THE UNIVERSITY OF CALGARY

Compositional variation in formation fluids and their relation to fluid flow and water-rock interaction in Devonian to Lower Cretaceous sedimentary rocks of southern Alberta

by

Dirk Kirste

A THESIS
SUBMITTED TO THE FACULTY OF GRADUATE STUDIES
IN PARTIAL FULFILMENT OF THE REQUIREMENTS FOR THE
DEGREE OF DOCTOR OF PHILOSOPHY

DEPARTMENT OF GEOLOGY AND GEOPHYSICS

CALGARY, ALBERTA

SEPTEMBER, 2000

Abstract

Variations in the chemical composition of waters in six aquifers ranging in age from Upper Devonian to Lower Cretaceous were examined to determine the chemical and hydrologic controls on the evolution of formation fluids in southern Alberta. The principal factors affecting fluid composition are mixing, water-rock interaction, and bacterial sulfate reduction. Mixing of chemically evolved formation waters with meteoric water has resulted in a complex regional distribution of chemical constituents. Several episodes of meteoric influx are recognized based on isotopic and chemical variations. Overlain on the fluid mixing signature are a number of chemical trends that are a product of water-rock interaction. Mineralogical control of the water chemistry is dominated by calcite-dolomite equilibrium in the carbonate and clastic reservoirs, although in the clastic reservoirs, calcium to magnesium activity ratios appear to be artifacts of earlier equilibria. The Nisku/Arcs formation waters are close to equilibrium with calcite, dolomite and anhydrite. Dissolved silica activities and pH of clastic-hosted waters are strongly influenced by the presence of clay minerals and smectite-aqueous solution metastable equilibrium. Bicarbonate and sulfate content and stable isotopes of sulfur and carbon are interpreted to reflect bacterial sulfate reduction that has occurred in areas affected by meteoric influx.

Fluid flow is dominated by south to north topography-driven flow with recharge in Alberta, Montana and Wyoming. Rapid changes in chemical composition and hydraulic head gradient indicate complex flow patterns that reflect changes in hydraulic conductivity and/or continuity of aquifers, and structural features like the Sweetgrass/Bow Island Arch and the Vulcan Low.

Acknowledgements

Three have been numerous people who have provided me with the support and inspiration needed to carry me through this endeavor. First and foremost, thanks are extended to Ian Hutcheon who could always be relied on for insight and clarity and cash when confusion or disillusion or poverty threatened. Terry Gordon, Larry Bentley, Ron Spencer, Dave Pattison, Ed Ghent all provided guidance and answers to questions only a grad student could ask. Graham Simpson, John Cody, Scott McLellan and all of the other grad students who entertained and enlightened. In particular I want to express my thanks to Cindy Riediger, Martin Fowler, Vern Stasiuk and Fari Goodarzi for encouraging me to return to research after a long hiatus. The stable isotope laboratory of Dr. H.R. Krouse and its occupants Maria, Jesusa and Nenita need to be thanked profusely. Special thanks to Maurice Shevalier for keeping the analytical and computational side of the research machine running.

I am grateful to the following who provided money or services needed to conduct the research. Kaush Rakhit of Rakhit Petroleum Consulting provided access to the AEUB database of water chemistry. Wayne Cox and PanCanadian Petroleum Ltd. provided money and a tremendous amount of logistic support. Lithoprobe for financial support. The AOSTRA COURSE funds also provided financial support. Ian Hutcheon's NSERC operating grant funded a substantial part of the sample collection and analyses.

Financial assistance is gratefully acknowledged from the University of Calgary Faculty of Graduate Studies through scholarships, AAPG Grants-in-Aid Foundation, Geological Society of America, and SPWLA.

I would also like to thank my parents and family for all that they have done.

CHAPTER 3 FLUID FLOW

LIST OF TABLES

List of Figures

Chapter One

Introduction

The composition of aqueous fluids in sedimentary basins is intimately related to the geochemical, biochemical, hydrogeologic, and thermal processes that occur during basin evolution. These processes are all recognized to occur in the western Canada sedimentary basin and are described to varying degrees in numerous publications. What is of particular importance is that these processes can leave characteristic chemical signatures on the fluid composition. The signatures are often subtle but can be distinguished. The purpose of this study is to try and identify the effects of these processes on waters from a series of aquifers. The choice of a series of aquifers allows for the recognition of interaction between fluids of different aquifers and to observe the effects of different lithologies on fluid composition.

The study examines the chemistry of formation waters within the Devonian Nisku/Arcs to Lower Cretaceous Viking/Bow Island Formations to determine the effects of mixing, mineralogical and biological controls, and fluid flow. This objective is realized through investigating:

1. Regional variations in the chemical and isotopic composition of the formation waters.
2. Changes in chemical composition related to mixing.

3. Water-mineral equilibria.
4. Origin and controls on bicarbonate and dissolved sulfide content.
5. Fluid flow potential and fluid flow paths as described by transport and isotopic composition of the fluids.

Study area

The study area is approximately 90,000 km^2 bordered on the south and east, by Montana and Saskatchewan, and extends north to township 30 and west to range 7 west of the 5^{th} meridian on the Dominion Land Survey co-ordinates (49° to 51.6°N, 110° to 114.6°W). Water samples were collected from throughout the region, but sampling was limited by the availability of producing wells and sufficiently high water cuts. The work is an extension of previous studies conducted by Cody and Hutcheon (1994, 1999) and McLellan (1995).

There are some additional questions that a study such as this can broach. The answers are perhaps beyond the scope of this study but they are almost certainly entangled within the implications of the results. They are:

1. What is the extent of fluid flow in a sedimentary basin that has undergone uplift and erosion in which flow is dominated by topography driven recharge?

2. To what extent do processes other than mixing affect the chemical composition of formation waters?
3. Given that fluid flow, mixing and mineralogical controls on fluid composition exist, what are the implications for mass transport?

This study does not directly address these questions and yet provides insight as to their solution. Chapter 2 is an in depth look at the formation water chemistry, linking together mixing and water-rock interaction in order to identify the processes and perhaps illustrate how very different they are. Chapter 3 investigates fluid flow, from the potential for flow to actual flow paths. Chemically conservative behavior is identified in chapter 2 and utilized in chapter 3 but non-conservative behavior, especially in stable isotopes, is also proven to be useful in interpreting fluid flow paths.

Chapter 2

Regional Water Chemistry

Introduction

The composition of aqueous fluids in sedimentary basins is intimately related to the geochemical, biochemical, hydrogeologic and thermal processes that occur during basin evolution. These processes have ramifications for hydrocarbon exploration and production as they influence reservoir quality and the economic value of extractable hydrocarbons. The composition of the fluids influences the kinds of dissolution and precipitation reactions that occur, the potential for biodegradation of oils, and may affect bulk sediment properties like resistivity and seismic velocity. Fluid flow may be a mechanism for the transport of dissolved solids. The distribution of different dissolved species can provide insight into reservoir continuity and compartmentalization, the potential for porosity reduction by cementation or enhancement by dissolution, and the occurrence of biologically mediated reactions such as sulfate reduction or methane oxidation, all of which are critical components in the assessment of hydrocarbon plays.

Understanding of the origin of variations in the composition of formation fluids in the western Canada sedimentary basin (WCSB) has evolved considerably since first addressed in a series of publications initiated by the Alberta Research Council (Hitchon

1964, 1969a,b; Billings et al., 1969; Hitchon and Friedman, 1969; Hitchon et al., 1971). Hitchon and Friedman (1969) and Hitchon et al. (1971) suggest extensive mixing of meteoric water and modified seawater as the origin of salinity variations in the WCSB. They proposed seawater modification through solution of evaporites, exchange with carbonates, clays and organic matter, membrane filtration and formation of new minerals. Sources of chloride in excess of seawater were interpreted to be from dissolution of halite and membrane filtration (Hitchon *et al.*, 1971). Spencer (1987) attributed high salinity in Devonian formation waters to significant contributions from residual evaporitic brines with brine composition modified by reactions with Precambrian basement rocks followed by dilution by meteoric waters. Loss of Na, Mg and increase in K and Ca was attributed to albitization and dolomitization (Spencer, 1987). Connolly *et al.* (1990) studied formation waters of Devonian through Cretaceous age rocks in central Alberta. Connolly *et al.* (1990) interpreted the waters to comprise three distinct groups. The first two groups (Group I and II) are from carbonate and clastic reservoirs respectively and consist of mixtures of residual evaporite brines and meteoric waters. The third group was interpreted to be of meteoric origin. Mineral reactions among clay minerals, ankerite precipitation and, possibly, ion exchange were suggested as having exerted some influence on the composition of fluids in carbonate reservoirs (Connolly *et al.*, 1990). Clastic-hosted waters were interpreted to be modified by dissolution of feldspar and clay

minerals and ion exchange (Connolly *et al.*, 1990). Cody (1993), Cody and Hutcheon (1994) interpreted variations in fluid composition of the Mannville Group of southern Alberta to reflect dilution by meteoric waters, reactions between clay minerals and feldspars, and bacterial sulfate reduction introducing carbon dioxide and hydrogen sulfide.

This study concentrates on the chemistry, origin and evolution of formation waters of six aquifers ranging in age from Devonian to Lower Cretaceous in southern Alberta. The study integrates chemical data from the extensive Alberta Energy and Utilities Board (AEUB) formation water database with 137 water samples collected for detailed chemical analyses and stable isotopic compositions of C, O, H, and S. Variations in the distribution of dissolved constituents are related to mixing, water-rock interactions and bacterially mediated processes to develop an understanding of the evolution and present day composition of the formation fluids.

Geology

The study area is located in the southern portion of the WCSB and includes the southern part of the Alberta basin and the western portion of the Williston basin (**Figure 2.1**). There are three principal tectonic and geophysical features included in the study area: The Rocky Mountain Fold and Thrust Belt and associated hinge zone; the Vulcan Low;

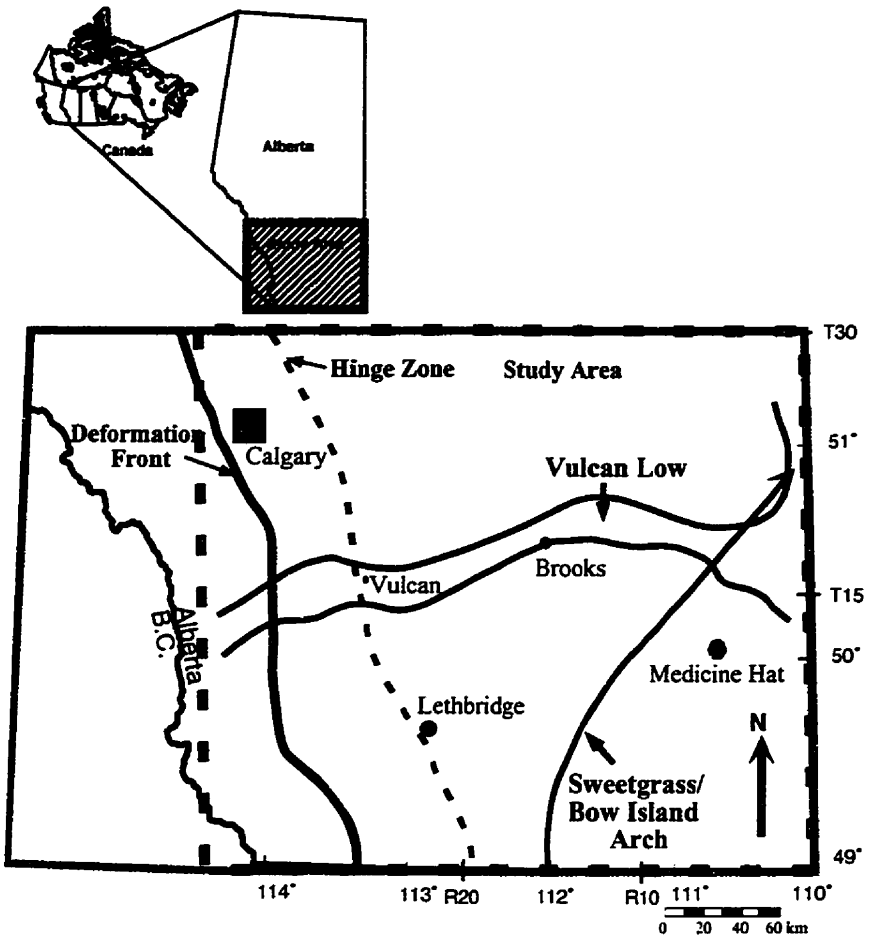

Figure 2.1 Map of the study area including the major structural features identified in the text. The study area is indicated by the dashed box.

and the Sweetgrass/Bow Island Arch. The Mesozoic deformation front and the associated hinge zone is marked by a rapid increase in dip, to the west, of the crystalline basement through a series of deep-rooted block faults with overlying foredeep strata thickening to the west (Wright *et al.*, 1994). The Vulcan Low is an aeromagnetic and gravity low interpreted to be a collision suture bordered on the south by the Medicine Hat Block and on the north by the Matzhiwin High (Ross *et al.*, 1991). Brandley *et al.* (1993) recognized Paleozoic displacement along vertical faults in the region of the Vulcan Low and suggest fault movement may have affected some Mesozoic deposition. In the south, the Sweetgrass/Bow Island Arch has been identified as a composite feature of basement structures that manifest themselves as a broad, low-angle, northeastward plunging anticline (Lorenz, 1982). Topographic highs identified with movement of the complex have been recognized from at least Ordovician to latest Tertiary time (Lorenz, 1982).

This study focuses on Upper Devonian to Lower Cretaceous sedimentary rocks in the southern part of the Alberta basin. The general Devonian to Cretaceous stratigraphy is given in **Figure 2.2**.

The Devonian Nisku/Arcs Formation consists of a shoaling upward cycle of sedimentation (Switzer *et al.*, 1994). Initial deposition of marine to marginal marine mudstones to wackestones was followed by the development of a northeast-southwest trending carbonate bank. East of the bank restricted and hypersaline conditions resulted

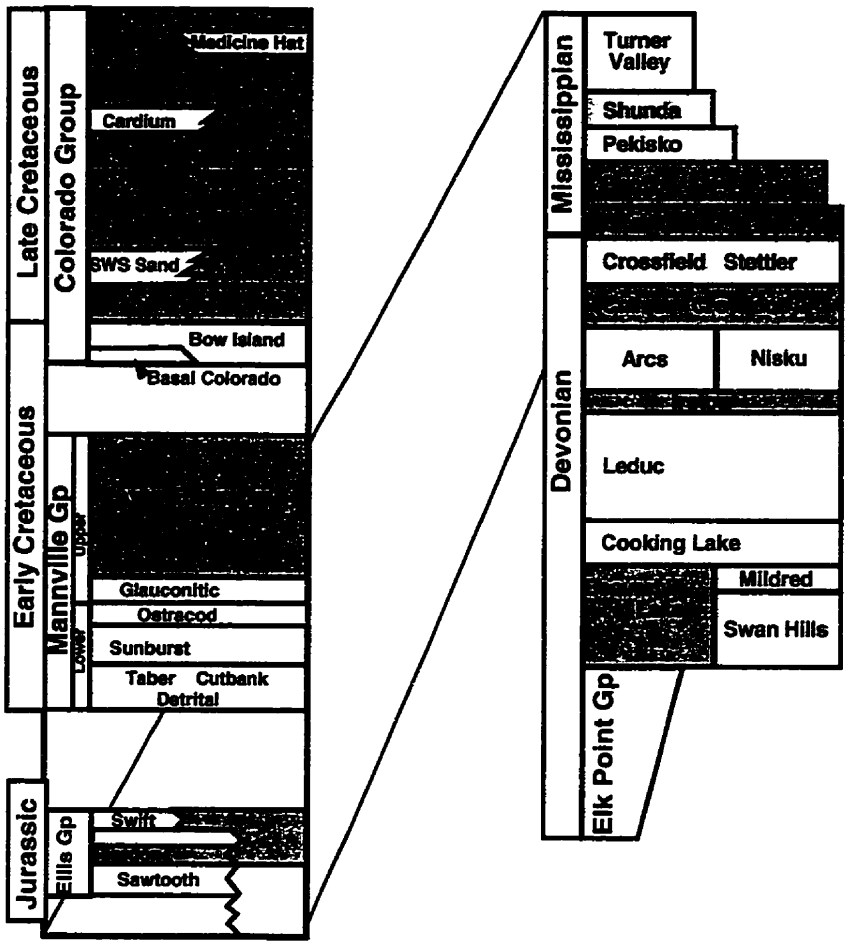

Figure 2.2. General stratigraphy of the study area. Blank spaces reflect unconformable contacts.

in deposition of carbonate muds and evaporites, to the west and north, shallow shelf carbonates were deposited (Kissling and Slingsby, 1992). The top of the Nisku Formation is recognized as a regional unconformity with karst features. Thin sands of the Calmar Formation were deposited on the Nisku during late stages of Winterburn Group deposition. The overlying Wabumun Group consists of thick anhydritic units of the Stettler Formation.

Mississippian strata conformably overlie Devonian carbonates in southern Alberta. An eustatic sea level rise resulted in deepening and anoxic conditions in the Late Devonian (Richards *et al.*, 1994). After the initial deposition of the Late Devonian to Early Mississippian lower Exshaw Formation, upwarping in conjunction with block faulting re-established carbonate platform deposition. A period of deepening through flexural subsidence and local block faulting followed. The reactivation of basement faults resulted in sagging of Paleozoic strata and deposition of substantial amounts of Carboniferous sediments. Shallow marine carbonates of the Pekisko Formation developed, followed by, and coeval with, restricted marine carbonates and anhydrite of the Shunda/Livingstone Formations. Subsequent transgressions resulted in deposition of carbonates of the Turner Valley and Mt. Head Formations. In southern Alberta significant erosion of Mississippian strata began in the Late Carboniferous and continued until Jurassic deposition commenced (Richards *et al.*, 1994).

The Upper Jurassic marks the onset of the Columbian Orogen and the development of a narrow foredeep trough towards the craton (Smith, 1994). The Middle Jurassic Sawtooth Formation, a shallow marine shelf sandstone, was deposited around Paleozoic erosional remnants on the sub-Jurassic surface (Poulton *et al.*, 1994). The erosional surface exhibits considerable local relief with karst features and collapse related to salt dissolution. Overlying shelf sandstone and shale cycles of the Rierdon and Swift Formations make up the remainder of Jurassic sediments in southern Alberta. A long period of uplift and erosion followed as movement of the Sweetgrass Arch of southern Alberta produced a positive topographic feature until late in Lower Cretaceous deposition.

The Mannville Group unconformably overlies the Jurassic Ellis Group and Mississippian strata. The Mannville Group is subdivided into Upper and Lower sections, separated by the calcareous mudstone to limestone Ostracod Member. The Cutbank and Sunburst members are fluvial-dominated sandstones within the Lower Mannville Formation (Hayes, 1986, Farshori and Hopkins, 1989). Deposition typically followed a southeast to northwest trend of sandstone channels. The Upper Mannville Glauconitic sandstone and A, B, and C units have been identified as non-marine incised valleys surrounded by interfluvial deposits completing a highly complex stratigraphic architecture (Wood and Hopkins, 1992). Deposition of the Upper and Lower Mannville Formation channels and

incised valley systems was controlled by topographic highs of Mississippian strata whose orientation was largely the result of north-south to northwest-southeast oriented block faults (Zaitlin, 1997)

Lower Cretaceous basal Colorado Formation sediments, marked by a thin conglomerate, unconformably overlie the Mannville Group. The formal units are the Basal Colorado Formation sandstone and the Joli Fou Formation shale, which pass laterally into the Viking/Bow Island Formation in southern Alberta. The Viking/Bow Island Formation consists of interbedded fine to coarse grained marine offshore to shoreface sandstones and conglomerates grading into non-marine sandstones in southeast Alberta overlying the Sweetgrass Arch (Poulton *et al.*, 1994). A major transgression followed Viking/Bow Island deposition resulting in the thick succession of marine shales of the Colorado Group.

Mineral Stability Diagrams

The relationship between an aqueous solution and mineral phases is often understood through the use of mineral stability diagrams. In surface and near surface environments mixing, weathering and diagenesis are the principal processes that affect aqueous solution composition. Of these, weathering and diagenesis are the processes that relate directly to the composition of the mineral phases and, perhaps the most common mineral phases

associated with weathering and diagenesis are clay minerals. Unfortunately clay minerals are also the most poorly constrained in terms of composition and thermodynamic properties.

The clay minerals smectite and illite display considerable compositional variability (Tardy and Fritz, 1981; May et al., 1986; Güven, 1988; Ransom and Helgeson, 1993). To accurately determine the role that clay minerals play in mineral reactions and in controlling solution chemistry, a broadly applicable method of obtaining their thermodynamic properties must be utilized. Two methods have been applied to account for the compositional variations in clays; (1) thermodynamic properties are calculated from experimental solubility data (Kittrick, 1971; Routson and Kittrick, 1971; Weaver et al., 1971) or estimated using chemical analogues for specific compositions (Tardy and Garrels, 1974; Nriagu, 1975; Chermak and Rimstidt, 1989); and (2) using mixing equations that consider clay minerals as solid solutions of end-member components (Tardy and Fritz, 1981; Aagard and Helgeson, 1983; Garrels, 1984; Tardy et al., 1987). Using specific compositions is limited as a rather large data set would be required to fully describe the range in chemical composition of clay minerals. On the other hand, mixing models allow for greater applicability because of the generality of solid solution models and the ability to constrain end member thermodynamic data.

The method used in this study utilizes a solid solution model that assumes ideal mixing on homological sites based on the procedure defined by Aagard and Helgeson (1983). Chemically complex smectites can be depicted on mineral stability diagrams by calculation of the activities of the thermodynamic components that make up the smectite solid solution. The thermodynamic components used are those recommended by Aagard and Helgeson (1983) and Ransom and Helgeson (1993; 1995). The smectites are represented by the stoichiometric thermodynamic components pyrophyllite, muscovite, paragonite and two fictive calcium and magnesium components that are structural analogues to the potassium and sodium micas. The mixing on sites model of Aagard and Helgeson (1983) takes into account independent and coupled substitution on tetrahedral, octahedral, and exchange sites. This method differs from those of Tardy and Garrels (1974), Tardy and Fritz (1981), Tardy et al. (1987), Tardy and Duplay (1992) in that it does not involve the use of cation exchange coefficients. Although the amount of experimental data on cation exchange in soils and clays is quite large, the values for clay minerals display considerable scatter (Bruggenwert and Kamphorst, 1982). Tardy and Garrels (1992) report the variability of exchange coefficients results in an up to 10kJ/mol difference in the calculated free energy of exchange. Although Tardy and Garrels (1992) dismiss the difference as insignificant, a 10kJ/mol change in free energy of a phase will result in a considerable shift in equilibrium curves on a mineral stability diagram.

The practical application of the Aagard and Helgeson (1983) method is that on an activity-activity diagram the stability curves between the end-member components represent equilibrium for clay minerals and coexisting aqueous solution. Plotting the smectite end-member components using activities calculated with the Aagard and Helgeson (1983) solid solution model at the temperature and pressure of the coexisting aqueous solution essentially defines a stability field of smectite. If the aqueous solution compositional data plot within the stability field, then equilibrium between water and smectite can be assumed. The problem with this technique is that the composition of the clay mineral has to be known. Smectite clays display limited variability of the octahedral, tetrahedral and interlayer site charges (Aagard and Helgeson, 1983; Ransom and Helgeson, 1993). Aluminum occupancy on octahedral and tetrahedral sites shows a narrow range for natural smectites, and tetrahedral site occupancy itself defines smectites from illites. (Ransom and Helgeson, 1993). The narrow range in tetrahedral and octahedral site occupancy suggests that it may be possible to use a smectite compositional analogue for which only the exchangeable cation composition needs to be determined if no clay mineral compositional data exists.

The method of Aagard and Helgeson (1983) requires knowledge of the clay mineral composition, in particular the mole fraction of each of the exchangeable cations. The composition of the clay minerals for the Sawtooth, Lower Mannville and Upper

Mannville clastic reservoirs is not known. The relatively low abundance of clay minerals (generally less than 3-5%) makes compositional analyses difficult and XRD techniques require the separation of the fine fraction using distilled water which will alter the exchangeable cation composition to favour calcium and magnesium over sodium and potassium because of exchange site preference at low ionic strengths (Appello and Postma, 1993). Instead, the Belle Fourche montmorillonite (Kittrick, 1971) was chosen as a representative compositional analogue for the aluminum and silicon tetrahedral and octahedral site occupancy. Knowledge of the mole fraction of each of the major cations on the exchange site is also required to complete the calculation. End member activities were determined by calculating the clay mineral exchangeable cation composition in equilibrium with each sampled water using the chemical modeling program PHREEQC. The program models ion exchange as ion association reactions in the form of half reactions. The Na-Ca exchange reaction:

$$\tfrac{1}{2}Ca^{2+} + Na - X \Leftrightarrow \tfrac{1}{2}Ca - X_2 + Na^{+} \qquad K_{Ca\,Na}$$

gives two half reactions:

$$Ca^{2+} + 2X^{-} \Leftrightarrow CaX_2 \qquad K_{CaX2}$$

$$Na^{+} + X^{-} \Leftrightarrow NaX \qquad K_{NaX}$$

Where X^- represents the exchangeable cation site, and CaX_2 and NaX are the exchangeable cations occupying the sites. The PHREEQC database contains association

constants relative to K_{NaX} (i.e. $K_{CaX2}=(K_{Ca\backslash Na}\bullet K_{NaX})^2$) where the exchange coefficient $K_{Ca\ Na}$ is derived from the literature. The composition of exchangeable cations of a clay mineral in equilibrium with an aqueous solution can then be determined. Calculated paragonite and pyrophyllite activities for a number of smectite mineral compositions are given in **Table 2.1**.

Calculation of thermodynamic properties

The stability of mineral phases and coexisting aqueous solutions is often represented using activity diagrams. Solution compositions plotted on these diagrams can be used to interpret mineralogical controls on the dissolved constituents. If chemical equilibrium between fluids and minerals is achieved, measured values of fluid composition calculated as activities plot on the stability curves of the mineral phases. Phase diagrams are calculated using thermodynamic properties of the mineral, water, and aqueous species involved in the equilibria. A number of thermodynamic databases exist that can be applied to this purpose (Robie et al., 1978; Helgeson et al., 1978, 1981; Berman, 1988; Johnson et al., 1992). The databases contain thermodynamic data determined from experimental work and calculated using equations of state for a large

Table 2.1. Calculated activities of the thermodynamic components Paragonite and Pyrophyllite for different smectite compositions

	Mole fraction of the exchangeable cation on the exchange site								Mica component activities			
	Na	K	Ca	Mg	Li	Sr	H	sum	Paragonite	log a (Parag)	Pyrophyllite	log a (Pyr)
Montana LT-42	8.22E-01	6.73E-03	5.82E-02	1.56E-02	5.04E-04	1.12E-02	2.68E-06	1.00	0.06	-1.26	0.24	-0.63
Wyoming	8.22E-01	6.73E-03	5.82E-02	1.56E-02	5.04E-04	1.12E-02	2.68E-06	1.00	0.06	-1.24	0.34	-0.47
Belle Fourche	8.22E-01	6.73E-03	5.82E-02	1.56E-02	5.04E-04	1.12E-02	2.68E-06	1.00	0.02	-1.73	0.39	-0.41
Upton	8.22E-01	6.73E-03	5.82E-02	1.56E-02	5.04E-04	1.12E-02	2.68E-06	1.00	0.03	-1.58	0.37	-0.43
Chambers	8.22E-01	6.73E-03	5.82E-02	1.56E-02	5.04E-04	1.12E-02	2.68E-06	1.00	0.04	-1.37	0.28	-0.55
Lorena	8.22E-01	6.73E-03	5.82E-02	1.56E-02	5.04E-04	1.12E-02	2.68E-06	1.00	0.04	-1.36	0.32	-0.50
Wyoming Clay Spur	8.22E-01	6.73E-03	5.82E-02	1.56E-02	5.04E-04	1.12E-02	2.68E-06	1.00	0.02	-1.70	0.38	-0.43

Smectite compositions from Tardy and Fritz (1981) and Ransom and Helgeson (1993)

number of stoichiometric minerals. Nonstoichiometric minerals like the clay minerals illite and smectite are generally not included because of variation in composition.

Smectite thermodynamic behavior can be fully determined when regarded as a regular solid solution described in terms of nine thermodynamic components (Ransom and Helgeson, 1993). Ransom and Helgeson (1993, 1994, 1995) recommend a number of stoichiometric and fictive thermodynamic components to account for the compositional and octahedral site variations in smectites. Of these, four provide explicitly for the contribution of the interlayer cations sodium, potassium, calcium and magnesium. The stoichiometric minerals paragonite and muscovite account for sodium and potassium and the fictive components $Ca_{0.5}Al_3Si_3O_{10}(OH)_2$ and $Mg_{0.5}Al_3Si_3O_{10}(OH)_2$ describe the calcium and magnesium contribution (Ransom and Helgeson, 1993, 1994).

The use of fictive components requires calculation of the thermodynamic properties needed to portray the phase on an activity diagram. A number of techniques exist for estimating thermodynamic properties (Nriagu, 1975; Tardy and Garrels, 1974, 1976, 1977; Helgeson et al., 1978; Robinson and Haas, 1983; Berman and Brown, 1985; Chermak and Rimstidt, 1989). The methods of Helgeson et al. (1978), Berman and Brown (1985) and Chermak and Rimstidt (1989) were used to calculate the Gibbs free energy and enthalpy of formation, third law entropy, volume and heat capacity of the

fictive thermodynamic components. The thermodynamic databases of Berman et al. (1985) and Berman (1988) were used in all of the calculations.

Table 2.2. Thermodynamic properties of the fictive smectite end-member components Ca-Mica and Mg-Mica, calculated using the methods of Helgeson *et al.* (1978), Chermak and Rimstidt (1989), and Berman and Brown (1985).

25°C, 1 bar	$\Delta G°_f$ (kJ/mol)	$\Delta H°_f$ (kJ/mol)	S° (J/mol)	V° (J/bar)
$Ca_{0.5}Al_3Si_3O_{10}(OH)_2$	-5583.31	-5959.48	262.181	12.906
$Mg_{0.5}Al_3Si_3O_{10}(OH)_2$	-5530.83	-5907.32	256.631	12.631

	k_o	k_1*10^{-2}	k_2*10^{-5}	k_3*10^{-7}
$Ca_{0.5}Al_3Si_3O_{10}(OH)_2$	632.5955	-41.4757	-146.226	209.51285
$Mg_{0.5}Al_3Si_3O_{10}(OH)_2$	631.856	-41.09995	-153.2492	219.82115

The Gibbs free energy of formation was estimated using the method of Chermak and Rimstidt (1989). The technique involves summing the polyhedral contributions of the different oxide and hydroxide components. Estimated values for the micas muscovite, pyrophyllite and paragonite are within 0.1% of the Berman (1988) database values. The polyhedral contribution of MgO in 8-fold coordination was not determined by Chermak and Rimstidt (1989) and had to be calculated separately using a multiple regression technique. A total of 11 minerals were used following structural sites outlined by

Robinson and Haas (1983) and Chermak and Rimstidt (1983) to calculate the MgO contribution. The free energy of the 8-fold coordinated MgO polyhedral unit was estimated to be –605.00 kJ/mol.

Molar volumes and third law entropies were calculated following the structural analogue algorithm of Helgeson et al. (1978). The structural analogues used were muscovite and paragonite. Estimated volumes and entropies using this procedure for micas are accurate to within 1% (Ransom and Helgeson, 1994).

Enthalpies of formation were calculated using the Gibbs free energy of formation, third law entropies, and entropies of formation from the elements. Heat capacities were estimated using the method of Berman and Brown (1985). Summation of the tabulated oxide component heat capacity coefficients results in calculated heat capacities within 2% of measured values (Berman and Brown, 1985).

Expansivity and compressibility was not determined as pressure and temperatures in the system under study do not exceed 200 bar and 80°C, and effects of pressure and temperature changes on volume are expected to be small.

The Berman (1988) thermodynamic database does not contain data for anhydrite and Simpson (1999) suggests the Berman (1988) calcite and dolomite thermodynamic data are not representative for complex aqueous solutions like natural waters. Simpson (1999) found the thermodynamic data for calcite and dolomite of Harvie et al. (1984) to be more

consistent with aqueous solution chemistry and mineral saturation states than that of Berman (1988). In this study, the thermodynamic data for anhydrite, calcite and dolomite is that of Harvie et al. (1984), this data is the same as that listed in the appendix of Nordstrom and Munoz (1996). The anhydrite, calcite and dolomite thermodynamic data are not used when considering silicate mineral stability and thus do not introduce any problems with internal consistency of the database.

Methods

The regional chemical data used in this study were extracted from the Alberta Energy and Utilities Board (AEUB) database of chemical analyses for waters collected from drill stem tests (DST), production tests and surface facilities. The data were made available in digitized form by the Geological Survey of Canada and Rakhit Petroleum Consulting Ltd. The AEUB chemical analyses primarily report K, Ca, Mg, Cl, total alkalinity as HCO_3, CO_3, SO_4 and Na, where Na is either determined directly, or calculated by difference to achieve charge balance. Some analyses report a combination of the univalent cations Na and K as Na by calculation where charge balance is assumed.

Data Culling

The AEUB water analyses are subject to a number of potential inaccuracies and those analyses must be identified and removed (Bachu *et al.*, 1987; Hitchon and Brulette, 1984). Contamination associated with drilling, completion and production methods, incorrect sampled intervals, multiple tested intervals, data entry errors, and multiple entries are the most common forms of error. The following culling methods are modified from those described by Bachu *et al.* (1987). Analyses missing any of the major ions Na, Cl, Ca and alkalinity, were deleted, as well as those collected from production locations down-stream of the separators (facilities where water-oil or water-gas mixtures are separated). Waters with densities less than 1, pH less than 4 or greater than 10, and those with lab analysis dates more than 1 month after sample collection dates were also culled. Data entry error was removed by calculating charge balance, with imbalances of greater than 5% being culled. Contamination by drilling mud, acid washes or washes from cement jobs was determined by cross-plotting the major cations and anions and by reviewing the recovery descriptions, waters indicating contamination were removed. Duplicate analyses, and analyses from larger test intervals, multiple intervals, and incorrect intervals were removed by scrutinizing the individual well samples. The resulting regional distributions of water chemistry can then be considered as representative, although not rigorously precise.

In total, 708 Devonian Nisku/Arcs Formation, 4597 Mississippian, 1244 Jurassic Sawtooth Formation, 4529 Lower Mannville, 2133 Upper Mannville, and 3458 Viking/Bow Island Formation water chemical analyses were obtained from the database. After culling, the numbers were reduced to 184 Devonian Nisku/Arcs Formation (26%), 876 Mississippian (19%), 426 Jurassic Sawtooth Formation (34%), 1040 Lower Mannville (23%), 559 Upper Mannville (26%) and 1161 Viking/Bow Island Formation (34%).

In addition to the regional bulk chemical analyses a number of wells were selected for controlled sampling for high quality chemical analyses, including major cations and anions, isotopes of carbon, oxygen, hydrogen and sulfur and organic acids. Water samples were collected from wells that had not been exposed to water flood or other forms of contamination. Gas wells were generally avoided, but some waters were collected from production tests on gas wells and from separators on high water content gas wells. In total 137 samples were collected from the Nisku/Arcs, Mississippian, Sawtooth, Upper and Lower Mannville and Viking/Bow Island reservoirs. The waters were sampled and preserved following procedures based on those developed and used by the United States Geological Survey (Lico *et al.*, 1982).

A field laboratory was used to measure and record pH and alkalinity and to preserve the samples for later laboratory analyses. Water and oil-water emulsions were collected from

high water cut (>30% water) wells and water source wells. Samples were collected in clean 9 litre Nalgene carboys and emulsions were allowed to separate. Temperature and pH were immediately recorded and two small (125 ml) aliquots were collected for alkalinity measurement and sulfide preservation. Conductivity was measured using a portable conductivity meter and alkalinity titrations were performed in the field. Sulfide was preserved using 50:50 water-sulfide anti-oxidant buffer (SAOB) mixture. The remaining water sample was filtered through a prefilter and a 0.45 μm filter using a N_2 pressure driven filtration device. Samples were preserved for various analyses using the following methods. A 125 ml aliquot for cation analyses was acidified to a pH of 2 using nitric or hydrochloric acid. 30 ml was collected for short chain aliphatic acids in amber glass bottles containing a small quantity of sodium azide as bactericide. In a 60 ml Nalgene bottle, a 10 ml aliquot was diluted to 60 ml with doubly distilled water and sealed for subsequent silica analysis. An uncoated Vacutainer® containing approximately 2 ml of NH_4OH solution saturated with $SrCl_2$ (ammoniacal strontium chloride) was filled with filtered water to precipitate $SrCO_3$ for ^{13}C isotopic analyses. To preserve for sulfur isotopes, two dark flint glass bottles were filled with filtered water. In one, $BaCl_2$ was added to precipitate sulfate as $BaSO_4$. In the other, cadmium acetate ($CdCH_3COOH$) was added to precipitate dissolved sulfide as CdS. Water for ^{18}O and D analyses was collected in two separate vacutainers.

Cation concentrations were measured by Atomic Absorption spectrometry on a Perkin Elmer 5000 AA spectrophotometer. Filtered unacidified samples were used for anion analysis on a Waters® ion liquid chromatograph using a Waters® anion column. Dissolved sulfide determinations were made using Orion® sulfide specific and double junction electrodes.

Stable isotopes of water (^{18}O and D), total dissolved carbonate (^{13}C), and dissolved sulfate and sulfide (^{34}S) were analyzed in the Stable Isotope Laboratory of Dr. H.R. Krouse, Department of Physics and Astronomy, University of Calgary. Oxygen isotopic measurements of water were made by equilibrating $CO_2(g)$ with water at 25°C (Epstein and Mayeda, 1953). The $^{15}O/^{16}O$ ratio of the $CO_2(g)$ was then measured on a Micromass MS903 mass spectrometer and the $\delta^{18}O$ reported as ‰ relative to Vienna Standard Mean Ocean Water (V-SMOW) with an error of $\pm$0.2‰. δD of H_2O was measured following the Zn reduction procedures outlined in Coleman *et al.* (1982). The produced hydrogen gas was analyzed on a Micromass 602 mass spectrometer with the δD reported as ‰ relative to V-SMOW. Error is estimated to be $\pm$2‰. Carbon isotopic composition was measured on the dissolved carbonate species precipitated as $SrCO_3$. Dried $SrCO_3$ was dissolved in orthophosphoric acid and the evolved $CO_{2(g)}$ was collected in glass tubes. The $\delta^{13}C$ of the $CO_{2(g)}$ was determined using a Micromass MS903 mass spectrometer. The carbon isotopic composition was reported as ‰ relative to the PeeDee Belemnite

(PDB) standard. Error is estimated to be ±0.3‰. The isotopic composition of the sulfate and sulfide was determined on a Micromass 602 mass spectrometer using the methods described by Thode (1954). The sulfur isotopic composition is reported in ‰ units relative to the Canyon Diablo Triolite (CDT) standard with estimated error of ±1‰.

The geochemical modeling program SOLMINEQ (Kharaka *et al.*, 1987) was used to compute the aqueous species distribution and mineral saturation states. The program calculates activity coefficients of charged species using the Helgeson (1969) B-dot method or the Pitzer ion-interaction method. The B-dot equation is considered reliable up to stoichiometric ionic strengths of 2 molal, although it can be effective at I<3.5 molal (Langmuir, 1997). Solutions with stoichiometric ionic strengths of >2 molal are better modeled using the Pitzer equation which was formulated specifically for concentrated aqueous electrolyte solutions. Formation water in Mississippian and younger rocks has stoichiometric ionic strengths less than 1.5 molal and speciation was carried out using the B-dot equation. Ionic strengths in excess of 2 required aqueous speciation and mineral saturation states for the Devonian Nisku/Arcs formation waters to be calculated using the Pitzer ion-interaction equation.

All sampling took place at the well head making sampling conditions problematic for obtaining an accurate pH determination. Degassing due to pressure release and oxidation of iron and sulfide can result in changes in pH. Measured pH typically reflects the

surface pressure and temperature conditions so *in*-situ pH must be determined through modeling. *In-situ* pH was calculated in SOLMINEQ by assuming equilibrium with calcite. Connolly *et al.* (1990) provide justification for the calcite equilibration assumption on the following grounds: (1) rapid equilibration between carbonates and aqueous solutions compared to the residence time of the formation waters; and (2) the ubiquitous occurrence of calcite in the Paleozoic carbonates and calcite cements in the Mesozoic clastic rocks, especially as late stage authigenic phases, imply calcite saturation is likely.

Results

Locations, chemical compositions, calculated pH, densities, temperatures, pressures, and depths of the sampled wells are summarized in **Table 2.3**. Analyzed waters have a charge balance error of <+/-5%, as determined from analyses. Stable isotope composition and acid gas partial pressures are given in **Table 2.4**.

Piper Plots

The water chemical composition of the AEUB data for each of the intervals are presented as trilinear diagrams in a Piper plot format (**Figures 2.3, 2.4, 2.5, 2.6, 2.7, and 2.8**). The diagrams are drawn by plotting, in milli-equivalents, the relative proportions of the major

Table 2.3. List of wells sampled and results of chemical analyses including modeled pH.

DLS Location	Operator	Pool	depth (m)	Field	Density	T	P (kPa)	HCO3	Na	Ca	K	Mg	Sr	Li	Mn	Fe	Ba	SiO2	Cl	SO4	Br	S	pH CO2	pH calcite
1-36-14-11W4	PanCanadian	Viking	668	Alderson	1.005	26	6200	342	3060	25	9	10	5.10	0.66	0.03	0.13	1.26	14.3	4700	14	19		7.32	7.69
9-29-14-10W4	Union Pacific Resources	Bow Island	650	Little Bow	1.013	32	7300	392	7810	180	25	46	37.70	1.93	0.13	0.24	2.18	43.6	12971	3	51	0.0	7.16	7.09
9-21-15-11W4	PanCanadian	Viking	725	Alderson	1.01	28	6500	624	3060	19	11	10	4.40	0.70	0.00	0.00	2.30	38.8	4615				7.37	7.73
1-4-19-12W4	PanCanadian	Viking	719	Alderson	1.007	28	6600	643	3622	26	52	10	10.93	1.00	0.04	0.18		36.5	5310	0		0.0	6.56	7.61
1-2-18-18W4	PanCanadian	Viking	772	Alderson	1.008	30	7796	810	3135	21	9	9	5.50	0.61	0.02	0.00	1.00	16.7	4810	23	18	0.1	6.47	7.66
4-30-18-17W4	PanCanadian	Bow Island	678	Bedger	1.01	32	9100	767	6138	63	16	16	20.00	0.92	0.17	0.24	0.22	23.1	9200		26	0.0	6.49	7.19
14-24-18-18W4	PanCanadian	Viking	884	Bedger	1.01	31	7700	624	6488	66	19	22	26.70	1.43	0.06	0.34	1.41	19.3	9136		19	0.0	6.37	7.14
F1/10-8-17-14W4	PanCanadian	Viking	795	Newell	1.008	31	7700	462	4399	50	11	12	12.60	0.67	0.03	0.23	4.60	24.0	6744	0	0	0.0	6.68	7.5
02/10-8-17-14W4	PanCanadian	Viking	795	Newell	1.0068	31	7700	636	4090	51	9	13	13.00	0.50	0.03	0.25	4.40	23.5	6085	0		0.0	6.61	7.31
11-18-24-18W4	CNRL	Viking	887	Wintering Hills	1.01	31	8000	518	7230	131	23	65	32.40	1.35	0.06	2.60	24.30	21.4	12169	6	56	0.0	7.48	7.1
11-29-28-17W4/2	Beaver Lake Resources	Viking	1113	Willow	1.013	35	9336	939	6405	43	23	52	12.00	1.15		2.49		24.4	9041			0.0	7.61	7.3
1-23-8-17W4	Renaissance Energy	Glauconitic	887	Taber S	1.001	35	9962	3315	1627	20	39	15	1.57	1.75	0.00	0.06	4.33	16.5	995	7	0	74.1	6.39	6.94
14-2-10-18W4	Petrorep Resources	Glauconitic	901	Bow Island	1.005	32	9596	3387	2028	23	23	10	1.38	1.19	0.00	0.06	1.42	13.0	1110	41	8.7	83.7	6.4	6.92
10-28-12-6W4	Amber Energy	Glauconitic	860	Medicine Hat	1.006	26	9960	3117	2925	18	19	16	6.30	1.03	0.01	0.00	0.00	18.2	2723	50		0.0	5.96	7.15
13-33-14-7W3	Regata Resources	Glauconitic	907	Medicine Hat	1.005	32	10150	3964	2640	32	29	19	2.00	1.58	0.02	0.38	2.18	23.7	1836	20		9.2	6.27	6.73
02/11-33-14-17W4	Aquila Energy	Upper Mannville		Enchant	1.013	31	11300	7584	7400	56	113	46	3.10	0.44	0.00	0.19	0.45	49.8	8712	643	12	2.4	5.91	6.41
10-21-18-18W4	PanCanadian	Upper Mannville	1014.3	Alderson	1.013	30	11178	10510	6056	45	145	36	4.00	0.19	0.00	0.06		26.1	3662	104		12.0	6.22	6.4
14-20-18-18W4	PanCanadian	Upper Mannville	1002	Alderson	1.013	30	11150	6077	6834	30	64	25	13.40	3.10	0.02	0.05		28.0	5653	0		1.0	6.51	6.74
11-20-18-18W4	PanCanadian	Upper Mannville	1010	Alderson	1.013	30	11150	4909	7230	52	71	42	19.10	3.13	0.02	0.08		27.2	8168	306		9.0	6.8	6.8
11-9-14-18W4	Crystal Energy Inc.	Glauconitic	1099	Little Bow	1.015	34	13497	9259	10040	104	189	30	31.10	1.54	0.15	0.32	1.85	35.7	10332			0.0	6.09	6.09
04/10-18-18-12W4	Renaissance Energy	Upper Mannville	974	Alderson	1.012	38	10500	7186	4415	19	67	18	1.00	4.58	0.01	0.11	0.00	22.2	3408	143		3.6	6.37	6.66
6-30-19-14W4	PanCanadian	Glauconitic	1028	Johnson	1.014	29	10759	4965	5870	39	84	53	12.30	3.72	0.05	0.47	2.14	19.3	7068	84	25	85.7	6.12	6.72
7-6-17-14W4	PanCanadian	Glauconitic	1018	Johnson	1.017	32	11000	5201	6130	63	129	63	12.20	5.16	0.29	0.11		26.0	6319	689		1.0	6.15	6.38
15-6-17-14W4	PanCanadian	Glauconitic	1119	Johnson	1.017	32	11000	2433	5967	64	84	33	12.90	2.39	0.08	0.05		25.9	7004	117		5.0	5.71	6.72
02/14-28-17-15W4	PanCanadian	Upper Mannville	1026	Countess	1.017	32	11140	9249	9723	71	167	93	15.70	10.60	0.01	0.17		26.4	10579	178		61.0	6.25	6.26
02/10-8-20-18W4	Crystal Energy	Upper Mannville	1160	Jumpbush	1.012	39	11500	3304	9980	38	95	56	32.10	3.95	0.02	1.04	0.00	47.5	13842	755	25	0.4	6.3	6.91
10-26-20-20W4	Tarragon Oil and Gas	Upper Mannville	1358	Bassano	1.017	38	12000	1986	11830	345	89	122	97.40	3.48	0.12	0.91	0.00	26.4	17636	431	28	0.0	6.78	6.4
7-2-20-21W4	Tarragon	Upper Mannville	1405	Queenstown	1.022	40	12780	830	14450	464	96	180	121.00	2.60	0.23	1.04	2.30	18.6	22076	7	49	0.9	5.59	6.42
14-24-20-21W4	Barrington Petroleum	Upper Mannville	1346	Jumpbush	1.022	40	12780	820	15130	452	91	177	127.00	3.02	0.61	1.08	0.00	19.3	22251	97	7	7.2	5.63	6.42
1-21-21-20W4	Enron Oil	Upper Mannville	1325	Bassano	1.022	40	11695	1049	14960	571	118	225	120.00	5.28	0.22	1.13	0.00	19.5	22380	383	45	4.1	5.29	6.23
6-28-20-23W4	PanCanadian	Upper Mannville	1583	Rockyford	1.02	49	10093	2469	9544	210	72	57	36.95	2.40	0.00	2.80	0.00	25.7	12825	1015		0.1	6.22	6.24
8-16-26-12W4	Renaissance Energy	Upper Mannville	1027	Cessford	1.0116	37	10500	4654	6247	19	34	19	12.90	1.75	0.02	0.00	1.00	13.7	6846	21	19	1.3	7.48	6.98
10-21-29-11W4	Cannet Resources	Upper Mannville	1042	Stanmore	1.012	33	8600	1065	6632	170	37	57	26.50	1.40	0.41	1.10	0.34	25.2	10030	1055		0.2	7.4	6.66
02/11-6-28-20W4	Renaissance	Upper Mannville	1336	Wayne-Rosedale	1.02	46	9473	1406	9226	86	45	26	0.59	2.00		2.80		21.8	12366			0.0	6.75	7.75
02/9-21-28-20W4	Gascoyne Petroleum	Upper Mannville	1314	Drumheller	1.016	46	9258	1391	8684	92	31	25	34.60	1.50	0.20		0.26	19.7	8922	35		0.0	6.81	6.78
15-20-1-9W4	Roan Resources	Mannville	936	Black Butte	1.013	33	7871	3563	4982	54	40	41	12.00	2.18	0.05	0.34	0.45	23.3	4969	657		7.3	6.59	6.67
8-6-1-14W4	Truax Resources	Cutbank	781	Red Coulee	1.004	29	9100	2509	1226	112	43	39	5.96	2.00	0.18	0.09	5.83	21.4	575			48.9	6.18	6.32
9-18-9-17W4	Renaissance Energy	Lower Mannville	930	Ferguson	1.007	34	9100	3700	2712	67	63	73	5.33	3.69	0.08	1.99	0.76	61.0	2307	12		0.0	5.65	6.44
4-7-8-4W4	Anderson Exploration	Sunburst	1133	Manyberries	1.01	37	9500	3212	3852	36	51	28	10.31	2.26	0.03	0.84	0.66	38.3	4200			0.0	6.38	6.8
02/13-11-6-17W4	Renaissance Energy	Lower Mannville	955	Wrentham	1.004	35	10000	9313	1963	37	36	19	3.59	1.40	0.00	2.83	3.86	32.3	1312	0	15	2.3	7.16	6.79
02/6-36-9-9W4	Altana Exploration	Lower Mannville	900	Medicine Hat	1.008	30	10200	3274	3110	15	20	9	2.40	0.90	0.04	0.23	0.00	23.7	2574	218	9	0.2	6.36	7.19
16-16-9-17W4	Renaissance Energy	Taber	976	Taber	1.0044	35	10700	9038	1854	33	25	12	1.73	1.54	0.00	0.23	3.03	76.8	978	0	34	7.2	6.89	6.75
13-34-10-13W4	Rife Resources	Lower Mannville	917	Bow Island	1.0084	33	10500	3223	1901	41	27	16	1.36	1.49	0.00	0.05	12.16	66.2	1236	5	45	100.7	5.69	6.87
16-14-19-18W4/2	Acanthus Resources	Lower Mannville	1070	Turin	1.011	35	11500	7111	4660	42	137	51	3.70	7.00	0.07	0.12	0.36	62.4	3606	69	36	70.2	5.89	6.5
9-1-13-17W4	Renaissance Energy	Lower Mannville	1013	Turin	1.008	39	11500	9248	3475	29	97	24		3.40	0.00	7.00	10.00	45.6	2070	5	16	46.4	5.86	6.7
02/14-9-12-18W4	Murdoch Petroleum	Mannville		Pekisko	1.0159	33	12000	12194	6023	42	180	82	9.50	7.60	0.00	0.90	0.00	29.2	6475	477		7.4	5.90	6.43
7-16-13-18W4	Startech Energy	Mannville	1120	Pekisko	1.015	34	12221	6364	5579	47	117	49	2.81	6.28	0.00	0.13	7.64	24.4	5516	75		77.0	5.55	6.44
4-24-14-10W4	Intensity	Lower Mannville	927.0	Alderson	1.015	32	10400	6184	5740	32	61	27	13.40	3.80	0.02	0.04		26.6	5317	469	15	122.0	6.15	6.74
14-30-14-10W4	Regata	Lower Mannville	918	Alderson	1.015	33	10313	5794	7060	33	29	22	19.00	2.24	0.15	0.05		27.0	7352	274	27	58.6	6.09	6.93
14-34-13-13W4	PanCanadian	Lower Mannville	898	Alderson	1.0117	37	11228	7394	4978	23	65	30	7.90	3.24	0.01	0.20	0.00	76.4	3125	112	6	20.8	6.22	6.77
12-18-14-18W4	Merit Energy	Lower Mannville	1144	Little Bow	1.0095	33	12231	4788	4493	101	92	55	4.04	6.90	0.07	0.25	0.92	42.4	4488			7.8	5.35	5.81
13-19-19-10W4	Intensity	Lower Mannville	932	Alderson	1.01	35	10418	9737	5390	18	46	14	5.40	3.46	0.05	0.09		28.6	2761	21	10	0.0	6.75	6.81
4-17-19-10W4	Petro-Canada	Lower Mannville	941.5	Alderson	1.018	38	10480	4914	6010	46	41	36	26.70	2.67	0.06	0.05		27.4	9245	54	35	9.3	6.03	6.63
9-32-19-11W4	PanCanadian	Lower Mannville	928	Alderson	1.0104	32	10800	6845	4480	26	50	13	4.30	3.11	0.01	0.01		29.2	2454	25		40.1	6.79	6.66
10-3-19-11W4	D & R Oils	Lower Mannville	919.9	Alderson	1.013	32	10804	6821	4927	19	35	11	6.82	2.81	0.01	0.08		26.7	2899	0		19.0	6.81	6.79
8-14-19-11W4	PanCanadian	Lower Mannville	944	Alderson	1.013	32	10900	10915	5900	17	42	10	7.25	2.53	0.01	0.04		30.3	3424	18	18	4.0	6.66	6.6
12-24-19-11W4	PanCanadian	Lower Mannville	953	Alderson	1.0137	32	10850	9260	5420	23	48	12	7.59	3.06	0.02	0.05		31.0	3147	35		13.7	6.41	6.72
13-11-19-11W4	PanCanadian	Lower Mannville	937	Alderson	1.0137	32	10900	9399	5200	29	38	13	9.56	2.90	0.01	0.02		29.5	3089	55	14	21.9	6.85	6.66
8-05-19-11W4	PanCanadian	Lower Mannville	970	Alderson	1.0111	32	10750	8677	4240	41	67	15	1.13	5.06	0.00	0.01		29.2	2102	13	5	1.4	5.94	6.44
14-06-19-11W4	PanCanadian	Lower Mannville	966.5	Alderson	1.0111	32	10750	9300	4920	23	50	12	4.04	4.03	0.00	0.04		31.4	2282	80	17	0.0	6.21	6.7
2-9-19-12W4	PanCanadian	Lower Mannville	979	Alderson	1.0133	36	10825	10749	6100	38	75	23	5.23	5.45	0.03	0.04		27.4	3403	114		5.0	6.35	6.44
14-4-19-12W4	PanCanadian	Lower Mannville	971	Alderson	1.0133	36	10481	9676	5490	12	98	19	6.80	5.94	0.06	0.16		25.7	3266	0		2.0	6.14	6.96
11-34-19-13W4	PanCanadian	Lower Mannville	974	Alderson	1.0133	36	11103	9020	5568	17	89	19	9.90	4.34	0.05	0.23		25.7	3668	0		0.8	7.43	6.89
02/2-9-19-13W4	PanCanadian	Lower Mannville	979	Alderson	1.0133	36	10946	10350	6390	13	74	19	8.13	5.23	0.03	0.20		23.1	3394	140		8.2	6.35	6.96
12-9-19-13W4	PCC Energy	Lower Mannville	979	Alderson	1.0133	36	10825	10739	6860	13	109	28	9.52	7.58	0.03	0.16		21.8	4279	34		45.9	6.52	6.93
02/11-9-19-13W4	PanCanadian	Lower Mannville	982	Alderson	1.0133	36	10946	7357	5960	12	41	13	9.61	2.96	0.06	0.71		20.2	4720	0		0.4	6.34	7.02
14-9-19-13W4	PCC Energy	Lower Mannville	985	Alderson	1.0133	36	10873	10519	7138	19	98	24	10.48	5.99	0.02	0.21		19.0	4028	220		30.9	6.49	6.79
16-3-19-13W4/2	PanCanadian	Lower Mannville	981	Alderson	1.0133	36	10846	9447	6534	16	70	19	12.10	4.25	0.04	0.32		20.7	4102	0		0.1	6.28	6.88
10-9-19-13W4	PCC Energy	Lower Mannville	978	Alderson	1.0133	36	10783	10970	6730	13	75	22	14.90	5.31	0.05	0.16		21.8	3733	202		7.5	6.52	6.95
6-3-19-13W4	PanCanadian	Lower Mannville	981	Alderson	1.0133	36	10201	7466	6532	17	49	19	23.00	3.56	0.10	0.33		16.0	5660	142		33.1	6.34	6.9
8-23-19-22W4	Crystal Energy Inc.	Lower Mannville	1457	Long Coulee	1.0145	43	13679	7619	7768	108	347	102	6.42	27.00	0.16	0.46	0.09	24.4	7695	749		35.3	5.33	6.09
5-3-19-10W4	Renaissance Energy	Lower Mannville	1002	Alderson	1.0148	34	10319	6267	4920	29	63	25	1.10	4.95	0.02	0.29	0.00	42.4	3593	38	10	36.5	6.81	6.82
7-8-19-10W4	Regata Resources	Lower Mannville	982	Alderson	1.0148	34	10113	9299	5170	28	85	25	1.80	5.24	0.01	0.30	0.90	29.5	4292		4	37.6	6.96	6.81

Table 2.3. continued.

DLS Location	Operator	Pool	depth (m)	Field	Density	T	P (kPa)	HCO3	Na	Ca	K	Mg	Sr	Li	Mn	Fe	Ba	SiO2	Cl	SO4	Br	S	pH CO2	pH calcite
02/11-29-18-13W4	Chevron	Lower Mannville	1016	Bantry	1.0176	38	10700	7831	8271	39	119	64	7.60	6.94	0.07	0.58	0.00	33.8	8066	131	14	79.1	6.15	6.54
3-26-20-12W4	Chevron	Lower Mannville	1119	Princess	1.022	38	11200	8242	11380	70	107	70	30.30	5.35	0.07	0.85	16.80	21.6	13803	39.9		8.6	6.83	6.32
11-24-20-14W4	PanCanadian	Lower Mannville	1025	Bantry	1.0204	39	11228	2840	10310	132	78	95	54.30	4.31	0.06	0.55	0.00	23.1	15263	324	7	21.5	5.54	6.41
6-9-23-18W4	PanCanadian	Lower Mannville	1244	Countess	1.015	37	9845	2128	6944	182	38	68	48.00	2.16	0.11	0.65	2.30	29.5	12821	142	24	54.1	7.05	6.39
5-36-24-26W4	Canadian Occidental	Lower Mannville	2074	Crossfield	1.026	64	20580	4206	13627	704	290	164	66.50	10.90	4.37	0.14		39.4	19432			426.0	5.53	5.54
6-26-24-26W4	Canadian Occidental	Lower Mannville	2102	Crossfield	1.035	66	20580	402	17090	802	284	179	68.70	1.32	2.77	0.23		43.4	28290			706.0	4.96	6.21
11-36-24-26W4	Canadian Occidental	Lower Mannville	2100	Crossfield	1.06	66	17190	6240	32931	1572	910	361	150.00	21.00	1.24	0.64		91.0	52878	830		268.0	5.89	5.01
02/7-7-25-21W4	PanCanadian	Lower Mannville	880	Parfleah	1.015	50	10700	2861	6195	217	69	45		2.20	0.77	1.30	0.00	28.2	12999	321		0.0	6.58	6.17
7-26-25-26W4	Canadian Occidental	Lower Mannville	2105	Crossfield	1.06	66	16350	7065	33425	1574	905	388	143.00	21.20	1.28	0.68		86.0	53798	699		201.0	5.84	5.07
7-16-27-9W4	Gulf Canada	Lower Mannville	1003	Heathdale	1.016	32	9311	2488	6336	30	33	31	12.40	1.40	1.45	8.40	8.30	23.1	6250	49		0.2	7.12	6.03
12-10-27-20W4	APF	Lower Mannville	1395	Wayne-Rosedale	1.016	44	10200	3127	7380	41	43	19	31.00	1.70	0.22	1.05	39.70	22.0	10031			0.0	6.74	6.9
8-24-29-12W4	Cannat Resources	Lower Mannville	1072	Stanmore	1.01	41	9300	1148	6663	57	35	49	7.60	1.30	0.40	0.60	0.00	27.0	9297	825		0.1	5.9	7.1
15-1-6-5W4	Trimpn Energy	Sawtooth	1169	Manyberries	1.0024	40	11350	3395	1600	28	36	10	1.25	1.64	0.03	0.20	1.75	16.7	554	160		12.5	6.4	6.81
14-34-6-16W4	SAHH Resources	Sawtooth	975	24/5/83	1.003	32	8958	3444	1993	22	19	11	2.00	1.08	0.00	0.04	2.54	16.8	1224		18.9	11.2	6.12	6.91
14-13-6-17W4	Renaissance Energy	Sawtooth	963	Wrentham	1.002	33	10300	2313	1181	82	55	30	1.60	1.30	0.10	1.60	6.60	26.7	730	49		92.5	5.86	6.56
8-9-7-14W4	Mission Resources	Sawtooth	944	Chin Coulee	1.0024	31	9900	3161	1536	57	52	26	2.16	1.30	0.06	0.08	9.39	19.3	685	18	2	98.4	6.1	6.51
16-36-7-17W4/2	Mission Resources	Sawtooth	1019	Taber S	1.004	34	10200	2504	2255	65	66	49	4.54	2.40	0.06	0.21	9.18	35.9	2545	65	6	14.7	5.3	6.46
7-1-8-15W4	PanCanadian	Sawtooth	977	Chin Coulee	1.0024	32	10400	3450	1602	52	41	21	1.70	1.54	0.01	0.02		29.1	617	54		314.0	5.8	6.54
14-27-8-17W4/2	Renaissance Energy	Sawtooth	1007	Taber S	1.006	32	11558	3244	1860	63	46	28	19.66	1.97	0.00	0.07	15.31	27.0	1160			60.7	5.76	6.47
02/16-34-9-13W4	Renaissance Energy	Sawtooth	917	Bow Island	1.0042	34	10300	2844	1811	36	26	12	1.27	1.35	0.00	0.02	2.31	23.1	1036	28	3	115.5	5.98	6.76
02/3-34-10-15W4	Renaissance Energy	Sawtooth	979	Taber N	1.004	33	10100	2844	1619	34	49	24				1.10		13.0	1178	0	45	133.7	5.86	6.78
9-30-11-11W4	Startech	Sawtooth	925	Bow Island	1.004	34	9800	3888	2060	36	39	16	1.10	1.73	0.03	0.00	2.45	29.5	1246	40		73.3	6.06	6.66
2-17-11-18W4	Rangal Oil	Sawtooth	1100	Turin	1.015	34	11500	7022	4585	101	163	54	3.87	6.80	0.03	0.11	1.64	22.0	4030	142	10	88.4	5.39	6.12
9-12-11-19W4	NCE PetroAlund	Sawtooth	1103	Turin	1.01	35	12000	8000	5564	135	184	57	6.76	6.80	1.50	0.19	2.44	18.0	4649	70	11	75.6	5.73	5.96
02/8-36-12-13W4	Norcen Energy	Sawtooth	971	Hays	1.005	31	10100	4581	3175	39	75	20		2.80	0.00	7.20	4.40	24.4	2011	119		16.0	5.6	6.63
7-9-16-20W4	Rosza Petroleum	Sawtooth	1286	Long Coulee	1.027	41	12800	6326	13272	103	166	110	29.10	10.16	0.09	0.38	0.05	19.3	16785	239		9.3	5.56	6.27
12-23-1-18W4	Texas Resources	Medicine Hat	842	Coults	1.004	38	6593	3039	1253	74	37	21	1.88	1.93	0.02	0.35	2.76	18.0	482	80		58.9	6.34	6.38
1-6-1-19W4	Glencoe Resources	Rundle	1091	Reagan	1.007	38	7600	3566	1697	99	70	53	19.50	4.66	0.02	0.25	1.39	16.5	841	66		58.9	5.72	6.25
4-27-6-17W4	Renaissance Energy	Turner Valley	1009	Taber S	1.006	32	10444	2964	1460	71	64	27	23.60	1.96	0.04	0.01	0.47	12.8	785	13		84.5	5.75	6.42
03/1-8-10-17W4	Renaissance Energy	Livingstone	1091	Taber N	1.006	32	11300	3443	2220	66	51	22	6.90	2.92	0.04	0.25	15.80	15.1	1428	16.6	5	49.3	5.15	6.48
02/6-15-10-15W4	Acanthus Resources	Livingstone	1086	Turin	1.013	33	11091	6749	5000	118	119	48	11.80	7.63	0.01	0.20	4.69	18.0	3975	185	9	78.8	5.53	6.07
7-36-12-26W4	Crestar Energy	Rundle	2059	Carseholm	1.017	52	19429	6160	7242	187	295	59	5.00	13.00	0.00	0.20	0.00	24.8	8074	1107		123.9	5.44	5.9
03/1-33-13-14W4/2	Startech Energy	Livingstone	957	Hays	1.007	33	11175	4871	3162	42	59	15	3.88	3.27	0.03	0.19	0.66	21.6	2078	29	6	10.4	5.95	6.01
13-27-19-26W4	Crestar Energy	Medicine Hat			1.045	55	19778	1194	19470	2882	542	951	1.00	16.10	0.00	13.00	0.52	20.5	38254	1451	122	34.4	4.51	5.54
5-36-14-10W4	Renata Resources	Pekisko	929	Alderson	1.008	31	10164	5223	4591	30	61	15	9.41	3.85	0.05	0.18	0.81	15.4	3580	105		21.7	6.95	6.74
8-9-15-16W4	Mesa Petroleum	Livingstone	1011	Enchant	1.015	31	10561	5103	9084	26	204	59	15.40	7.88	0.23	0.14	1.76	12.8	10045	136	17	0.6	5.82	6.92
11-21-16-12W4	Renata Resources	Sunburst Pekisko	987	Bantry	1.014	52	10750	7087	6336	10	55	15	19.10	4.37	0.06	0.12	3.77	16.7	5914	159	7	22.5	5.94	7.18
10-19-16-12W4	Renata Resources	Pekisko	957	Bantry	1.014	52	10750	7605	7534	12	50	30	20.59	3.89	0.03	0.26	11.94	16.0	6351	0		28.7	6.95	7.07
02/10-18-16-22W4/2	Northstar Energy	Rundle	1481	Long Coulee	1.016	40	14100	7352	9150	117	326	71	3.61	19.70	0.07	0.05	0.12	41.9	9033	1237	47	37.3	5.21	6.1
4-6-19-10W4	Renaissance Energy	Pekisko	976	Princess	1.017	40	10600	3350	7950	41	66	61	31.10	3.61	0.06	0.79	14.26	11.6	11392	25	31	3.9	6.69	6.82
7-3-19-14W4	Renaissance Energy	Pekisko	1037	Brooks	1.023	40	11200	4849	10780	56	146	77	47.90	6.77	0.06	0.29	6.90	23.1	14500	72	25	28.4	6.09	6.57
12-21-20-9W4/2	Renaissance Energy	Pekisko	1078	Suffield	1.016	34	10604	6503	6522	31	55	15	11.90	3.92	0.03	0.20	0.76	16.7	5527		7	1.2	6.29	6.71
16-9-20-27W4	Compton Petroleum	Rundle	2058	Gladys	1.052	64.5	17824	1025	27750	1639	429	429		13.40	0.00	1.50	0.00	39.1	43281	575		0.5	5.31	5.81
7-33-23-26W4	Beaupaw Petroleum	Rundle	2111	Crossfield	1.063	73	19409	773	30250	1358	772	391		25.80	0.00	1.00	5.00	32.1	51182			39.2	4.73	6.02
10-12-23-14W4	Anderson Oil and Gas	Pekisko	1017	Mjtzhrin	1.02	33	9800	1498	6540	172	39	65	53.10	1.80	0.15	9.92	7.90	18.0	9711	3	25	0.0	7.42	6.35
6-22-30-24W4	Tarrason Oil and Gas	Pekisko	1664	Twinig	1.031	52	11400	840	17360	358	139	136	9.80	4.60		0.50		29.5	24779	478		24.8	6.01	6.51
6-16-30-24W4	Startech Energy	Pekisko	1667	Swalwell	1.031	52	11415	602	17430	901	126	176	145.00	5.30	0.10	0.50	5.50	23.1	30211			0.1	5.88	6.51
8-31-12-19W4	Norcen Energy	Arcs	1357	Enchant	1.03	38	12353	5257	10750	802	1418	221	1.28	22.02		3.50		27.6	9802	9100	10.7		5.07	5.51
16-20-12-19W4/2	Rosza Petroleum	Arcs	1392	Enchant	1.05	39	13000	3509	23010	1602	847	394	30.53	13.80	0.02	0.45	0.00	24.6	30699	8894	15	26.1	4.92	5.58
02/16-30-13-15W4	Norcen Energy	Arcs	1370	Enchant	1.024	49	12600	3151	10540	1012	636	312	24.77	13.80	0.00	0.30	0.00	22.2	14221	6960	25	38.0	5.01	5.57
14-32-13-15W4	Gulf Canada	Arcs	1403	Enchant	1.025	50	12400	4732	11900	956	1068	294	23.90	33.80	0.13	0.41	1.23	18.7	13688	7896	91	32.0	5.35	5.45
8-31-13-18W4	Eagle Resources	Nisku	1388	Enchant	1.033	50	12400	5039	15410	1388	1154	488	35.10	38.10	0.12	0.45	1.47	21.1	19214	8660	110	24.0	5.33	5.28
10-4-14-16W4	Norcen	Nisku	1365	Enchant	1.022	50	11647	3929	7087	875	1095	275	20.10	1.54	0.06	0.02	0.99	8.6	7255	5559	29	243.0	5	5.51
14-19-15-16W4	Norcen	Arcs	1360	Enchant	1.017	50	12085	4175	7965	760	760	237	16.10	15.20	0.15	0.25	0.86	18.4	8666	7939	64	60.0	5.19	5.58
02/9-13-20-20W4	Tarrason Oil and Gas	Nisku	1754	Jumpbush	1.017	66	14745	1502	6250	1370	741	566	38.70	12.30	0.05	0.96	0.00	47.5	11612	3162		93.6	4.39	5.66
3-16-22-16W4	PanCanadian	Nisku	1435	Countess	1.0282	38	12500	1340	10860	1405	534	394	47.80	9.48	0.11	0.61	0.00	19.3	14501	5100		70.5	4.53	5.62
02/6-13-26-21W4	PanCanadian	Nisku	1746	Wayne-Rosedale	1.023	62	14292	1459	9084	1447	955	328	3.72	10.40		1.20		30.8	16075	2077		61.4	4.55	5.67
6-29-29-19W4	Renaissance	Nisku	1800	Drumheller	1.0278	54	13000	1563	8127	1373	1007	419		12.10	0.17	1.30	0.50	19.5	17536	2310		66.0	4.65	5.69
9-29-29-20W4	Beaupaw Petroleum	Nisku	1845	Drumheller	1.043	59	13100	1310	15840	3870	1738	882		19.20	0.27	36.00	1.20	28.2	34606	1634		61.9	4.61	5.39
6-11-29-24W4	Chauvco	Nisku	1974	Swalwell	1.1	71	16500	614	36000	12160	4150	2150	466.00	47.40	0.32	0.66	4.99	30.9	88462	645	652	60.0	4.25	5.2
10-15-29-24W4	Chauvco	Nisku	1966.5	Swalwell	1.104	71	17981	621	38440	13670	4460	2340	548.00	48.70	0.31	0.63	5.48	30.9	93205	598	712	116.0	4.28	5.29
10-14-29-24W4	Saron Petroleum Inc.	Nisku	1913.4	Swalwell	1.15	71	16354	298	59280	23600	6525	3760	975.00	57.10	0.75	1.63	6.32	19.9	151565	120	1126	1361.0	4.41	5.61
4-1-29-24W4	Encal Energy	Nisku	2009	Swalwell	1.1	71	15879	898	33800	10900	4261	2096		37.30	0.00	4.30	0.00	44.7	85396	188		189.0	4.32	5.22
9-5-29-25W4	Rigel Oil and GAs	Wabamun	2180	Imicana	1.065	83	23215	808	32800	948	1478	1319	3.10	28.80		3.00		98.8	54317	3974		180.2	4.54	6.17

Table 2.4. Stable isotope composition of the sampled waters and acid gas partial pressures.

DLS Location	Formation	$\delta^{18}O‰$ in H_2O V-SMOW	$\delta D‰$ in H_2O V-SMOW	$\delta^{34}S‰$ in SO_4^{2-} CDT	$\delta^{34}S‰$ in HS^- CDT	$\delta^{13}C‰$ in HCO_3^- PDB	PH_2S kPa	PCO_2 kPa
1-36-14-11W4	Viking	-6.8	-79			-1.9	0	2
9-29-14-18W4	Bow Island	-4.7	-78			0.1	0	2
9-21-15-11W4	Viking	-6.6	-77			4.5	0	2
1-4-16-13W4	Viking	-6.1	-77			8.0	0	13
1-2-16-15W4	Viking	-6.0	-80			-4.2	0	0
4-30-16-17W4	Bow Island	-4.6	-77			9.8	0	18
14-24-16-18W4	Viking	-4.7	-76			-2.6	0	17
F1/10-8-17-14W4	Viking	-5.1	-81	31.6	4.8	6.0	0	7
02/10-8-17-14W4	Viking	-5.5	-79			8.7	0	7
11-19-24-15W4	Viking	-6.7	-78			0.6	0	0
11-29-28-17W4/2	Viking	-7.5	-85			-2.3	0	0
								0
1-23-8-17W4	Glauconitic	-15.1	-122		23.1	4.0	0	111
14-2-10-13W4	Glauconitic	-14.1	-122		15.6	7.9	0	107
10-28-12-5w4	Glauconitic	-9.6	-94			16.4	0	245
13-33-14-7W4	Glauconitic	-11.9	-108		24.4	11.2	0	176
02/11-33-14-17W4	Upper Mannville	-5.3	-87	27.2	19.4	-2.1	0	628
10-21-15-15W4	Upper Mannville	-8.2	-96		22.1	-1.6	0	447
14-20-15-15W4	Upper Mannville	-5.9	-84			-2.1	0	128
11-20-15-15W4	Upper Mannville	-4.7	-81	30.6	8.5	-3.3	0	56
11-8-15-18W4	Glauconitic	-4.5	-71			1.9	0	125
04/16-15-16-12W4	Upper Mannville	-9.3	-92	33.2	11.8	0.0	0	2
6-30-16-14W4	Glauconitic	-5.2	-77	27.8	23.3	1.3	8	264
7-5-17-14W4	Glauconitic	-5.6	-84	25.7		-0.9	0	253
15-6-17-14W4	Glauconitic	-5.1	-78	25.6	14.4	-1.5	21	354
02/14-26-17-15W4	Upper Mannville	-4.2	-81	11.5	19.5	-1.5	0	345
02/16-5-20-19W4	Upper Mannville	-4.4	-80			-0.9	0	113
10-28-20-20W4	Upper Mannville	-3.5	-74	28.7		-4.1	0	12
7-2-20-21W4	Glauconitic	-4.6	-79	21.4		-5.8	0	137
14-24-20-21W4	Upper Mannville	-4.0	-77			-10.6	0	125
1-21-21-20W4	Glauconitic	-4.0	-75	26.3		-2.3	0	351
6-22-25-23W4	Upper Mannville	-4.7	-79	21.8		-4.0	0	121
5-16-26-12W4	Mannville	-7.4	-84			9.8	0	11
16-21-29-11W4	Upper Mannville	-8.4	-83	26.1		-6.1	0	3
02/11-6-29-20W4	Glauconitic	-6.5	-82			6.0	0	19
02/6-21-29-20W4	Upper Mannville	-5.8	-78	35.8		-10.6	0	28
16-20-1-8W4	Mannville	-9.8	-84	31.4		16.4	0	74
8-5-1-16W4	Cutbank	-16.4	-128			14.1	1	145
9-12-3-17W4	Lower Mannville	-15.7	-116			20.4	0	68
4-7-5-4W4	Sunburst	-10.0	-86			21.0	0	114
02/13-11-6-17W4	Lower Mannville	-15.2	-121			2.5	0	12
02/6-36-9-8W4	Lower Mannville	-8.3	-94	20.7		4.0	0	103
16-16-9-17W4	Taber	-15.3	-119			1.1	0	32
13-34-10-13W4	Lower Mannville	-14.3	-121			8.2	0	558
15-14-10-19W4/2	Lower Mannville	-9.9	-102	18.7	20.0	0.8	10	741
9-1-12-17W4	Lower Mannville	-13.1	-111		23.2	1.7	13	593
02/14-3-12-19W4	Mannville	-5.8	-69	29.3	16.9	0.0	11	1015
7-16-13-19W4	Mannville	-6.8	-90			-1.4	17	1678
4-34-14-10W4	Lower Mannville	-7.6	-91	42.7	32.5	2.0	8	320
14-30-14-10W4	Lower Mannville	-6.7	-81	38.9	37.4	6.6	8	315
14-34-14-15W4	Lower Mannville	-9.1	-92	29.8		-1.3	0	336
12-18-14-18W4	Lower Mannville	-9.7	-97	23.9		-1.3	29	1487
13-19-15-10W4	Lower Mannville	-7.9	-88			9.9	0	127
4-17-15-10W4	Lower Mannville	-5.7	-86		168.8	7.9	8	322
5-03-15-11W4	Lower Mannville	-9.0	-98		62.1	7.2	0	99
10-3-15-11W4	Lower Mannville	-8.6	-97	29.5	19.8	4.5	0	93
8-14-15-11W4	Lower Mannville	-7.1	-86		68.3	10.4	0	164
12-24-15-11W4	Lower Mannville	-8.2	-94		149.2	8.8	0	257
13-11-15-11W4	Lower Mannville	-8.0	-93		63.0	11.5	0	99
5-05-16-11W4	Lower Mannville	-10.3	-100		154.2	4.9	0	733
14-06-16-11W4	Lower Mannville	-9.9	-96			5.5	0	527
2-9-16-13W4	Lower Mannville	-7.9	-92	28.7	12.8	-1.8	0	360
14-4-16-13W4	Lower Mannville	-8.0	-93	26.0		-1.5	0	524
11-34-15-13W4	Lower Mannville	-7.5	-90			-2.0	0	22
02/2-9-16-13W4	Lower Mannville	-8.0	-90			-1.8	0	371
12-9-16-13W4	Lower Mannville	-6.4	-84			-1.8	2	243
02/11-3-16-13W4	Lower Mannville	-7.1	-83				11	223

Table 2.4. Continued.

DLS Location	Formation	$\delta^{18}O‰$ in H_2O V-SMOW	$\delta D‰$ in H_2O V-SMOW	$\delta^{34}S‰$ in SO_4^{2-} CDT	$\delta^{34}S‰$ in HS^- CDT	$\delta^{13}C‰$ in HCO_3^- PDB	PH_2S kPa	PCO_2 kPa
14-9-16-13W4	Lower Mannville	-7.0	-90			-2.0	2	249
15-3-16-13W4/2	Lower Mannville	-7.7	-86	34.1		-2.7	0	368
10-9-16-13W4	Lower Mannville	-7.2	-90			-2.0	2	246
6-3-16-13W4	Lower Mannville	-6.6	-86			-3.7	0	0
6-23-16-22W4	Sunburst	-4.6	-83	27.7		1.5	6	2432
5-3-18-10W4	Lower Mannville	-7.4	-90		27.6	1.9	0	104
7-9-18-10W4	Lower Mannville	-7.5	-85		29.1	1.9	0	71
02/11-29-18-13W4	Mannville	-4.2	-82	29.9	24.2	0.5	17	392
3-26-20-12W4	Basal Mannville	-4.1	-79		32.5	14.4	0	82
11-24-20-14W4	Mannville	-5.1	-81	38.9	3.4	0.4	0	584
6-9-23-18W4	Ostracod	-5.3	-67	52.7	7.8	-9.4	0	0
5-36-24-28W4	Basal Quartz	-1.7	-59	21.3	18.9	2.3	412	1033
6-26-24-28W4	Basal Quartz	-1.8	-56	21.1	20.1	3.5	412	1033
11-35-24-28W4	Basal Quartz	-1.7	-48	25.8	24.2	-3.0	177	835
02/7-7-25-21W4	Lower Mannville	-4.5	-74	23.0		-4.5	0	59
7-26-25-28W4	Basal Quartz	-1.9	-49	27.1		5.4	90	772
7-16-27-9W4	Lower Mannville	-8.0	-86			15.9	0	13
12-10-27-20W4	Basal Quartz	-5.3	-78	25.1		12.9	0	43
8-24-29-12W4	Lower Mannville	-8.1	-83	62.7		-12.2	0	112
15-1-5-5W4	Sawtooth	-14.6	-115			2.6	0	127
14-34-6-15W4	Sawtooth	-13.9	-115		23.1	1.6	0	219
14-13-6-17W4	Sawtooth	-16.5	-127		23.5	2.0	77	276
5-9-7-14W4	Sawtooth	-15.2	-121		23.6	5.3	0	199
16-36-7-17W4/2	Sawtooth	-15.3	-121		22.2	3.1	10	998
7-1-8-15W4	Sawtooth	-15.1	-130	24.6	22.9	3.8	270	461
14-27-8-17W4/2	Sawtooth	-14.9	-125			6.1	0	462
02/16-34-9-13W4	Sawtooth	-15.4	-117		23.9	6.2	0	250
02/3-34-10-15W4	Sawtooth	-15.4	-122		24.1	3.4	0	316
5-30-11-11W4	Sawtooth	-13.8	-116		23.5	8.4	0	249
2-17-11-18W4	Sawtooth	-9.4	-99		20.3	-0.4	86	2067
9-12-11-19W4	Sawtooth	-8.6	-97	35.6	18.5	0.1	20	1070
02/8-36-12-15W4	Sawtooth	-13.7	-112		25.2	5.3	56	901
7-9-16-20W4	Sawtooth	-2.2	-78	27.3		0.0	0	1165
12-23-1-16W4	Mississippian	-16.6	-124			2.2	0	1
1-6-1-19W4	Rundle	-14.8	-119	23.3	24.1	1.1	8	623
4-27-8-17W4	Turner Valley	-14.7	-121		21.5	4.1	0	414
03/1-5-10-17W4	Livingstone	-14.3	-121			7.5	0	1806
02/8-15-10-19W4	Livingstone	-9.7	-102			-0.9	333	1287
7-36-12-26W4	Rundle	-5.3	-89	28.4	18.3	1.1	159	1822
03/1-33-13-14W4/2	Livingstone	-11.5	-106			8.3	0	383
13-27-13-26w4	Mississippian	-2.5	-80	24.1	21.8	2.0	6	2096
5-36-14-10W4	Pekisko	-8.3	-93			-2.3	0	42
8-3-15-16W4	Livingstone	-6.8	-84			0.0	12	554
11-21-15-12W4	Pekisko	-7.3	-89			-2.2	0	559
16-19-16-12W4	Pekisko	-5.9	-83			-3.0	0	63
02/10-12-16-22W4/2	Rundle	-5.4	-81	30.2		0.5	3	3195
4-6-19-10W4	Pekisko	-3.8	-81		32.0	2.2	0	50
7-3-19-14W4	Pekisko	-3.6	-78			2.6	0	277
12-21-20-8W4/2	Pekisko	-7.7	-80			7.1	0	252
16-9-20-27W4	Rundle	-0.6	-80	24.4		-2.0	2	346
7-33-23-28W4	Rundle	0.6	-70	22.2	16.8	1.2	163	1108
10-12-23-14W4	Pekisko	-6.9	-80			-8.5	0	4
8-22-30-24w4	Pekisko	-4.0	-80	39.2	5.1	-2.1	0	64
8-18-30-24W4	Pekisko	-3.5	-82			2.4	0	91
8-31-12-15W4	Arcs	-6.6	-79	25.3		-3.6	0	3026
16-20-12-16W4/2	Arcs	-2.1	-57	26.3	11.4	-2.1	0	2600
02/16-30-13-15W4	Arcs	-8.7	-92	23.7	16.5	-1.4	0	2281
14-32-13-16W4	Arcs	-8.1	-88	25.0	16.1	-2.9	144	1665
8-31-13-16W4	Nisku	-6.6	-76	26.0	16.0	-1.9	144	1665
16-4-14-16W4	Nisku	-9.3	-99	27.7	23.5	-2.4	34	3155
14-19-15-16W4	Arcs	-9.6	-93	24.7	12.5	-8.3	97	2127
02/9-13-20-20W4	Nisku	-12.3	-107	31.8	11.1	-4.7	221	5125
3-18-22-16W4	Nisku	-14.4	-121			-7.8	0	2500
02/6-13-28-21W4	Nisku	-10.7	-104	24.3	12.6	-4.1	653	3283
6-29-29-19W4	Nisku	-11.3	-104	25.1	11.0	-4.4	202	1712
9-26-29-20W4	Nisku	-8.8	-95	25.3	13.5	-3.4	145	1230
6-11-29-24W4	Nisku	0.9	-66	23.3	16.4		249	1937
10-15-29-24W4	Nisku	1.5	-65	23.5	18.4	-9.2	241	1268
10-14-29-24W4	Nisku	2.5	-56	22.7	15.0	-15.9	1904	334
4-1-29-24W4	Nisku	0.5	-94	24.7		-2.2	953	1923
9-5-29-26W4	Wabamun	3.7	-57	25.9	23.5	-6.1	0	0

cations and anions on ternary diagrams and by combining the two on a quadrilateral diagram. Piper plots provide a visual method of classifying water into types based on the dominant ions (for example Na-Cl or Na-HCO_3). The Piper plot can provide the ability to determine if a series of waters are mixtures of end-members. A two end-member mixture results in a straight line on the diagram although straight lines are not unequivocal proof that mixing is the controlling process. The following describe each series of waters with some of the distinctions between waters of a particular unit being made partially on the basis of location.

The AEUB database waters from the Devonian Nisku/Arcs Formations have total dissolved solid (TDS) content that varies from 8,000 to 242,000 mg/l. Compositions range from Na-Cl to Na-SO_4 (up to SO_4 = 85 % anions meq/l) dominated. The Na-SO_4 waters have higher HCO_3 content with increasing SO_4 (**Figure 2.3**). The highest TDS waters are of the Na-Cl type and have an increasing Ca and Mg content that correlates with Cl. There appear to be two clusters of data for the Devonian aquifer:

1. High Cl, plotting in a linear trend in all three diagrams.
2. Moderate to high SO_4 and HCO_3, plotting in linear trends in the ternary diagrams but scattered in the quadrilateral diagram.

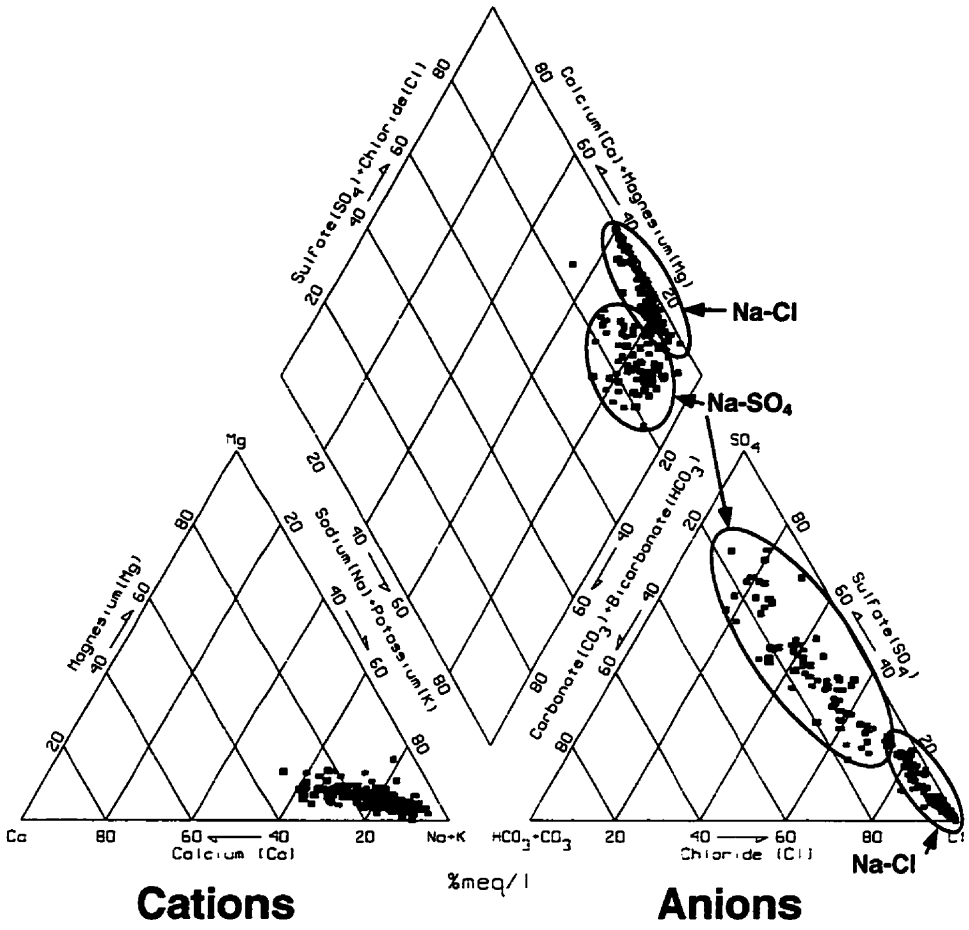

Figure 2.3. Nisku/Arcs aquifer water Piper plot. The two different groups, Na-Cl and Na-SO_4 are highlighted.

In distinct contrast to the Nisku/Arcs aquifer is the carbonate-hosted Mississippian aquifer (**Figure 2.4**). TDS range from 4,000 to 104,000 mg/l. The dominant water types are Na-Cl, and Na-HCO_3-Cl (HCO_3 > 10% anions). SO_4 contents do not exceed 25% (meq/l) and display little correlation with other cations or anions. Like the Nisku/Arcs hosted waters, high TDS correlates with Na-Cl type water and increasing Ca and Mg. Three clusters are differentiated for the Mississippian hosted waters:

1. High Cl, plotting as a cluster in the anion ternary diagram and as a linear trend in the cation ternary and in the quadrilateral diagram.
2. Na-HCO_3-Cl type waters with variable Ca, Mg, and SO_4 and plotting over a broad range of HCO_3 compositions.
3. Na-Cl waters that cluster in the region of chloride and sulfate (80:20). This grouping is made partially based on the map location of these data (see next section).

TDS values of the Jurassic Sawtooth aquifer waters range from 4,600 to 34,000 mg/l. The waters are predominately of the Na-HCO_3-Cl type similar to group 2 of the Mississippian aquifer (**Figure 2.5**). The more chloride-rich waters have the highest TDS and contain higher sulfate content. Two distinct groupings are recognized:

1. Na-HCO_3-Cl waters with relatively higher Cl and SO_4 content.
2. Na-HCO_3-Cl waters with variable Ca, and Mg.

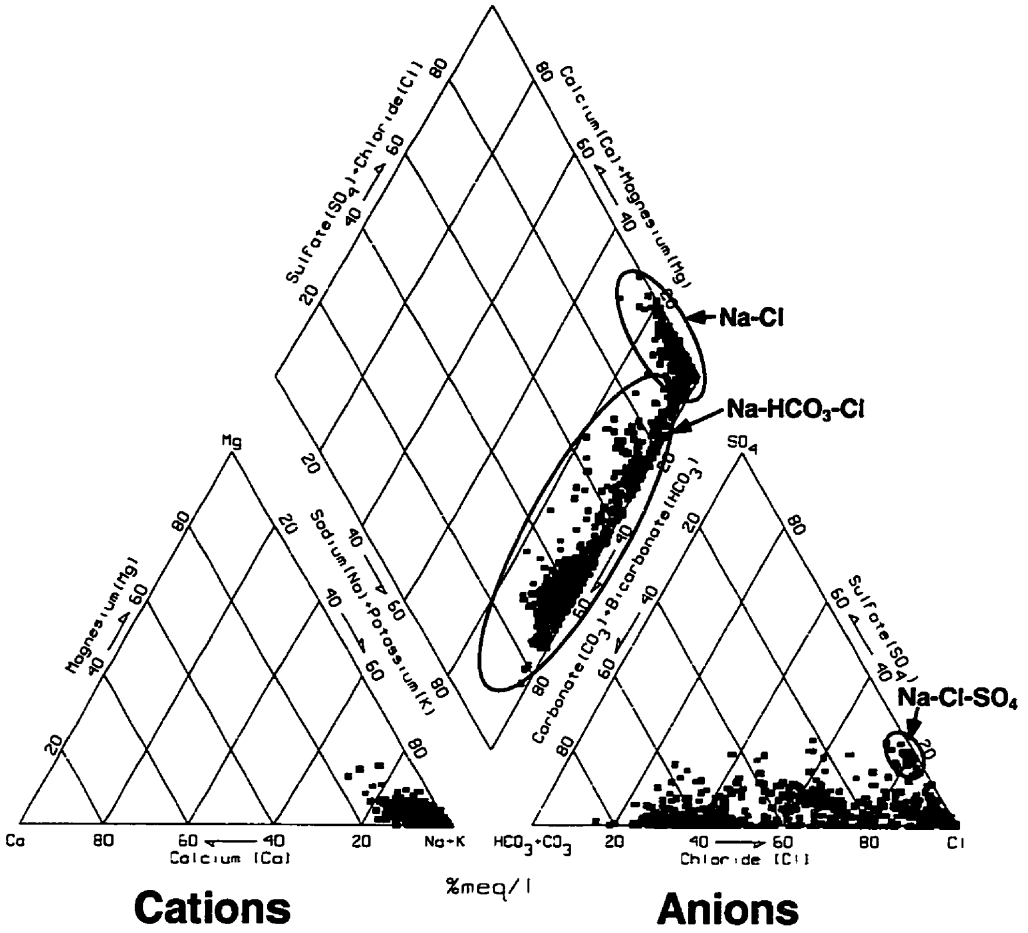

Figure 2.4. Mississippian aquifer water Piper plot. The three different groups, Na-Cl, Na-HCO_3-Cl and Na-Cl-SO_4 are highlighted.

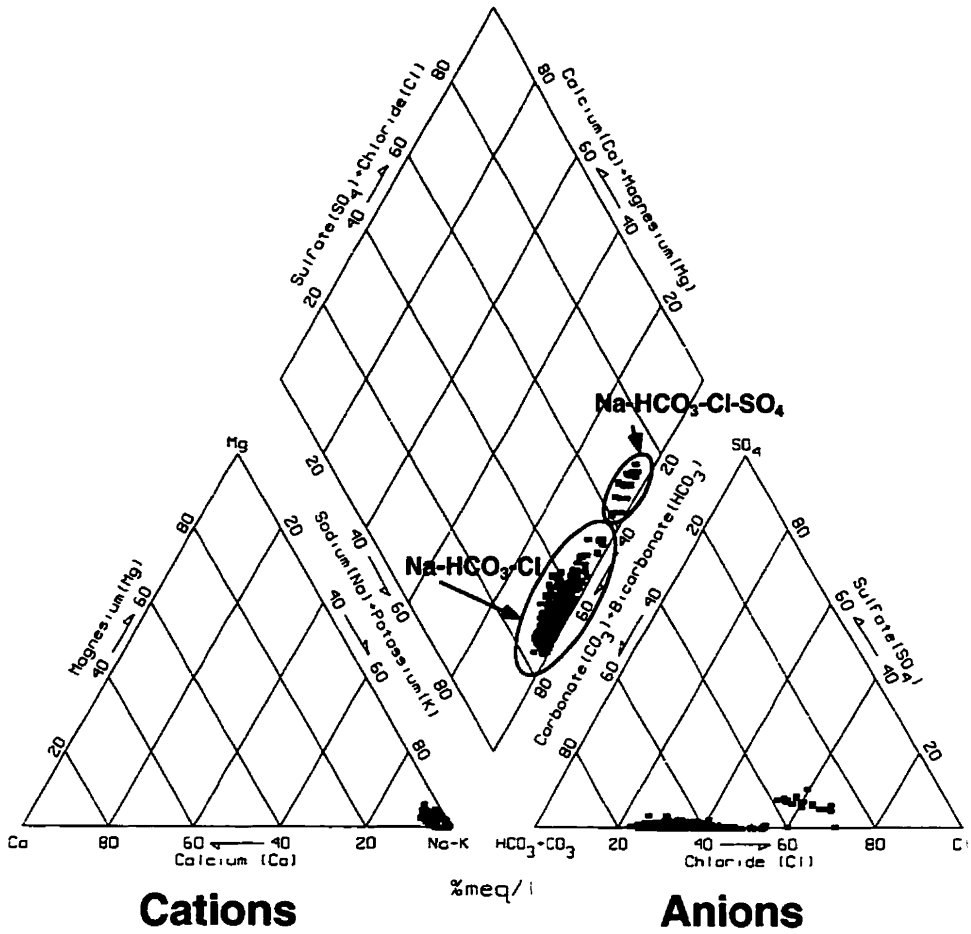

Figure 2.5. Sawtooth aquifer water Piper plot. The two different groups, Na-HCO_3-Cl, Na-HCO_3-Cl-SO_4 are highlighted.

The Lower Mannville aquifer waters plot in a very similar manner to those of the Mississippian (**Figure 2.6**). TDS ranges from 4,000 to 91,000 mg/l. The Na-Cl waters have the highest TDS and display increasing Ca and Mg content with increasing Cl. The three clusters of data defined for the Mississippian aquifer waters are also observed in the Lower Mannville aquifer, although the high sulfate group is less apparent on the Piper diagram.

The Upper Mannville aquifer water compositions are also very similar to the Mississippian and the Lower Mannville (**Figure 2.7**). The TDS contents range from 3,400 to 61,000 mg/l. Observations made for the Mississippian and Lower Mannville aquifers apply equally to the Upper Mannville although, like the Lower Mannville, the higher sulfate waters are not as well separated on this diagram compared to the waters in Mississippian strata.

Waters sampled from the Viking/Bow Island aquifer have considerably different compositional variations than those of the underlying units (**Figure 2.8**). TDS contents range from 3,500 to 30,000 mg/l. The waters are dominated by Na-Cl and Na-Cl-HCO_3. The higher TDS waters correspond to the highest Cl content waters, which also display the highest Ca and Mg. The Viking/Bow Island aquifer waters can be divided into two groups:

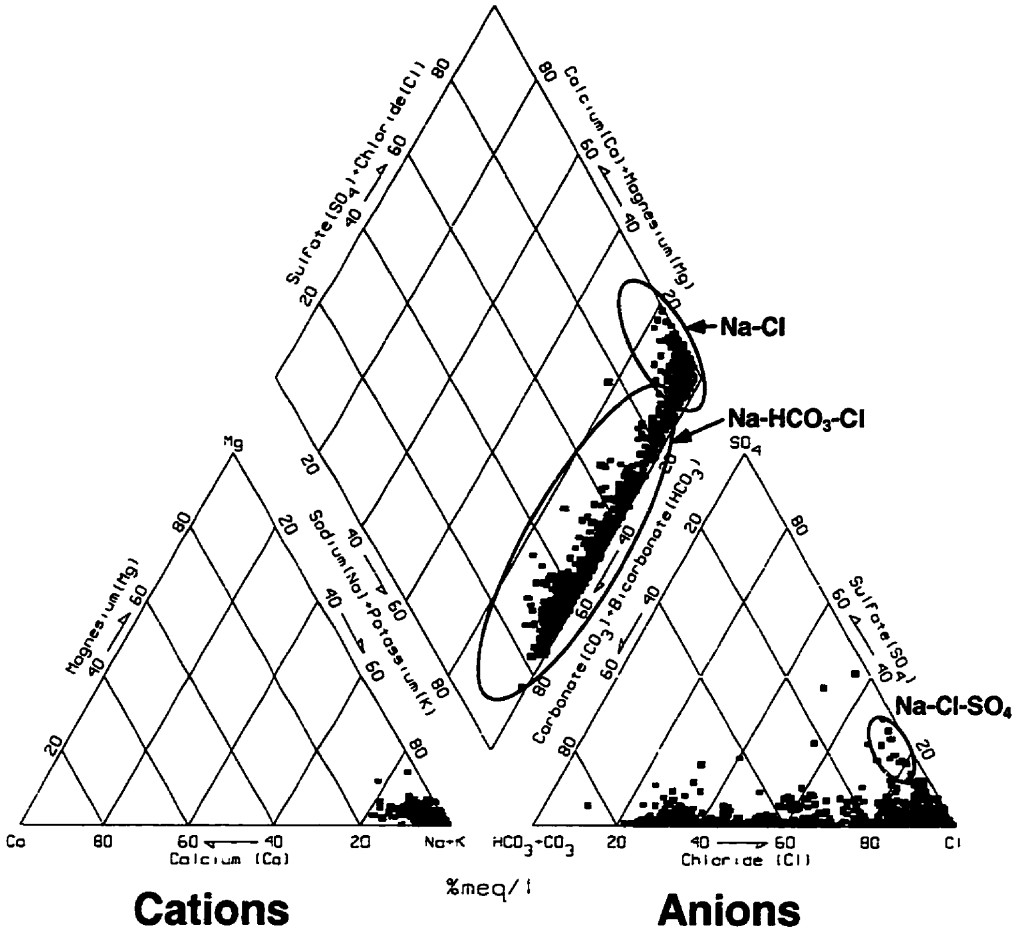

Figure 2.6. Lower Mannville aquifer water Piper plot. The three different groups, Na-Cl, Na-HCO_3-Cl and Na-Cl-SO_4 are highlighted.

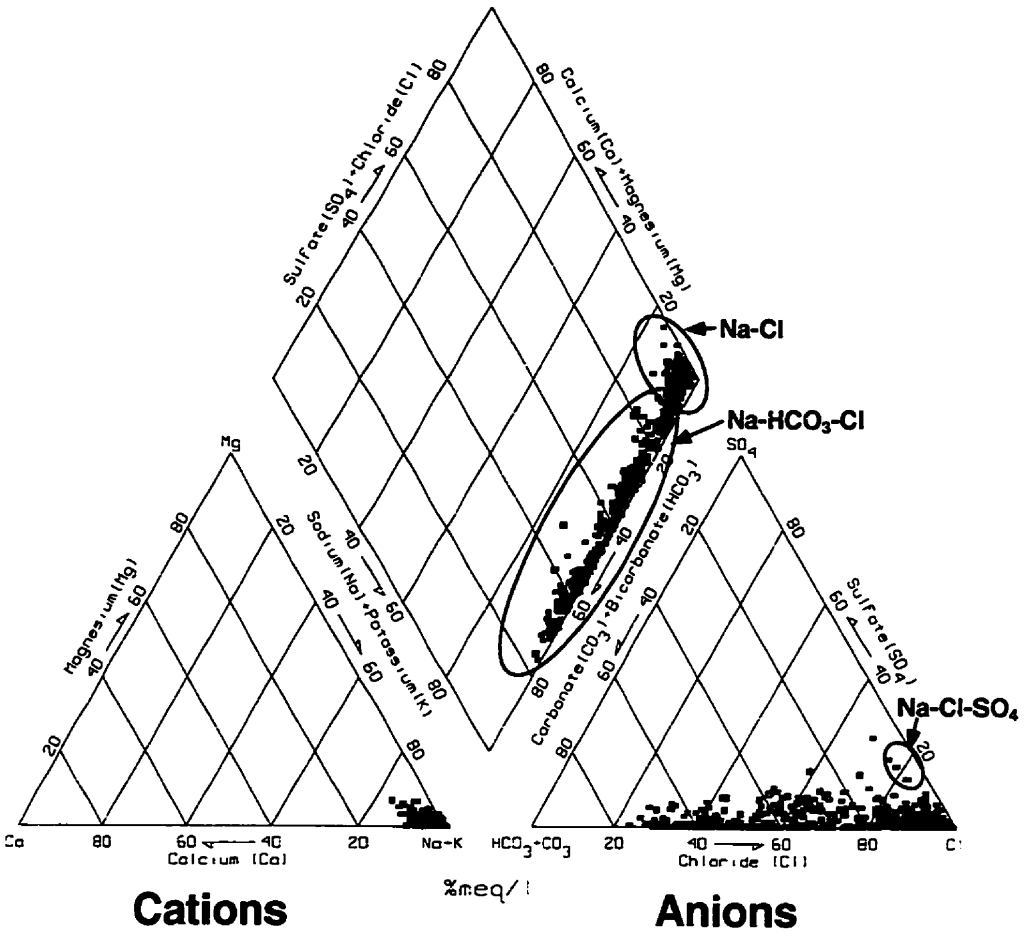

Figure 2.7. Upper Mannville aquifer water Piper plot. The three different groups, Na-Cl, Na-HCO_3-Cl and Na-Cl-SO_4 are highlighted.

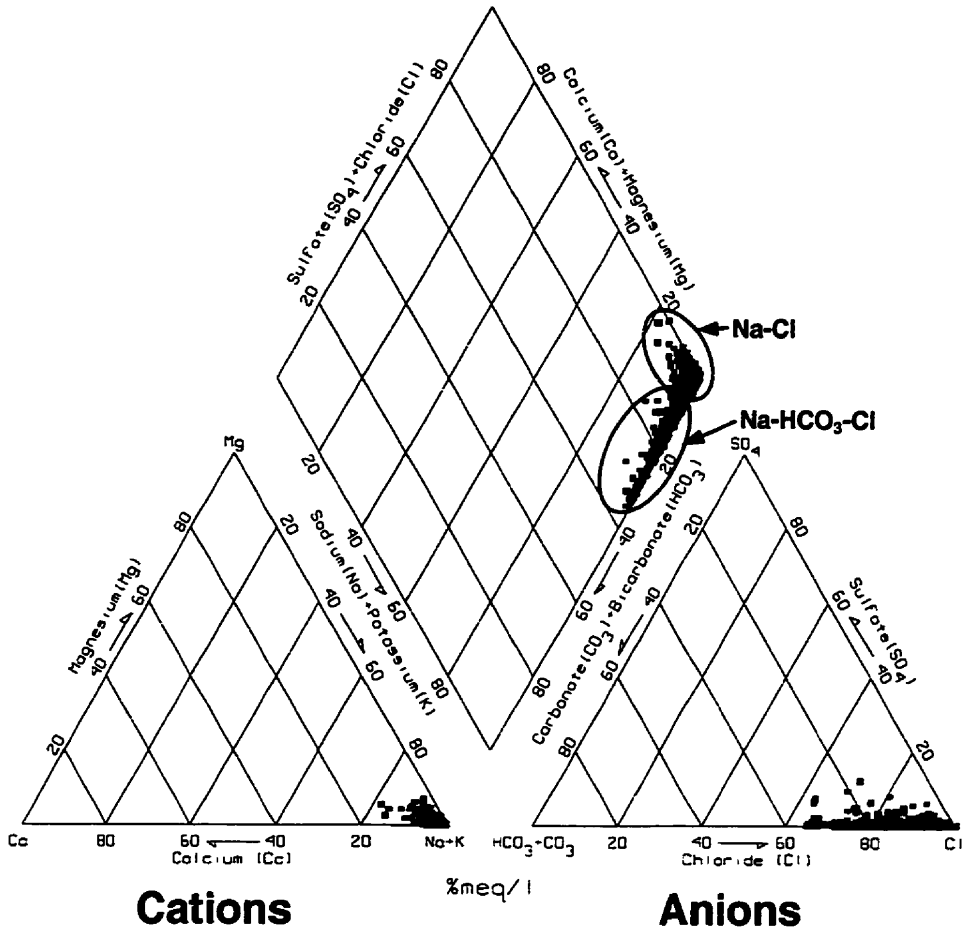

Figure 2.8. Viking/Bow Island aquifer water Piper plot. The two different groups, Na-Cl and Na-HCO_3-Cl are highlighted.

1. Na-Cl waters plotting as a cluster on the anion ternary diagram and as linear trends on the cation ternary and quadrilateral diagram.
2. Na-Cl-HCO_3 waters plotting as linear trends on all three diagrams.

Regional variations in chemical composition

Devonian Nisku/Arcs Aquifer

The distribution of Cl, HCO_3, and SO_4 for the Nisku/Arcs aquifer is illustrated in **Figure 2.9, 2.10 and 2.11**. Chloride concentration increases from 1,150 mg/l in the south, to in excess of 149,000 mg/l in the more deeply buried western portion of the study area. A second Cl low occurs in the northeast with chloride content at <15,000 mg/l. East of approximately 112.5°W, values do not exceed 25,000 mg/l and there is a relatively shallow concentration gradient. In comparison, the concentration gradient in regions of Cl contents greater than 25,000 mg/l is quite steep.

Concentration of bicarbonate ranges from 161 mg/l to greater than 6,300 mg/l. The highs occur in the central region with lows in the southeast, north and west. Lows in the west correspond to high Cl concentrations.

Sulfate concentration ranges from 152 mg/l to 13,300 mg/l. Highs generally correspond to those of bicarbonate and lows correspond to high Cl.

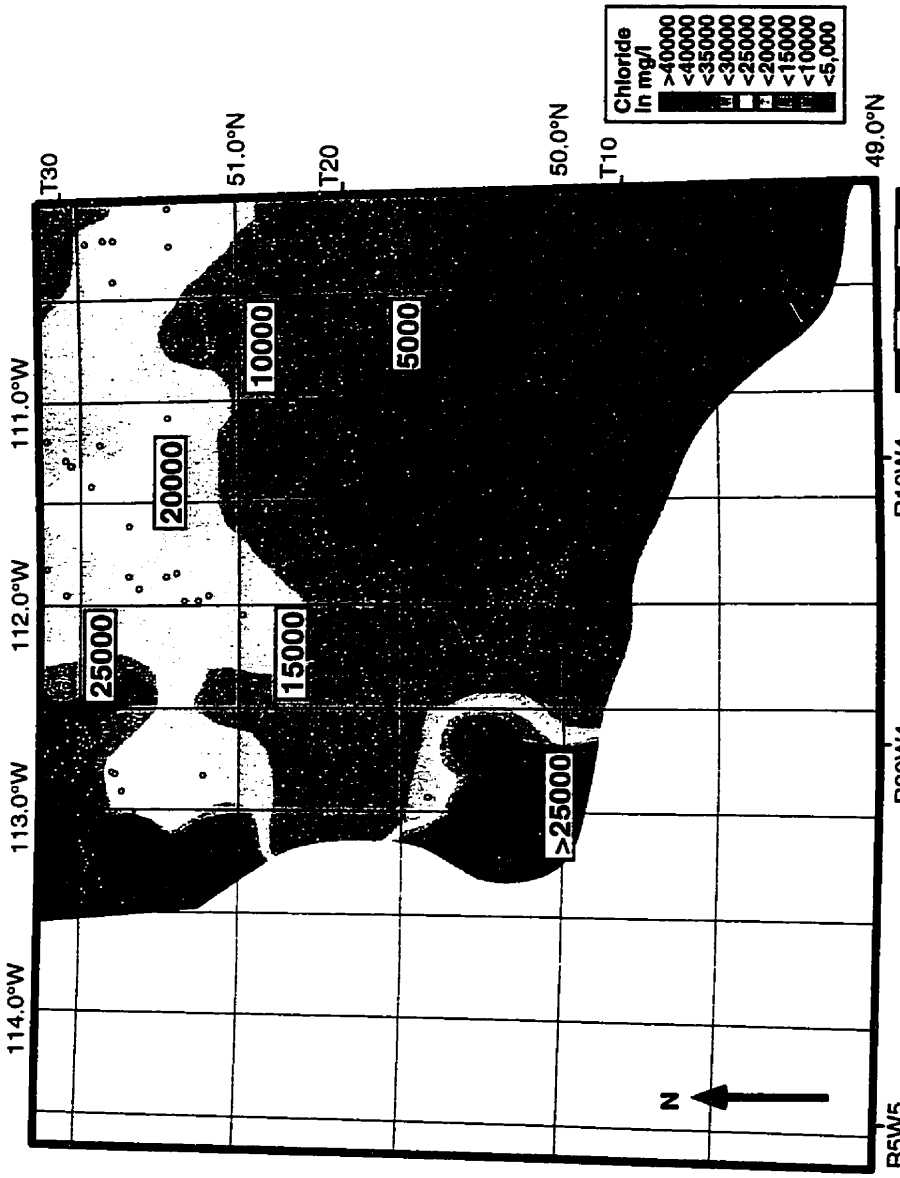

Figure 2.9 Nisku/Arcs aquifer map of the chloride distribution. Contours are in 5,000 mg/l intervals and well control of data is given by the small circles. Solid lines are chloride contours at 5,000 mg/l intervals

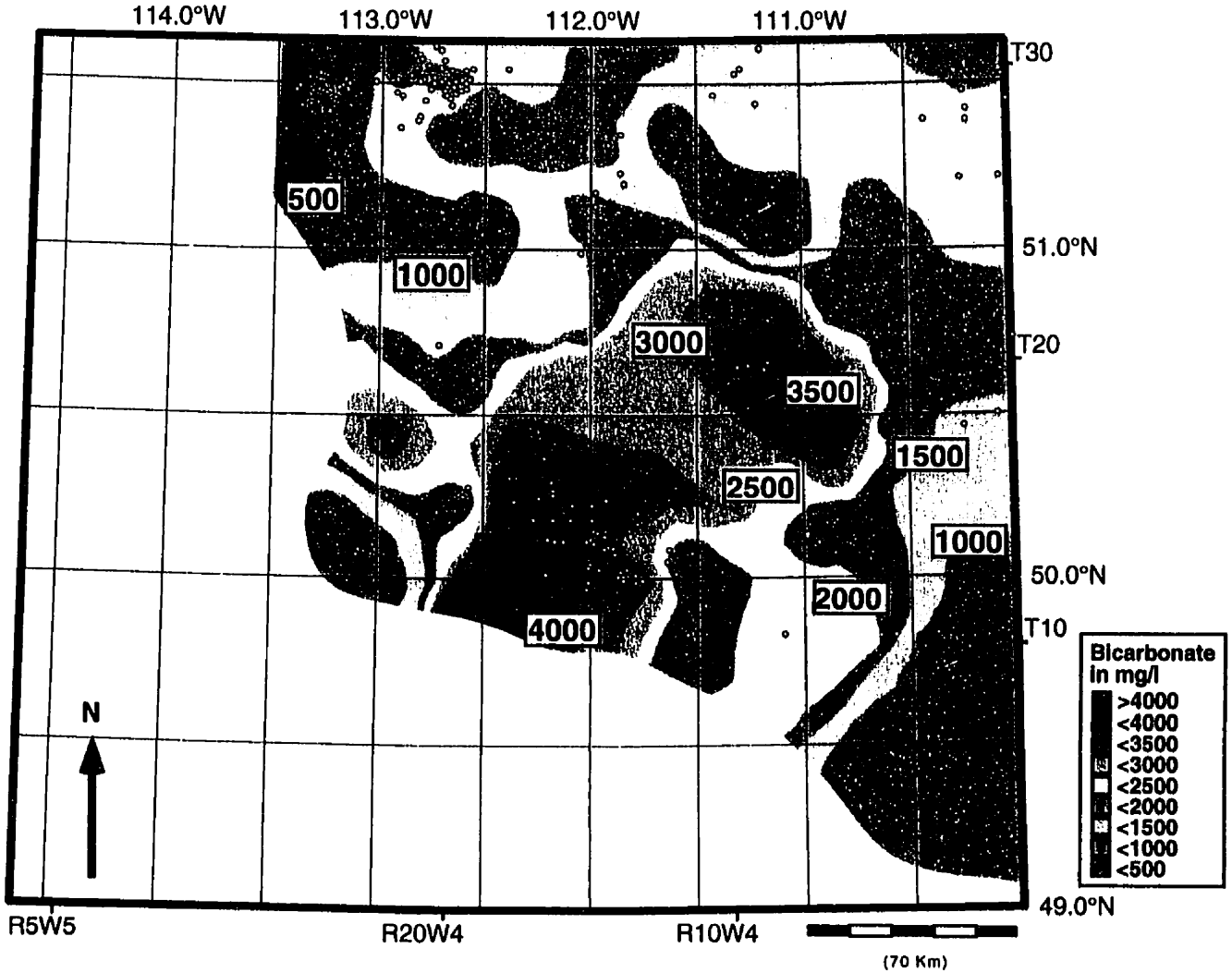

Figure 2.10. Regional distribution of Nisku/Arcs aquifer bicarbonate content. Contours are in 500 mg/l intervals and well control is shown.

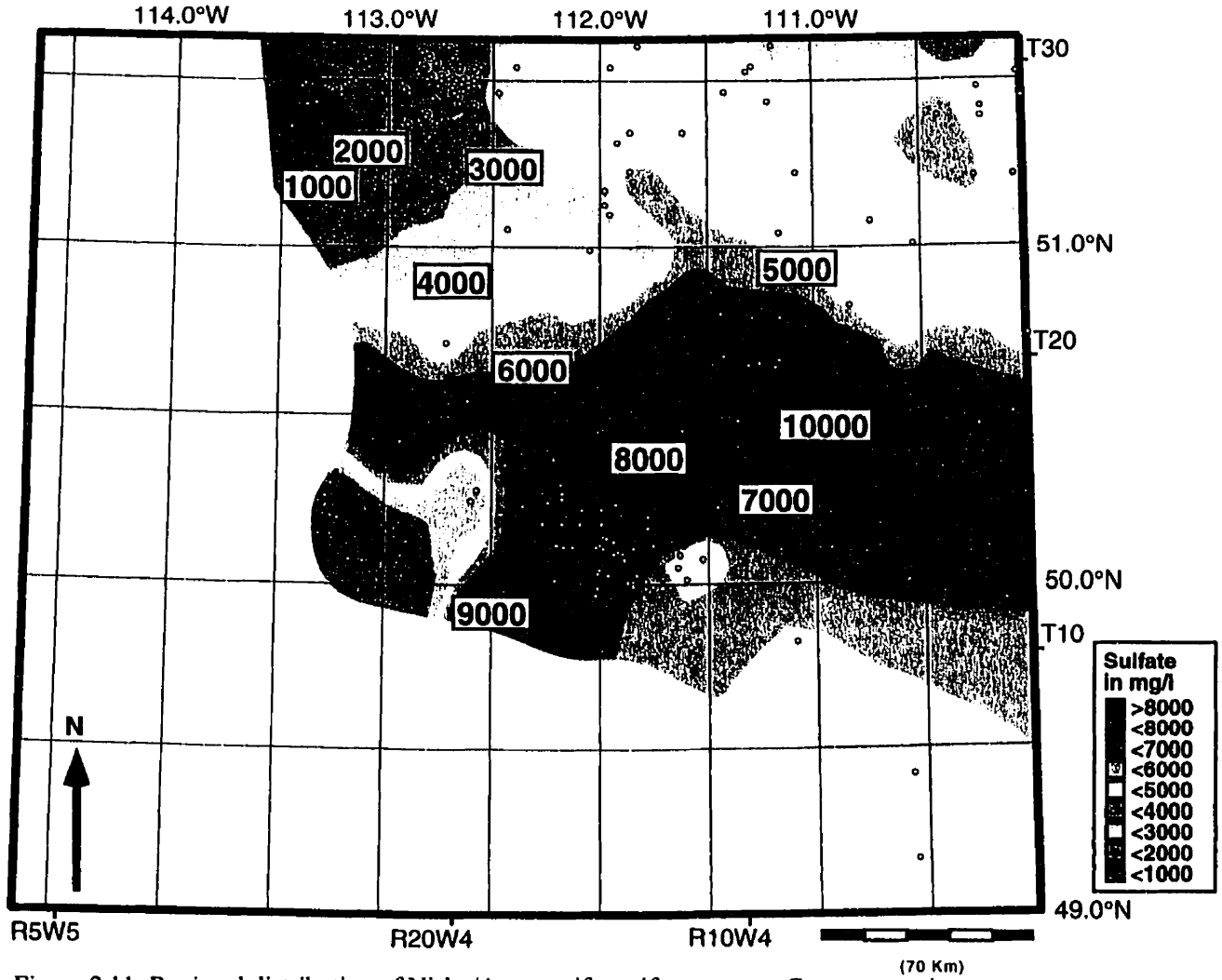

Figure 2.11. Regional distribution of Nisku/Arcs aquifer sulfate content. Contours are in 1000 mg/l intervals and well control is shown

Mississippian Aquifer

Regional variations in Cl, HCO_3, and SO_4 distribution of Mississippian hosted waters are illustrated in **Figures 2.12, 2.13, and 2.14**. Chloride concentration ranges from 500 mg/l to 62,000 mg/l. In the southeast, concentration is low (<5,000 mg/l) and the concentration gradient is relatively shallow. Toward the west and northwest the concentrations increase and a steeper concentration gradient is observed. Two areas show a lesser change in concentration gradient. The smaller region, centered on 50°N and 113°W, extends northward and westward. The larger of the two extends north and west of 51°N and 110.5°W.

Bicarbonate concentration ranges from less than 110 mg/l to 11,688 mg/l. Highs occur as a broad northeast trending band in the central area with lows in the south, north and west. Lows in the north and west correspond to highs in Cl concentration.

The concentration of sulfate ranges from 0 mg/l to 4100 mg/l. Highs are restricted to the north and northeast, and the southwest. High Cl areas tend to correspond to low HCO_3 and SO_4, and high HCO_3 correspond to low SO_4.

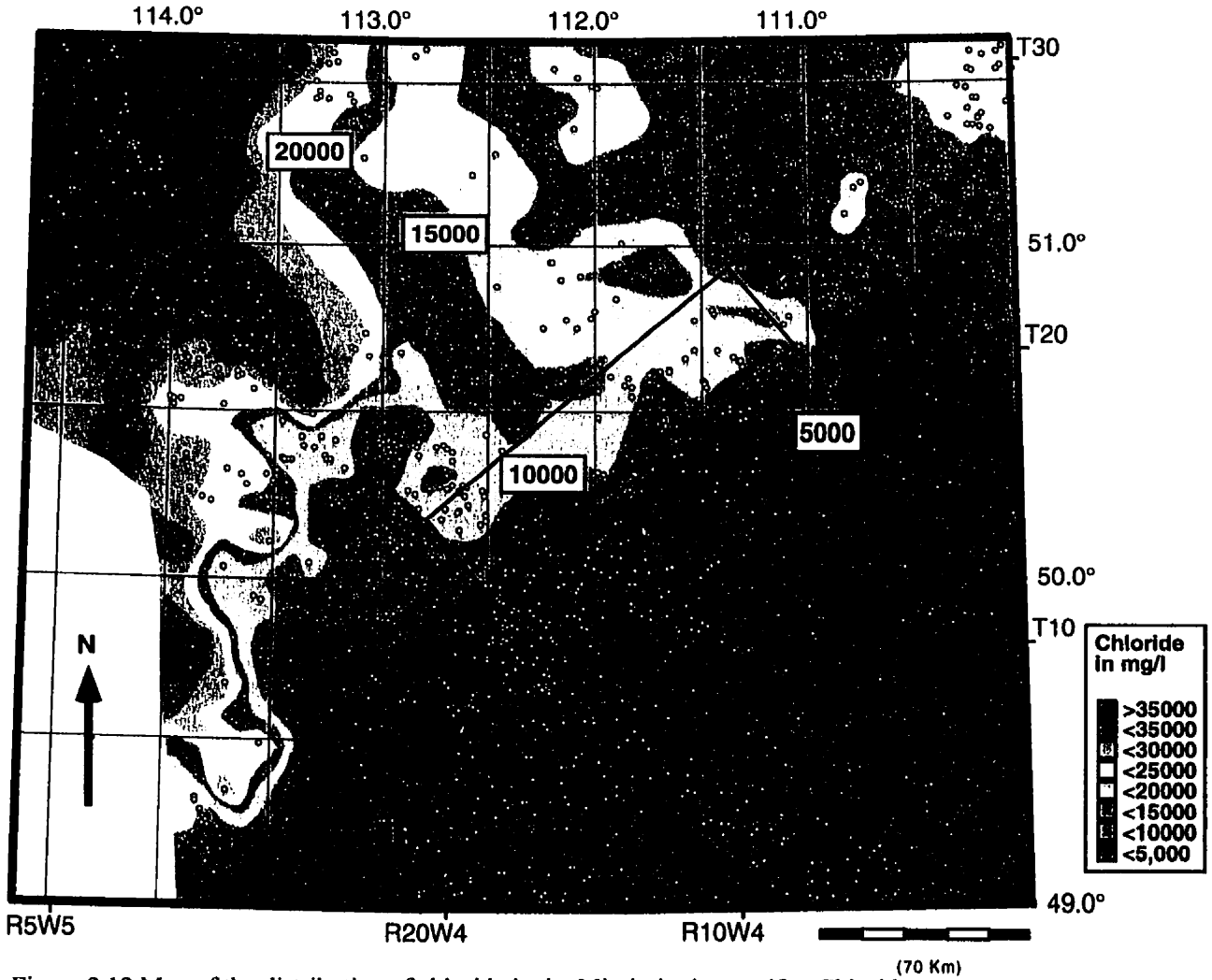

Figure 2.12 Map of the distribution of chloride in the Mississippian aquifer. Chloride contours are in 5000 mg/l intervals and well control is shown. The rectangle demarks the rapid increase in Cl gradient interpreted to be a narrow mixing zone.

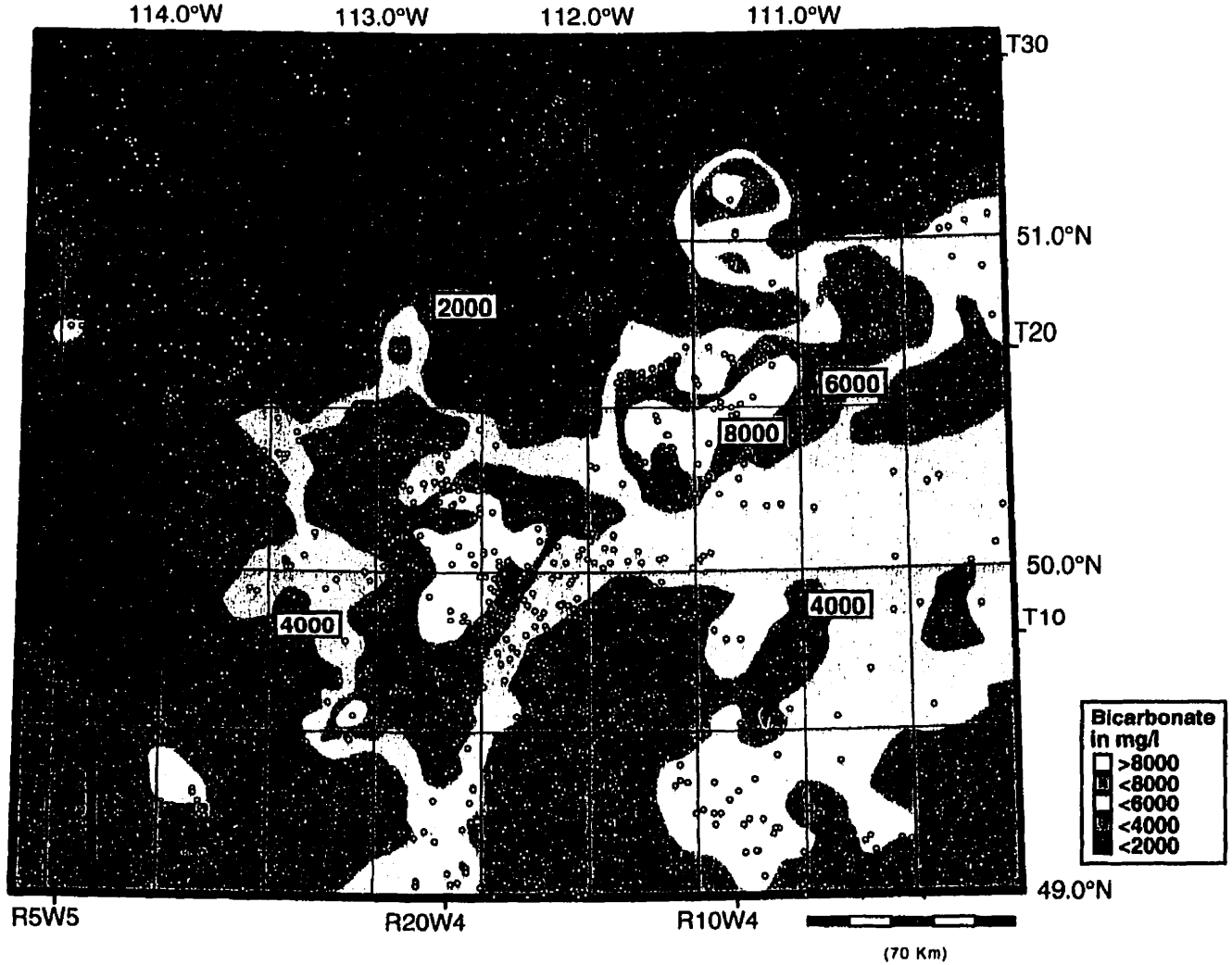

Figure 2.13 Map of the distribution of Mississippian aquifer bicarbonate content. Contours are in 2,000 mg/l intervals and well control is shown.

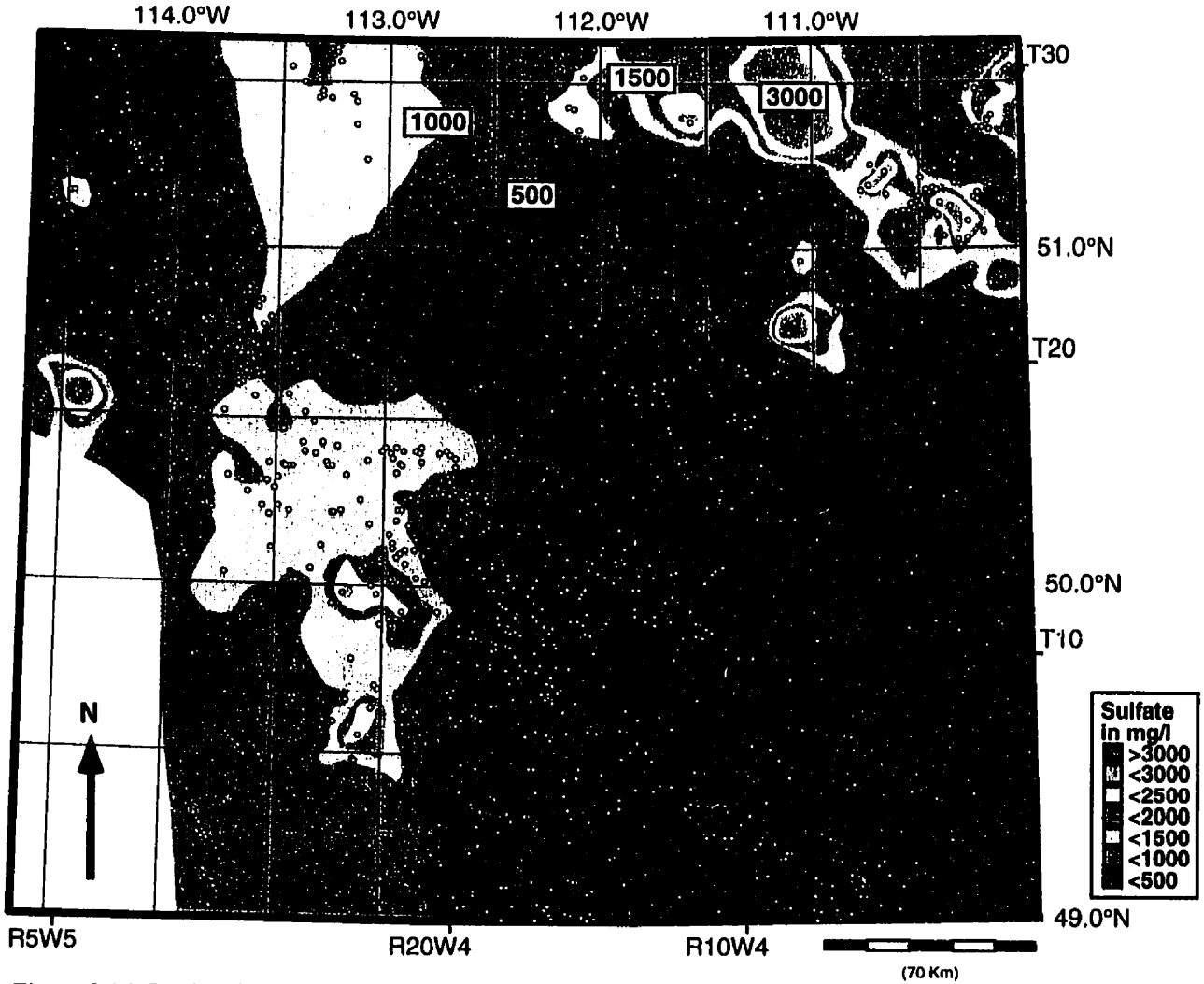

Figure 2.14. Regional distribution of Mississippian sulfate content. Contours are in 500 mg/l intervals and well control is shown.

Jurassic Aquifer

The distributions of Cl, and HCO_3 content of the Sawtooth aquifer are illustrated in **Figures 2.15, and 2.16**. The concentration of chloride ranges from 630 mg/l to 12,400 mg/l. On the map, two lows, divided by a band of higher Cl, are recognized. The low in the southwest is centred on 49.5°N by 112°W, and the other low occurs in the southeastern corner. Highs are observed in the northwestern extent of the Sawtooth Formation and coincide with a rapid increase in depth.

Bicarbonate content ranges from 2,203 mg/l to 10,000 mg/l. The distribution of bicarbonate mirrors that of chloride with highs in the west, and lows in the south-central and southeast. A map of the sulfate distribution is not included as the sulfate concentrations are low and quite variable although the highest sulfate contents occur in the northwest.

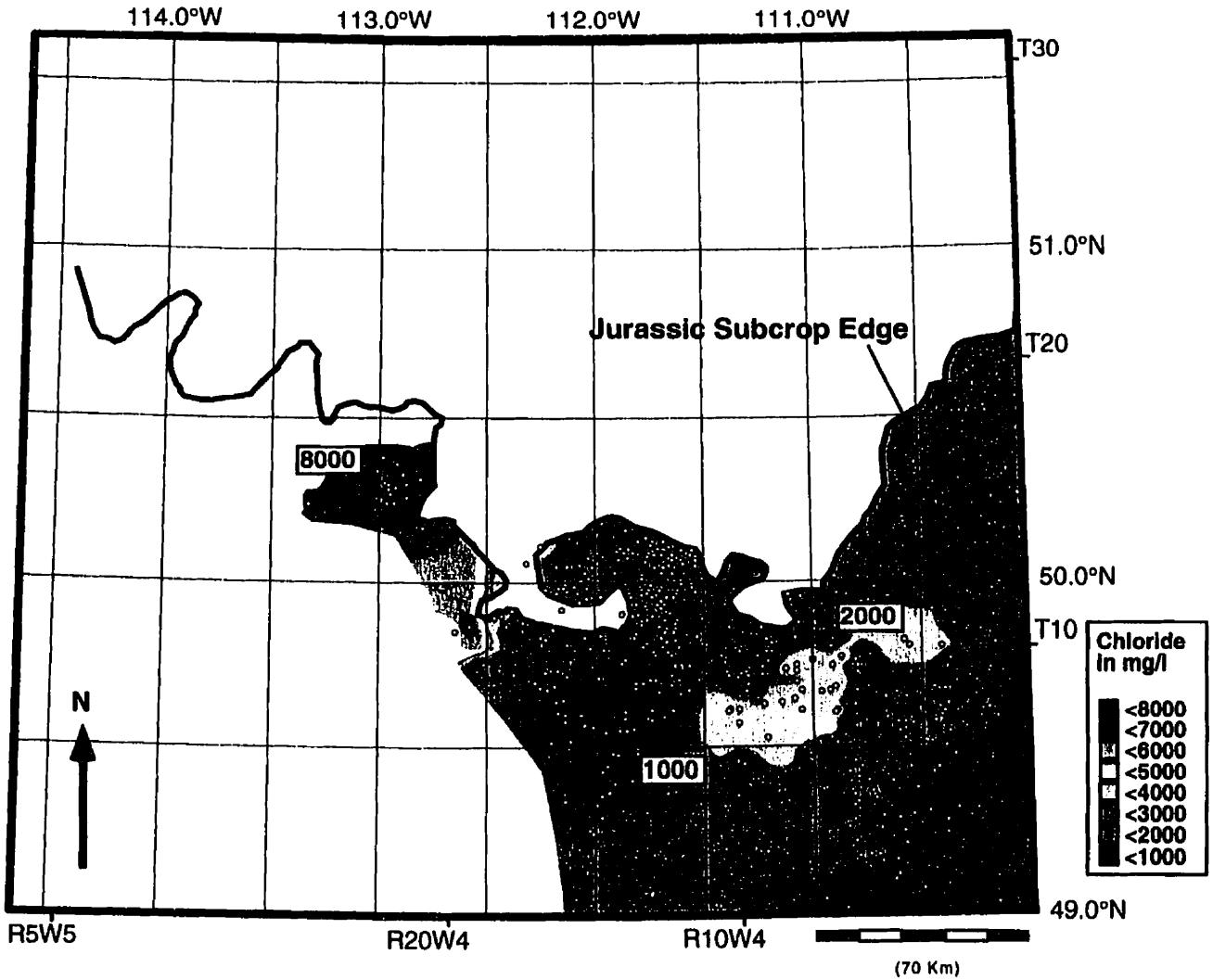

Figure 2.15 Map of the Sawtooth aquifer chloride distribution. Chloride contours are in 1,000 mg/l intervals and well control is shown.

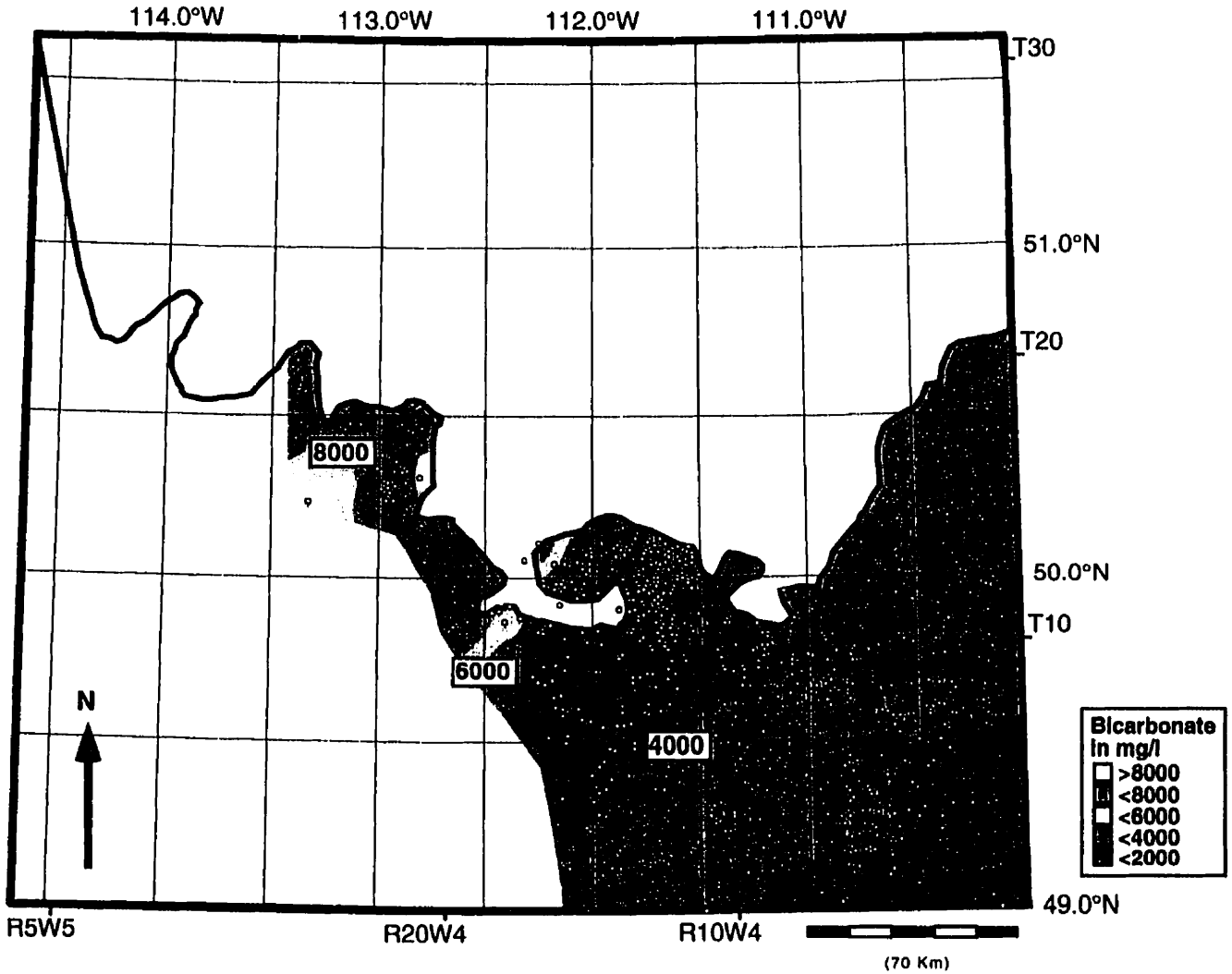

Figure 2.16 Regional distribution of Jurassic Sawtooth aquifer bicarbonate content. Contours are in 500 mg/l intervals and well control is shown

Lower Mannville Aquifer

The regional variations in Cl, HCO_3, and SO_4 are mapped in **Figures 2.17, 2.18, and 2.19**. Chloride concentrations range from 545 mg/l to 55,000 mg/l. Lows in chloride concentration occur in the south and east, and highs occur in the northwest. The concentration gradient is low in the south and increases towards the northwest. The change in the concentration gradient mimics that of the Mississippian waters, including the two regions recognized above which display an initially gradual gradient increase. The only major difference between the Lower Mannville and the Mississippian occurs between 49.5° and 50.5° west of 112.5°. The chloride content of the Lower Mannville, above the Jurassic aquitard, increases from south to north then decreases as the subcrop edge is approached (**Figure 2.20**). Values north of 49.6° are similar to those of the underlying Mississippian (**Figure 2.21**).

Bicarbonate concentration ranges from 29 mg/l to 12,041 mg/l. Lows are in the north and west and highs occur in the south and central regions of the study area. The highs coincide with those observed in the Mississippian and the overall distribution mirrors that of the Mississippian.

The concentration of sulfate ranges from 0 mg/l to 4,800 mg/l. The highest sulfate content is in the northeast. The high west of 50.5° by 112.5° correlates with highs observed in the Jurassic and Mississippian.

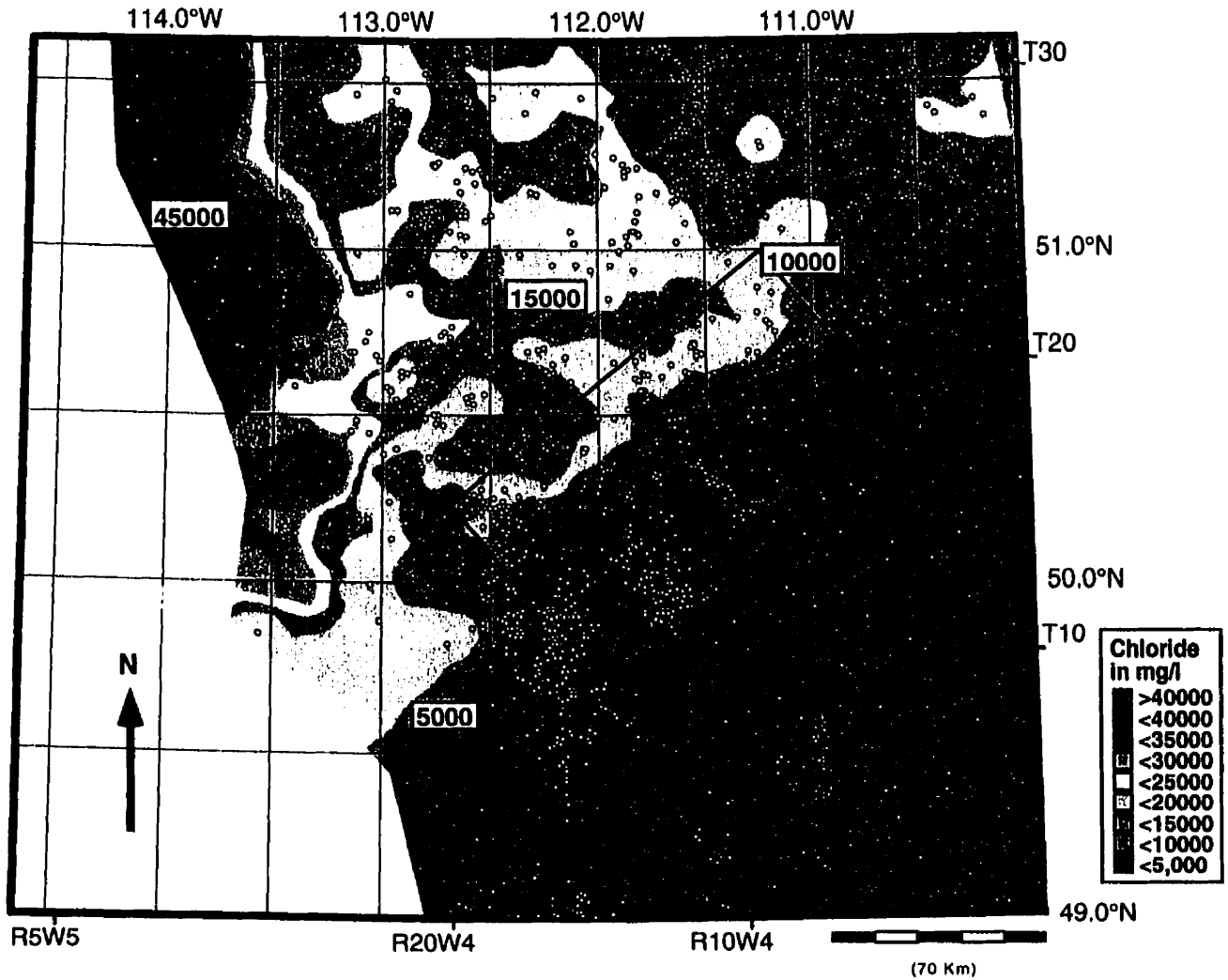

Figure 2.17. Map of the Lower Mannville aquifer chloride distribution. Chloride contours are in 5,000 mg/l contour intervals and well control is shown. The rectangle demarks the rapid increase in Cl gradient interpreted to be a narrow mixing zone.

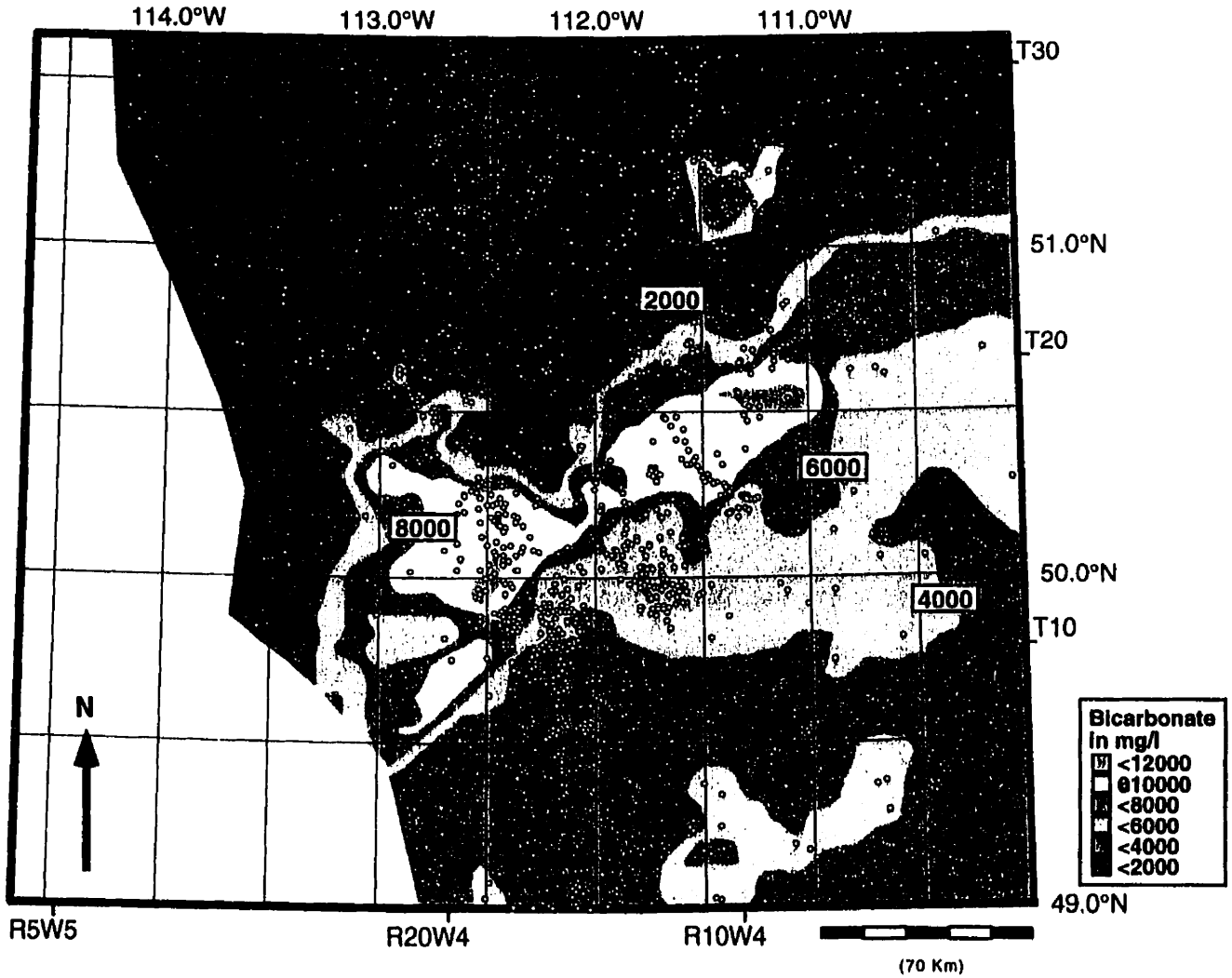

Figure 2.18 Map of the distribution of Lower Mannville aquifer bicarbonate content. Contours are in 2,000 mg/l intervals and well control is shown

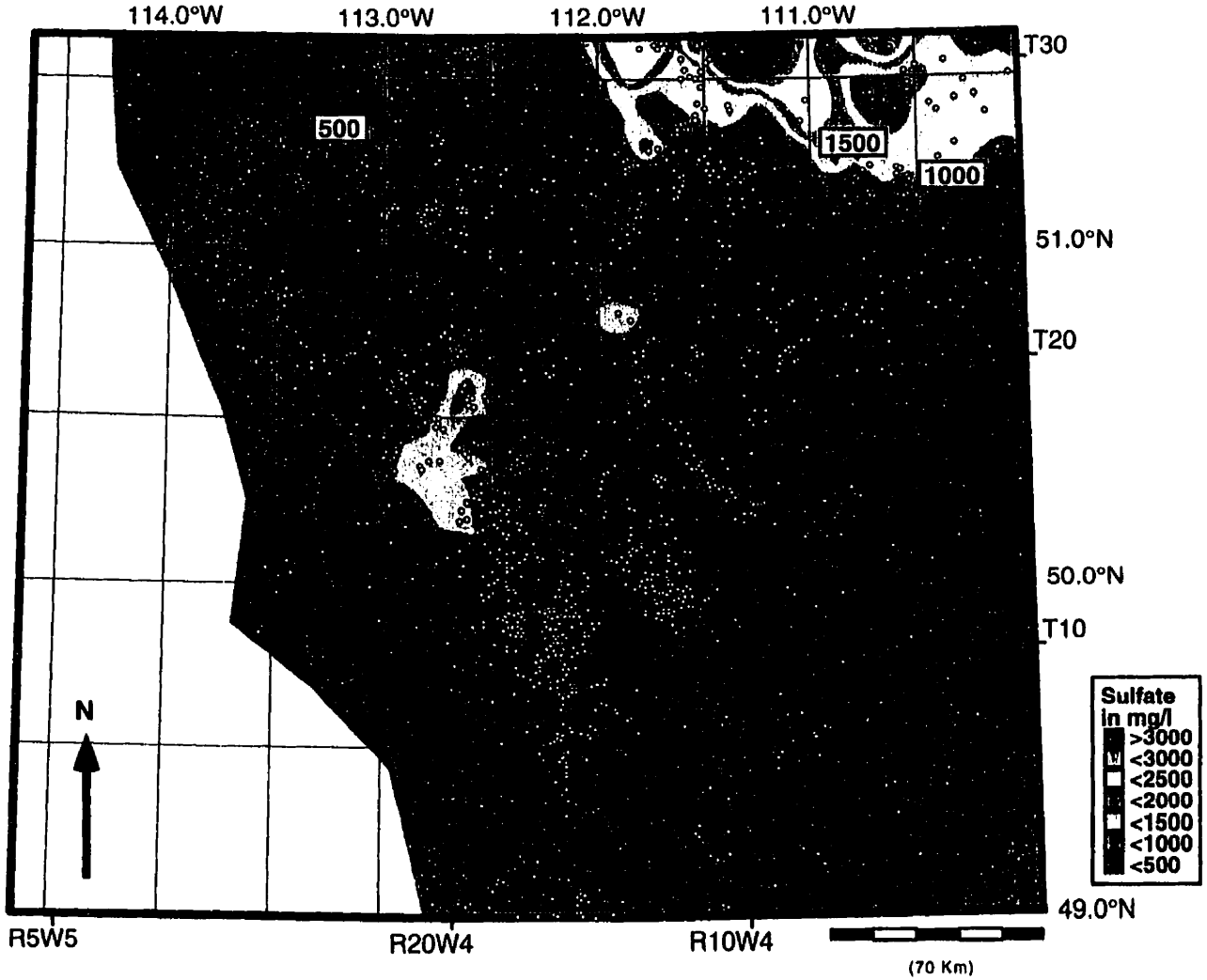

Figure 2.19. Regional distribution of Lower Mannville aquifer sulfate content. Contours are in 500 mg/l intervals and well control is shown.

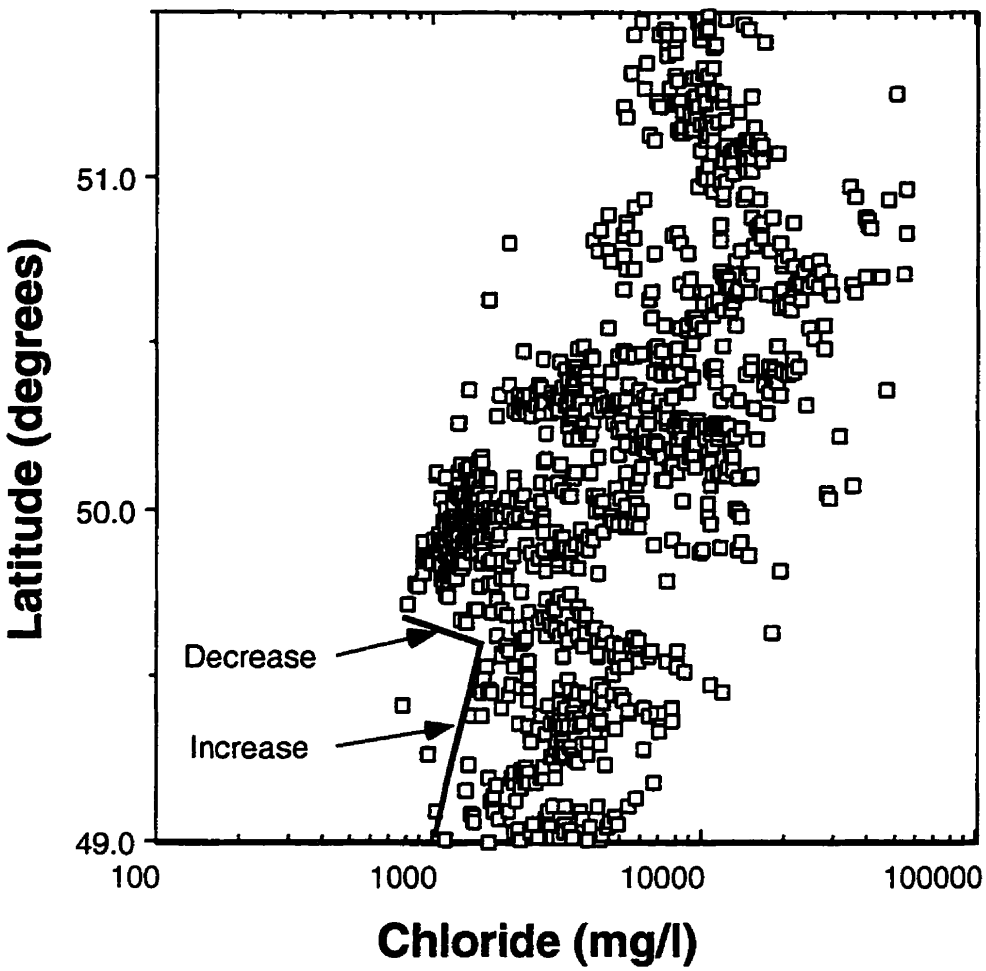

Figure 2.20. Plot of the Lower Mannville aquifer chloride content vs latitude. The Cl content increases from 49°N and decreases at approximately 49.6°N.

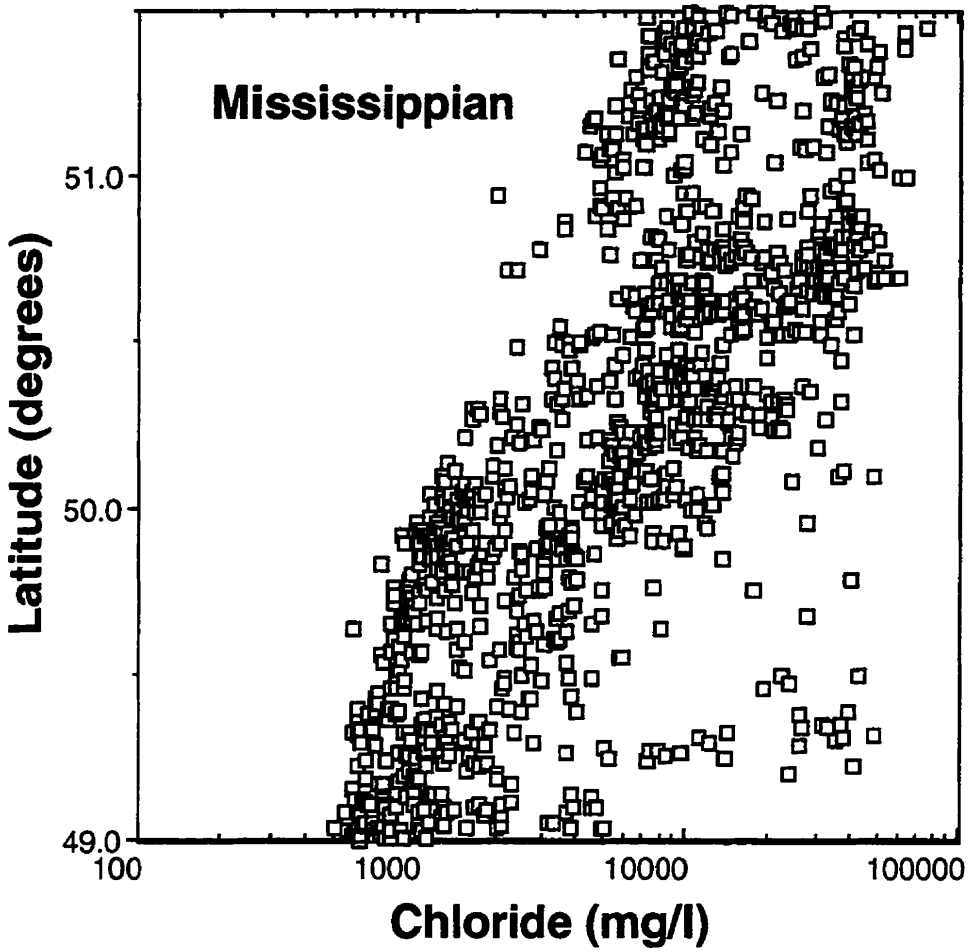

Figure 2.21. Plot of the Mississippian aquifer chloride content vs latitude. The Cl content increases steadily from 49°N. The Cl content at 49.6°N is the same as that of the Lower Mannville

Upper Mannville Aquifer

Regional variations in the distribution of Cl, HCO_3, and SO_4 for the Upper Mannville aquifer are illustrated in **Figures 2.22, 2.23, and 2.24**. Chloride concentration ranges from 650 mg/l to 35,000 mg/l. Chloride concentration is low in the south with the lows extending up along the eastern edge of the study area. Highs occur in the west and a steeper concentration gradient demarks the salinity change. The 10,000 mg/l contour coincides with that of the Lower Mannville and Mississippian aquifers.

The concentration of bicarbonate ranges from 140 mg/l to 11,250 mg/l. A broad band of high bicarbonate content water extends across the study area, coinciding with similar highs in the Lower Mannville and Mississippian. Lows occur in the north and west. Sulfate content ranges from 0 mg/l to 3000 mg/l.

High sulfate content correlates with highs observed in the Mississippian and Lower Mannville. The sulfate highs approximately correspond to bicarbonate highs in the region between 112° and 113°.

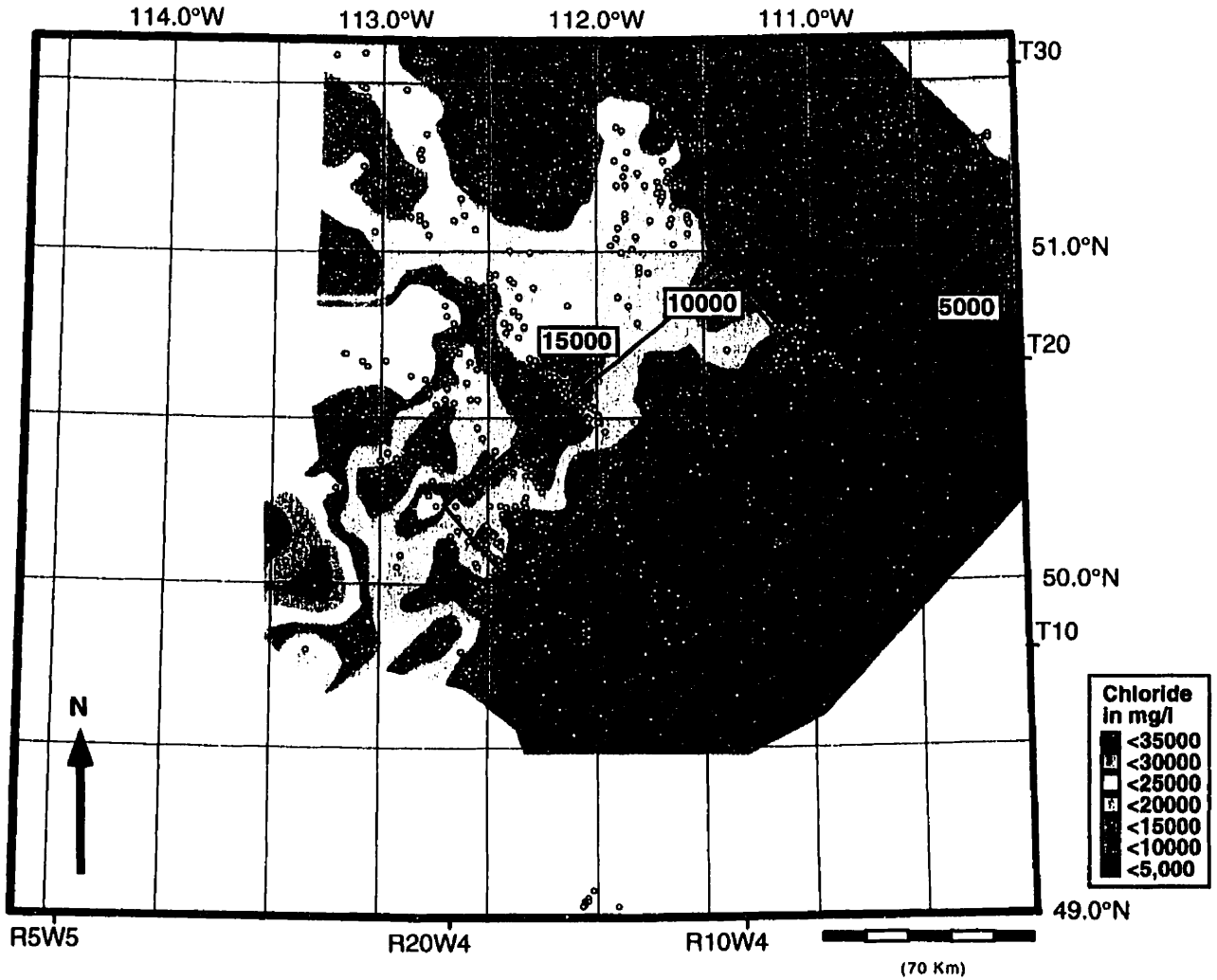

Figure 2.22. Map of the Upper Mannville aquifer chloride distribution. Chloride contours are in 5,000 mg/l contour intervals and well control is shown. The rectangle demarks the rapid increase in Cl gradient interpreted to be a narrow mixing zone.

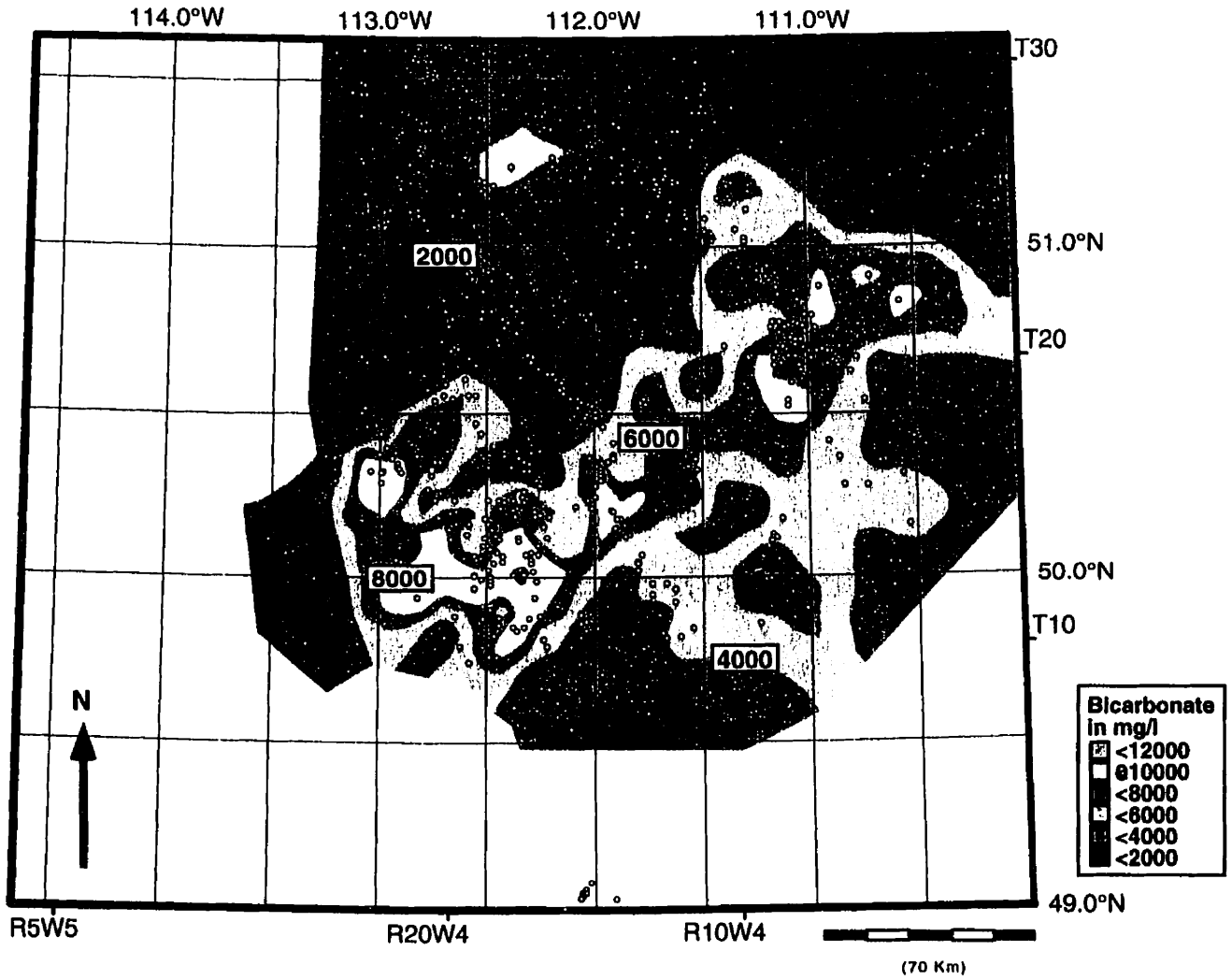

Figure 2.23. Regional distribution of Upper Mannville aquifer bicarbonate content. Contours are in 500 mg/l intervals and well control is shown

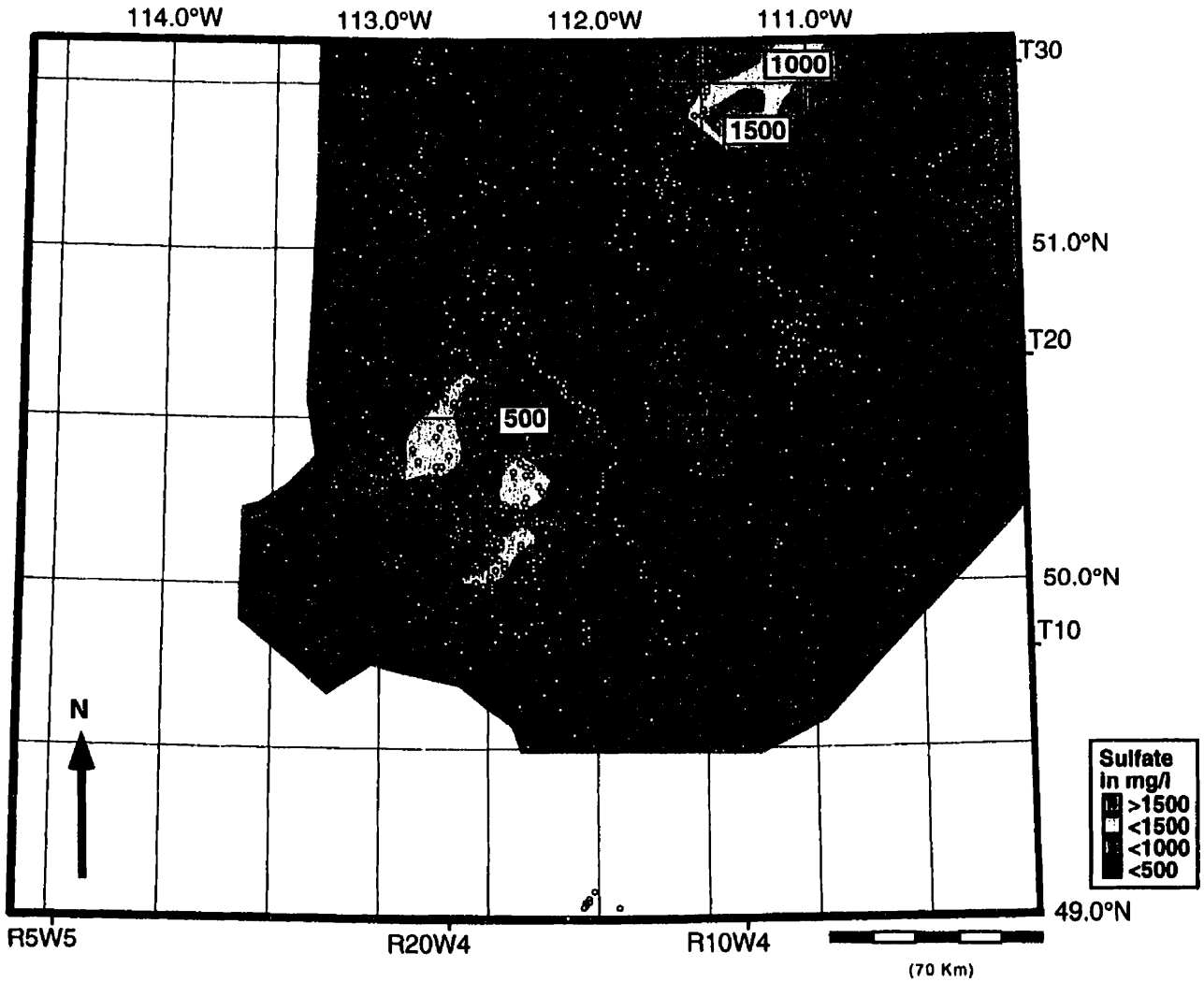

Figure 2.24. Regional distribution of Upper Mannville aquifer sulfate content. Contours are in 500 mg/l intervals and well control is shown

Viking/Bow Island Aquifer

Regional variations in the Viking/Bow Island aquifer Cl, and HCO_3 content are illustrated in **Figures 2.25 and 2.26**. Chloride concentration ranges from 1370 mg/l to 18,000 mg/l. The regional lows occur in the south. A second low is also present in the northwest. A broad band of higher Cl water extends from the west-central portion of the study area to the northeast. The concentration of bicarbonate ranges from 30 mg/l to 4150 mg/l. Isolated highs are widely distributed except in the west where the highest concentrations occur. The lowest bicarbonate contents occur in the northeast. Sulfate concentrations in the Viking/Bow Island culled data are low, typically less than 200 mg/l. The narrow range in data limits the practical application of sulfate distribution and the map of sulfate is not included.

Discussion

Chemical trends

The compositional evolution during evaporation of seawater is well documented and generally follows a predictable pathway (Carpenter, 1978; McCaffrey *et al.*, 1987). Plots of the variation in the major cations and anions in relation to chloride concentration for each of the aquifer units are given in the following figures. Included in the diagrams is the composition of present-day seawater, and the dilution and the evaporation up to Mg-

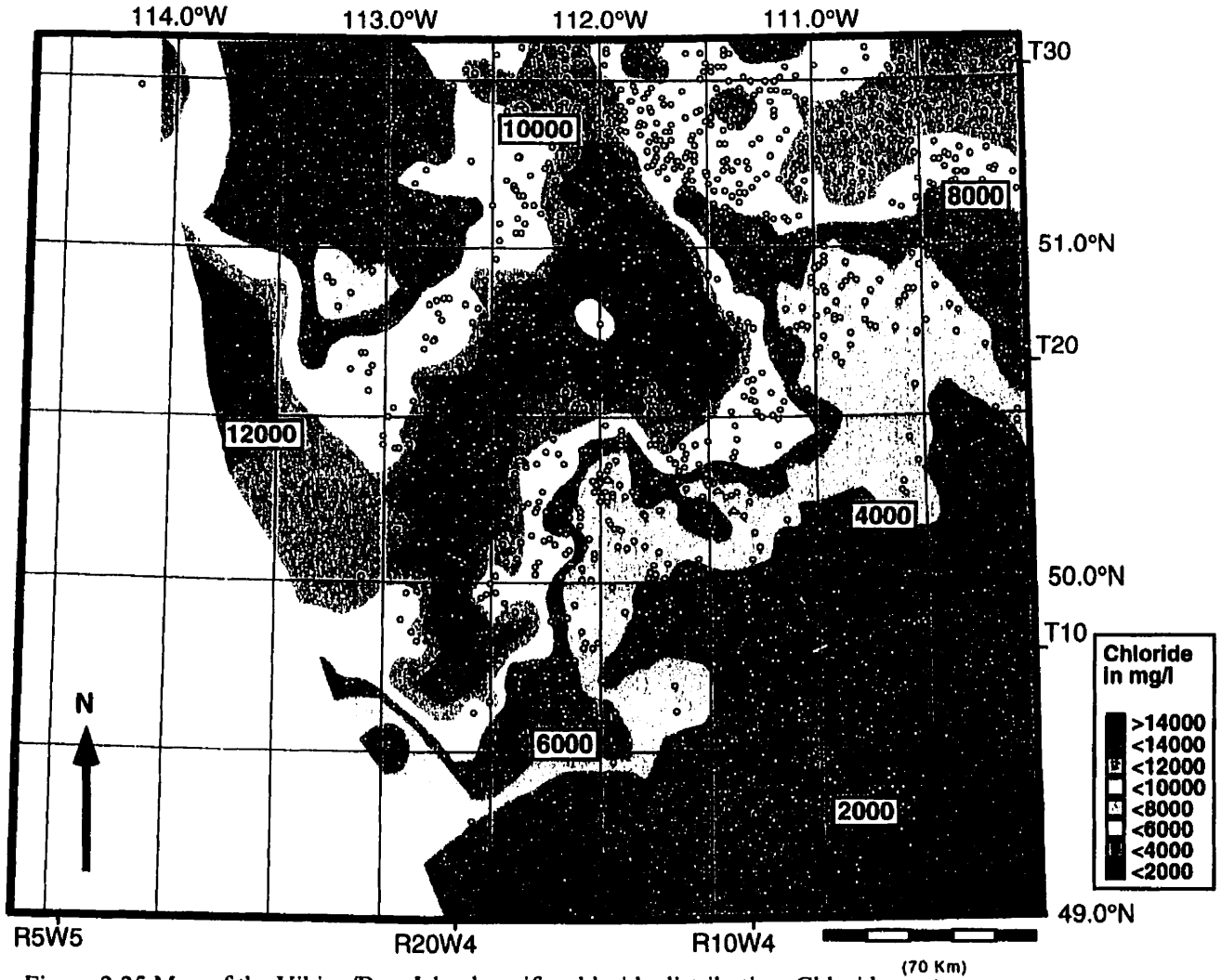

Figure 2.25 Map of the Viking/Bow Island aquifer chloride distribution. Chloride contours are in 2,000 mg/l intervals and well control is shown.

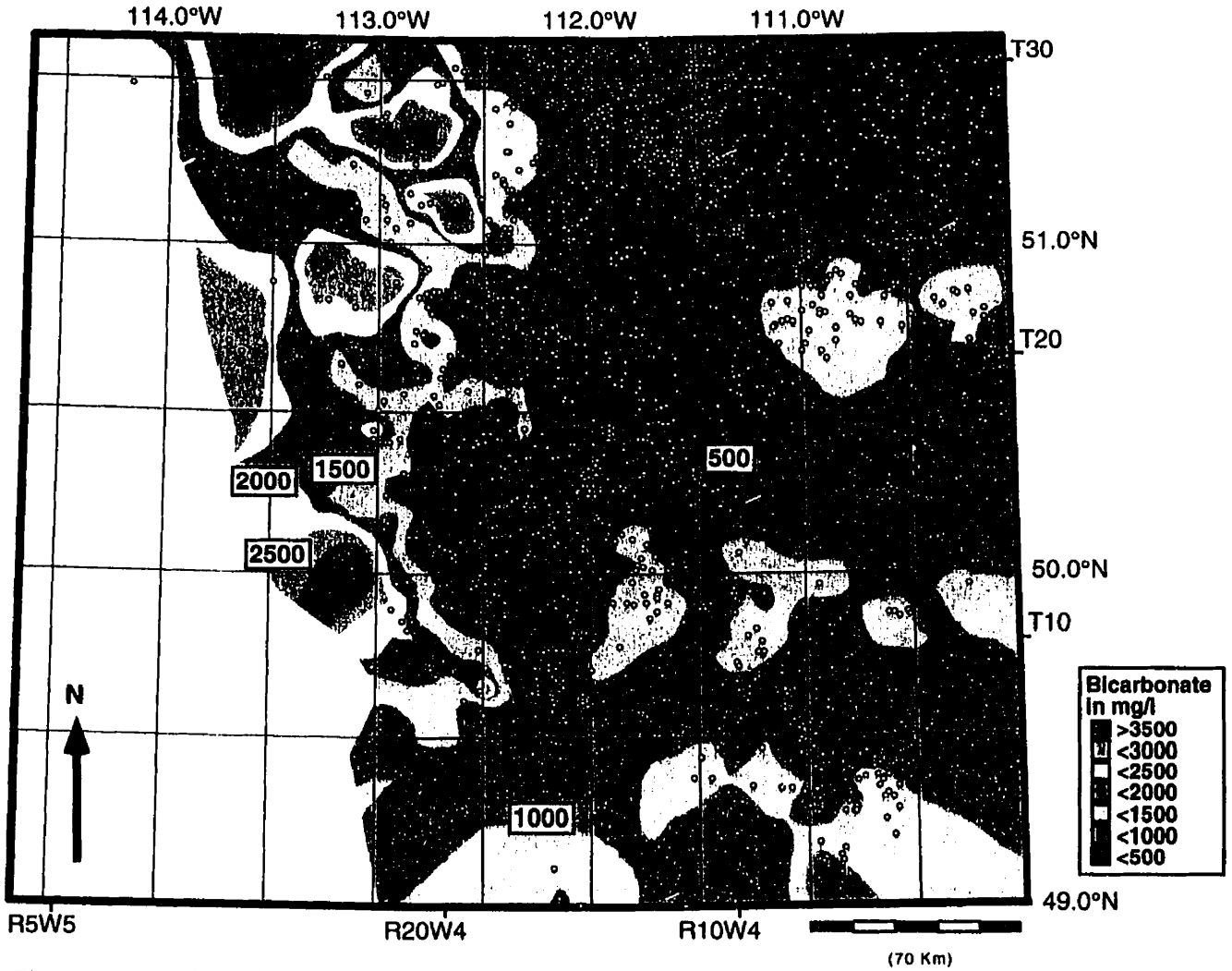

Figure 2.26. Regional distribution of Viking/Bow Island aquifer bicarbonate content. Contours are in 500 mg/l intervals and well control is shown

sulfate precipitation curves derived from diluting seawater and by concentrating seawater through subaerial evaporation (Carpenter, 1978). The range of concentrations of the dissolved constituents of the culled database and sampled waters coincide, indicating that the culling methods were effective in removing the majority of the analyses in the AEUB database that were not representative of formation waters. Some of the data for K, Mg, and Ca from the AEUB database fall below the general trends observed and are obviously inaccurate but these were not discarded, as the Cl content, used to show regional variations on the map scale, appear to be reasonably accurate.

Devonian Nisku/Arcs Aquifer

Variations in cation composition

The Nisku/Arcs aquifer water sodium and potassium contents show a strong linear correlation with chloride (**Figure 2.27a**). Sodium data plot above the evaporation-dilution (E-D) curve at less than 30,000 mg/l Cl and below the curve at greater than 30,000 mg/l. The high Cl (>30,000 mg/l) portion of the sodium trend would intersect the E-D curve at a point beyond halite saturation and precipitation. The majority of the potassium data lie above the seawater evaporation-dilution curve (**Figure 2.27b**). Above 20,000 mg/l, potassium concentration varies linearly with chloride concentration. Below 20,000 mg/l K displays considerable scatter but, in general, displays a continuation of the

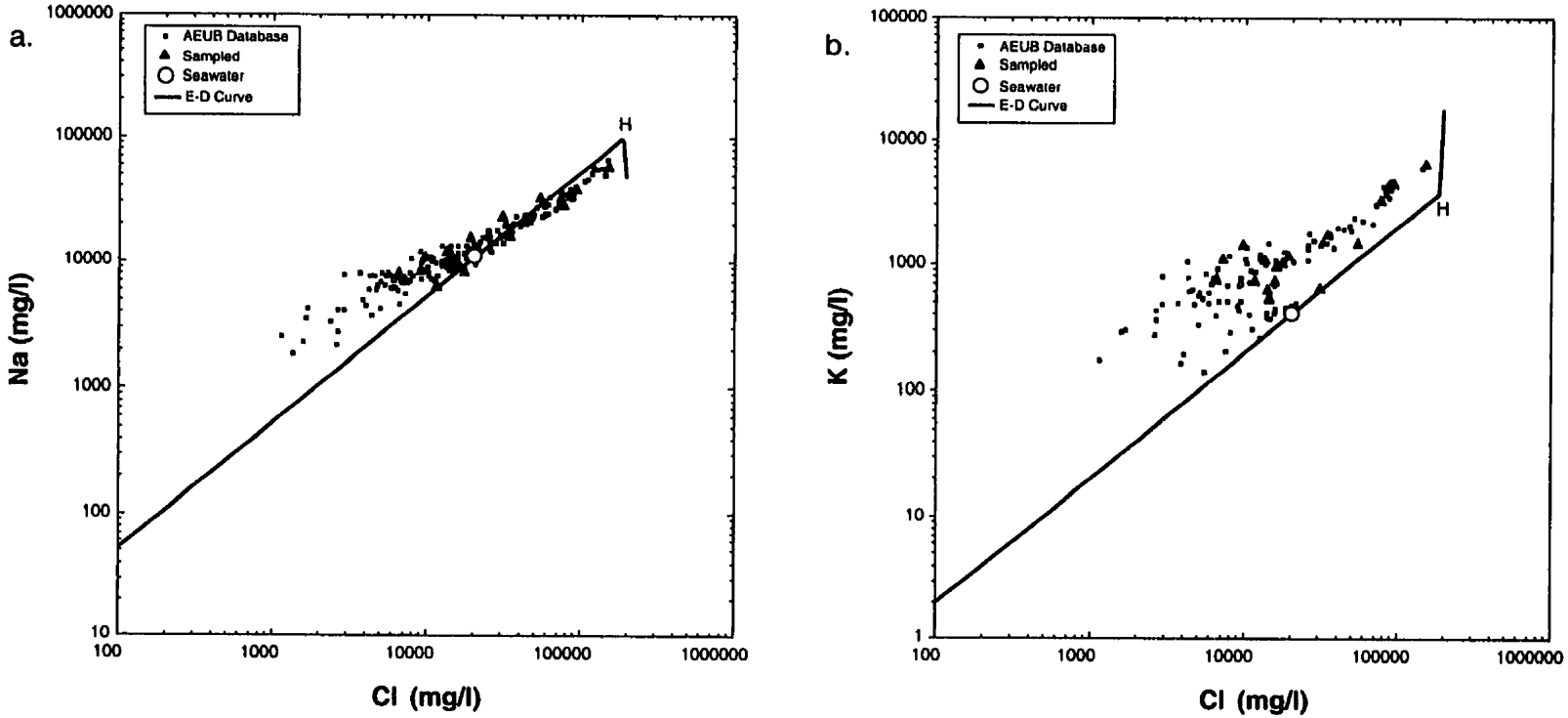

Figure 2.27a,b. Plots of the Nisku/Arcs sodium and potassium vs chloride. A good linear correlation, especially at higher Cl is apparent. Data includes that of Hitchon et al. (1971). The E-D curve is the seawater evaporation-dilution curve of Carpenter (1978). H marks the point at which halite saturation and precipitation initiates.

trend for higher Cl. The decrease in sodium and increase in potassium relative to the seawater E-D curve is consistent with dilution by meteoric water of seawater evaporated beyond halite saturation.

Calcium contents plot above the seawater evaporation-dilution curve indicating that there is addition of calcium relative to that expected during seawater evaporation (**Figure 2.27c**). Two trends are apparent, one at higher than 15,000-20,000 mg/l concentration and the other at lower concentrations. The magnesium data generally plots below the E-D curve (**Figure 2.27d**). The same two trends observed for Ca are evident for Mg. The lower chloride waters correspond to the Na-SO_4 dominated waters identified in the Piper diagram and the higher Cl corresponds to the Na-Cl group.

The concentration of bicarbonate is highest at low chloride concentrations and decreases considerably at Cl concentrations greater than 20,000 mg/l (**Figure 2.27e**). Sulfate content decreases with increasing chloride content (**Figure 2.27f**). There appears to be a change in the slope of the curve at approximately 20,000 mg/l. Sulfate contents lie both above and below seawater composition and the slope is opposite to that expected with evaporation-dilution.

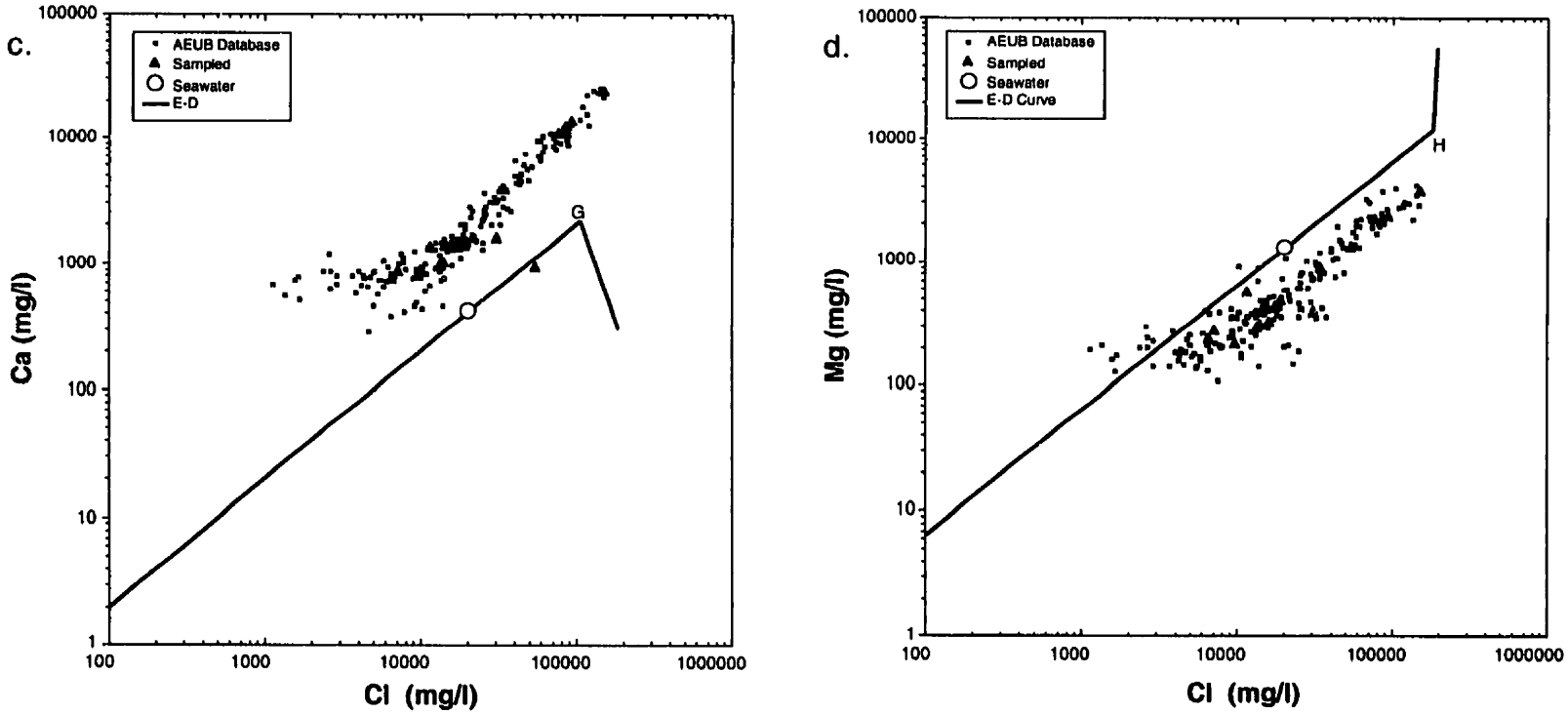

Figure 2.27c,d. Plot of the Nisku/Arcs calcium and magnesium vs chloride. A good linear correlation at higher Cl is apparent. Below 20,000 mg/l Cl a distinct change in slope occurs. Data includes that of Hitchon et al. (1971). The E-D curve is the seawater evaporation-dilution curve of Carpenter (1978). G and H mark the points at which gypsum and halite saturation and precipitation initiate.

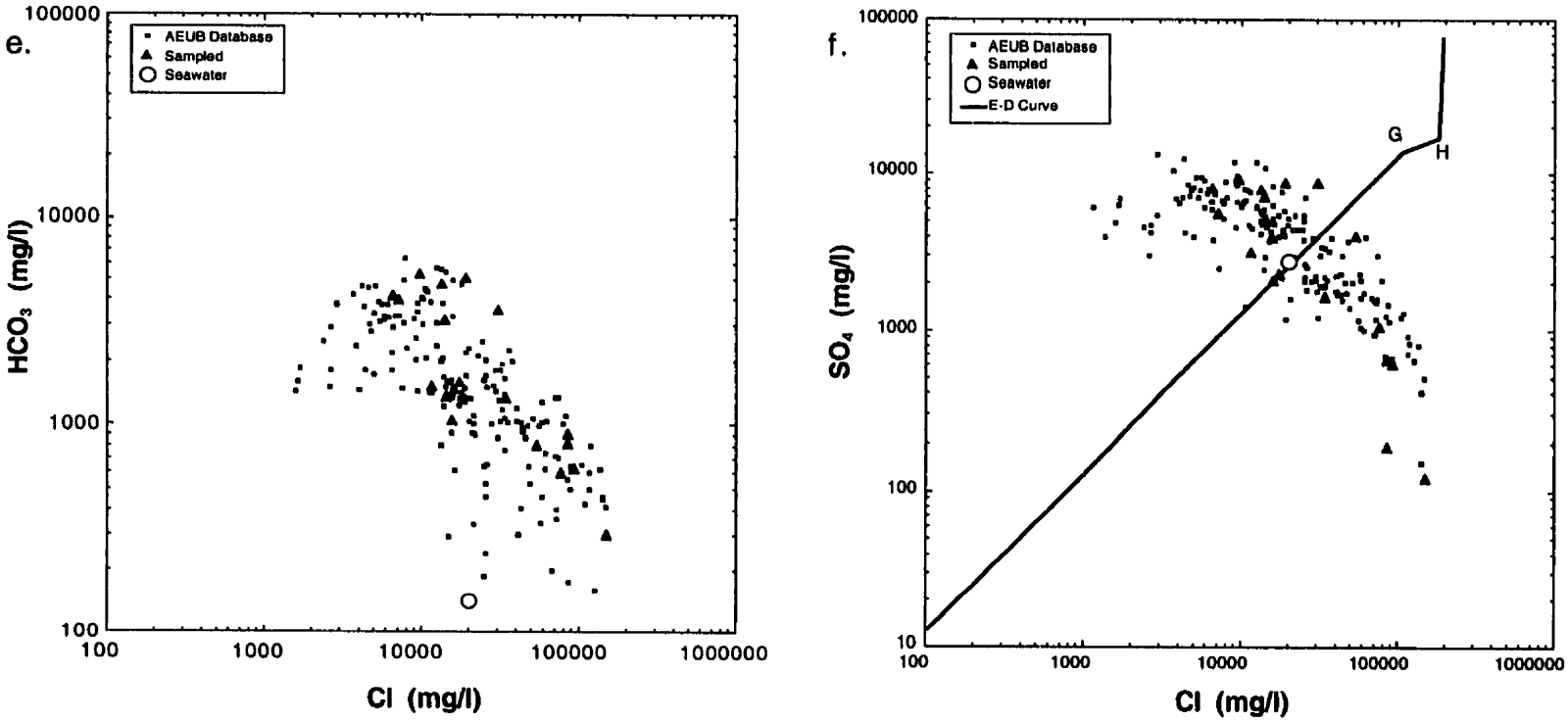

Figure 2.27e,f. Plot of the Nisku/Arcs bicarbonate and sulfate vs chloride. Both bicarbonate and sulfate decrease with increasing chloride. Below 20,000 mg/l Cl a distinct change in slope occurs. Data includes that of Hitchon et al. (1971). The E-D curve is the seawater evaporation-dilution curve of Carpenter (1978). G and H mark the points at which gypsum and halite saturation and precipitation initiate.

Mineralogical controls on solution composition

Significant changes in the concentrations of calcium, magnesium, bicarbonate and sulfate relative to chloride occur at approximately 15,000-20,000 mg/l Cl. Unlike sodium and potassium, dilution does not seem to be the only factor controlling the concentrations of these ions. Thermodynamic controls on the composition of aqueous solutions can be investigated by evaluating saturation states of mineral phases and through diagrams that show mineral stability relative to the activity of aqueous components.

High sulfate content occurs in a relatively localized area in the Devonian Nisku/Arcs aquifer. Anhydrite occurs throughout the region of high sulfate content (Slingsby and Kissingly, 1992). The localized occurrence and the relatively dilute formation waters suggest the increase in sulfate content reflects dissolution of anhydrite. Anhydrite saturation indices indicate the waters are saturated with respect to anhydrite. The anhydrite dissolution reaction:

$$CaSO_4 \Rightarrow Ca^{2+} + SO_4^{2-} \qquad 1$$

releases an equal molar amount of calcium and sulfate into solution. An increase of 4,000 mg/l sulfate should result in an increase of over 1,600 mg/l in calcium. However, calcium concentrations are generally less than 1,000 mg/l at low chloride, high sulfate concentrations. Inspection of **Figures 2.27c and 2.27d** shows that at low chloride concentrations, the calcium and magnesium concentrations are higher than expected

relative to the trend of the data at Cl >20,000 mg/l. Calcium content is approximately 500 to1000 mg/l higher and magnesium is 100 to 200 mg/l higher. The 500 to 1,000 mg/l increase in calcium does not fully compensate for the 4,000 to 6,000 mg/l increase in sulfate from anhydrite dissolution. These lower than expected (from anhydrite dissolution) calcium concentrations indicate removal of Ca. Some other process must account for the lower calcium content.

Two reactions have the potential to reduce Ca in solution, precipitation of calcite and reaction of dolomite with Ca^{2+} to produce calcite. The reactions with are:

$$Ca^{2+} + HCO_3^- \Leftrightarrow CaCO_3 + H^+ \qquad 2$$

$$Ca^{2+} + CaMg(CO_3)_2 \Leftrightarrow 2CaCO_3 + Mg^{2+} \qquad 3$$

Calcite precipitation results in a decrease in calcium, bicarbonate and pH. The number of moles of Ca and Mg added to the system using 1000 mg/l Ca and100 mg/l Mg from above for a 4000 mg/l sulfate increase is insufficient (25 mmol + 4 mmol vs 42 mmol sulfate) to account for all of the Ca that would be added by anhydrite dissolving. Some of the calcium (in this example 13 mmol) must be removed by precipitation of calcite.

The possibility of the equilibria 1+2 and 1+3 controlling the chemistry can be tested by plotting activity diagrams. **Figures 2.28, 2.29** show the equilibrium for the reactions:

$$CaSO_4 + HCO_3^- \Leftrightarrow CaCO_3 + H^+ + SO_4^{2-} \qquad 4$$

$$0.5CaSO_4 + CaMg(CO_3)_2 + 0.5Ca^{2+} \Leftrightarrow 2CaCO_3 + Mg^{2+} + 0.5SO_4^{2-} \qquad 5$$

at temperatures of 40°C and 80°C. Note that reactions 4 and 5 do not contain H^-, so the assumption of calcite equilibrium to estimate pH does not influence the plotted position of water compositions. The water data plot on or close to the calcite-anhydrite equilibrium curve at low temperatures (**Figure 2.28**). The curve shifts an insignificant amount at higher temperatures and the higher T water data plot in the calcite stability field. This suggests that at low temperature, reaction between calcite and anhydrite may be influencing the water composition and approaching equilibrium. In **Figure 2.29**, the water data plot on or near the equilibrium curves for most of the samples at formation temperature, except the most saline waters. The implication is that a reaction among calcite-dolomite-anhydrite may be close to equilibrium and influencing water compositions throughout the temperature range of the sampled water. A plot of the calcite-dolomite equilibrium (**Figure 2.30**) for the temperature range of the data indicates that the ratio of calcium to magnesium is controlled by the calcite-dolomite reaction.

Origin of the Devonian Nisku/Arcs aquifer waters

A mass balance calculation was undertaken to determine the origin of the formation waters and the potential reactions influencing water chemistry. Spencer (1987) determined that the majority of Devonian-hosted formation waters consist of residual

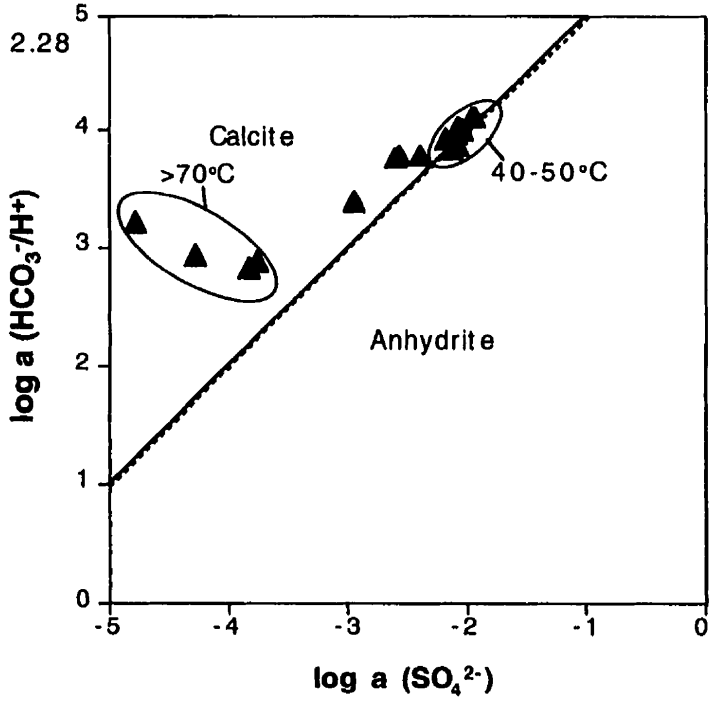

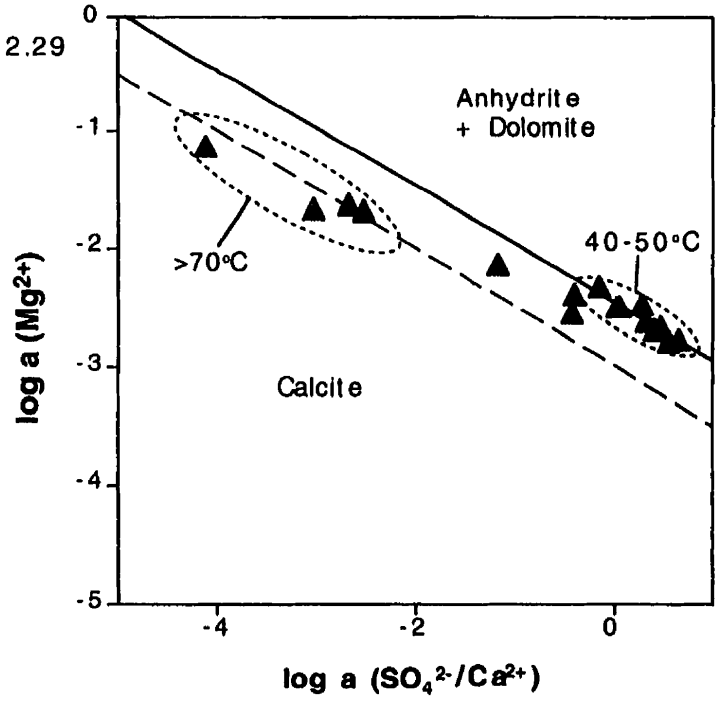

Figures 2.28 and 2.29. Log activity-activity plots of Nisku/Arcs aquifer waters showing the stability of calcite and anhydrite (2.28) and calcite, dolomite and anhydrite (2.29) at temperatures and pressures of 40°C and 100 bar (solid line), and 70°C and 200 bar (dashed line). Low temperature waters appear to reflect equilibrium between calcite and anhydrite but high T waters do not (high T curve in 2.28 is virtually unchanged from the low T curve). The water composition may also be influenced by equilibrium between calcite-dolomite-anhydrite through the range in temperatures.

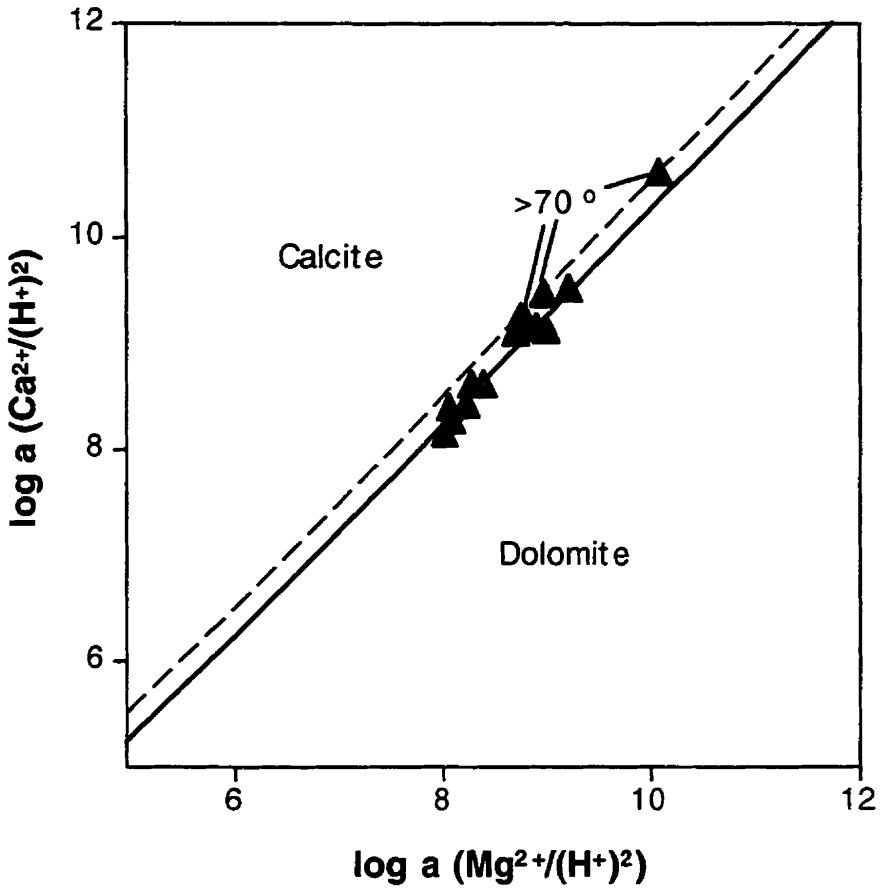

Figures 2.30. Log activity-activity plot showing the stability of calcite and dolomite at temperatures and pressures of 40°C and 100 bar (solid line), and 70°C and 200 bar (dashed line). Triangles represent the Nisku/Arcs aquifer water composition. Calcite-dolomite equilibrium appears to be influencing the the ratio of calcium to magnesium in the waters.

evaporite brines diluted by meteoric water. Ratios of cations and anions to bromide were used to determine the extent of evaporation, dilution, and water-rock interaction (Spencer, 1987). In this study, analytical difficulties in establishing accurate bromide concentrations made a calculation similar to Spencer (1987) impractical.

A mass balance calculation based on establishing the chloride concentration of the brine end-member, and through that the concentration of Ca, Mg and SO_4 in the evaporite brine, was attempted. **Table 2.5** summarizes the results of the mass balance approach. The seawater evaporation curves of Carpenter (1978) were used for the calculation. The first step is to determine the chloride composition of the brine end-member. The linear correlation of sodium and potassium with chloride suggests that dilution of the residual evaporite brine is the dominant factor in the compositional variation of Na and K. Calculation of the chloride content at the intersection of a linear regression of the sodium data and the E-D curve past halite precipitation gives 185,973 mg/l Cl for the AEUB database and 187,417 mg/l Cl for the samples collected in this study. Similar calculations for potassium are in close agreement with the sodium calculation (185,788 and 185,574 mg/l respectively for the AEUB and samples collected in this study). A value of 186,000 mg/l chloride was chosen as the composition of the evaporated brine end-member. Calcium and magnesium content at 186,000 mg/l Cl determined from linear regression of the >30,000 mg/l chloride waters are listed in **Table 2.5**. The composition of evaporite

Table 2.5. Mass balance calculations used to determine the origin of Nisku/Arcs formation water.

	Devonian		Linear regression	E-D curve int.	Concentration at		Brine concentration	
Ion	Data Source	Data Range	R^2	Cl mg/l	Cl 186,000 mg/l	mmol/l	at Cl 186,000 mg/l	mmol/l
Na	AEUB	>30,000 mg/l Cl	0.95	185,973				
Na	Sampled	>30,000 mg/l Cl	0.99	187,417				
K	AEUB	>30,000 mg/l Cl	0.92	185,788				
K	Sampled	>30,000 mg/l Cl	0.98	185,574				
Ca	AEUB	>30,000 mg/l Cl	0.9		29,579	738		
Ca	Sampled	>30,000 mg/l Cl	0.99		29,329	732		
Mg	AEUB	>30,000 mg/l Cl	0.67		4,524	186	34,023	1,400
Mg	Sampled	>30,000 mg/l Cl	0.98		4,609	190		
SO4							44,945	468

brine with a Cl content of 186,000 mg/l produced by seawater evaporated beyond halite saturation was also calculated. The calcium, magnesium and sulfate contents determined by extrapolating the AEUB data to a chloride content of 186,000 mg/l are listed in the column titled "Brine concentration at Cl 186,000 mg/l". The results as mmol/l are also listed. The magnesium and sulfate in the evaporated brine would result in dolomitization and anhydrite precipitation when in contact with calcite. Dolomitization would produce calcium and reduce magnesium at a 1:1 ratio, and precipitation of anhydrite would remove calcium and sulfate at a 1:1 ratio. The amount of magnesium would be reduced by: (1) the amount of calcium in the formation water at 186,000 mg/l Cl minus the calcium in the residual evaporite brine; (2) the amount of sulfate in the residual evaporite brine minus the sulfate in the formation water at 186,000 mg/l Cl; and (3) the amount of magnesium in the formation water at 186,000 mg/l Cl. The mass balance equation for 1 liter of water is:

$$Mg^{2+}_{brine} - \left(Ca^{2+}_{fm.water} - Ca^{2+}_{brine}\right) - \left(SO_4^{2-}{}_{brine} - SO_4^{2-}{}_{fm.water}\right) - Mg^{2+}_{fm.water}$$

Inserting the numbers from **Table 2.5** gives:

$$1{,}400 - (735 - 0) - (468 - 1) - 188 = 8 mmol$$

The residual of 8mmol/l is insignificant to the overall calculation. The mass balance indicates that there is sufficient magnesium in the evaporated brine to account for the calcium content in the formation water and the loss of sulfate from the brine.

These results are not being proposed as a model for the extensive dolomitization of the Nisku/Arcs Formation. They merely reflect the water-rock reactions required to account for the present day composition of the fluids through reaction with an evaporated brine end-member.

The net change in porosity due to dolomitization and anhydrite precipitation can also be determined. One liter of brine would result in the production of 83cc of dolomite and the precipitation of 18.5cc of anhydrite. The resultant porosity change in a limestone with 10% porosity would be +12cc for the calcite-dolomite reaction and –18.5cc for the anhydrite precipitation giving a net change of –6.5cc or a decrease in porosity from 10% to 9.35%.

Spencer (1987) applied a mass balance approach to determine the origin of Devonian brines in central and northern Alberta. He interpreted the brines as being residual evaporative brines modified by albitization, dolomitization, and gypsum or anhydrite precipitation, followed by dilution with meteoric water (Spencer, 1987). The Devonian Nisku/Arcs Formation waters in southern Alberta appear to have a similar origin. Seawater evaporated beyond halite precipitation is interpreted to be the precursor brine. Spencer (1987) assumes bromide and chloride behave conservatively during mixing and uses the Cl/Br ratio to determine the extent of evaporation. Decreases in sodium content and increases in potassium content in formation water relative to the diluted evaporative

brine were attributed to albitization (Spencer, 1987). In southern Alberta, it appears that potentially, sodium and potassium have not been influenced by interaction with sialic rocks. Modification of calcium, magnesium and sulfate content reflects the process of dolomitization and anhydrite precipitation as described by Spencer (1987) and there may be sufficient magnesium in the evaporite brine to fully account for the high in calcium and low sulfate observed in the formation waters. Subsequent to the dolomitization and anhydrite precipitation, the formation waters have been diluted to varying degrees by meteoric water and dissolution of anhydrite and precipitation of calcite have further modified the composition.

Mississippian, Jurassic Sawtooth, Lower Mannville and Upper Mannville Aquifers

Variations in cation composition

The Mississippian, Sawtooth, Lower Mannville and Upper Mannville aquifers display similar compositions and regional distributions of dissolved constituents and will be treated as a single hydrostratigraphic group. The plots of sodium versus chloride content for the aquifers display three distinct trends recognized by a change in slope of the Na vs Cl data: Trend I lies on or near the seawater evaporation dilution curve and extends from Cl = 5,000 mg/l to >60,000 mg/l; Trend II has chloride values of 5,000 to 20,000 mg/l with higher Na concentrations; and Trend III displays high Na and low Cl (300 to 5,000

mg/l) (**Figures 2.31a, 2.31b, 2.31c, and 2.31d**). The linear nature of these trends indicates simple mixing dominates the sodium and chloride composition of the formation waters. Trend I represents the more saline waters in the west and north. The low chloride values of trend 1 are from the northeastern region, north of 51° (**Figures 2.13, 2.17, and 2.22**). Trend III waters are from the southern portion of the study area and trend II represents the narrow mixing zone between low chloride waters in the south and higher chloride waters in the north and west as seen on the chloride distribution maps. Intermediate data on the chloride diagrams (lower Na values than trend III between Cl 1,000 and 5,000 mg/l and waters with Na values that lie between trend II and trend I for Cl <20,000 mg/l) represent mixing between the lower Cl portion of trend I with waters from trend III.

The calcium, magnesium, and potassium contents, although quite variable, show several distinct features. Above 20,000 mg/l Cl, calcium is enriched relative to the seawater E-D curve (**Figure 2.32a-d**). Below 20,000 mg/l Cl, the calcium data lie above and below the E-D line. There is large decrease in Ca with decreasing chloride at less than10,000 mg/l Cl and an increase in Ca below 2,000-3,000 mg/l Cl. The majority of the magnesium values are below the seawater curve (**Figure 2.33a-d**). The magnesium content decreases linearly with decreasing chloride above 5,000-6,000 mg/l Cl and has a lower positive slope below 5,000 mg/l Cl. Potassium displays a similar trend with a steep positive slope

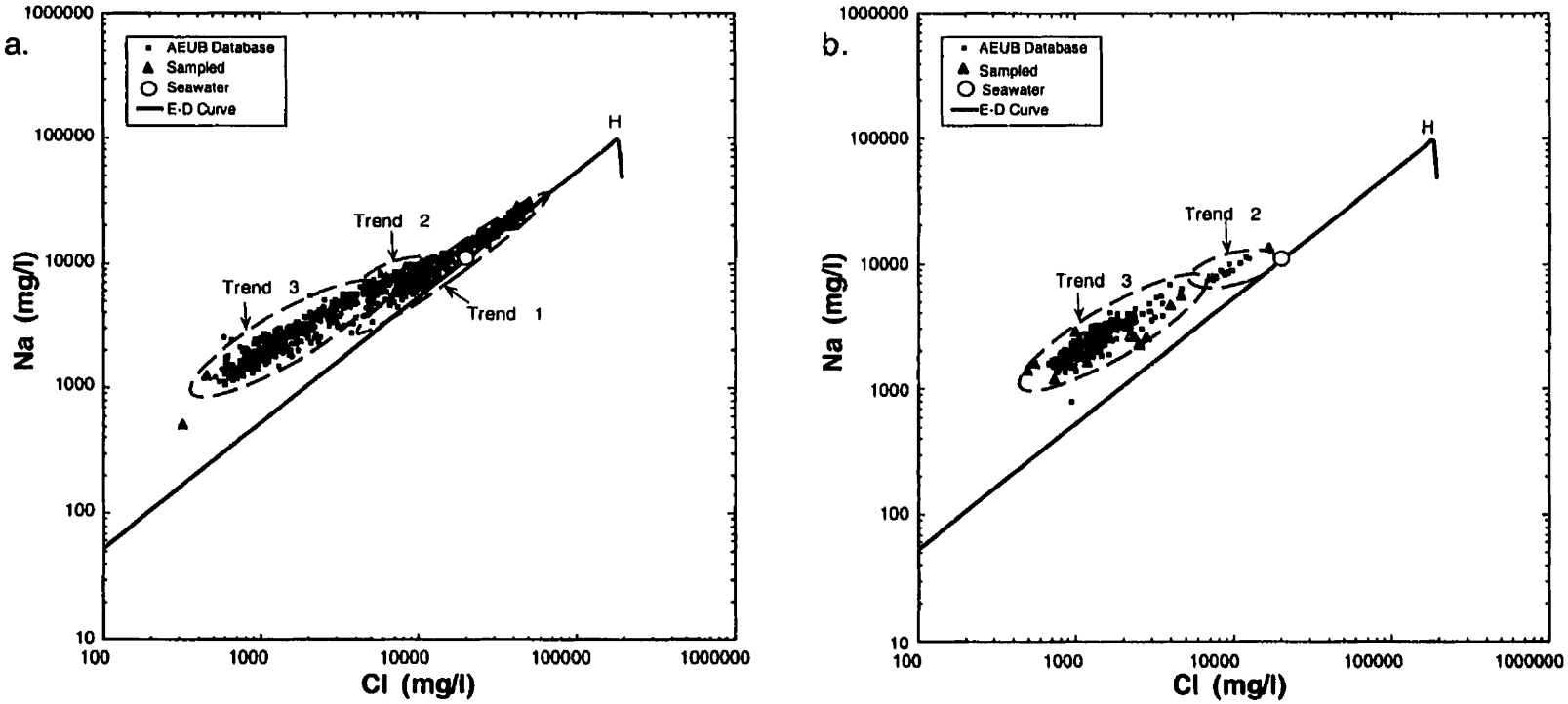

Figure 2.31a,b. Plot of the Mississippian (a) and Sawtooth (b) sodium vs chloride. The three trends, identified by slope changes, are indicated. The data point that lies close to the Seawater composition in b) is from west of 113° and corresponds to trend 1 waters. Data includes that of Hitchon et al. (1971) and Cody and Hutcheon (1994). The E-D curve is the seawater evaporation-dilution curve of Carpenter (1978). H marks the points at which halite saturation and precipitation initiates.

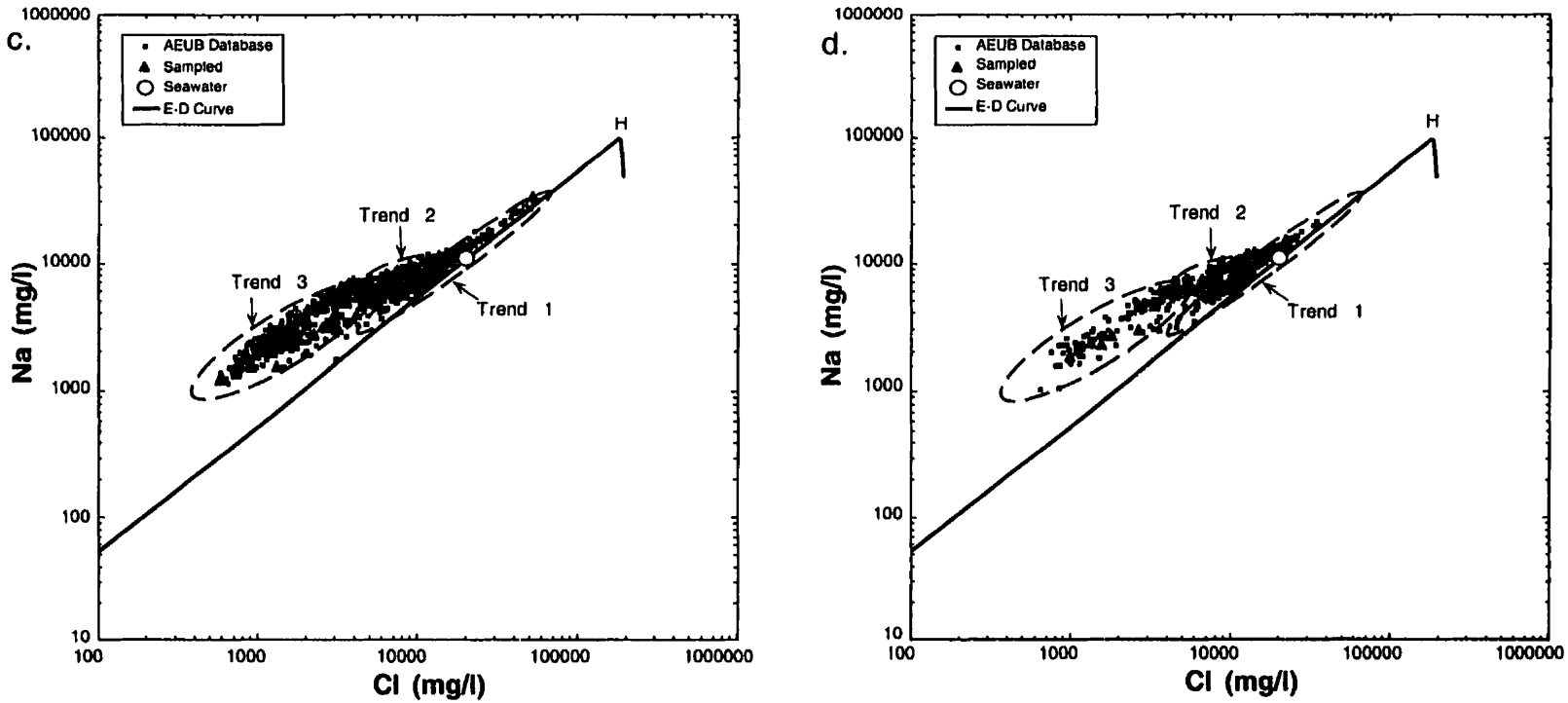

Figure 2.31c,d. Plot of the Lower (a) and Upper (b) Mannville sodium vs chloride. The three trends, identified by slope changes, are indicated. Data includes that of Hitchon et al. (1971) and Cody and Hutcheon (1994). The E-D curve is the seawater evaporation-dilution curve of Carpenter (1978). H marks the points at which halite saturation and precipitation initiates.

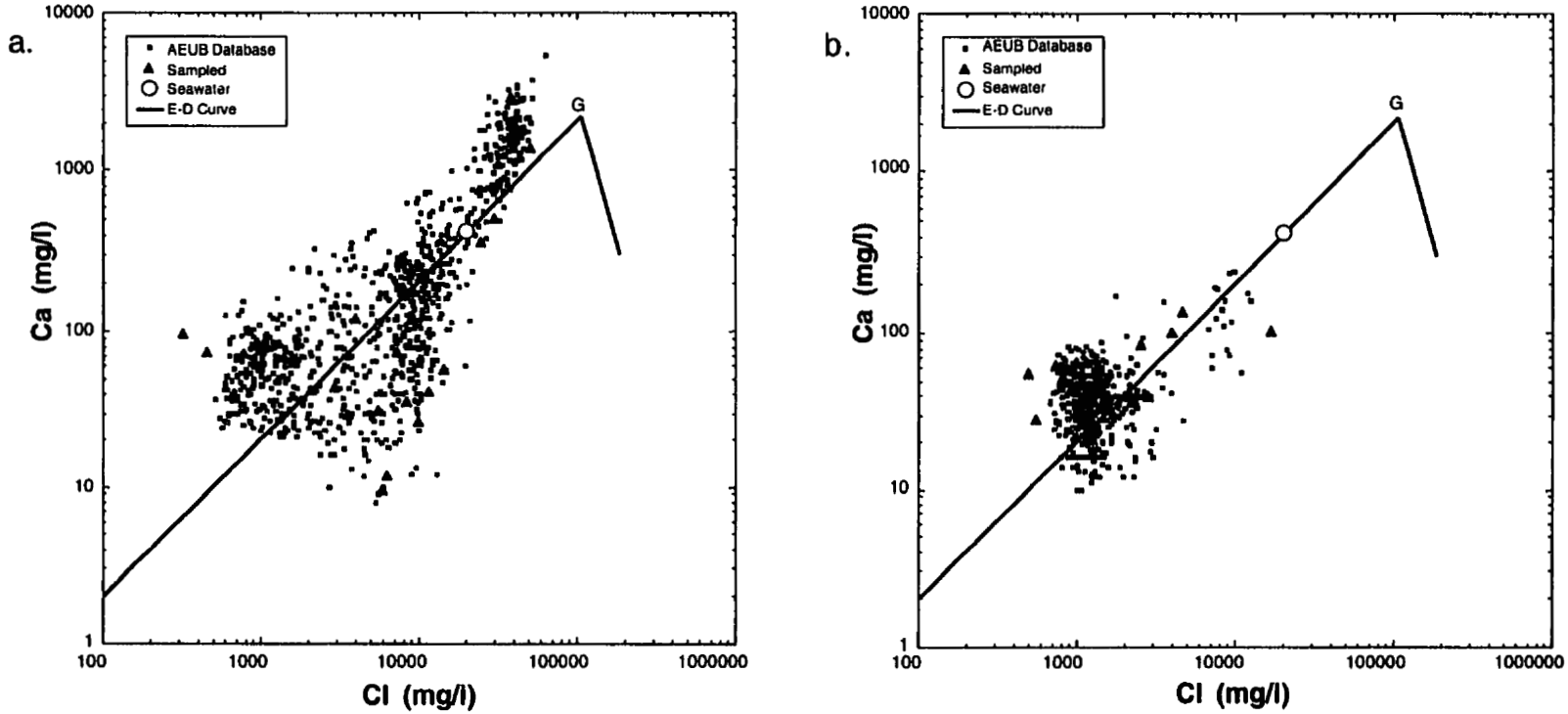

Figure 2.32a,b. Plot of the Mississippian (a) and Sawtooth (b) calcium vs chloride. Note the sharp decrease in calcium at Cl between 2,000 and10,000-11,000 mg/l in (a). Data includes that of Hitchon et al. (1971) and Cody and Hutcheon (1994). The E-D curve is the seawater evaporation-dilution curve of Carpenter (1978). G marks the points at which gypsum saturation and precipitation initiates.

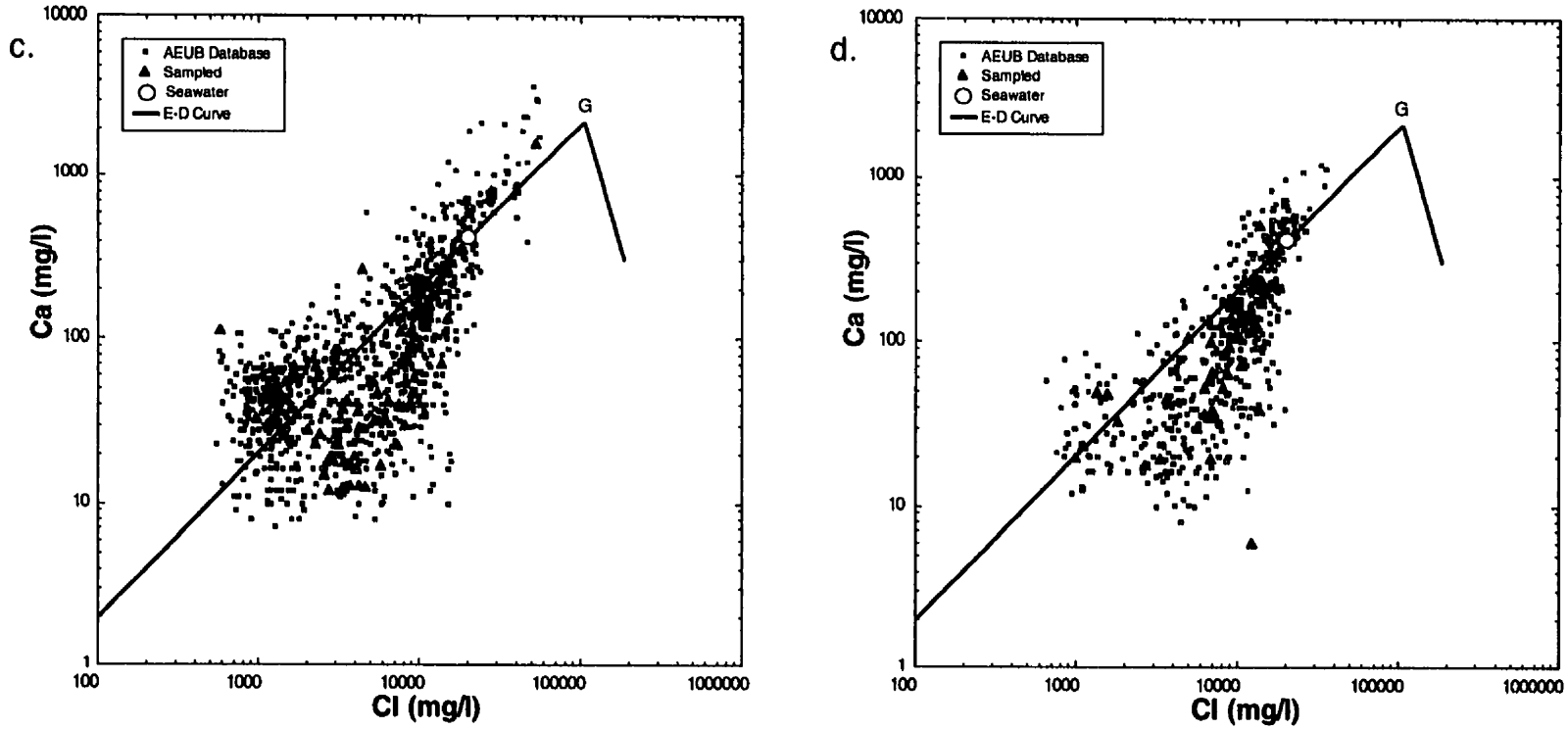

Figure 2.32c,d. Plot of the Lower (c) and Upper (d) Mannville calcium vs chloride. The Lower and Upper Mannville also show the decrease in calcium between 2,000 and 10,000-11,000 mg/l Cl. Data includes that of Hitchon et al. (1971) and Cody and Hutcheon (1994). The E-D curve is the seawater evaporation-dilution curve of Carpenter (1978). G marks the points at which gypsum saturation and precipitation initiates.

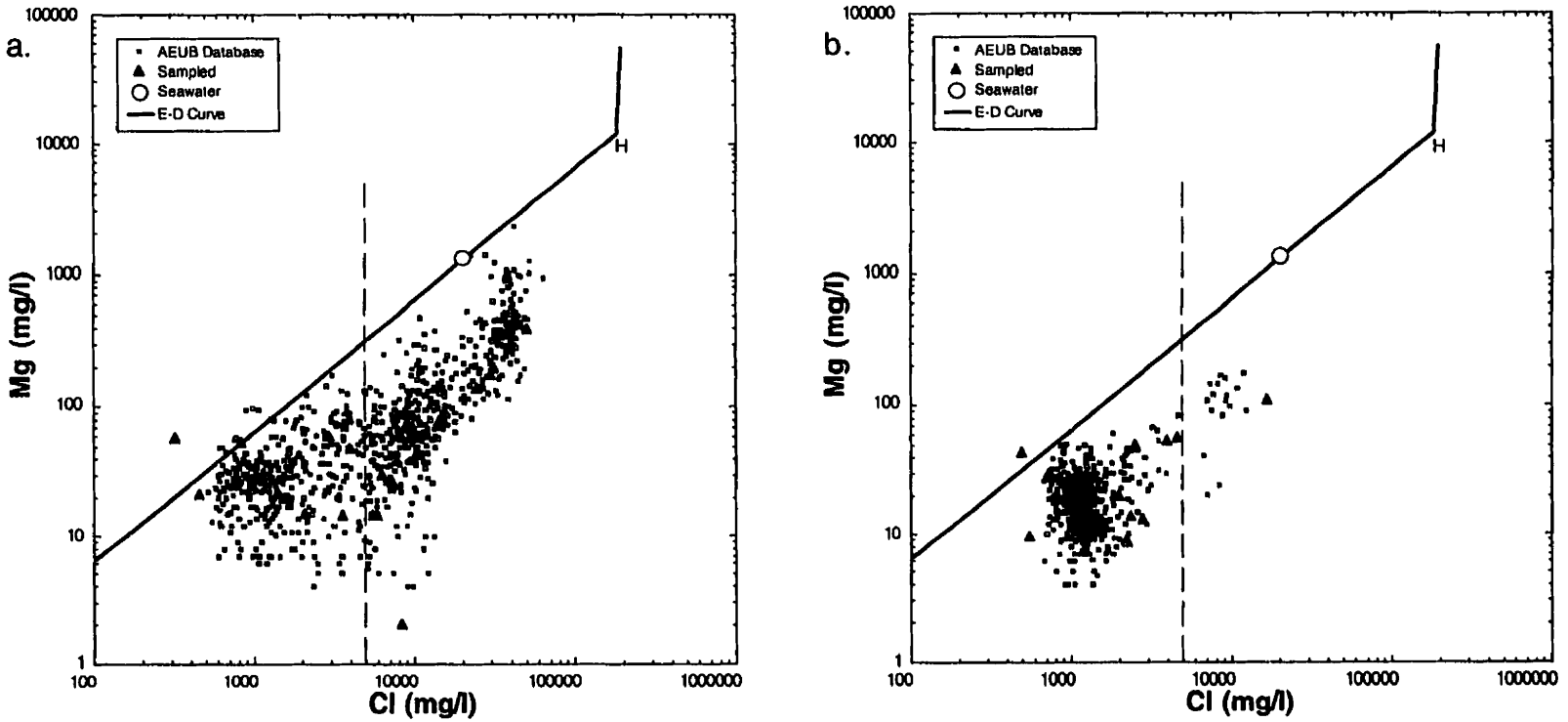

Figure 2.33a,b. Plot of the Mississippian (a) and Sawtooth (b) magnesium vs chloride. The dashed line marks the 5,000 mg/l Cl content where a change in slope of the data is interpreted to occur. Data includes that of Hitchon et al. (1971) and Cody and Hutcheon (1994). The E-D curve is the seawater evaporation-dilution curve of Carpenter (1978). H marks the points at which halite saturation and precipitation initiates.

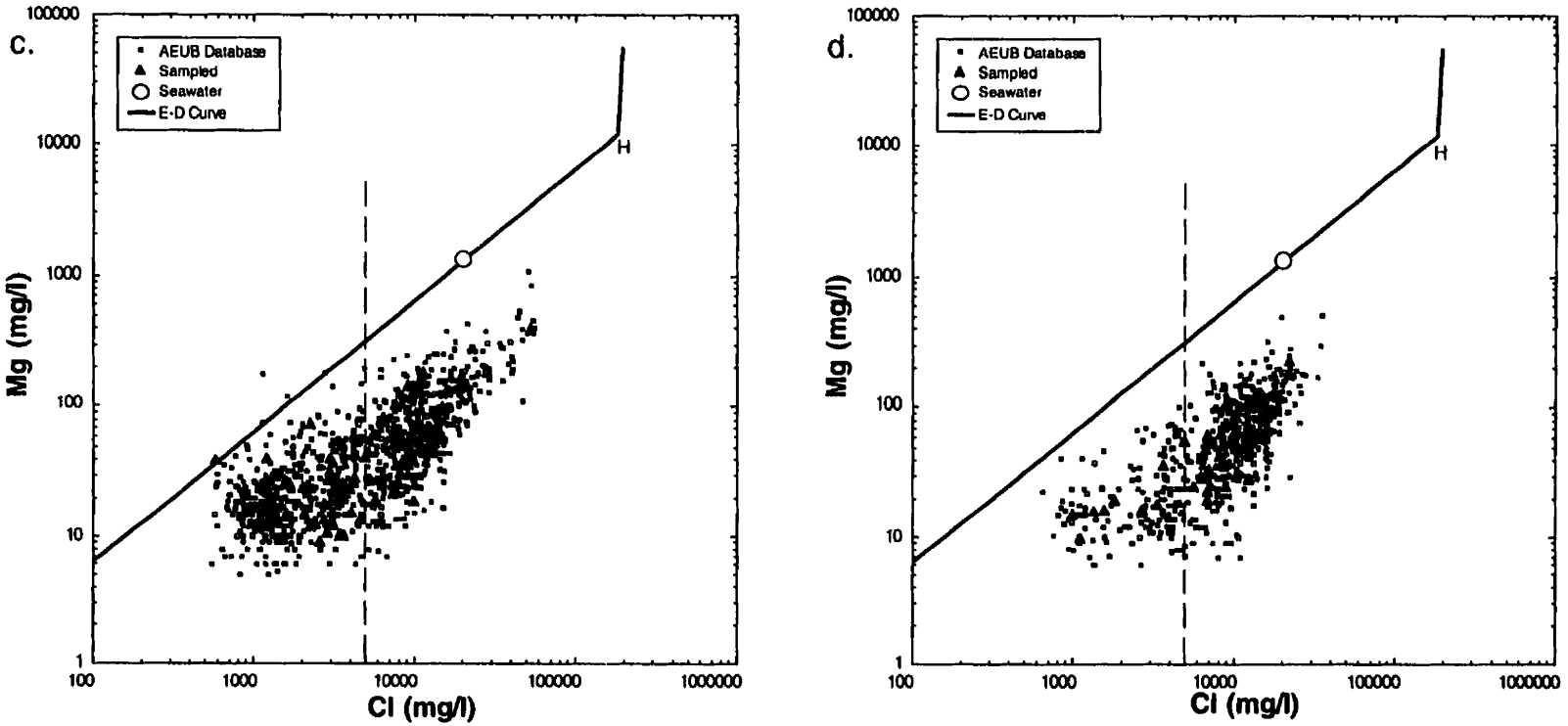

Figure 2.33c,d. Plot of the Lower (c) and Upper (d) Mannville magnesium vs chloride. The dashed line marks the 5,000 mg/l Cl content where a change in slope of the data is interpreted to occur. Data includes that of Hitchon et al. (1971) and Cody and Hutcheon (1994). The E-D curve is the seawater evaporation-dilution curve of Carpenter (1978). H marks the points at which halite saturation and precipitation initiates.

at high chloride concentrations (> 20,000 mg/l) and a lower slope at lower Cl (**Figure 2.34a-d**). The potassium data also lie above the seawater curve at lower Cl and below at higher. The variations in calcium, magnesium and potassium with chloride are complicated considerably by their aerial distribution. Trend I waters have high Ca, Mg, and K in the west and much lower values in the north, east of 113°. The result is considerable scatter on the diagrams depending on whether Trend I mixes with Trend III along the Trend II curve or below it. Mixing lines drawn on the potassium vs. chloride diagram (**Figure 2.34a-d**) suggest that potassium does behave conservatively in the context of the regional distribution whereas calcium and magnesium are subject to lithologic controls as well. Potassium content shows variations that can be explained by 3 end-member mixing. The mixing relations are perhaps best illustrated in **Figure 2.34b** where the Jurassic Sawtooth Formation does not display the low potassium content attributed to the north of 51° mixing because the unit subcrops south of 51°. The different mixing lines suggest that more than one event of meteoric water intrusion has occurred and waters in the north (Cl >~5,000 mg/l) reflect an earlier event while waters in the south reflect present day meteoric recharge.

The variations in Ca are more likely the result of water-rock interaction and are perhaps better understood in relation to the distribution of bicarbonate. At low chloride content, bicarbonate concentrations are high and increase nearly linearly with Cl. Trend II and III

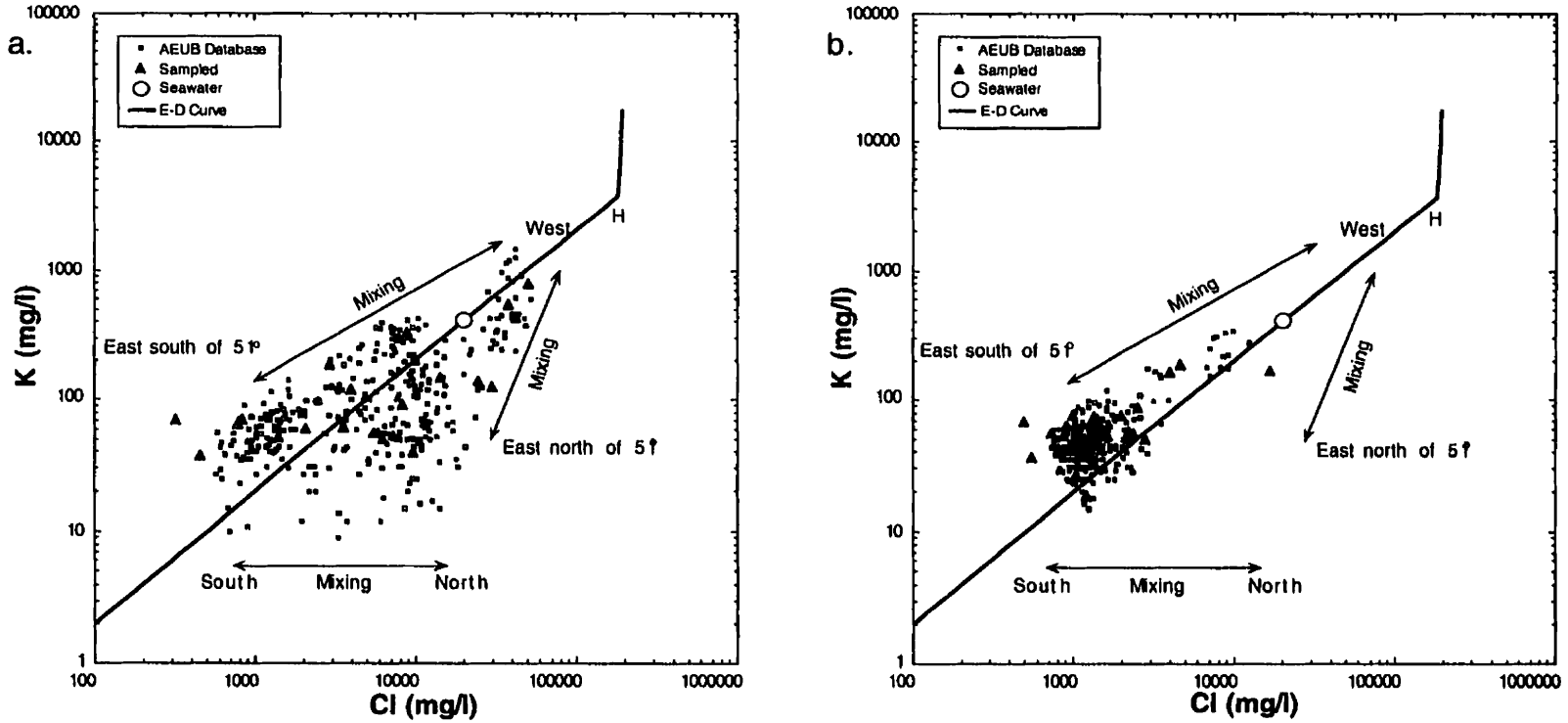

Figure 2.34a,b. Plot of the Mississippian (a) and Sawtooth (b) potassium vs chloride. Included in the plots are mixing lines showing the effect of 3 end-member mixing. Waters in the northeast tend to have lower K at higher Cl than those of the south, the result is distinct east-west and north-south compositional variations. The Sawtooth Formation subcrops in the south so only the east-west mixing for south of 51° is observed. Data includes that of Hitchon et al. (1971) and Cody and Hutcheon (1994). The E-D curve is the seawater evaporation-dilution curve of Carpenter (1978). H marks the points at which halite saturation and precipitation initiates.

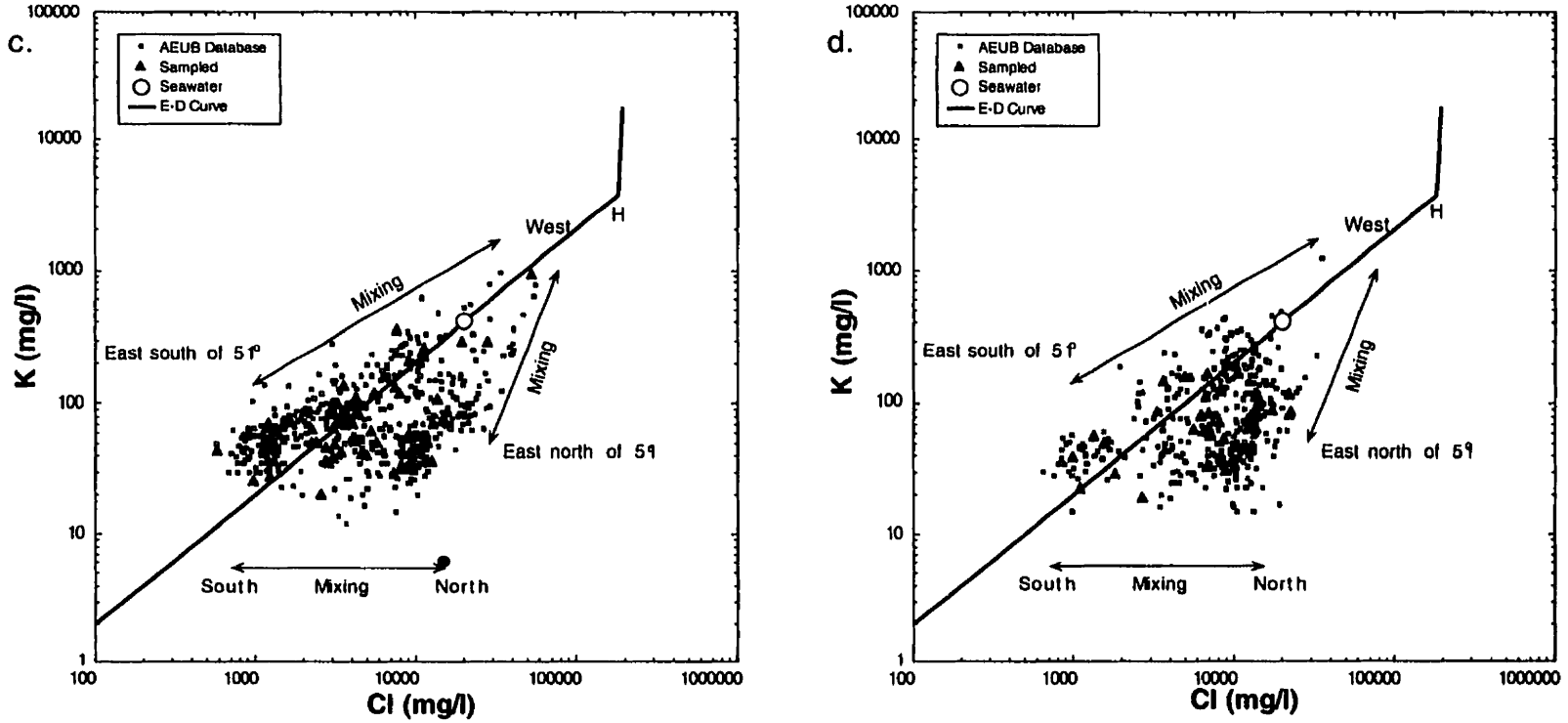

Figure 2.34c,d. Plot of the Lower (c) and Upper (d) Mannville potassium vs chloride. Included in the plots are mixing lines showing the effect of 3 end-member mixing. Waters in the northeast tend to have lower K at higher Cl than those of the south, the result is distinct east-west and north-south compositional variations. Data includes that of Hitchon et al. (1971) and Cody and Hutcheon (1994). The E-D curve is the seawater evaporation-dilution curve of Carpenter (1978). H marks the points at which halite saturation and precipitation initiates.

waters all display high bicarbonate content and Trend I waters have intermediate to low values. Bicarbonate content decreases significantly above 10,000 mg/l Cl along two paths, one at lower Cl, and the other at higher (**Figure 2.35a,c,d**). The lower HCO_3-Cl curve reflects the broad region of low Cl concentration gradient in the northern portion of the study area and the higher Cl trend reflects the region in the central and western portions of the area. The highest bicarbonate corresponds to Trend II on sodium versus chloride plot. The increase in bicarbonate observed on both the map and the concentration plot indicates that bicarbonate has been added to the formation water. The effect on calcium content is apparent from the concentration plots and **Table 2.3** with the lowest calcium corresponding to the highest bicarbonate concentrations. The sulfate plotted against chloride diagram illustrates the lack of correlation between sulfate and chloride observed on the maps (**Figure 2.36a-d**). All of the sampled waters are undersaturated with respect to anhydrite.

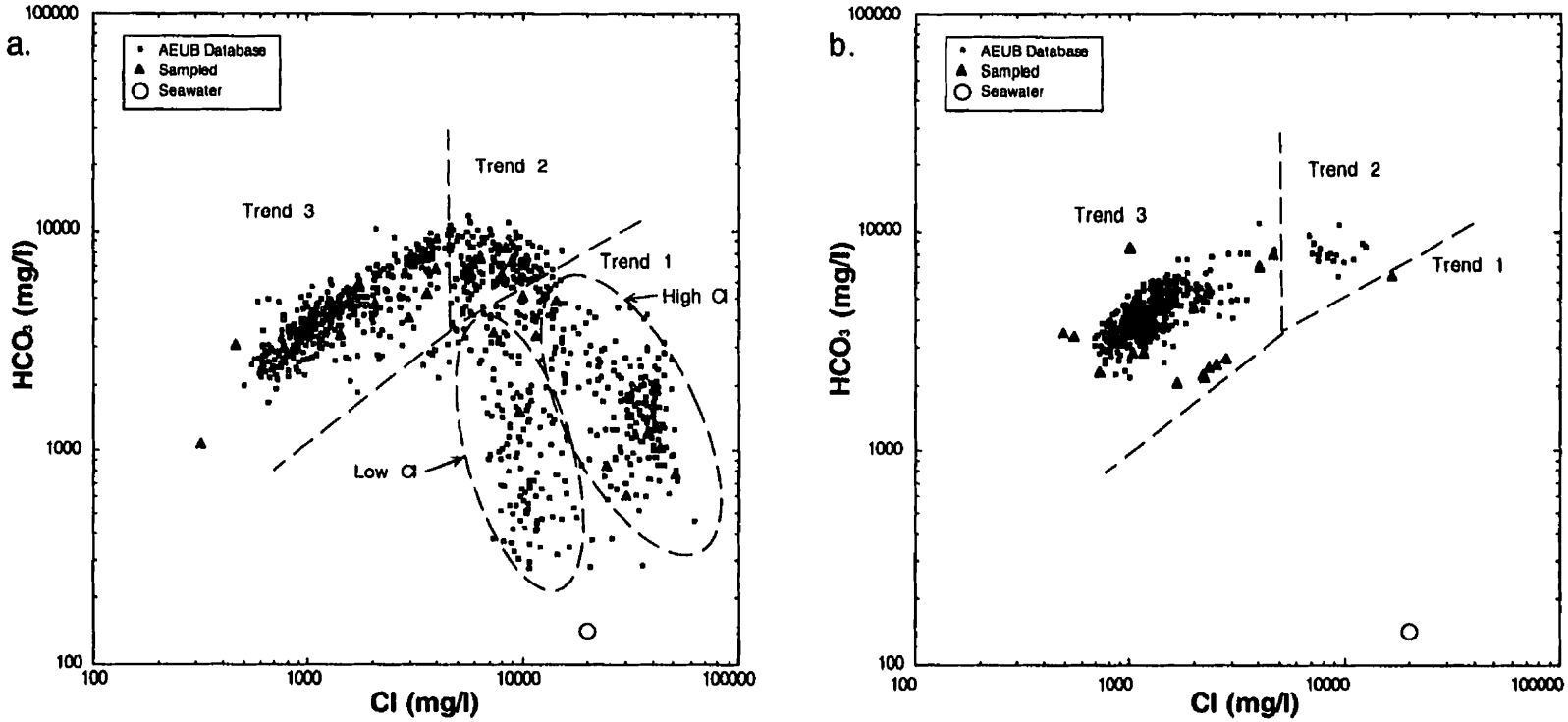

Figure 2.35a,b. Plot of the Mississippian (a) and Sawtooth (b) bicarbonate vs chloride. The trends defined in the Na vs Cl plot can be recognized on the bicarbonate vs chloride diagrams. Increasing bicarbonate with chloride in the Trend 3 waters, high bicarbonate at higher Cl in the trend 2 waters and decreasing bicarbonate with Cl in the trend 1 waters is shown. The decrease in calcium between 2,000 and 11,000 mg/l Cl is related to the increase in bicarbonate. The high and low Cl regions defined in a) are from lower Cl waters in the north of the study area and higher Cl waters in the central and western regions. Data includes that of Hitchon et al. (1971) and Cody and Hutcheon (1994).

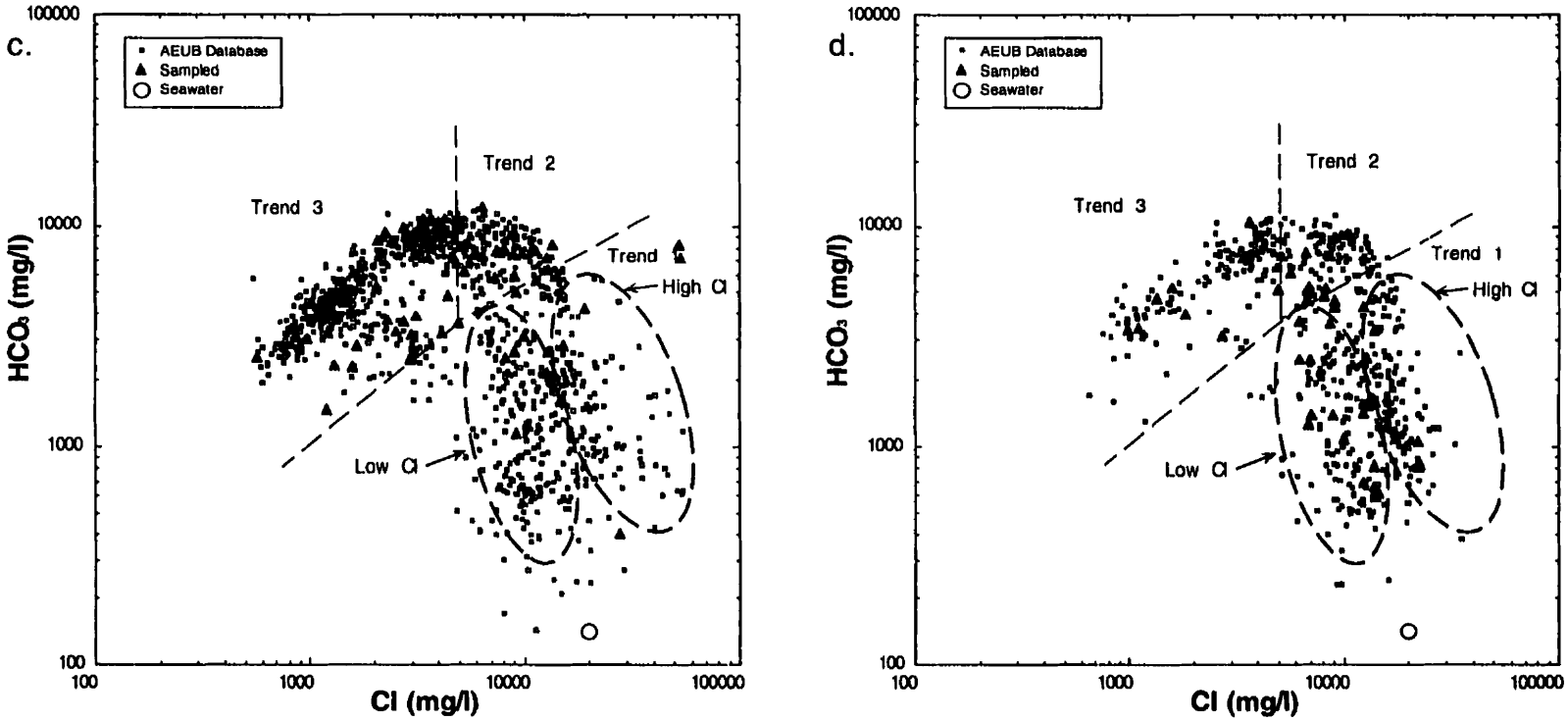

Figure 2.35c,d. Plot of the Lower (c) and Upper (d) Mannville bicarbonate vs chloride. The trends defined in the Na vs Cl plot can be recognized on the bicarbonate vs chloride diagrams. Increasing bicarbonate with chloride in the Trend 3 waters, high bicarbonate at higher Cl in the trend 2 waters and decreasing bicarbonate with Cl in the trend 1 waters is shown. The decrease in calcium between 2,000 and 11,000 mg/l Cl is related to the increase in bicarbonate. The high and low Cl regions are not as well defined as in the Mississippian, but are from similar locations. Data includes that of Hitchon et al. (1971) and Cody and Hutcheon (1994).

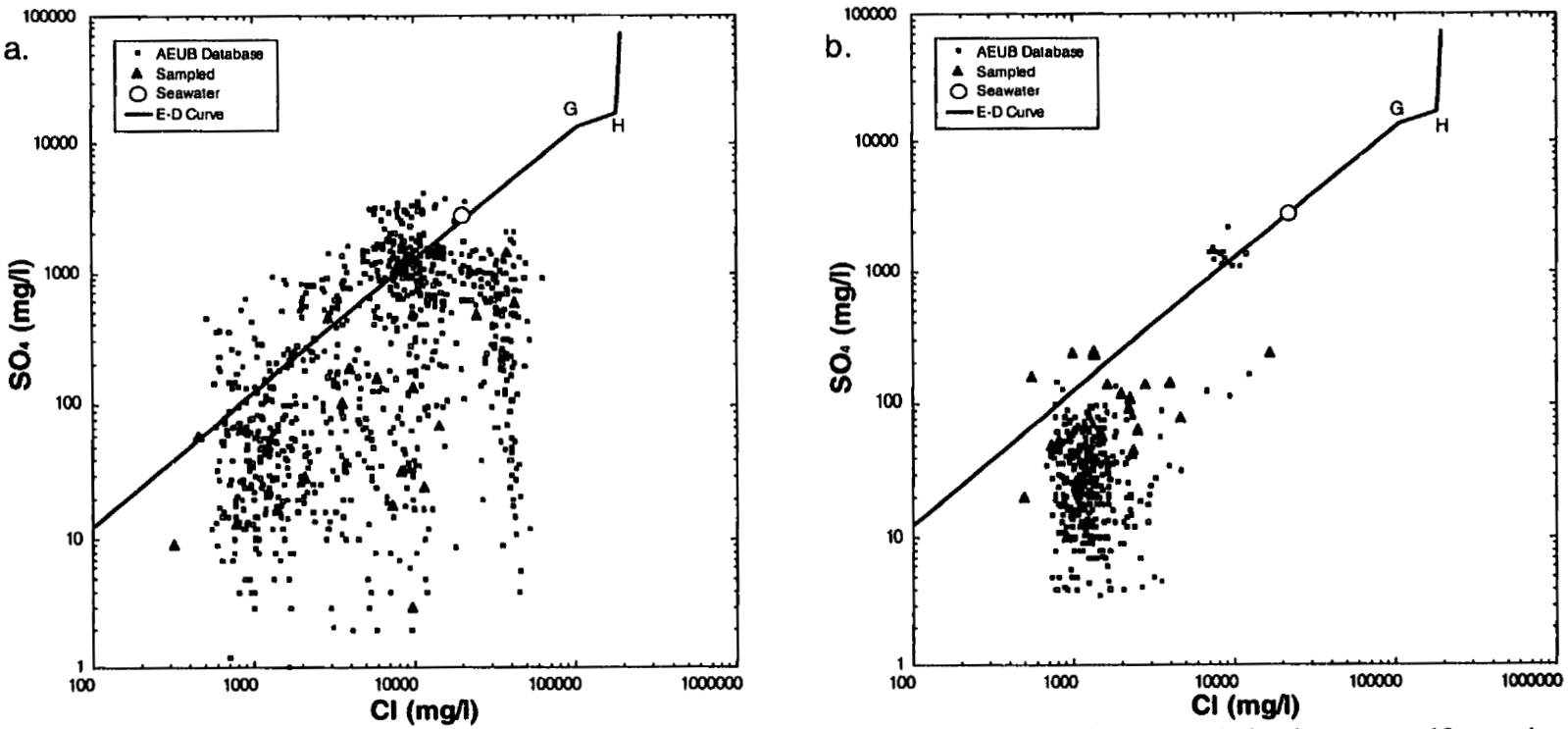

Figure 2.36a,b. Plot of the Mississippian (a) and Sawtooth (b) sulfate vs chloride. There is no correlation between sulfate and chloride except for in a) at high Cl. The high sulfate group identified in the Piper plot of the Sawtooth are also well defined. Data includes that of Hitchon et al. (1971) and Cody and Hutcheon (1994). The E-D curve is the seawater evaporation-dilution curve of Carpenter (1978). G and H mark the points at which gypsum and halite saturation and precipitation initiate.

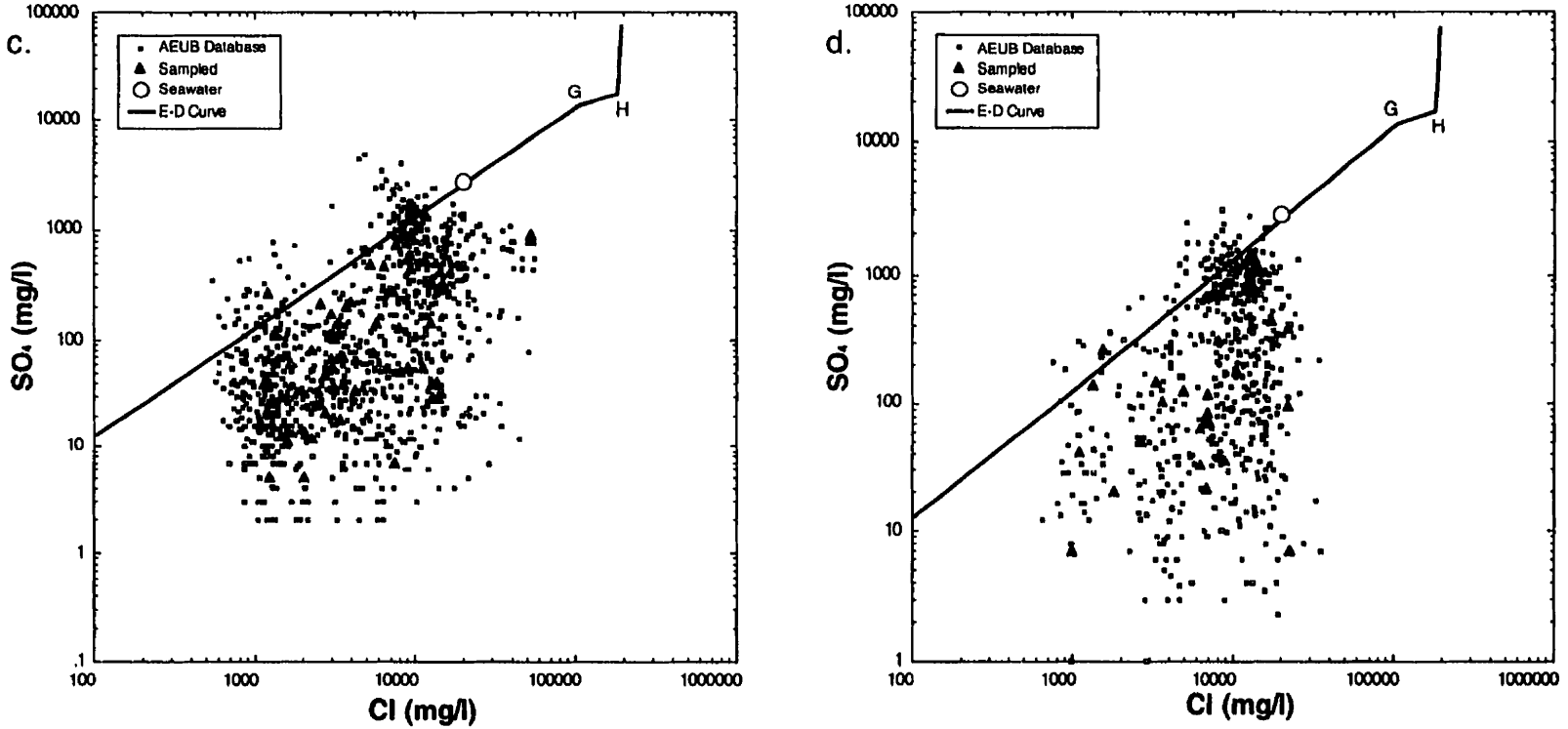

Figure 2.36c,d. Plot of the Lower (c) and Upper (d) Mannville sulfate vs chloride. There is no correlation between sulfate and chloride. Data includes that of Hitchon et al. (1971) and Cody and Hutcheon (1994). The E-D curve is the seawater evaporation-dilution curve of Carpenter (1978). G and H mark the points at which gypsum and halite saturation and precipitation initiate.

Mineralogical controls on solution composition

The change in lithology from the Mississippian carbonate to the Jurassic and Lower Cretaceous clastic rocks introduces the possibility of chemical variations that relate to interaction between fluids and aluminosilicates. By plotting mineral stability diagrams that include clay minerals and feldspars, the potential for water-rock interaction can be tested. The following diagrams include clay mineral-fluid equilibria calculated following the procedure of Aagard and Helgeson (1983) as described in the introduction to this chapter. It must be reiterated that the lines separating the fields for muscovite, paragonite, Ca-mica, or Mg-mica, and pyrophyllite, represent contours along which an aqueous solution coexists with smectite that has a fixed log $((a_{mica})^2/(a_{pyrophyllite})^3)$ (where a represents activity).

The reaction involving the muscovite and pyrophyllite end members is:

$$2KAl_2(AlSi_3O_{10})(OH)_2 + 2H^+ + 6SiO_{2(aq)} = 3Al_2Si_4O_{10}(OH)_2 + 2K^+ \qquad 6$$

(muscovite) (pyrophyllite)

The equation for equilibrium (6) on an activity-activity diagram is given by:

$$\log(a_{K^+}/a_{H^+}) = 3\log a_{SiO_2(aq)} + \log a_{misc.} - 1.5\log a_{pyroph.} - 0.5\log K$$

where K is the equilibrium constant for equilibrium (6). Changes in the activities of muscovite or pyrophyllite and the effect of temperature on K result in changes in the y-intercept and a corresponding up or down shift in the curve. In the following diagrams,

the activity of pyrophyllite is set by the smectite analogue chosen. Mica activities are determined using the smectite exchangeable cation composition calculated using the program PHREEQC, as described in the introduction. The diagrams contain two smectite curves, the first is calculated at 25°C and pressure according to the measured reservoir pressures at the lowest temperatures, and the second is at the highest temperature and pressure for the sampled waters. Calcium, magnesium and potassium mica activities at low temperatures were found to show a range of up to an order of magnitude because of variations in the composition of the water. At a given temperature, the exchangeable cation composition is dependent on the concentration of the cation in the aqueous phase and on the total concentration of the aqueous solution (Appelo and Postma, 1996). A water with similar Na/K ratios but with different ionic strengths will result in different exchangeable cation compositions of the clay mineral (or exchanger) because of the selectivity of the exchanger is greater at low total concentrations. There is also a difference in the exchangeable cation composition of an exchanger for waters with differing cation ratios but similar ionic strengths. The mica activities show a range in values because of this dependence of the exchanger composition on the composition and ionic strength of the water.

The value selected for the activity-activity diagram is either the lowest or the highest mica activity for the low temperature samples. On a phase diagram, a decrease in the

activity of a component in a phase results in an increase in the size of the stability field of the phase. An example of the low and high activity effects at 25°C on the equilibrium curve is given in **Figure 2.37**. The result is that the water data, if in equilibrium with smectite of similar octahedral and tetrahedral site occupancy as the analogue, should plot on or below the curve when the highest mica activity was chosen and on or above the curve when the lowest mica activity was chosen (the equilibrium curves essentially define a "stability field" of the smectite at a particular temperature). In general, the highest activity was used for the cation-hydrogen activity ratio vs dissolved silica diagrams so the data should plot on or below the curve. The highest temperature samples should plot on or near the high temperature curves.

Laumontite was chosen as the calcium aluminosilicate phase over anorthite for two reasons: (1) laumontite and plagioclase are difficult to distinguish in thin section and laumontite has been recognized in Mannville Formation equivalent rocks (Ghent and Miller, 1974); and (2) anorthite as a component in the plagioclase solid solution can be represented using the activity of the component, and even at very low activity ($a=10^{-3}$) does not plot on the activity diagrams.

The relationship between the aqueous solutions and aluminosilicates is illustrated in **Figures 2.38-2.42**. The carbonate hosted Mississippian aquifer waters (**Figure 2.38**) do not show a significant correlation to the aluminosilicate mineral phase stability

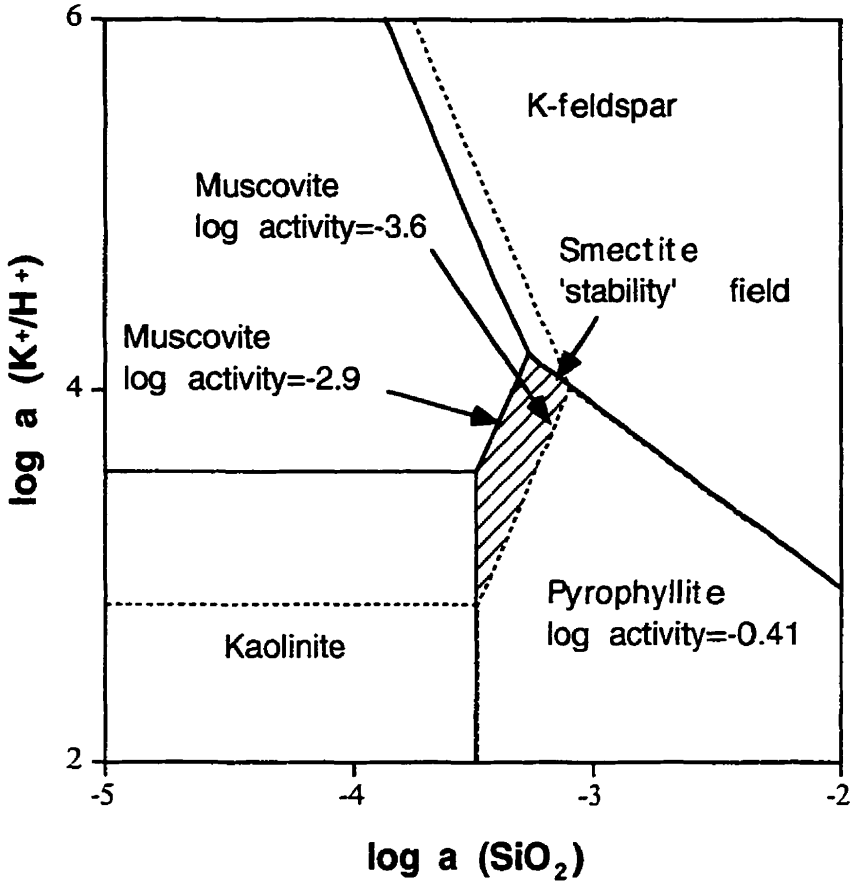

Figures 2.37. An example of a log activity-activity plot showing the stability of smectite, kaolinite and K-feldspar at 25°C and 100 bar. The diagram shows the change in the muscovite stability field as the calculated muscovite activity varies when the exchangeable cation composition of the smectite analogue varies. The highest muscovite activity (-2.9) is represented by the solid line and the lowest activity is the dashed line. A series of water data, used to calculate the exchangeable cation composition and therefore the mica activity, in equilibrium with smectite at 25°C, should fall on or between the lines. In the diagrams used below, the highest mica activity will generally be used so water data should plot on or below the line marking pyrophyllite stability (in this case musc. log a = -2.9).

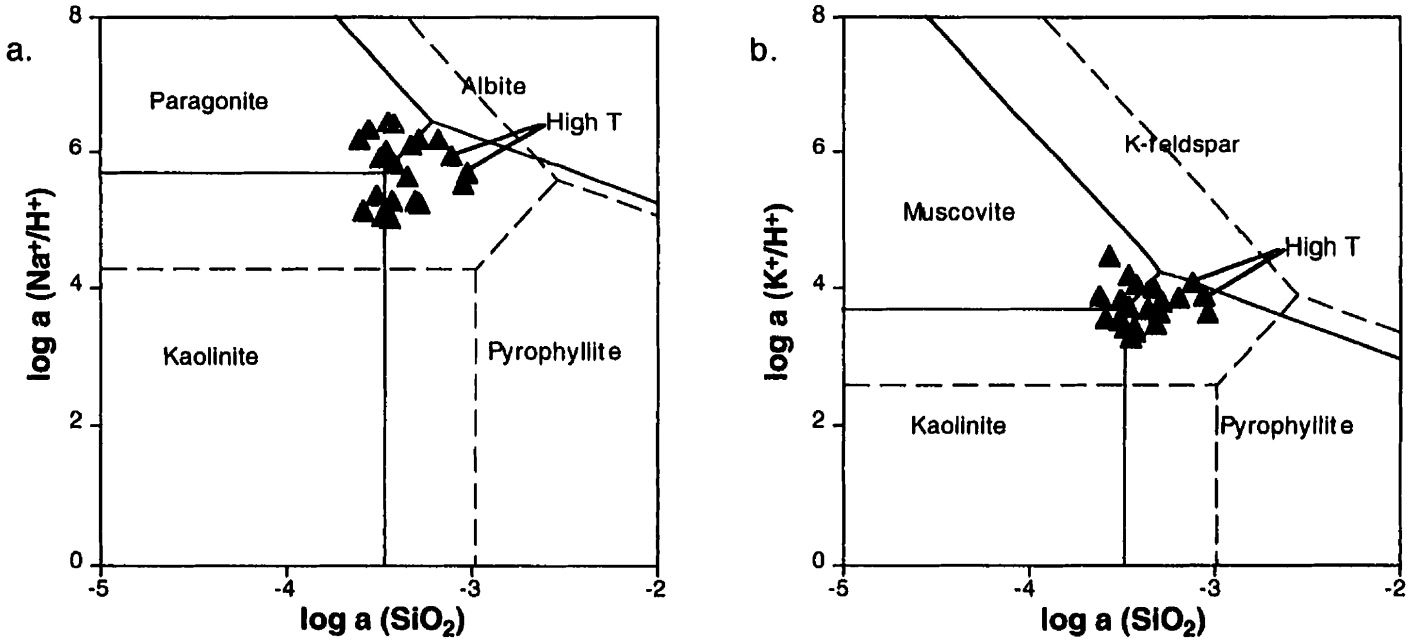

Figures 2.38a,b. Log activity-activity plots showing the stability of aluminosilicate phases at temperatures and pressures of 25°C and 100 bar (solid line), and 75°C and 200 bar (dashed line). The triangles represent the Mississippian aquifer waters. The data do not show a strong correlation to the phase boundaries, particularly at high temperatures. The high T data should plot on or near the high T boundaries if smectite is influencing the water chemistry.

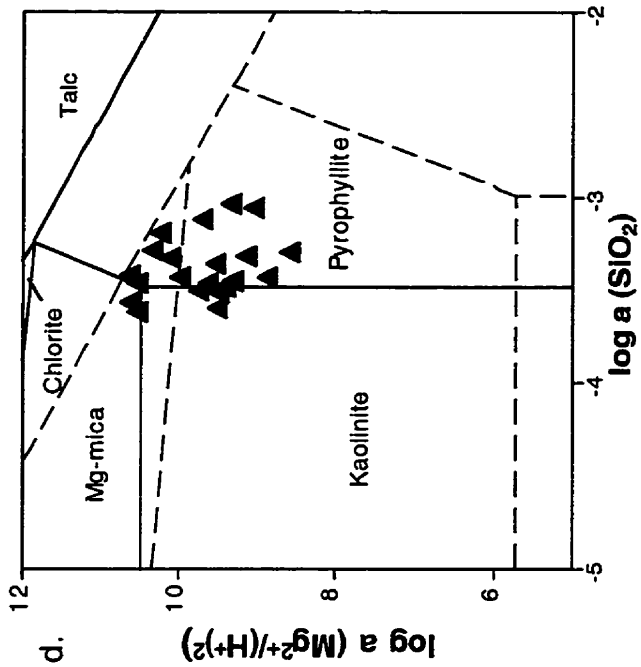

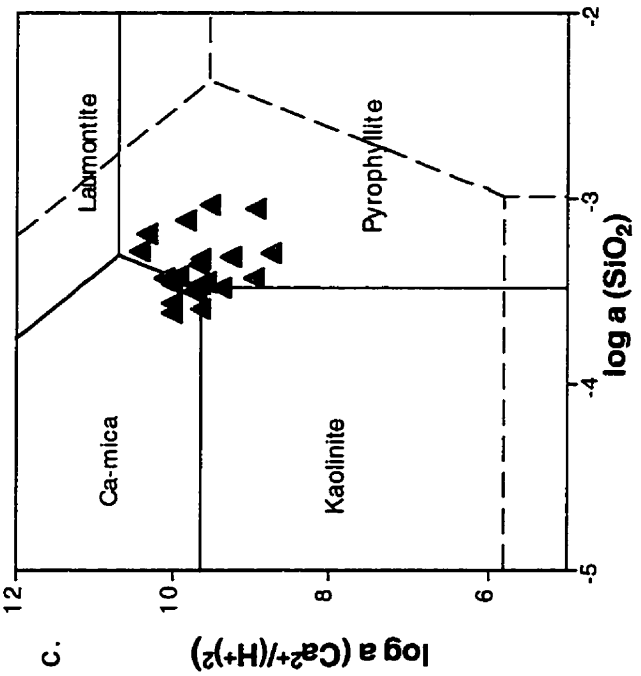

Figures 2.38c,d. continued.

boundaries in the diagrams. The Mississippian aquifer consists predominantly of carbonates and anhydrite with few silicate minerals and equilibrium with aluminosilicate mineral phases is not expected. Moreover, the smectite analogue is Cretaceous in age and it cannot be expected to be representative of detrital clay in Mississippian-aged rocks. The waters hosted in clastic rocks appear to display a close relationship to the clay mineral stability boundaries. The data from the waters collected in this study fall on, or below, the 25°C curves and the high temperature data are reasonably close to the high T curves. The implication is that a clay mineral of composition similar to the Belle Fourche montmorillonite analogue may be in equilibrium with the water. This implies that smectite is present in the rocks and has come to metastable equilibrium with the pore waters.

Visual inspection of Jurassic Sawtooth, Lower Mannville and Upper Mannville thin sections and data from James (1985), Wood (1990), and Cody (1993) indicate that clay minerals do occur (<1-5%) predominantly as smectite and mixed layer smectite-illite with minor amounts of kaolinite. There appears to be equilibrium between kaolinite, smectite and the fluid in some of the samples (data that plot near the kaolinite stability field). Kaolinite is observed in a number of thin sections but, as the water data imply, does not occur in the majority of the samples. Relatively little feldspar is recognized in the Sawtooth, Lower Mannville and Upper Mannville Glauconitic aquifers of southern

Alberta (Potocki and Hutcheon, 1992; Cody, 1993). The majority of water data in **figures 2.39-2.41** do not plot close to the smectite-feldspar, smectite-laumontite or smectite-talc-chlorite phase boundaries, and it can be assumed that these phases do not react significantly with pore waters to influence solution chemistry. **Figure 2.42** illustrates the relationship between the water composition and the albite-K-feldspar stability boundaries. At low T and high T the data do not plot near the smectite-feldspar boundaries.

If the dominant control on cation content is mixing with dilute meteoric waters then from equation 6, clay minerals may exert some control on the pH and silica activity. A plot of silica activity versus temperature **(Figure 2.43)** shows that silica content does not fall on the saturation curves of quartz, chalcedony or alpha-cristobalite. The silica activities are generally higher than silica polymorph saturation for many of the samples and fall between chalcedony and amorphous silica saturation. The highest silica activities are from the western portion of the study area at high (>65°C) and lower (35°C) temperatures. The elevated silica activities fit the prediction of the smectite solid solution equilibrium model both through the effect of temperature and compositional changes. Equation 6 indicates that as the cation activity increases, the pyrophyllite activity and pH should decrease and mica and silica activity should increase. The mica activities are 1.5 to 2.5 orders of magnitude lower than the pyrophyllite activity, thus only a very small

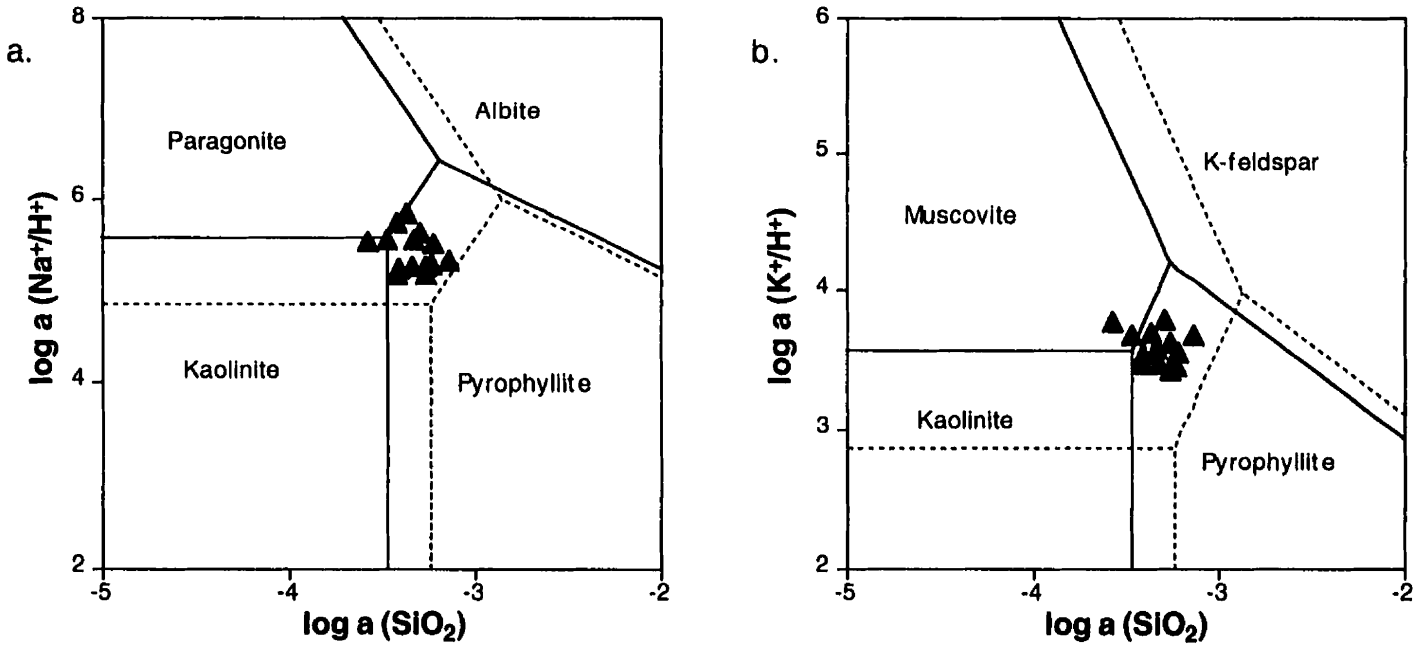

Figures 2.39a,b. Log activity-activity plots showing the stability of aluminosilicate phases at temperatures and pressures of 25°C and 100 bar (solid line), and 45°C and 120 bar (dashed line). The triangles represent the Sawtooth aquifer waters. The majority of data plot within the range defined by the low T and high T smectite stability boundaries. Some of the data plot on or near to the smectite-kaolinite phase boundary suggesting equilibrium between smectite and kaolinite is influencing the water composition.

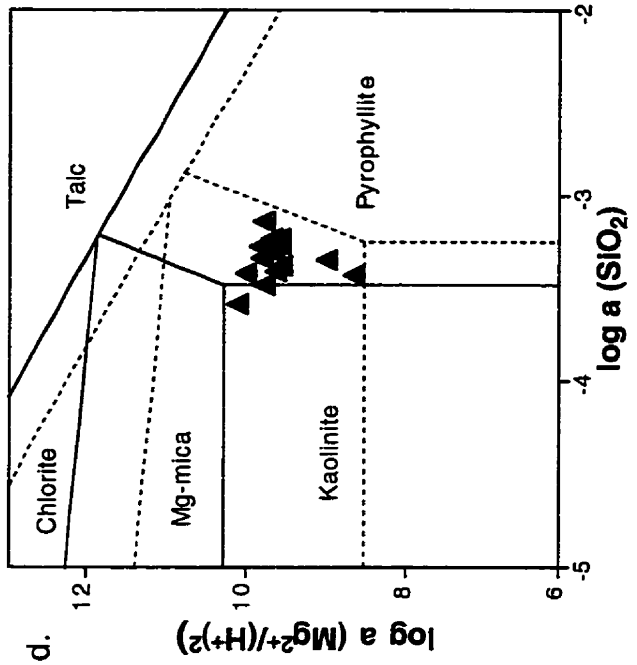

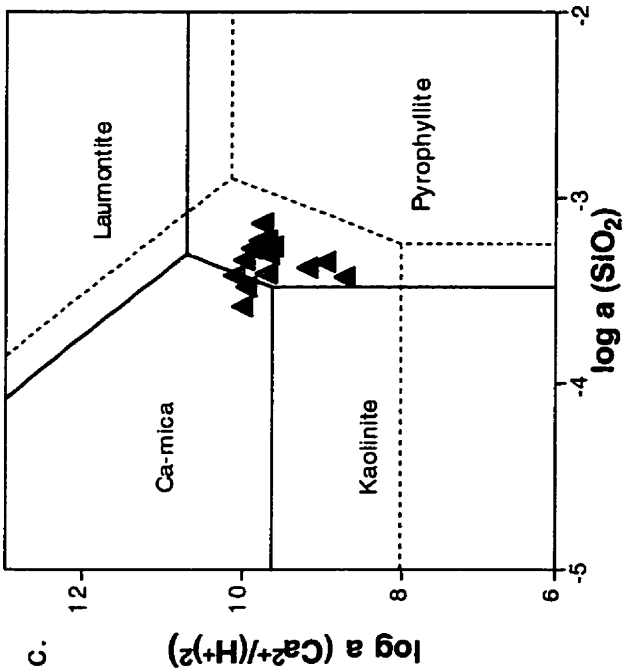

Figures 2.39c,d. continued.

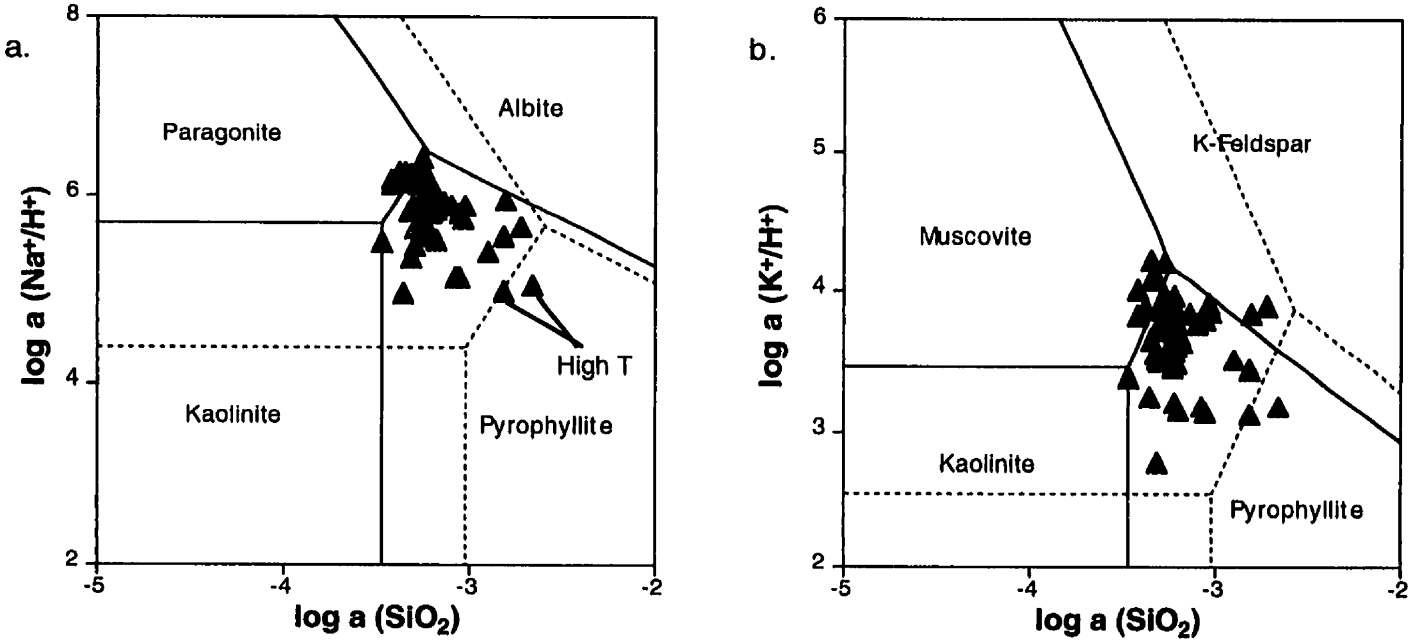

Figures 2.40a,b. Log activity-activity plots showing the stability of aluminosilicate phases at temperatures and pressures of 25°C and 100 bar (solid line), and 70°C and 200 bar (dashed line). The triangles represent the Lower Mannville aquifer waters. The Lower Mannville data fall on or near the smectite analogue stability boundaries at low and high temperatures. Some of the data lie near the albite-smectite, K-feldspar-smectite and laumontite-smectite as well as the kaolinite-smectite phase boundaries.

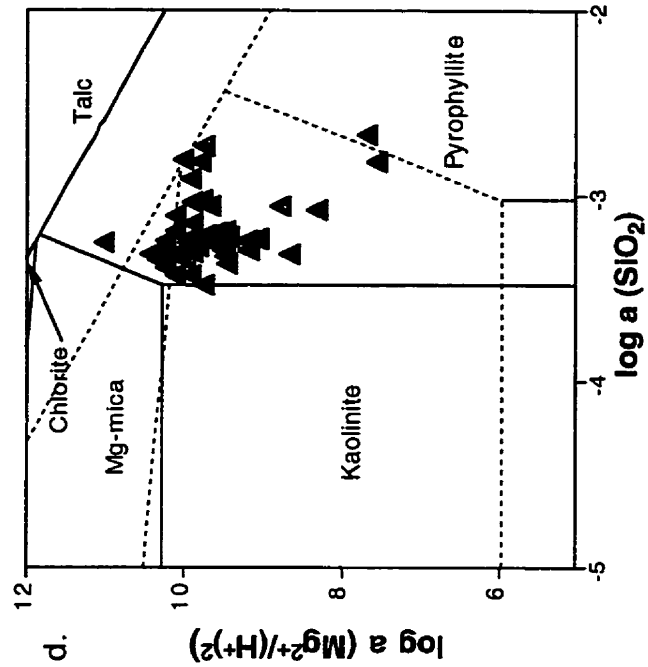

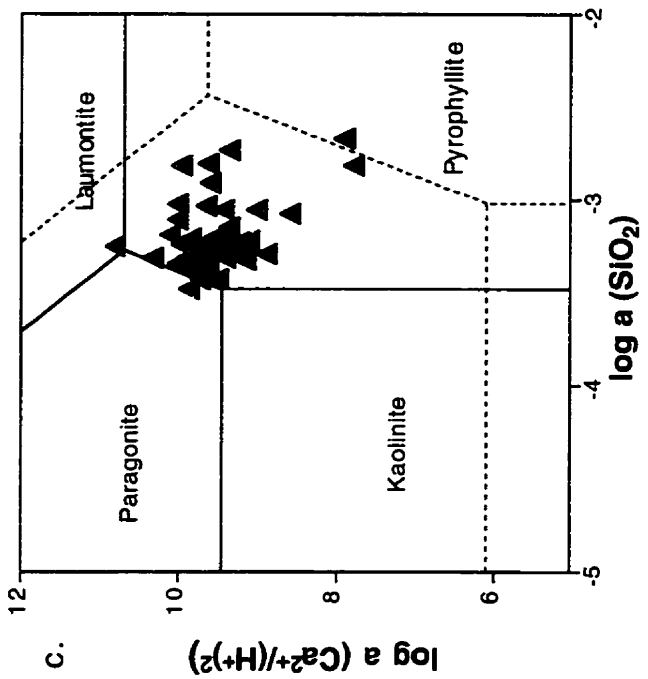

Figures 2.40c,d. continued.

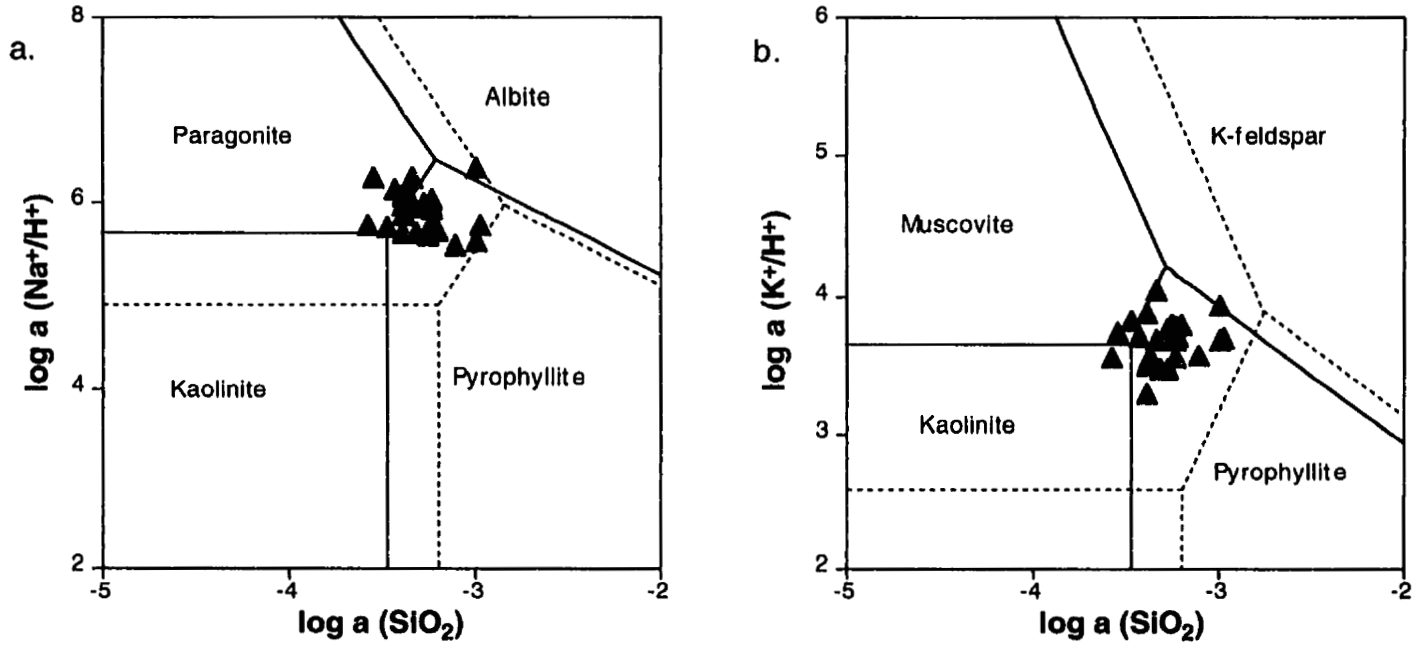

Figures 2.41a,b. Log activity-activity plots showing the stability of aluminosilicate phases at temperatures and pressures of 25°C and 100 bar (solid line), and 50°C and 130 bar (dashed line). The triangles represent the Upper Mannville aquifer waters. The data correlate reasonably well with the smectite analogue stability boundaries. The high T data do not plot near the high T curve, but the majority of the waters plot within the range of mica activities at reservoir temperature.

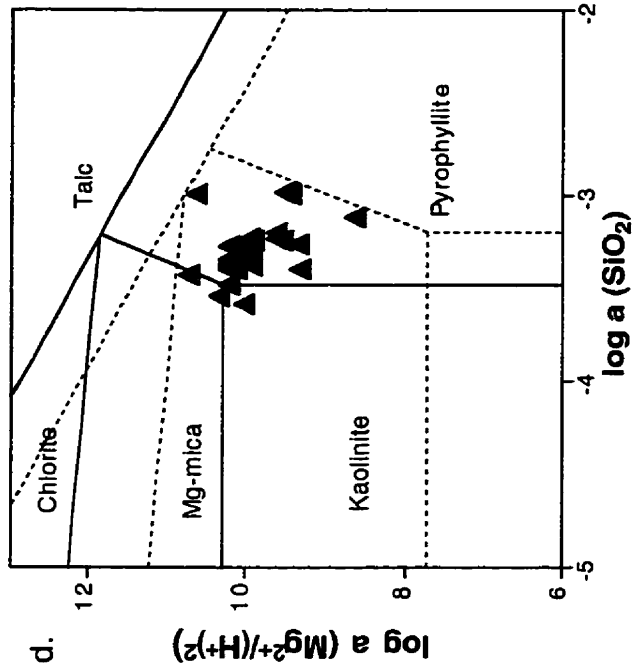

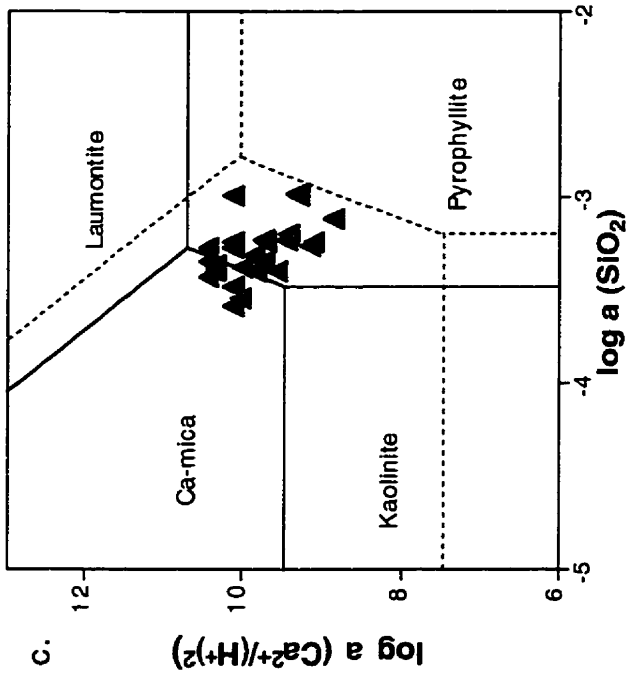

Figures 2.41c,d. continued.

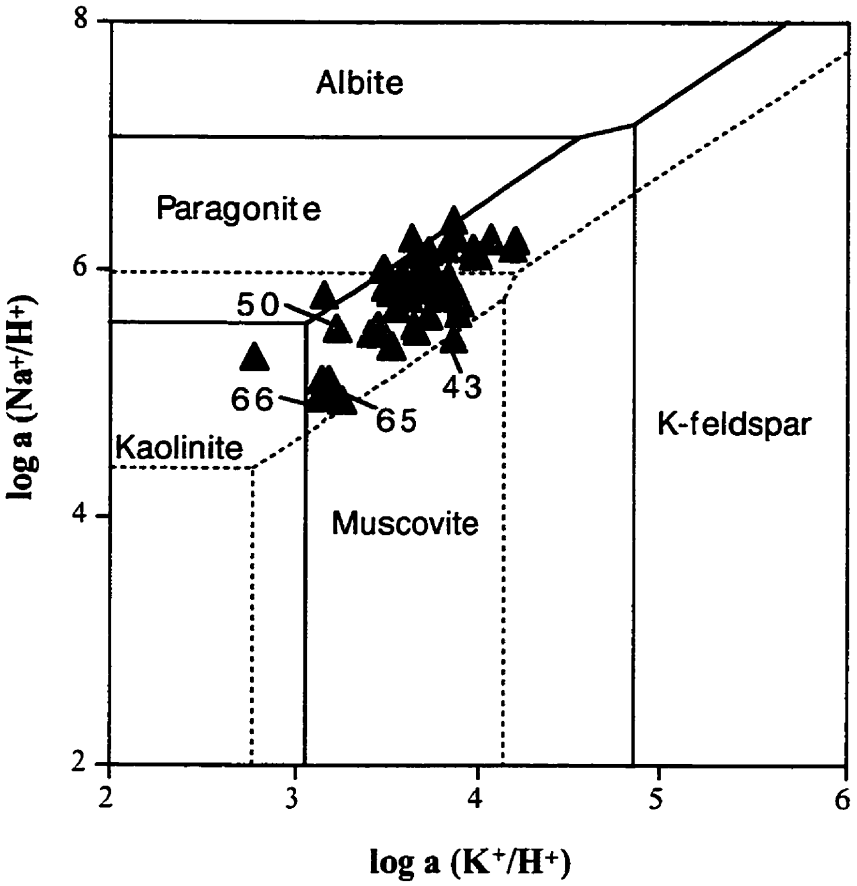

Figures 2.42. Plot of the log activity (Na^+/H^+) vs log activity (K^+/H^+) for the aluminosilicate phases shown at 25°C, 100 bar (solid line) and 70°C, 200 bar (dashed line). Water data is from the Lower Mannville aquifer. The waters do not plot near the feldspar stability boundaries in this diagram and the data plot over a wider range than that defined by the albite-K-feldspar equilibrium between 25 and 70°C. The highest T samples (T given on the diagram) plot well below the stability boundaries. The data do, however plot in the area defined by the smectite analogue coexisting with an aqueous solution. Log activities used in the diagram are at 25°C Paragonite=-1.7, Muscovite=-3.4, Silica=-3.4 and at 70°C Paragonite=-1.8, Muscovite=-2.9, Silica=-2.7

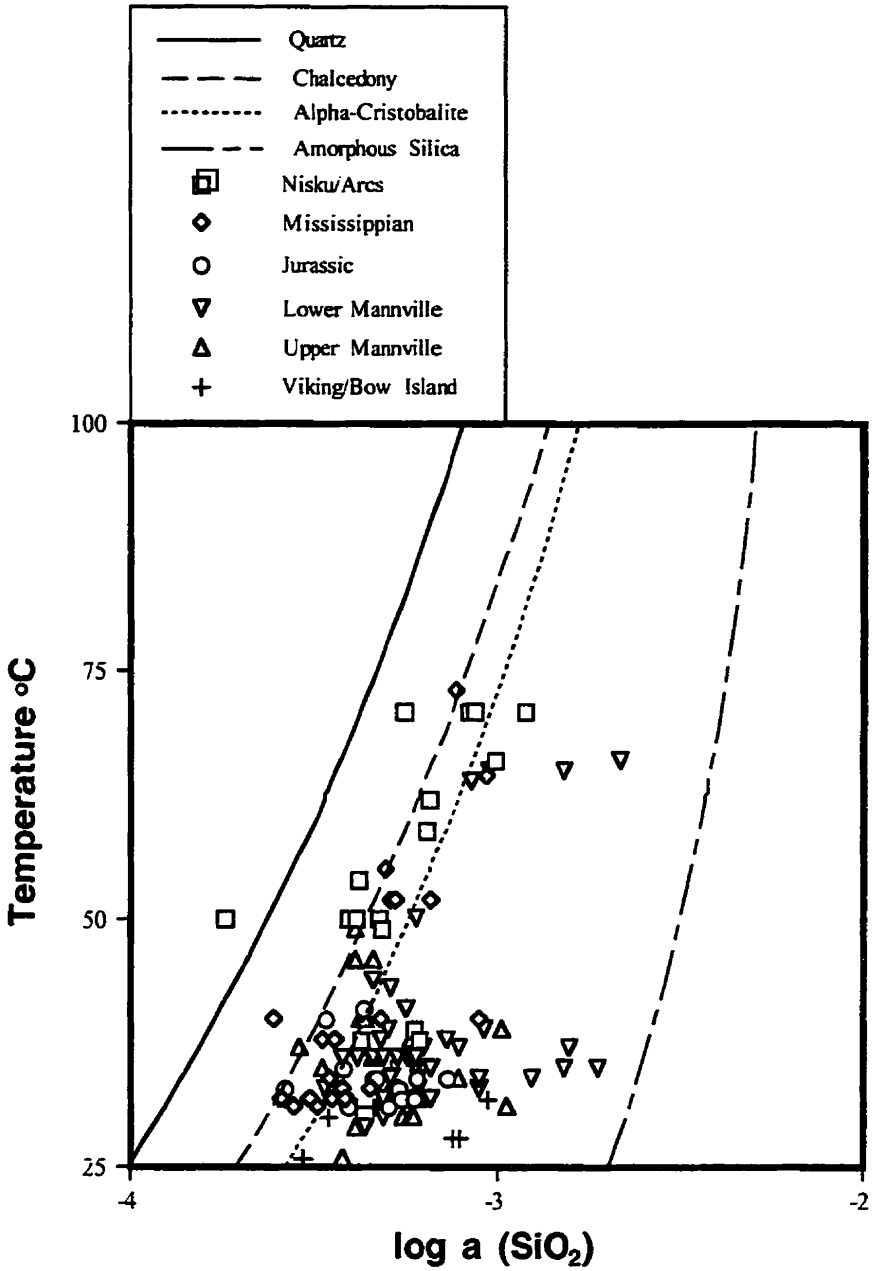

Figures 2.43. Temperature vs log activity of dissolved silica plot. The majority of the data plot between alpha-cristobalite and amorphous silica saturation. It can be seen from this diagram that the silica activity of the clastic-hosted waters tend to be higher than those of the carbonate-hosted waters.

change in the pyrophyllite activity is required to compensate for changes in the cation and silica content observed. Silica activities in excess of quartz saturation in marine sediments containing smectite and K-feldspar have long been recognized (Tardy and Garrels, 1974). Mackenzie and Garrels (1965) measured elevated silica activities in experiments in which different clay minerals were submersed in seawater and allowed to equilibrate over an extended period of time. In fact, the silica content of seawater in contact with montmorillonite was 4 to 8 times greater that of than kaolinite, chlorite, illite, or muscovite after only 6 months (Mackenzie and Garrels, 1965). Aagard and Helgeson (1983) used phase relations to determine that at temperatures below 200°C, smectite is not stable in aqueous solutions that are saturated with respect to quartz. Abercrombie *et al.* (1994) propose that the smectite to illite reaction may in fact be the result of the reduction in silica activity as the quartz SiO_2 polymorph becomes stable. Using a number of data sources they point out that at low temperatures in the presence of smectite, aqueous silica activities are high and choosing a silica polymorph to define the aqueous silica activity is problematic. The results of this study and Abercrombie *et al.* (1994) indicate that at low temperatures, silica activity may be largely controlled by the presence of smectite.

The relationship between the calcium and magnesium content of the Mississippian to Upper Mannville aquifers can be determined by plotting activity diagrams similar to

those plotted for the Devonian aquifer. Formation waters are undersaturated with respect to anhydrite, therefore only the dolomite reaction needs to be taken into consideration. **Figure 2.44a-d** shows the relationship between fluid composition and calcium-magnesium mineral equilibria. The majority of the Mississippian data plot on the calcite-dolomite curve (**Figure 2.44a**). The data that plot below the curve are from the mixing zone between low and higher Cl waters (**Figure 2.13**). Precipitation of calcite is the most likely process to account for the decrease in calcium. In carbonate host rocks, the addition of CO_2 to the aqueous phase results in calcite dissolution due to the decrease in pH. However, mixing of bicarbonate-rich, low calcium waters with higher calcium, low bicarbonate fluids can produce oversaturation and precipitation of calcite (Runnels, 1969). The mixing zone in the study area represents just such an environment. Formation water with high calcium content mixes with bicarbonate-rich water. The net result is that in carbonates some calcite precipitation occurs as evidenced from **Figure 2.32 and 2.35**. In the clastic aquifers (**Figures 2.44b,c,d**) the majority of the data plot below the calcite-dolomite equilibrium curve. Calcite precipitation through mixing may also be taking place, however reactions between the silicate minerals and an aqueous solution can buffer pH (Smith and Ehrenberg, 1989; Hutcheon and Abercrombie, 1990; Hutcheon *et al.*, 1993) and have to be considered. Hutcheon and Abercrombie (1990)

suggest the reaction between kaolinite and smectite regulates the a_{Na^+}/a_{H^+} of a fluid via the equilibrium:

$$Na^+ + kaolinite \Leftrightarrow Na - smectite + H^+ \qquad 7$$

The activity diagrams (**Figures 2.39-2.41**) indicate that equilibrium between smectite and kaolinite in several of the samples exists, suggesting pH may be buffered by an equilibrium similar to equation 7. In samples where kaolinite is not noted to occur, equation 6 indicates that with dilution, pH should increase as the smectite end-member reaction favours the right hand side as the cation (Na, K, Ca, Mg) activity decreases. If pH is increased by aluminosilicate equilibria, calcite precipitation will result. In clastic rocks containing clay minerals or other pH buffers, calcite will precipitate until equilibrium at the buffered pH is reached. Waters in the Jurassic, Lower Mannville, and Upper Mannville aquifers are interpreted to have migrated into the units from the Mississippian. The majority of sampled waters from the Mississippian aquifer indicate that calcite-dolomite equilibrium is being approached and is influencing the water chemistry. It can be assumed that prior to flow into the clastic aquifers, waters had calcium to magnesium activity ratios that reflected calcite-dolomite equilibrium. Equilibria like 6 and 7 are potential pH buffers in the clastic aquifers and decreases in calcium activity relative to the calcite-dolomite equilibrium curve are interpreted to be the result of calcite precipitation in a pH buffered system.

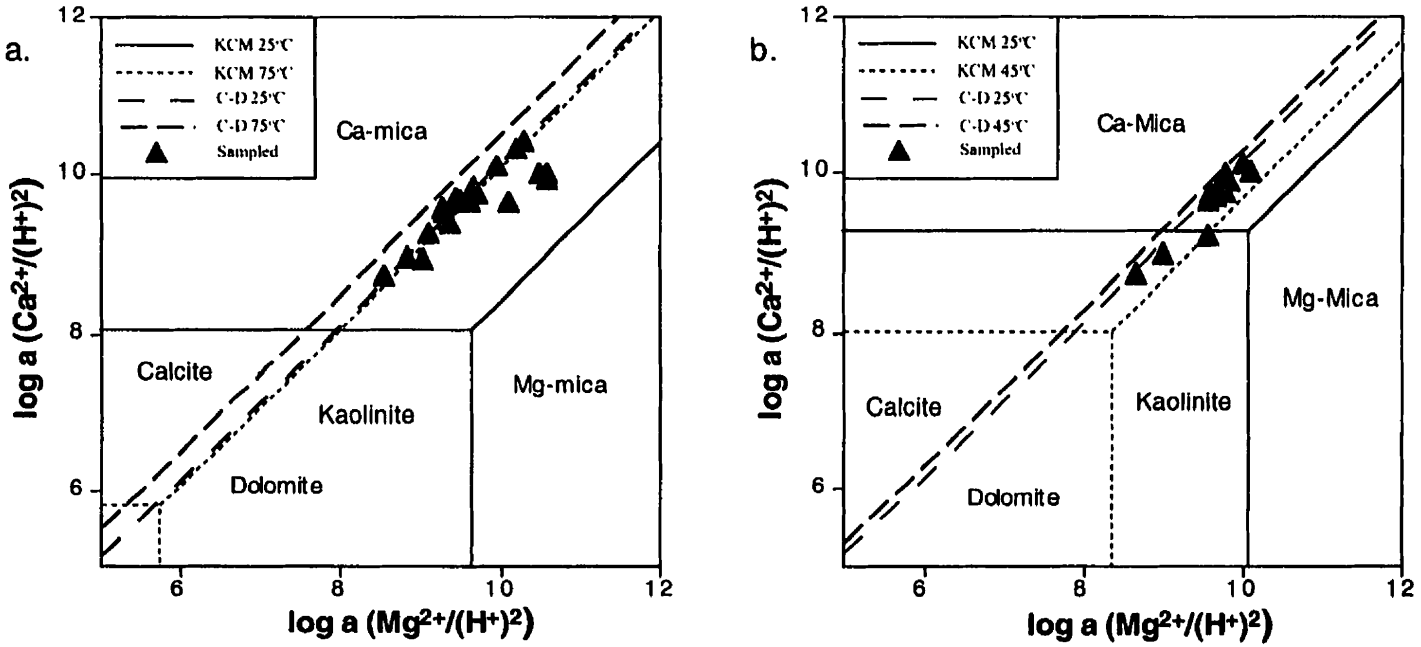

Figures 2.44a,b. Log activity-activity plots showing the stability of aluminosilicate phases and calcite-dolomite at temperatures shown. The triangles represent the Mississippian aquifer waters in (a), Sawtooth aquifer waters in (b), Lower Mannville aquifer waters in (c) and Upper Mannville aquifer waters in (d). KCM refers to the kaolinite-Ca mica-Mg mica phase boundaries at the given T, and C-D refers to the calcite-dolomite boundary at the given T. The C-D lines are the diagonal lines that span the diagram and the calcite and dolomite stability fields encompass the upper and lower portions of the diagram respectively.

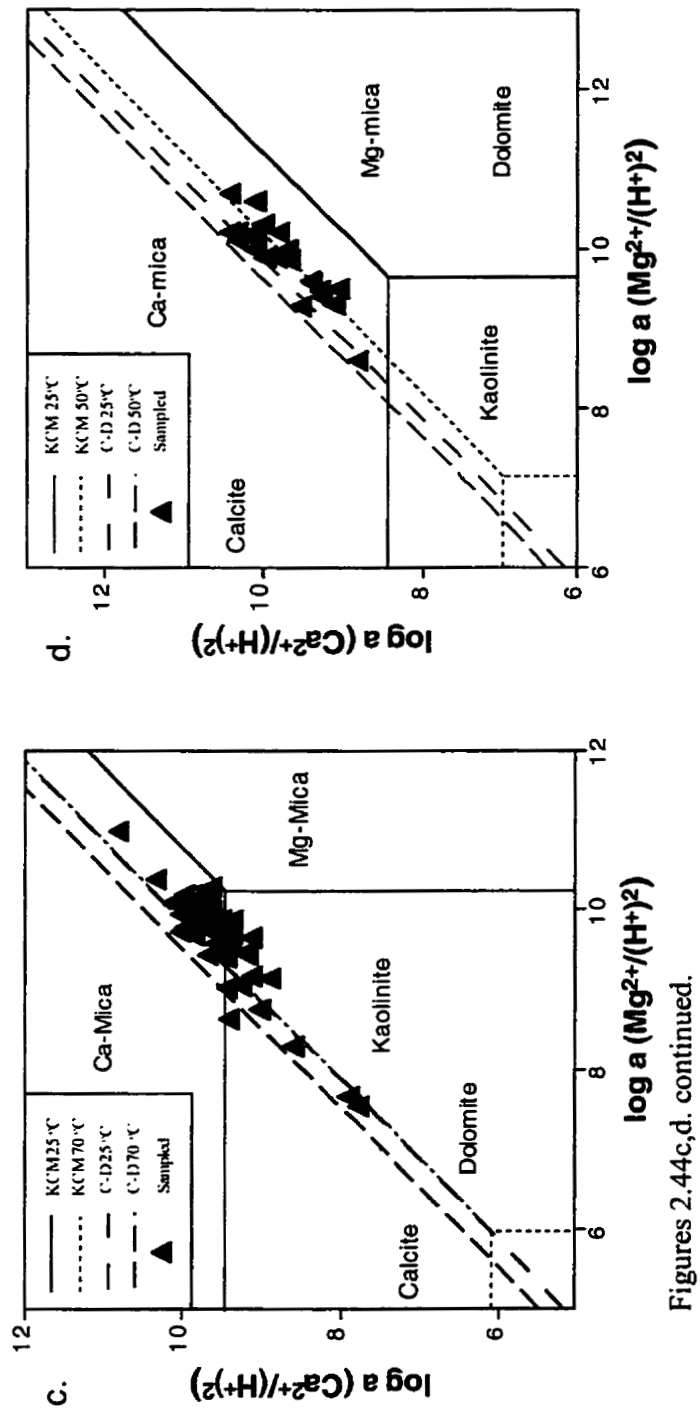

Figures 2.44c,d. continued.

Origin of Mississippian to Upper Mannville aquifer waters

Chloride content in excess of seawater indicates two possible sources for the high salinity waters. Halite dissolution would result in high sodium and chloride content, but the high potassium content at greater than seawater chloride and the lack of proximal halite deposits makes this unlikely. An evaporative marine brine origin, similar to that suggested for waters in the Devonian, is more probable. There are several possible compositions of the brine end member. A potential restriction on the degree to which evaporation proceeded is that the sodium data lie on the evaporation-dilution curve, and halite saturation may not have been achieved. Unfortunately, mass balance does not provide any other constraints on the Mississippian- to Lower Cretaceous-hosted brine end-member. However, the regional geology does perhaps allow for a qualitative interpretation. The Mississippian strata of southern Alberta was extensively eroded prior to deposition of the Jurassic and again prior to and during deposition of the Lower Cretaceous. It is unlikely that formation waters present prior to the erosion events would have survived a near complete flushing of the system by freshwater. The underlying Devonian aquifers do contain saline brines and the brine end-member of the Mississippian and younger units may be related to the Devonian hosted brines. Connolly et al. (1990b) interpreted the saline formation waters of Mississippian, Jurassic and

Lower Cretaceous aquifers of central Alberta to be genetically related to Devonian formation waters. It appears that a similar conclusion is valid for southern Alberta.

Viking/Bow Island Aquifer

Variations in major ion composition

The Na-Cl data for the Viking/Bow Island aquifer lie on the seawater evaporation-dilution curve (**Figure 2.45a**). The linear correlation of sodium with chloride suggests that mixing between seawater and dilute meteoric water is the dominant control on sodium content. Calcium content ranges from compositions approximating seawater to below the seawater curve at lower Cl (**Figure 2.45b**). The data display a steeper slope at higher Cl (> 8,000 mg/l) and a lesser slope at lower Cl concentrations. Magnesium and potassium data display trends similar to calcium, but plot well below the seawater curve (**Figure 2.45c, d**). Bicarbonate content decreases with increasing chloride following two trends that reflect the regional variations in composition (**Figure 2.45e**). There is no correlation in sulfate to chloride content (**Figure 2.45f**).

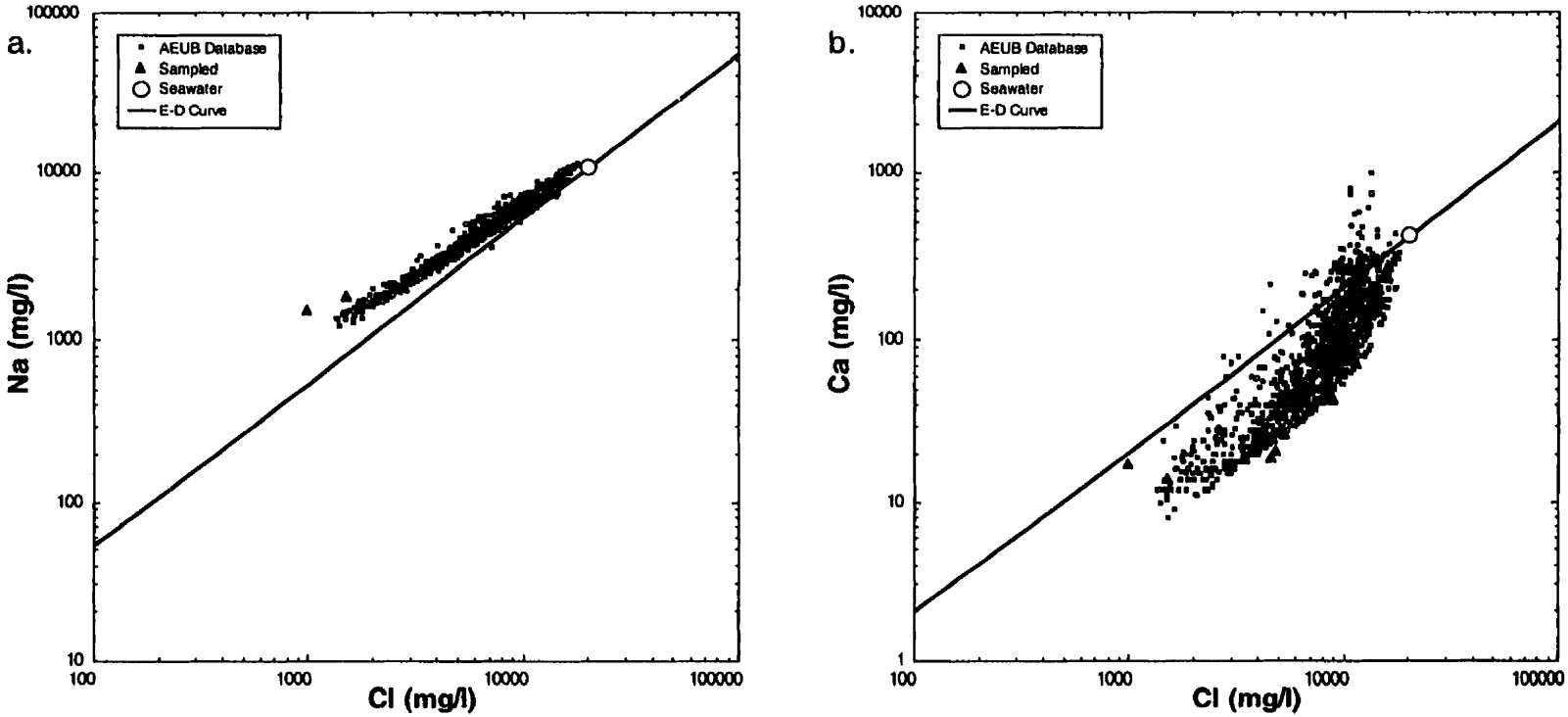

Figure 2.45a,b. Plots of the Viking/Bow Island sodium and calcium vs chloride. A good linear correlation of sodium with chloride is apparent. The calcium data displays a change in slope at approximately 8,000 mg/l Cl. Data includes that of Hitchon et al. (1971). The E-D curve is the seawater evaporation-dilution curve of Carpenter (1978).

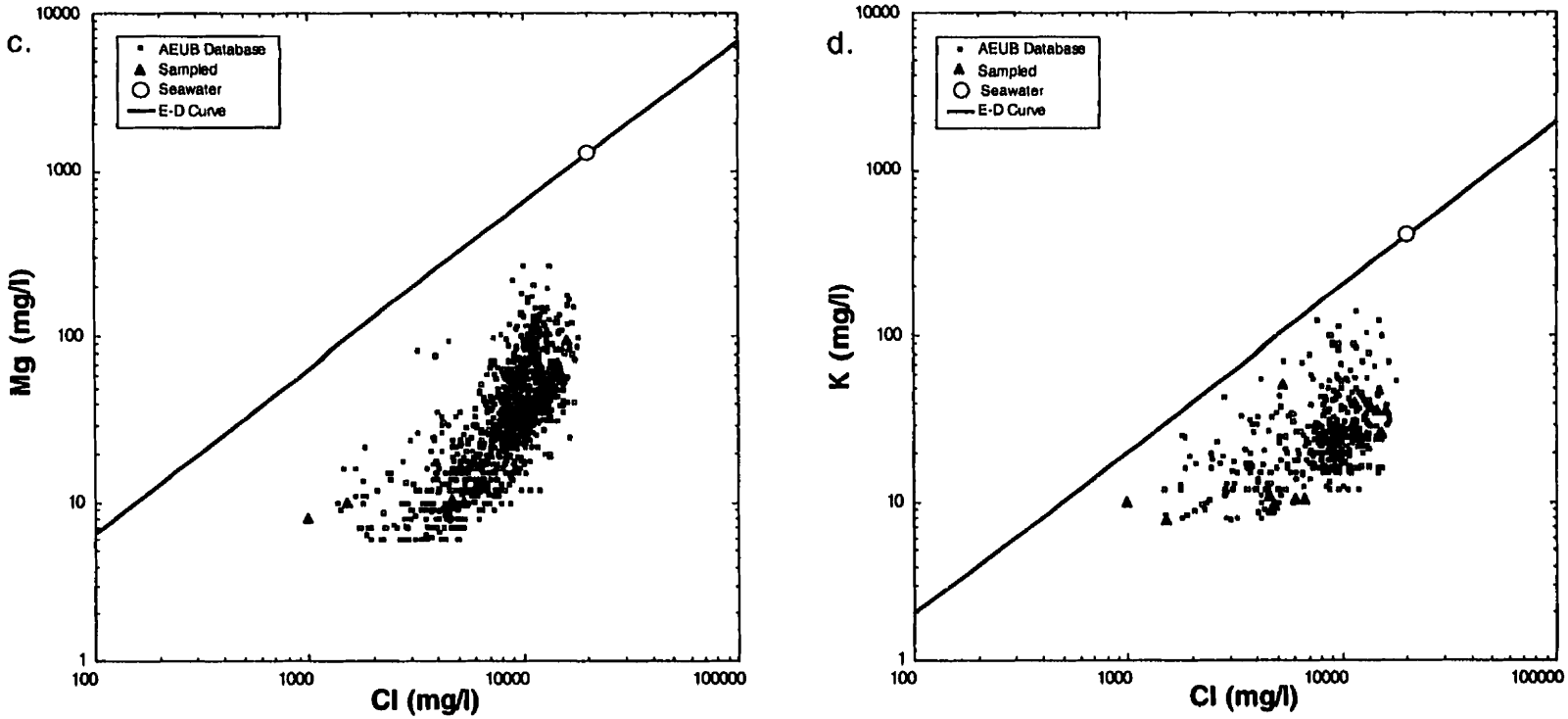

Figure 2.45c,d. Plots of the Viking/Bow Island magnesium and potassium vs chloride. Both potassium and magnesium data display relatively smooth curves (especially for the sampled analyses) suggesting a mineralogical influence on water composition. Data includes that of Hitchon et al. (1971). The E-D curve is the seawater evaporation-dilution curve of Carpenter (1978).

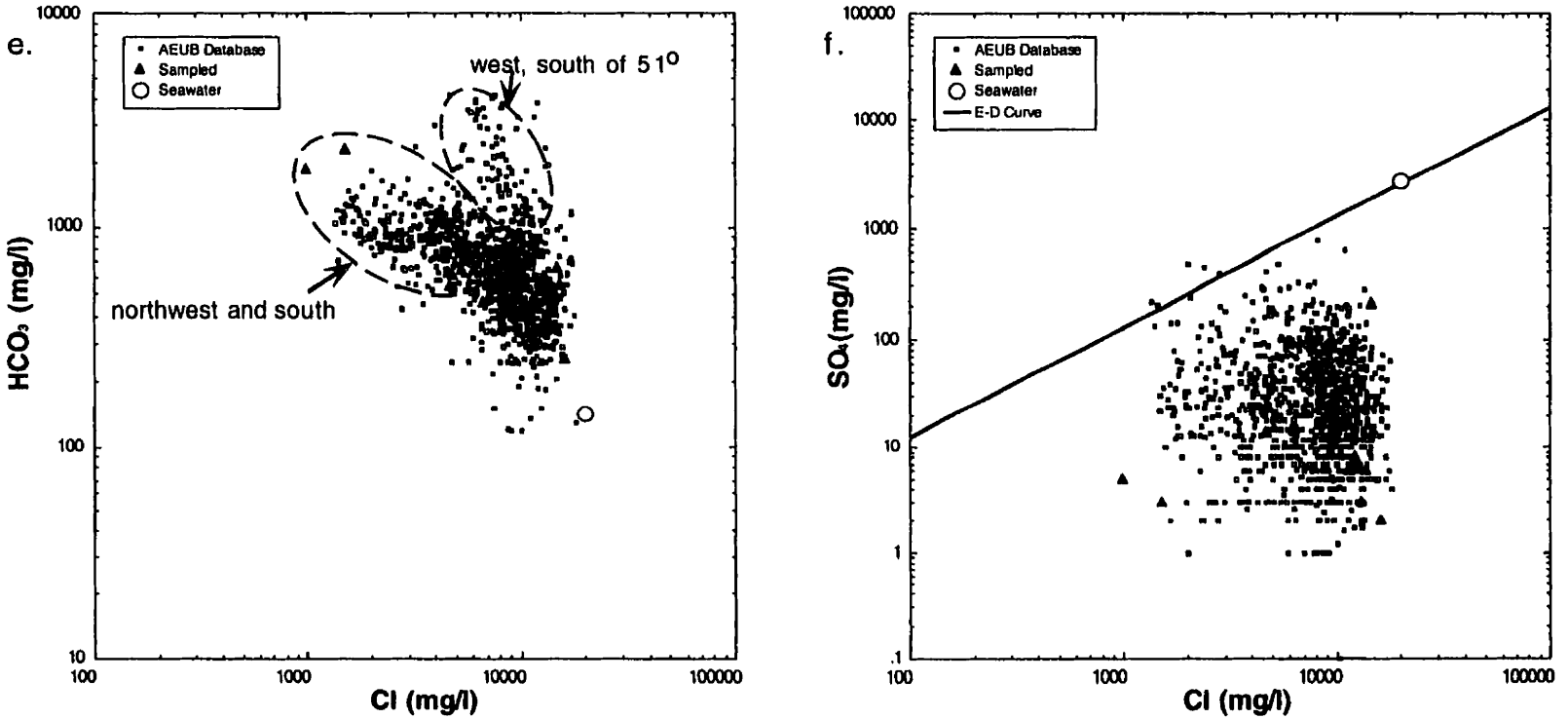

Figure 2.45e,f. Plots of the Viking/Bow Island bicarbonate and sulfate vs chloride. The two groups identified in e) reflect the regional distribution of bicarbonate and chloride. Data includes that of Hitchon et al. (1971). The E-D curve is the seawater evaporation-dilution curve of Carpenter (1978).

Mineralogical controls on solution composition

Plots of cation to hydrogen ion ratios versus dissolved silica show no consistent relationship between the waters and the smectite analogue (**Figure 2.46**). The Belle Fourche smectite may be an inappropriate analogue to use for evaluating the Viking/Bow Island formation water chemistry. However, **figures 2.46 b and d** show water data plotting near to the muscovite-pyrophyllite and Mg-mica-pyrophyllite boundary suggesting potassium and magnesium to hydrogen activity ratios may be influenced by the presence of smectite. There appears to be some indication that equilibrium between smectite and potassium feldspar, and smectite and chlorite is being approached for some of the samples. Chlorite and K-feldspar have been identified in the Viking/Bow Island by Longstaffe and Ayalon (1987) and McLellan (1995). The sodium data plot near to the smectite-albite stability boundary suggesting the smectite-albite reaction is approaching equilibrium and pH and silica activity may reflect a mineralogical control. Whether there is equilibrium between laumontite and smectite is difficult to determine, the data plot along the Ca-mica-laumontite boundary but the interpretation is equivocal. Mixed layer illite/smectite clays occur in the Viking/Bow Island Formation sands but may not be exerting an strong influence on fluid composition, or are metastable relative to other mineral phases that are controlling the solution composition. Petrologic observations indicate that precipitation of authigenic K-feldspar overgrowths and

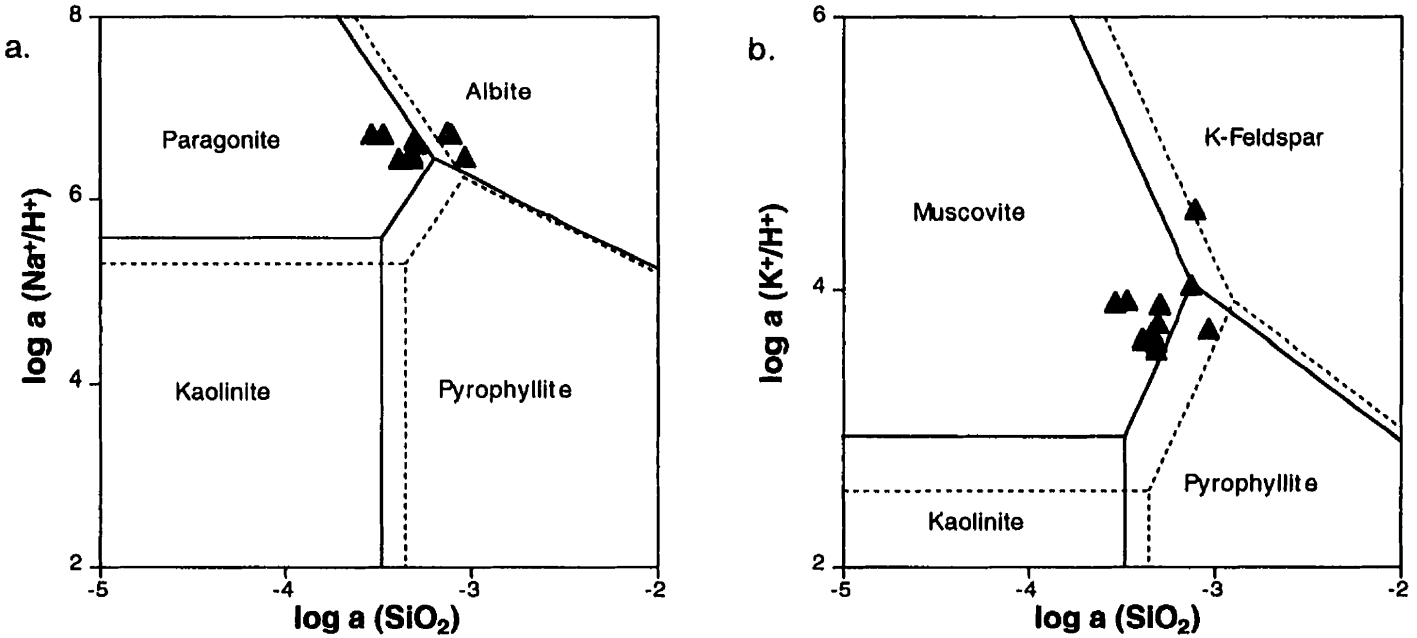

Figures 2.46a,b. Log activity-activity plots showing the stability of aluminosilicate phases at temperatures and pressures of 25°C and 60 bar (solid line), and 35°C and 90 bar (dashed line). The triangles represent the Viking/Bow Island aquifer waters. The data do not show a consistent relationship with the mineral phase boundaries like that observed in the Sawtooth to Upper Mannville aquifers. The sodium (a), potassium (b), and magnesium (d) plots have water data falling close to the albite, K-feldspar, and chlorite stability boundaries indicating a potential for clay-mineral-feldspar and -chlorite equilibrium influencing the water composition.

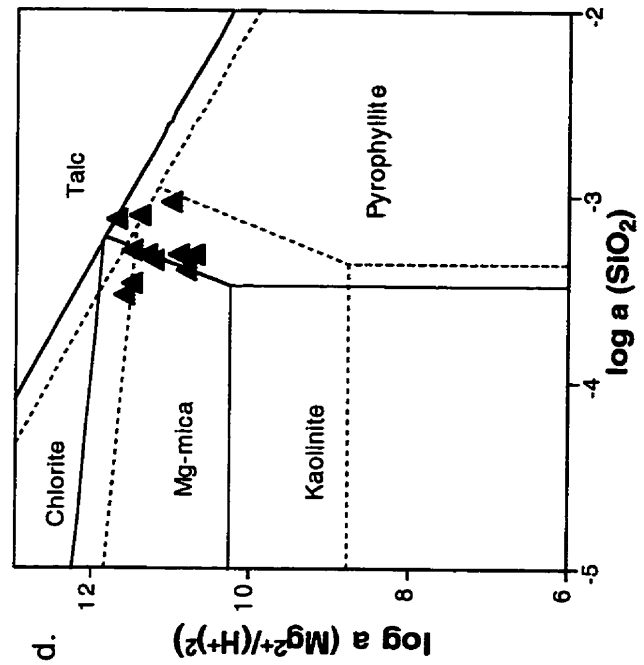

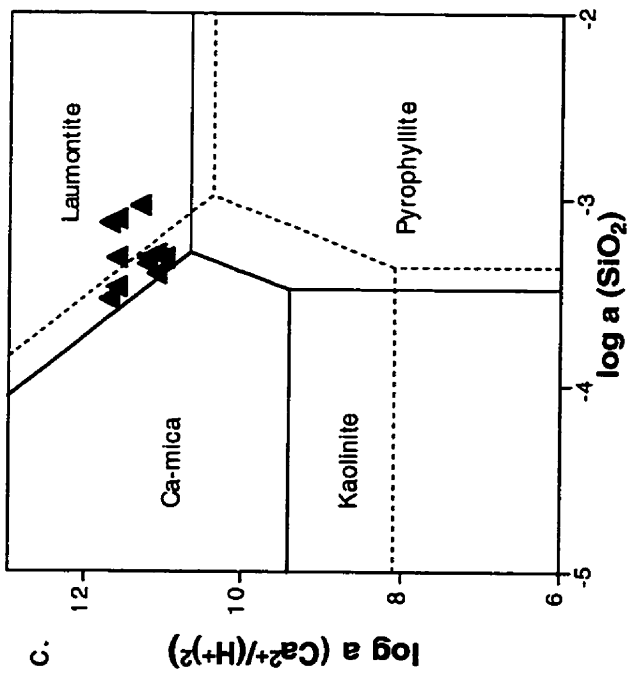

Figures 2.46c,d. continued.

dissolution of plagioclase has occurred (McLellan, 1995). The small change in potassium (<100 mg/l) would result in a very small increase in sodium (<60 mg/l) and could not be recognized within the scatter of sodium data.

A plot of calcium versus magnesium shows a strong correlation to calcite-dolomite equilibrium (**Figure 2.47**). The samples that fall off of the curve show a calcium decrease relative to magnesium, probably due to calcite precipitation. The samples that fall off the curve are from mixing zone areas where low chloride bicarbonate-rich meteoric waters mix with higher chloride waters. Authigenic dolomite and calcite were observed in thin section and have been reported to occur in Viking/Bow Island sandstones from within and to the north of the study area (Foscolos *et al.*, 1982; Longstaffe and Ayalon, 1987; McLellan, 1995). The dolomite is interpreted to be of early to mid-stage diagenesis and calcite precipitation occurs as an early phase and/or later in the paragenetic sequence (Longstaffe and Ayalon, 1987). The calcium-magnesium relationship may reflect early dolomitization and dolomite precipitation followed by dilution with meteoric water and calcite precipitation.

Origin of the Viking/Bow Island Formation water

The sodium vs chloride data suggests that the Viking/Bow Island Formation water originated as seawater. Calcium and magnesium contents reflect dolomitization of calcite

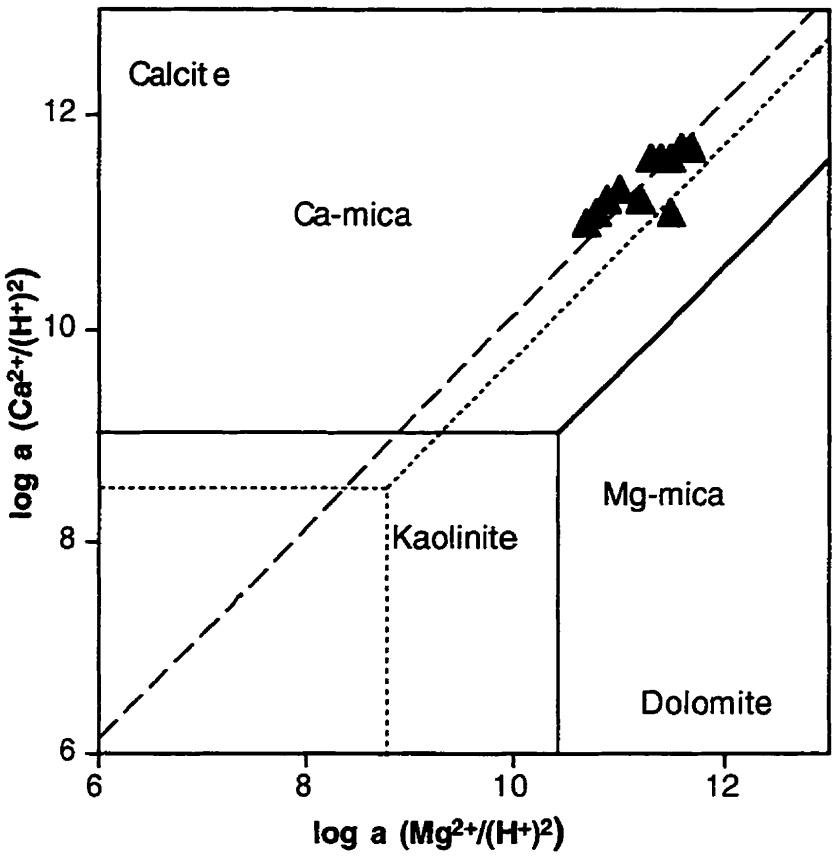

Figures 2.47. Log activity-activity plots showing the stability of aluminosilicate phases and calcite-dolomite at temperatures shown. The triangles represent the Viking/Bow Island aquifer waters. The lines represent the mineral phase stability bondaries of the aluiminosilicates at 25°C (solid line) and 35°C (fine dashed line) and the calcite-dolomite boundary at 25°C. The C-D stability boundary is the line that spans diagonally across the diagram and the calcite and dolomite stability fields encompass the upper and lower portions of the diagram respectively. The majority of data plot on or near the calcite-dolomite boundary.

and loss of potassium is attributed to feldspar overgrowth precipitation. Subsequent dilution by meteoric water has modified the composition.

Origin of high bicarbonate waters

Elevated bicarbonate concentrations in regionally restricted areas are observed in all of the aquifers (**Figures 2.10, 2.13, 2.16, 2.18, 2.23 and 2.26**). A common source of bicarbonate in formation waters at low temperatures (<80°C) is the bacterially mediated oxidation of organic matter (Bailley *et al.*, 1973; Orr, 1977; Connan, 1984). The majority of high bicarbonate waters have measurable amounts of dissolved H_2S and elevated CO_2 in the gas phase. High CO_2 partial pressures and the presence of dissolved sulfide (**Table 2.3 and 2.4**) may be the result of bacterial sulfate reduction (BSR) (Orr, 1977; Berner 1985; Machel *et al.*, 1995; Cody and Hutcheon, 1999). A simplified reaction equation describing anaerobic destruction of an alkane hydrocarbon can be written as (from Rueter et al., 1994):

$$C_{10}H_{22} + 7.75SO_4^{2-} + 5.5H^+ \Rightarrow H_2O + 7.75H_2S + 10HCO_3^- \qquad 7$$

BSR requires a source of sulfate, hydrocarbons, and the presence of bacteria. Production fluids from oil wells have been shown to contain sulfate reducing bacteria (Olson et al., 1981; Stetter et al., 1993). Evidence of the anaerobic degradation of crude oils in

hydrocarbon reservoirs was, until recently, largely circumstantial. Experimental work in the last few years has demonstrated that sulfate reducing bacteria can directly utilize hydrocarbons (Rueter et al., 1994; Caldwell et al., 1998).

Hydrocarbon reservoirs in southern Alberta show appreciable biodegradation, particularly in the areas that correspond to the bicarbonate-rich fluids of this study (Karavas, 1998; Manzano et al., 2000). The sulfur isotopic composition of sulfate and sulfide and the low temperature of the reservoirs (**Tables 2.3, 2.4**) indicate the most likely process is bacterial sulfate reduction. Sulfate and sulfide sulfur isotopes in the Nisku/Arcs formation show a shift of –7‰ to –20‰ (**Table 2.4**) consistent with open-system BSR. The isotopic composition of sulfate is similar to anhydrite sulfate composition in Devonian aged rocks (Krouse et al., 1988) and the abundance of anhydrite results in an easily utilized source of sulfate.

The sulfur isotopic composition of sulfate and sulfide are more variable in the Mississippian and younger aquifers (**Table 2.4**). Anhydrite is far less common in the Mississippian carbonates and the majority of the waters are undersaturated with respect to anhydrite indicating a system where the sulfate supply is restricted. The variable and often large difference in sulfur isotopic values for aqueous sulfate and sulfide are indicative of BSR. Equally compelling is the observation that regionally, high bicarbonate contents coincide with low sulfate content. According to equation 7, sulfate

is removed from the system and bicarbonate is produced. Without a local source of sulfate, there should be low concentrations of sulfate in areas of high bicarbonate. Cody and Hutcheon (1994) and Cody et al. (1999) attribute high CO_2 and H_2S content and sulfur isotopic compositional variations in produced waters to BSR in Mannville reservoirs. The results of this study are consistent with their (Cody and Hutcheon, 1994; Cody et al., 1999) interpretation and extend the data down into the Mississippian and Devonian.

Sulfide content is generally much lower than bicarbonate in all of the sampled waters and CO_2 partial pressures are typically an order of magnitude higher than H_2S partial pressures in the associated gas phase (**Tables 2.3, 2.4**). The BSR reaction (equation 7) produces sulfide and bicarbonate at a ratio of 7.75:10 and, written in other forms, at ratios of 1:2. Sulfide must be consumed by some reaction to account for the discrepancy. Cody and Hutcheon (1994) observed large quantities of pyrite in the Mannville reservoir rocks and attribute the loss of sulfide to pyrite precipitation. Pyrite is observed in all of the aquifers and iron contents in waters are typically low (**Table 2.3**). Whether sufficient iron is available to account for the difference in bicarbonate and dissolved sulfide is not known. A simple mass balance calculation indicates that for a 6,000 mg/l increase in bicarbonate, approximately 15 mmol of iron would completely precipitate out the sulfide produced by BSR (using the sulfate1:2 bicarbonate ratio) as pyrite. Potential sources of

iron include ankerite, siderite and magnetite along with a host of other phases that contain iron in trace amounts. In a rock containing 10% porosity, dissolution of less than 1cc (or 0.01 volume %) of any of the above minerals would provide sufficient iron to precipitate the sulfide.

Variations in the carbon isotopic composition of bicarbonate are considerable, indicating that a number of processes are in effect. Carbon isotope values range from –16‰ to +21‰ PDB (**Table 2.4**). The majority of waters indicate carbon isotope equilibrium with carbonates of the Mississippian and Devonian with values of 0+/-2‰. Whether values reflect carbonate dissolution or temperature-isotopic equilibrium cannot be determined from these data. BSR results in little carbon isotope fractionation between the organic matter and bicarbonate. Values should fall in the range of –18 to –33‰ depending on the isotopic composition of the precursor hydrocarbon (Carothers and Kharaka, 1980). Reduction of dissolved CO_2 by methanogenic bacteria produces a positive shift in carbon isotopic composition (Whiticar et al., 1986). Positive $\delta^{13}C$ values can generally be attributed to methanogenesis (Carothers and Kharaka, 1980). The wide range in isotopic compositions observed in this study suggests interpretation of the source of carbon is not possible from carbon isotopes alone.

Conclusions

1. Formation waters of the Devonian Nisku/Arcs aquifer in southern Alberta are comprised of Na-Cl dominated and Na-HCO_3-SO_4 dominated components. The regional distribution of chloride indicates mixing with fresher water in the east. The influx of low salinity water has resulted in the dissolution of anhydrite and BSR, producing high bicarbonate contents associated with high sulfate.
2. Calcium, magnesium, and sulfate contents reflect equilibrium between calcite, dolomite and anhydrite. At low temperatures (<50°C) the waters are also in equilibrium with calcite and anhydrite, independently of dolomite, and high sulfate with low calcium contents reflect anhydrite dissolution and calcite precipitation. The composition of sodium and potassium appear to reflect the original brine composition and have not been modified extensively by water-rock interactions.
3. The Nisku/Arcs Formation waters of southern Alberta originated as seawater evaporated beyond halite precipitation, compatible with the conclusions of Spencer (1987) and Connolly (1991) for Devonian hosted waters in central and northern Alberta. Subsequent reaction of the brine with calcite resulted in dolomitization and anhydrite precipitation significantly altering the brine composition.
4. The Mississippian to Upper Mannville aquifers show similar distributions of chemical composition. The formation waters are of three recognizable types, Na-Cl, Na-

HCO_3-Cl, and Na-Cl-SO_4 whose distribution reflects mixing with meteoric water and perhaps, bacterial sulfate reduction.

5. The Mississippian to Upper Mannville aquifer waters originated as a marine evaporative brine, probably related to brines in Devonian-aged aquifers. The waters show considerable dilution by meteoric water, particularly in the south and east. The unconformity bounded contact between the Mississippian and overlying units, the southeast to northwest regional orientation of the Lower and Upper Mannville, and similarities in fluid composition indicate that cross-formational flow from the Mississippian up into the Jurassic Sawtooth and Lower Cretaceous Mannville controls the chemical composition of waters in the clastic units. Two distinct groups of waters are present on a regional basis, with a narrow mixing zone separating them. Sodium and potassium mix conservatively, however differences in regional composition suggest that more than one mixing event has occurred.
6. The clastic hosted waters have compositions that are suggest equilibrium with clay minerals, particularly smectite and in some cases smectite and kaolinite. Silica activities and pH reflect mineralogical control consistent with the presence of smectite. Calcium and magnesium content in the Mississippian to Upper Mannville aquifers reflects control by dolomitization, although calcite precipitation has subsequently decreased the calcium content in many of the waters. The processes

that have resulted in calcite precipitation are mixing of high Ca/HCO_3 fluids with low Ca/HCO_3 fluids and CO_2 addition to systems in which pH is buffered by clay minerals.

7. Two Viking/Bow Island water compositional types are recognized, Na-Cl and Na-Cl-HCO_3. Variations in chloride content reflect mixing with dilute meteoric water. Although the Viking/Bow Island formation waters display a complex regional pattern, the waters appear to have originated as seawater.

8. Activity diagrams indicate that smectite is present but does not exert a dominant influence on the solution chemistry. Sodium, calcium and magnesium activity ratios plot near the feldspar, laumontite, and chlorite/talc stability fields and fluid compositions may reflect mineralogical control of pH and dissolved silica. Dolomitization and dolomite precipitation has resulted in calcium and magnesium contents that reflect calcite-dolomite equilibrium. The potassium content differs appreciably from the conservative mixing curve suggesting loss of potassium. Feldspar overgrowths are observed in thin section indicating the decrease in potassium content may reflect K-feldspar precipitation.

9. High bicarbonate contents and trace amounts of hydrogen sulfide indicate bacterial mediated sulfate reduction has occurred in a large but aerially restricted region. Stable isotopes of sulfur support BSR as the most likely source of the sulfide.

However the source of bicarbonate is more ambiguous. A lack of correlation between bicarbonate and dissolved sulfide content and variable carbon stable isotope compositions may indicate some of the bicarbonate is from dissolution of calcite although low calcium contents would require some other sink for calcium such as Ca-smectite of laumontite.

10. The use of a smectite compositional analogue has proven to be an effective method to evaluate mineralogical controls on fluid composition in a system where no clay mineral compositional data is available. The Aagard and Helgeson (1983) solid solution model for approximating the thermodynamic behavior of smectite is shown to have applicability for a sedimentary basin system displaying a moderate range in temperature, pressure and aqueous solution composition.

Chapter 3

Fluid Flow

Introduction

Migrating groundwater acts as a medium of mass transport that chemically and thermally alters the sediments through which it flows. Evidence that fluids migrate distances of meters to hundreds of kilometers can be found throughout sedimentary basins as ore deposits and oil pools. Numerous numerical models utilizing basic flow and transport equations have been generated to describe the conditions leading to fluid migration and the resultant ore deposits and hydrocarbon accumulations (Cathles and Smith, 1983; Bethke, 1985; Garven, 1985, 1989; Deming *et al.* 1990; Deming and Nunn, 1991; Ge and Garven, 1994). As well, current flow regimes have been extensively studied and described for the WCSB (Hitchon 1969a,b; Schwartz *et al.*, 1981; Toth and Corbet, 1987; Toth, 1989; Hitchon *et al.*, 1990; Bachu and Underschultz, 1993; Cody and Hutcheon, 1994; McClellan 1995; Bachu, 1995, and Bachu and Underschultz, 1995). These studies indicate that although models may describe the possible mechanisms that create flow potentials, the basins and the sediments within, dictate how that flow is manifested.

The present-day patterns of fluid flow in the basin reflect hydraulic head gradients produced by both elevation differences and pressure differences caused by erosional

rebound (Bachu, 1995). The Alberta basin has been divided into two hydrostratigraphic systems based on water chemistry, lithology and hydrologic parameters: the post-Jurassic hydrostratigraphic group; and the pre-Cretaceous hydrostratigraphic group (Bachu, 1995).

In southern Alberta, the post-Jurassic hydrostratigraphic group consists of predominantly shales alternating with thin sandstones. Salinities are low and reflect periodic flushing by fresher waters (Hitchon, 1969a,b). Flow systems are largely driven by local topography in the shallow aquifers (Toth and Corbet, 1987). In deeper aquifers flow is transient, driven by the erosional rebound of the shale sequences causing inward lateral flow from the permeable boundaries (Neuzil and Pollock, 1982). The flow is from the south and east towards the fold and thrust belt, opposing the topography (Toth and Corbet, 1987; Bachu and Underschultz, 1995).

The pre-Cretaceous hydrostratigraphic group waters in southern Alberta have high salinities except in the proximity of recharge areas in the south (Schwartz *et al.*, 1981; Bachu and Underschultz, 1995) and in the northeast where aquifers subcrop and waters from overlying formations mix with the pre-Cretaceous waters (Hitchon *et al.*, 1990; Bachu and Underschultz, 1993). The high salinities of these waters suggest that Laramide induced flushing was incomplete (Bachu, 1995) and there is no isotopic evidence of Tertiary meteoric fluids even entering the Devonian strata (Nesbitt and

Muehlenbachs, 1994), suggesting that Laramide induced flushing may never have taken place. Flow is from the south towards the northeast, with recharge in Montana along the margin of the Sweetgrass Arch (Hitchon, 1969 a, b; Schwartz *et al.*, 1981). Flow does not appear to be fed by topographic recharge in the fold and thrust belt possibly due to the overlying thick Cretaceous shale sequences (Bachu, 1995). Eastward flow appears to be a remnant of tectonic compression with high density fluids retarding flow resulting in long residency times for the tectonically expelled waters (Bachu, 1995).

The present-day patterns of fluid flow in the Western Canada Sedimentary Basin describe a complex three dimensional flow system that bears little resemblance to those predicted by simple flow models. Flow driving mechanisms are operative to varying degrees throughout the basin but to understand the nature of the flow, models must be constrained by the available geochemical and hydrologic data. Integration of measurable geochemical data, including chemical and isotopic composition of waters and fluid inclusions, with hydrologic data like hydraulic head, permeabilities, and temperatures may make it possible to understand the present-day flow regime. By understanding the mechanisms of the present-day flow regime we might open a window on to paleoflow systems.

The objective of this chapter is to examine the salinity variation and flow paths of formation waters in the southern part of the Western Canada Sedimentary Basin (WCSB) (**Figure 3.1**). To do this, chemical and isotopic compositions of formation waters, the oxygen isotopic composition of rocks and minerals, and the fluid potentiometric data are combined. Fluid flow in the southern part of the WCSB has been examined by (Hitchon, 1969a,b; Schwartz *et al.*, 1981; Hitchon, 1984; Toth and Corbet, 1987a,b; Corbet and Bethke, 1992; Bachu and Underschultz, 1995; Cody, 1993; Cody and Hutcheon, 1994; McLellan, 1995), primarily using potentiometric data. Some studies (Schwartz *et al.*, 1981; Cody, 1993; Cody and Hutcheon, 1994) report variations in salinity related to the flow paths interpreted from potentiometric data. This approach is taken one step further, showing in detail how the spatial distribution of salinity is related to the potentiometric surfaces and fluid flow pathways. Further, the oxygen isotopic data for formation waters are integrated with that for rocks and minerals to examine the possibility that some areas have experienced more fluid flow than others.

Flow models

The four principle mechanisms for fluid flow are: topography induced flow; compaction/decompaction ; buoyancy; and tectonics (Garven, 1995).

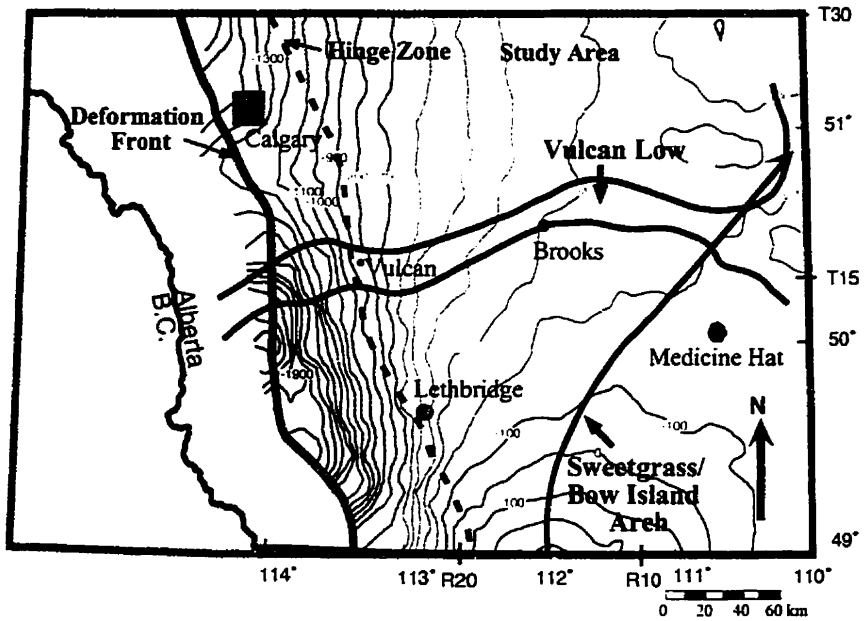

Figure 3.1 Map of the study area including the major structural features. Contours are of the sub-Mannville unconformity surface relative to sealevel given at 100 meter intervals.

Topography driven flow results from hydraulic head gradients caused by variations in elevation of the water table. Erosionally sculptured land forms exhibit considerable influence on local flow systems and intermediate flow systems of over 1 km depth depending on the permeability (Toth and Corbet, 1987). On a regional scale, topography driven flow systems are mechanistically linked to orogenic activity (Hitchon, 1969a,b). Fresh water infiltrates in elevated areas, acquiring heat and dissolved constituents as it moves downward. Eventually the fluid encounters a permeable aquifer and flows laterally and upward to the basin edge (Hitchon 1969a,b). The controlling factor on water volume is the rate of recharge in the elevated areas, resulting in a potentially unlimited supply.

Equivalent freshwater head is commonly used in the modeling of groundwater flow in systems that display considerable variations in fluid density. It is generally assumed that fluid flow in nearly horizontal aquifers is approximately horizontal and that density related gravity effects and spatial variations in density are negligible (Bachu, 1995). The assumption of constant density allows the use of the concept of a potential field described by a potentiometric surface. The use of a potentiometric surface in analytical and numerical methods coupled with isotropic rock properties allows for the representation, analysis and simulation of a number of hydrogeological problems. However, studies in contaminant hydrogeology, hazardous waste disposal, and petroleum reservoir

hydrogeology indicate that assumption of constant density is not valid in some situations (Bachu, 1995b). Variable density waters introduce a vertical component to fluid flow. Flow patterns of variable density fluids cannot be accurately determined from equivalent freshwater pressure or head gradients because a single potential field does not exist under these conditions. The relative significance of this vertical force can be determined using an equation for the driving force ratio, an expression of the relative magnitude of a density related error term to the magnitude of the equivalent freshwater head. Numerical simulations of fluid flow in variable density systems can indicate changes in flow patterns induced by buoyancy. In simple models, flow can be effectively represented but complex models are hindered by uncertainties caused by heterogeneity and anisotropy in the calculated and measured parameters and in the selection of boundary conditions.

Davies (1987) investigated the relative importance of density related effects on fluid flow and defined the dimensionless driving force ratio (DFR) as:

$$\mathrm{DFR} = \frac{\Delta\rho|\nabla \mathrm{E}|}{\rho_o|\nabla h_o|} \qquad 1$$

The DFR is the ratio of the buoyancy component of flow to the pressure component of flow. Buoyancy drives flow in the maximum direction of ∇E (gradient in elevation), which corresponds to the greatest dip of the confining surface. Driving forces, as expressed by ∇h_o, drive the flow in the direction of the maximum hydraulic gradient. Davies (1987) determined that DFR values greater than 0.5 indicate flow in which

significant error can be introduced if buoyancy is neglected. The DFR illustrates that even when the dip of an aquifer is small, dense fluids may retard or even reverse flow if the calculated freshwater head gradient is small.

Stable isotopes of oxygen and hydrogen

The use of stable isotopes in groundwater hydrology has proven effective because of the conservative behavior of the isotopes of water in low temperature (<50°C) systems where residence times of the fluid are small relative to the kinetics of isotope exchange reactions between water and minerals (Whelan, 1987). Gat (1981) defined three categories of subsurface waters based on the isotopic composition and origin: 1) Meteoric waters that reflect modern precipitation; 2) Older meteoric waters that reflect meteorological or recharge conditions different from the current regime; 3) Formation waters that have, over long periods of time and/or at elevated temperatures, had water-rock interaction result in non-conservative behavior of the oxygen and hydrogen isotopes. Studies of the stable isotopes of oxygen and deuterium of saline waters in sedimentary basins have proven to be effective in the interpretation of fluid origins (Clayton *et al.*, 1966; Hitchon and Friedman, 1969; Kharaka and Carothers, 1986). Clayton *et al.* (1966) determined that formation waters of the Illinois and Michigan basins are predominantly of meteoric origin, and variations in the deuterium content did not reflect exchange or fractionation

processes while oxygen content was subject to considerable exchange with the surrounding aquifer rocks. Hitchon and Friedman (1969) used the stable isotopes of hydrogen and oxygen in the WCSB to interpret the origin and geochemistry of formation waters. Salinity variations were related to the movement of fresh water through the basin and mixing with diagenetically modified seawater (Hitchon and Friedman, 1969). The oxygen isotopic composition was interpreted to reflect exchange of oxygen isotopes between water and carbonate minerals that was dependent on the relative amount of carbonate available.

Hydrostratigraphy

The Upper Devonian to Lower Cretaceous succession in southern Alberta can be described within a hydrostratigraphic framework that relates to the hydraulic properties of the rock. Relatively permeable sandstones and carbonates are identified as aquifers and less permeable shales and carbonates are identified as aquitards (Schwartz *et al.*, 1981; Toth and Corbet, 1987). A hydrostratigraphic unit consists of a single layer, formation, or group of formations, that display similar hydraulic properties. A hydrostratigraphic group is made up of a series of hydrostratigraphic units and may be termed an aquifer or aquitard, depending on the ability to display flow on a regional scale, even if the unit contains both aquifers and aquitards.

The Upper Devonian to Upper Cretaceous strata of southern Alberta have been subdivided into hydrostratigraphic units and groups by Schwartz *et al.*, (1981), Toth and Corbet (1987), and Bachu and Underschultz, (1995) (**Figure 3.2**). The Nisku/Arcs Formation is the basal aquifer in this study because it is the lowest unit from which abundant chemical and hydrologic data was available in the database. The overlying Calmar/Crowfoot to Exshaw and Lower Banff Formations form an aquitard. The upper portions of the karsted, truncated Mississippian carbonates and the lowermost Jurassic sandstone, the Sawtooth Formation, form a regional aquifer system. In the southern and western portions of the study area shales of the Jurassic Rierdon Formation behave as an aquitard. The overlying Lower Mannville forms an aquifer system, however, the southeast-northwest trend (Fashori and Hopkins, 1989; Zaitlin, 1997) of the sand channels limits the lateral (east-west) continuity of the aquifer. The Upper Mannville consists of an aquifer unit at the base, the Glauconitic sandstone, that is not well developed in the southern portion of the study area, but forms distinct southeast-northwest trending sandstone channels in the central and northern regions (Hopkins *et al.*, 1982; Wood and Hopkins, 1992; Karvonen and Pemberton, 1997). Like the Lower Mannville, east-west hydraulic continuity in the Upper Mannville is limited. The Mississippian to Lower Cretaceous Upper Mannville aquifers form a single hydrostratigraphic group (Schwartz *et al.*, 1981; Toth and Corbet, 1986; Bachu and

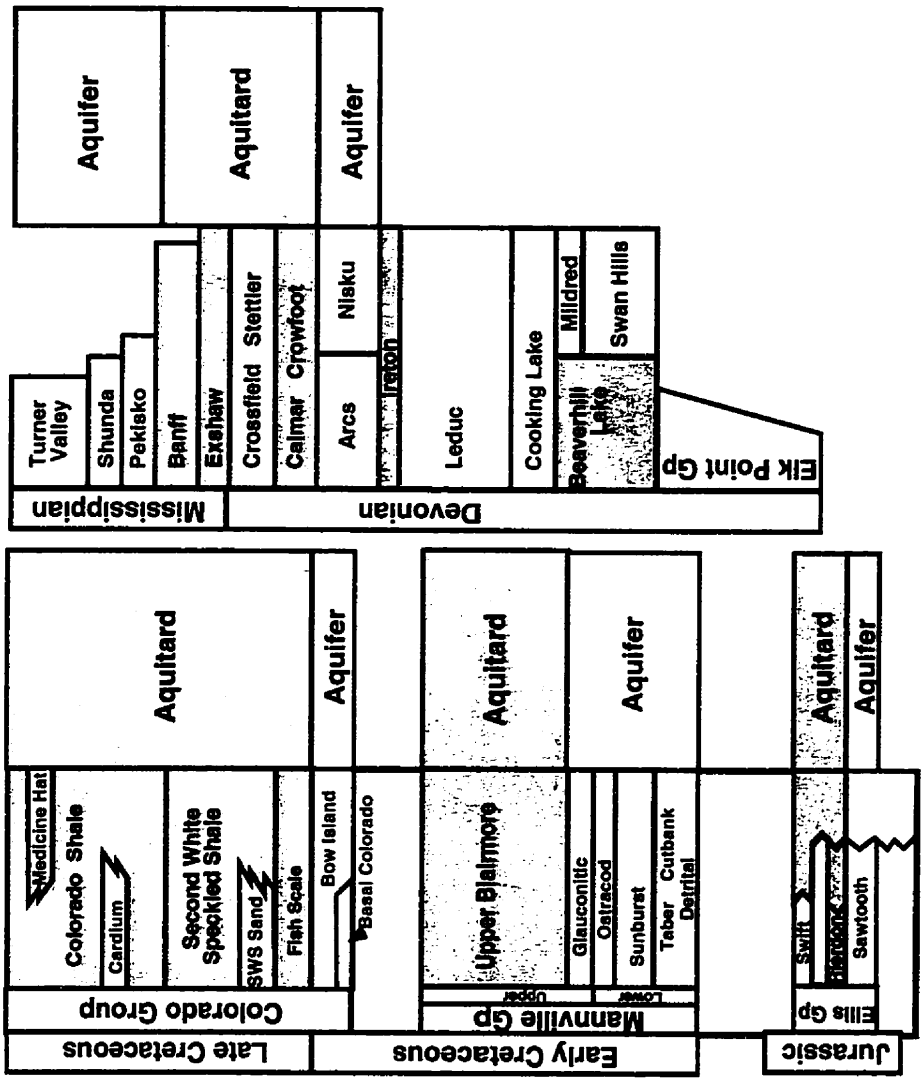

Figure 3.2. Hydrostratigraphy of the study area. Hydrostratigraphic units are defined as 'aquitards' or 'aquifers' based on Schwartz et al. (1981),Toth and Corbet, (1987), and Bachu and Underschultz, (1995).

Underschultz, 1995). The remainder of the Upper Mannville forms an aquitard system. Overlying the Upper Mannville is the thick, predominantly shaley Colorado Group, which forms the Colorado aquitard. The Viking/Bow Island Formation, near the base of the Colorado Group, is defined as an aquifer.

Results

$\delta^{18}O$-δD composition of the formation water

Values of $\delta^{18}O$ of water from the study area range from –16.5‰ to +4‰ (V-SMOW) and –130‰ to –48‰ V-SMOW for deuterium (**Table 3.1, Figure 3.3**). The data follow the general trend for Alberta basin waters observed by Hitchon and Friedman (1969), Connolly *et al.* (1990), Cody and Hutcheon (1994), and Simpson (1999). A linear regression intersects the global meteoric water line (GMWL, Craig, 1961) at $\delta^{18}O$=-17‰ and δD= –129‰, similar to values of local surface water in southern Alberta (-16.8‰ and -141‰ respectively, Hitchon and Friedman, 1969). Most of the waters plot below the meteoric water line indicating a large enrichment in ^{18}O and comparatively smaller enrichment of D relative to meteoric water. Waters that deviate considerably from this trend may reflect some production-related contamination such as water flood or introduction of water condensed from the gas phase. The data imply meteoric water forms a significant component of formation water from southern Alberta. Mixing of

Table 3.1. Well location, formation name, chloride content and isotopic composition of sampled waters.

DLS Location	Formation	Chloride (mg/l)	$\delta^{18}O‰$ in H_2O V-SMOW	$\delta D‰$ in H_2O V-SMOW
1-36-14-11W4	Viking	4700	-6.8	-79
9-29-14-18W4	Bow Island	12971	-4.7	-78
9-21-15-11W4	Viking	4615	-6.6	-77
1-4-16-13W4	Viking	5310	-6.1	-77
1-2-16-15W4	Viking	4810	-6.0	-80
4-30-16-17W4	Bow Island	9200	-4.6	-77
14-24-16-18W4	Viking	9136	-4.7	-76
F1/10-8-17-14W4	Viking	6744	-5.1	-81
02/10-8-17-14W4	Viking	6085	-5.5	-79
11-19-24-15W4	Viking	12199	-6.7	-78
11-29-28-17W4/2	Viking	9041	-7.5	-85
1-23-8-17W4	Glauconitic	995	-15.1	-122
14-2-10-13W4	Glauconitic	1116	-14.1	-122
10-28-12-5w4	Glauconitic	2723	-9.6	-94
13-33-14-7W4	Glauconitic	1836	-11.9	-108
02/11-33-14-17W4	Upper Mannville	6712	-5.3	-87
10-21-15-15W4	Upper Mannville	3662	-8.2	-96
14-20-15-15W4	Upper Mannville	5682	-5.9	-84
11-20-15-15W4	Upper Mannville	8165	-4.7	-81
11-8-15-18W4	Glauconitic	10332	-4.5	-71
04/16-15-16-12W4	Upper Mannville	3408	-9.3	-92
6-30-16-14W4	Glauconitic	7068	-5.2	-77
7-5-17-14W4	Glauconitic	8319	-5.6	-84
15-6-17-14W4	Glauconitic	7004	-5.1	-78
02/14-26-17-15W4	Upper Mannville	10579	-4.2	-81
02/16-5-20-19W4	Upper Mannville	13842	-4.4	-80
10-28-20-20W4	Upper Mannville	17638	-3.5	-74
7-2-20-21W4	Glauconitic	22676	-4.6	-79
14-24-20-21W4	Upper Mannville	22251	-4.0	-77
1-21-21-20W4	Glauconitic	22380	-4.0	-75
6-22-25-23W4	Upper Mannville	12825	-4.7	-79
5-16-26-12W4	Mannville	6848	-7.4	-84
16-21-29-11W4	Upper Mannville	10030	-8.4	-83
02/11-6-29-20W4	Glauconitic	12398	-6.5	-82
02/6-21-29-20W4	Upper Mannville	8922	-5.8	-78
16-20-1-8W4	Mannville	4969	-9.8	-84
8-5-1-16W4	Cutbank	575	-16.4	-128
9-12-3-17W4	Lower Mannville	2307	-15.7	-116
4-7-5-4W4	Sunburst	4200	-10.0	-86
02/13-11-6-17W4	Lower Mannville	1312	-15.2	-121
02/6-36-9-8W4	Lower Mannville	2574	-8.3	-94
16-16-9-17W4	Taber	976	-15.3	-119
13-34-10-13W4	Lower Mannville	1236	-14.3	-121
15-14-10-19W4/2	Lower Mannville	3606	-9.9	-102
9-1-12-17W4	Lower Mannville	2070	-13.1	-111
02/14-3-12-19W4	Mannville	6475	-5.8	-69
7-16-13-19W4	Mannville	5516	-6.8	-90
4-34-14-10W4	Lower Mannville	5317	-7.6	-91
14-30-14-10W4	Lower Mannville	7352	-6.7	-81
14-34-14-15W4	Lower Mannville	3126	-9.1	-92
12-18-14-18W4	Lower Mannville	4486	-9.7	-97
13-19-15-10W4	Lower Mannville	2761	-7.9	-88
4-17-15-10W4	Lower Mannville	9245	-5.7	-86
5-03-15-11W4	Lower Mannville	2454	-9.0	-98
10-3-15-11W4	Lower Mannville	2899	-8.6	-97
8-14-15-11W4	Lower Mannville	3424	-7.1	-86
12-24-15-11W4	Lower Mannville	3147	-8.2	-94
13-11-15-11W4	Lower Mannville	3089	-8.0	-93
5-05-16-11W4	Lower Mannville	2102	-10.3	-100
14-06-16-11W4	Lower Mannville	2282	-9.9	-96
2-9-16-13W4	Lower Mannville	3403	-7.9	-92
14-4-16-13W4	Lower Mannville	3268	-8.0	-93
11-34-15-13W4	Lower Mannville	3686	-7.5	-90
02/2-9-16-13W4	Lower Mannville	3394	-8.0	-90
12-9-16-13W4	Lower Mannville	4279	-6.4	-84
02/11-3-16-13W4	Lower Mannville	4720	-7.1	-83
14-9-16-13W4	Lower Mannville	4028	-7.0	-90
15-3-16-13W4/2	Lower Mannville	4102	-7.7	-86
10-9-16-13W4	Lower Mannville	3733	-7.2	-90
6-3-16-13W4	Lower Mannville	5860	-6.6	-86
6-23-16-22W4	Sunburst	7695	-4.6	-83
5-3-18-10W4	Lower Mannville	3593	-7.4	-90

Table 3.1. continued.

DLS Location	Formation	Chloride (mg/l)	$\delta^{18}O‰$ in H_2O V-SMOW	$\delta D‰$ in H_2O V-SMOW
7-9-18-10W4	Lower Mannville	4292	-7.5	-85
02/11-29-18-13W4	Mannville	8086	-4.2	-82
3-26-20-12W4	Basal Mannville	13803	-4.1	-79
11-24-20-14W4	Mannville	15263	-5.1	-81
6-9-23-18W4	Ostracod	12821	-5.3	-67
5-36-24-28W4	Basal Quartz	19432	-1.7	-59
6-26-24-28W4	Basal Quartz	28290	-1.8	-56
11-35-24-28W4	Basal Quartz	52876	-1.7	-48
02/7-7-25-21W4	Lower Mannville	12995	-4.5	-74
7-26-25-28W4	Basal Quartz	53798	-1.9	-49
7-16-27-9W4	Lower Mannville	8250	-8.0	-86
12-10-27-20W4	Basal Quartz	10031	-5.3	-78
8-24-29-12W4	Lower Mannville	9297	-8.1	-83
15-1-5-5W4	Sawtooth	554	-14.6	-115
14-34-6-15W4	Sawtooth	1224	-13.9	-115
14-13-6-17W4	Sawtooth	730	-16.5	-127
5-9-7-14W4	Sawtooth	885	-15.2	-121
16-36-7-17W4/2	Sawtooth	2545	-15.3	-121
7-1-8-15W4	Sawtooth	817	-15.1	-130
14-27-8-17W4/2	Sawtooth	1160	-14.9	-125
02/16-34-9-13W4	Sawtooth	1036	-15.4	-117
02/3-34-10-15W4	Sawtooth	1178	-15.4	-122
5-30-11-11W4	Sawtooth	1246	-13.8	-116
2-17-11-18W4	Sawtooth	4030	-9.4	-99
9-12-11-19W4	Sawtooth	4669	-8.6	-97
02/8-36-12-15W4	Sawtooth	2011	-13.7	-112
7-9-16-20W4	Sawtooth	16785	-2.2	-78
12-23-1-16W4	Mississippian	462	-16.6	-124
1-6-1-19W4	Rundle	841	-14.8	-119
4-27-8-17W4	Turner Valley	785	-14.7	-121
03/1-5-10-17W4	Livingstone	1428	-14.3	-121
02/8-15-10-19W4	Livingstone	3975	-9.7	-102
7-36-12-26W4	Rundle	8074	-5.3	-89
03/1-33-13-14W4/2	Livingstone	2076	-11.5	-106
13-27-13-26w4	Mississippian	38254	-2.5	-80
5-36-14-10W4	Pekisko	3580	-8.3	-93
8-3-15-16W4	Livingstone	10045	-6.8	-84
11-21-16-12W4	Pekisko	5914	-7.3	-89
16-19-16-12W4	Pekisko	6351	-5.9	-83
02/10-12-16-22W4/2	Rundle	9033	-5.4	-81
4-6-19-10W4	Pekisko	11592	-3.8	-81
7-3-19-14W4	Pekisko	14500	-3.6	-78
12-21-20-6W4/2	Pekisko	5527	-7.7	-80
16-9-20-27W4	Rundle	43281	-0.6	-80
7-33-23-28W4	Rundle	51162	0.6	-70
10-12-23-14W4	Pekisko	9711	-6.9	-80
8-22-30-24w4	Pekisko	24779	-4.0	-80
8-18-30-24W4	Pekisko	30211	-3.5	-82
8-31-12-15W4	Arcs	9802	-6.6	-79
16-20-12-16W4/2	Arcs	30698	-2.1	-57
02/16-30-13-15W4	Arcs	14221	-8.7	-92
14-32-13-16W4	Arcs	13668	-8.1	-88
8-31-13-16W4	Nisku	19214	-6.6	-76
16-4-14-16W4	Nisku	7255	-9.3	-99
14-19-15-16W4	Arcs	6686	-9.6	-93
02/9-13-20-20W4	Nisku	11612	-12.3	-107
3-18-22-16W4	Nisku	14501	-14.4	-121
02/6-13-28-21W4	Nisku	16075	-10.7	-104
6-29-29-19W4	Nisku	17536	-11.3	-104
9-26-29-20W4	Nisku	34608	-8.8	-95
6-11-29-24W4	Nisku	86462	0.9	-66
10-15-29-24W4	Nisku	93205	1.5	-65
10-14-29-24W4	Nisku	151565	2.5	-56
4-1-29-24W4	Nisku	85398	0.5	-94
9-5-29-26W4	Wabamun	54317	3.7	-57

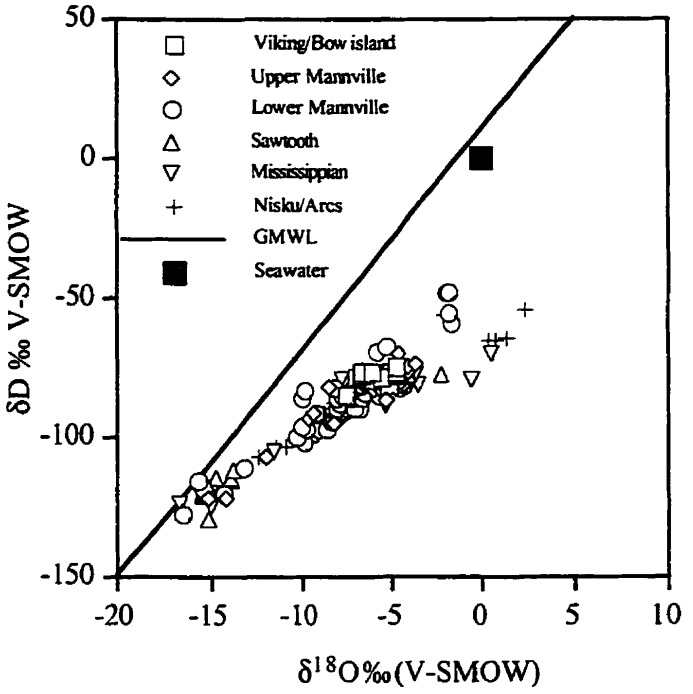

Figure 3.3. Plot of the oxygen and deuterium isotopic composition of formation waters. GMWL is the Global Meteoric Water Line of Craig (1961). Data fall on the trend observed by Hitchon and Friedman (1969) for formation waters of the Alberta basin.

meteoric water with isotopically evolved water results in the compositional variations observed on the δD vs $\delta^{18}O$ (Hitchon and Friedman, 1969; Connolly *et al.*, 1990; Cody and Hutcheon, 1994; and Simpson, 1999). The following sections will investigate the distribution of the freshwater hydraulic head, chloride composition, and isotopic composition of the waters and relate these to the fluid flow regime.

Regional distribution of freshwater hydraulic head, chloride composition, and $\delta^{18}O$ values

The potential for fluid flow can be represented by mapping the distribution of freshwater hydraulic head determined from pressure and elevation data derived from drill stem tests (DST) and production tests. Freshwater hydraulic head was calculated from A and B quality coded drillstem tests. **Table 3.2** summarizes the criteria used by the American Institute of Formation Evaluation (AIFE) for the quality coding. The A and B data are from the highest quality tests, but DST and production induced inconsistencies required a culling procedure to remove inaccurate data. Culling was accomplished through removal of tests that showed a large test interval (>50m) or the testing of more than one aquifer. The removal of tests displaying production induced drawdown was achieved by scrutinizing the data based on testing and production dates and distance to nearest

neighbour producing wells. After culling, 251 Nisku/Arcs, 679 Mississippian, 966 Lower Mannville, 458 Upper Mannville and 2356 Viking/Bow Island wells remained.

Table 3.2. American Institute of Formation Evaluation (AIFE) Quality Coding System Criteria for Coding

A Code – Best Quality

1. Test mechanically sound
2. Recorder used – chart good
3. Flow pressures verify recoveries and/or flow rates
4. Bottom packer held on straddle tests
5. Recorder depths given
6. Recorder within the tested interval
7. ISI stabilized, or near stabilization with increments
8. Preflow time long enough to release hydrostatic head
9. KB elevation given
10. Two good shut-ins required
11. PMAX range of approximately 7 to 69 kPa from read shut-in pressure
12. Fluid to surface on flows
13. Flow incremented

B Code – Nearing stabilization

1. Slight mechanical difficulties, but does not affect the test
2. Shut-ins not fully stabilized
3. Recorder pressures disagree from 7 to 131 kPa after recorder drag and depth difference
4. PMAX range of approximately 138 to 241 kPa from read shut-in pressure
5. Flow pressures do not verify recoveries
6. Plugging, fluid to surface, resets on flows (flow irregularities)
7. Flows incremented

Freshwater equivalent hydraulic head was calculated using:

$$h = z + \frac{P}{\rho g} \qquad 2$$

where z is elevation of the tested interval relative to sea level, P is pressure in kPa, ρ is freshwater density (1,000 kg/m^3), and g is the acceleration due to gravity (9.8 m/s^2).

Contours generated from the distribution of freshwater hydraulic head describe the potentiometric surface. A potentiometric surface is defined as "an imaginary surface, the topography of which reflects the fluid potential of the formation water from place to place within a subsurface reservoir in terms of the elevation to which a column of water would rise above a reference datum within a vertical tube" (Dahlberg, 1982). Two restrictions on evaluating a potentiometric surface are that the aquifer be horizontal and confined. If constant density is assumed, the potential for flow is from areas of high head to areas of low head.

A number of different factors may affect the shape of the potentiometric surface. Changes in permeability are indicated by changes in the distance between contours. A decrease in permeability results in an abrupt decrease in the slope (steeper slope) of the potentiometric surface (Dahlberg, 1982). Density variations in the fluid also affect the head or height of the water column. Heavier, or more dense fluids require lower head values to equilibrate a pressure, thus changes in fluid density may also result in changes in the slope of the potentiometric surface. If the fluid densities are known, a simple calculation can determine the effect, if any, of changes in fluid density on freshwater equivalent head values.

Another factor which may affect the interpretation of flow within an aquifer is the presence of fluids of different densities in a sloping aquifer. Gravity will add a downward component to flow for variable density fluids. The relative significance of this vertical force can be determined using an equation for the driving force ratio (DFR, equation 3.1), an expression of the relative magnitude of a density related error term to the magnitude of the equivalent freshwater head.

On the accompanying maps, the potentiometric surfaces are overlain on the chloride and $\delta^{18}O$ ratio distributions in order to differentiate potential for flow from actual evidence of flow as described by transport or displacement of dissolved species and recharge by meteoric waters. Chloride is chosen as it behaves as a conservative species at Cl <180,000 mg/l and the chloride content of recharge waters (precipitation) is low. Conservative behavior occurs if halite (or other Cl bearing salts) is not encountered along a flow path and increases in chloride content occur only through mixing. Undersaturation of the waters with respect to halite (Cl <180,000 mg/l) suggests that halite is not contributing to the chloride content, thus, mixing is assumed to be the dominant control on chloride content. The chloride distribution can be used as a proxy for density, as increasing chloride content corresponds to increasing density. The oxygen isotopic composition reflects the origin and the extent to which dilution by meteoric water and

water-rock isotope exchange has occurred. In particular, the regional distribution of $\delta^{18}O$ ratios is useful in recognizing meteoric water input and flow paths.

Nisku/Arcs aquifer fluid flow paths

The freshwater equivalent hydraulic head map overlain on the Cl and $\delta^{18}O$ distribution for the Nisku/Arcs aquifer is given in **Figure 3.4**. High head values occur in the southwest, northwest and southeast. A regional low can be found in the north, centered between 112.5° and 113°W and 51°N. Potential for flow is from regions of higher head to regions of lower head, suggesting that possible flow directions described by the potentiometric surface are from the southwest and southeast towards the north, towards the west, north of 50°, and from west to east, west of 113°. Driving force ratios of 1.5 to 2 were calculated for the region west of 113° and north of 51°. The DFR are significantly greater than 0.5 suggesting updip flow potential is considerably decreased by a density-driven downdip component. The steep gradients observed in the west may also reflect permeability changes that result from a lack of hydraulic continuity of the aquifer. The change in head gradient and DFR values in the west, and the widely spaced contours in the east, are interpreted to describe flow in the Devonian Nisku/Arcs aquifer as dominated by a south to north component in the eastern half of the study area. The

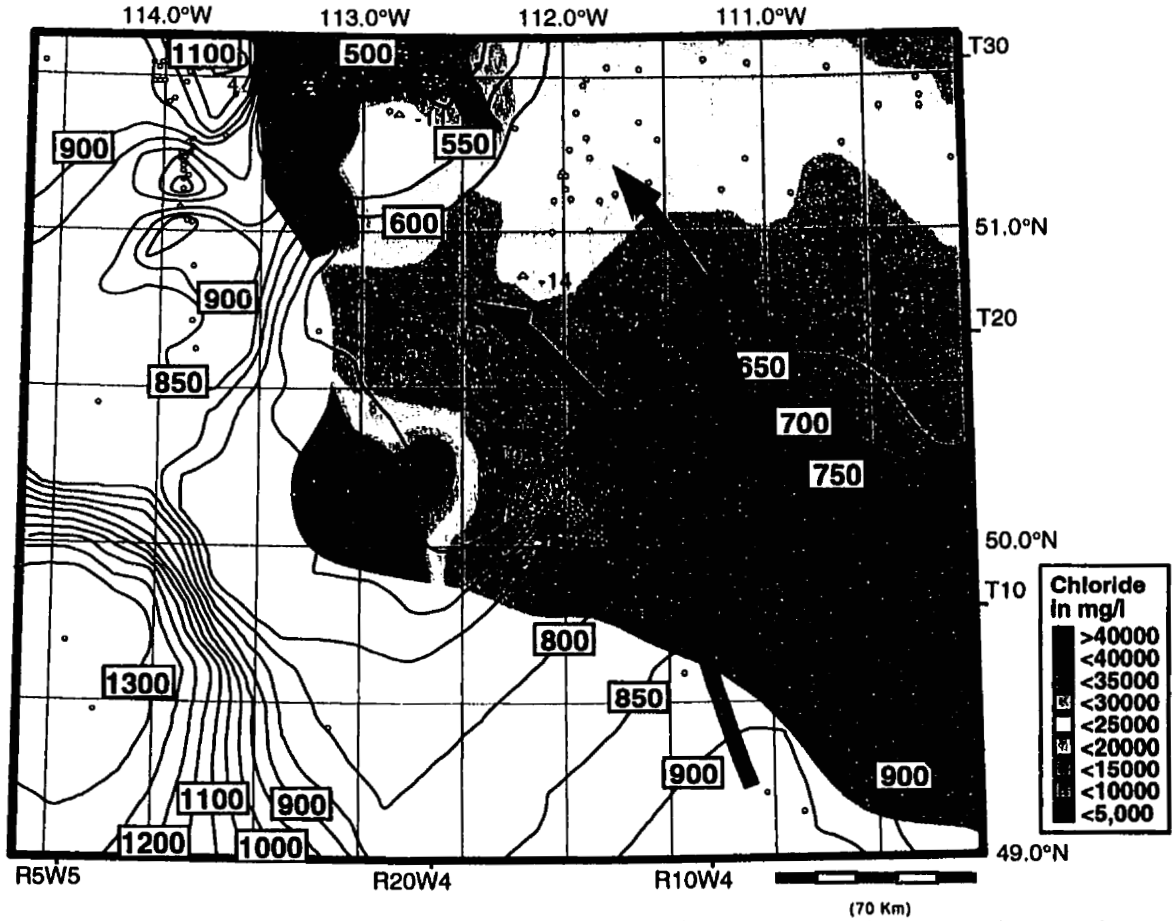

Figure 3.4. Nisku/Arcs potentiometric surface (labelled solid contour lines) overlain on the chloride (coloured contours 5,000 mg/l) and $\delta^{18}O$ distribution (shown as numbers). Arrows show the interpreted flow paths.

distribution of chloride corresponds to the flow directions defined by the potentiometric surface indicating transport and flow directions coincide. The regional distribution in oxygen isotopic composition does not show a consistent relationship with chloride content. South of 50.5°, $\delta^{18}O$ values increase with increasing chloride. The $\delta^{18}O$ ratios north of 50.5° are lower at higher Cl (-14 to –11‰ at Cl >10,000 to 30,000 mg/l) than in the south and decrease to the west.

Mississippian aquifer fluid flow paths

The map of the potentiometric surface overlain on the chloride and oxygen isotope content distribution for the Mississippian aquifer is shown in **Figure 3.5**. Freshwater equivalent head varies from 1650 m to less than 400 m. The southwestern and northwestern regions display steep head gradients. East of 113.4°W, head gradients are less steep with widely spaced contours in the south and more tightly spaced contours north of 50.5°. The potential for flow as described by the potentiometric surface is from the south towards the northeast and northwest. The shallow head gradient roughly corresponds to low chloride concentrations (<5,000 mg/l). The increase in head gradient coincides with an increase in the salinity gradient defined in the previous chapter as a narrow mixing zone between low chloride (<5,000 mg/l) water with higher chloride (5,000-15,000 mg/l Cl) water. The change in chloride content and steeper head gradient

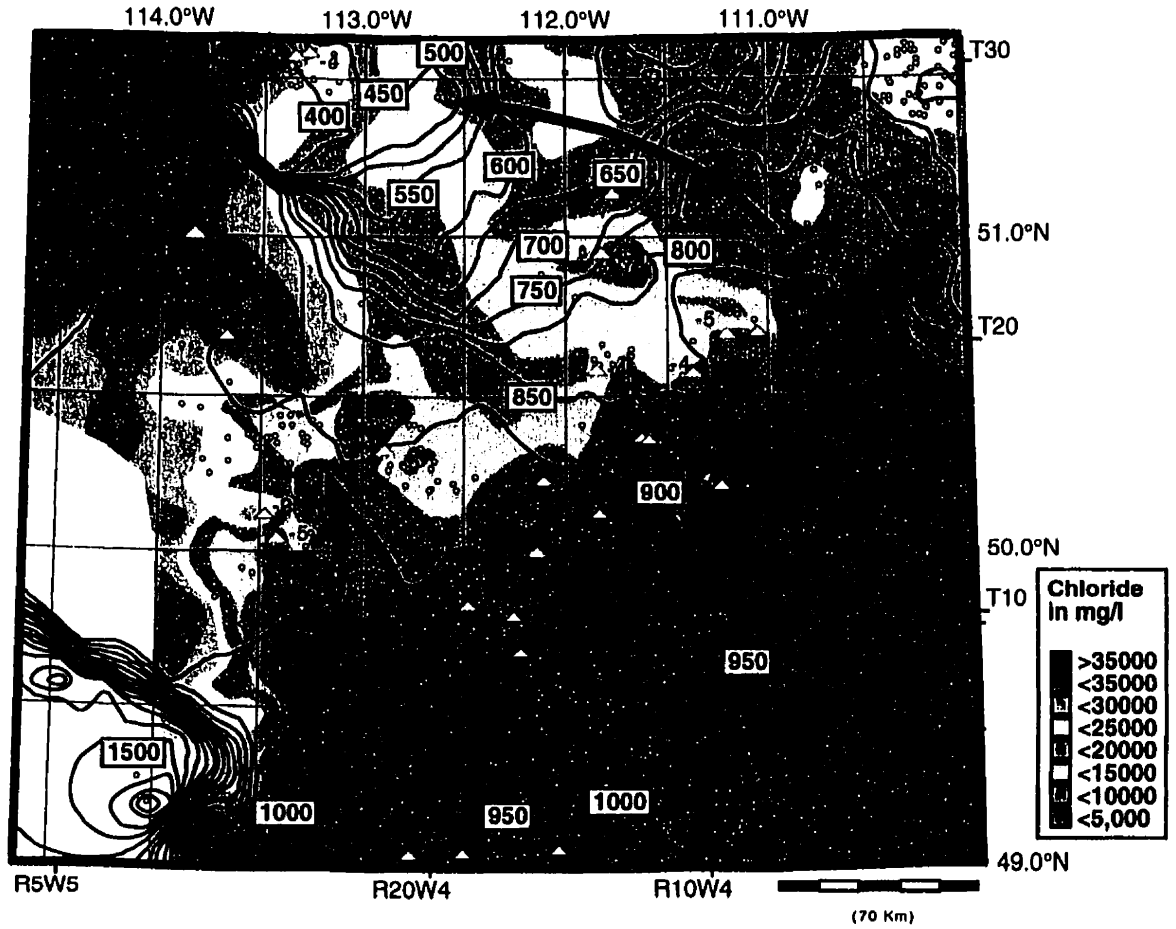

Figure 3.5. Mississippian aquifer potentiometric surface (labelled solid contour lines) overlain on the chloride (coloured contours 5,000 mg/l) and $\delta^{18}O$ distribution (shown as numbers). Arrows show the interpreted flow paths. Oxygen isotope data includes that of Hitchon and Friedman (1969).

suggest a decrease in the permeability or continuity of the aquifer. A decrease in permeability would result in reduced flow producing the rapid increase in the chloride content as the dilution effect of the meteoric water is diminished. Density effects are minimal as head values recalculated to higher salinity do not significantly change the contours. Areas in the south- and northwest, where the head gradient is very steep, may be due to a lack of hydraulic continuity.

The $\delta^{18}O$ values are lowest in the south and increase to the north. Values in the south are consistent with meteoric recharge waters and the increase in $\delta^{18}O$ coincides with increasing chloride content. Chloride content and oxygen isotopic composition suggest recharge from the south and flow directions corresponding to those described by the potentiometric surface with restricted flow in areas where the head contours are closely spaced. In the north (north of 51°) there appears to be a westward component to the flow towards the regional low.

Jurassic aquifer fluid flow paths

The map of the Sawtooth aquifer potentiometric surface, overlain on the chloride and oxygen isotope content distributions, indicates high fluid potential in the southeast and southwest centred on the chloride lows (**Figure 3.6**). Low freshwater

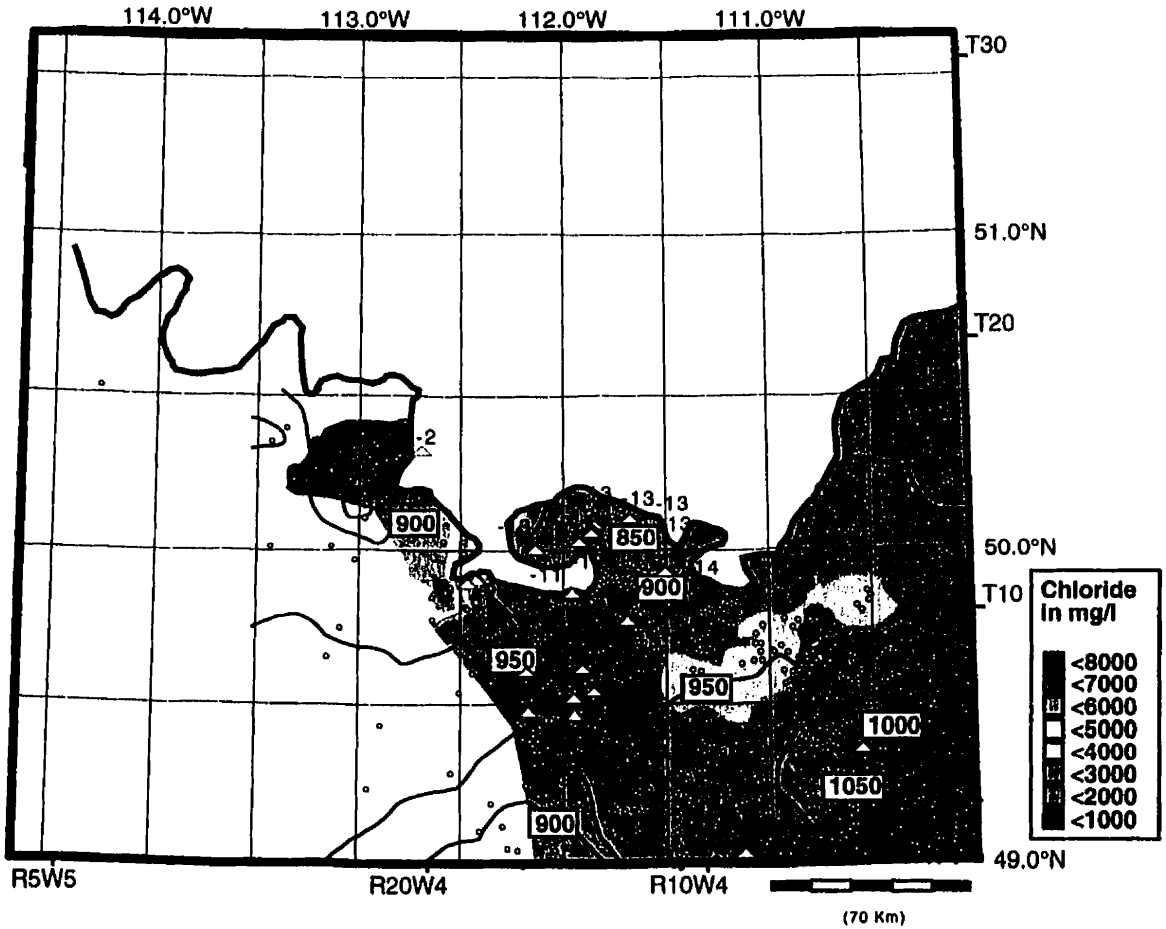

Figure 3.6. Sawtooth aquifer potentiometric surface (labelled solid contour lines) overlain on the chloride (coloured contours 1,000 mg/l) and $\delta^{18}O$ distribution (shown as numbers). Arrows show the interpreted flow paths. Oxygen isotope data includes that of Cody and Hutcheon (1994).

values of hydraulic head occur in the north and northwest. The potential for flow suggests north and northwestward directed flow paths issuing from the high in the southeast, and northwest to east-northeast flow from the high in the southwest. Chloride content is lowest in the southeast and in the area centered on 49.5°N and 112°W, highs are in the northwest. An increase then decrease in the chloride content from southeast to northwest is observed, perhaps indicating sluggish flow or restricted flow paths. The $\delta^{18}O$ distribution indicates meteoric recharge in the regions of chloride lows. An increase in $\delta^{18}O$ values occurs towards the north and northwest. The distribution in chloride content and $\delta^{18}O$ values is consistent with flow directed from the southwest to the north and northeast, issuing from the 950m contour between 49.4° and 49.7°N and west of 112°, and suggests relatively little contribution to regional flow from the southeast.

Lower Mannville aquifer fluid flow paths

The map of the potentiometric surface of the Lower Mannville aquifer, overlain on Cl distribution, is given in **Figure 3.7**. High head values occur in the south and northwest and a regional low occurs in the northwest between 113° and 113.7°. North of the

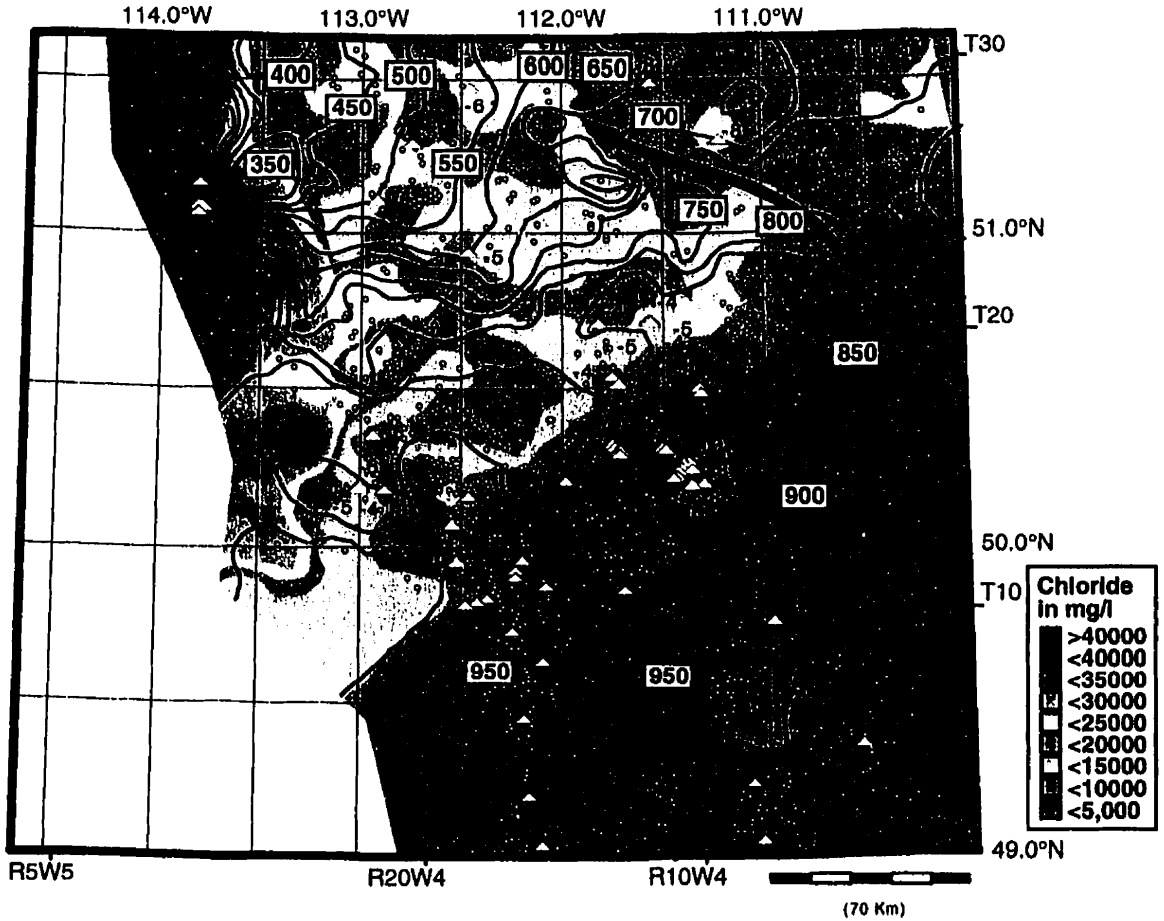

Figure 3.7. Lower Mannville aquifer potentiometric surface (labelled solid contour lines) overlain on the chloride (coloured contours 5,000 mg/l) and $\delta^{18}O$ distribution (shown as numbers). Arrows show the interpreted flow paths. Oxygen isotope data includes that of Hitchon and Friedman (1969), and Cody and Hutcheon (1994).

Jurassic subcrop edge, head values are similar to those found in the underlying Mississippian aquifer (**Figure 3.5**). In the south and east, head contours are widely spaced suggesting reservoir continuity. An increase in the head gradient that roughly coincides with the increasing Cl content occurs north of 50.3° indicating that, like the Mississippian, flow is reduced by a loss of reservoir permeability or continuity. The flow paths described by the potentiometric surface are from south to north towards the regional low and from west to east in the region west of 113.5° and north of 50.5°. A small, northwest directed component to flow is recognized east of 112° and north of 50°. Chloride content is low in the south and displays a narrow mixing or transition zone at Cl >5,000 mg/l between 113° and 111°W.

The $\delta^{18}O$ values increase from south to north and east to west except south of 50°. The flow, as defined by head and chemical composition, is directed from the south (north of 49.5° and east of 112°) towards the northeast with a small component of flow towards the northwest as described above.

Upper Mannville aquifer fluid flow paths

The distribution of freshwater equivalent head for the Upper Mannville aquifer is overlain on a map of the chloride concentration and $\delta^{18}O$ values in **Figure 3.8**. The highest head values (>950 m) occur in the south. The regional low lies in the north, just

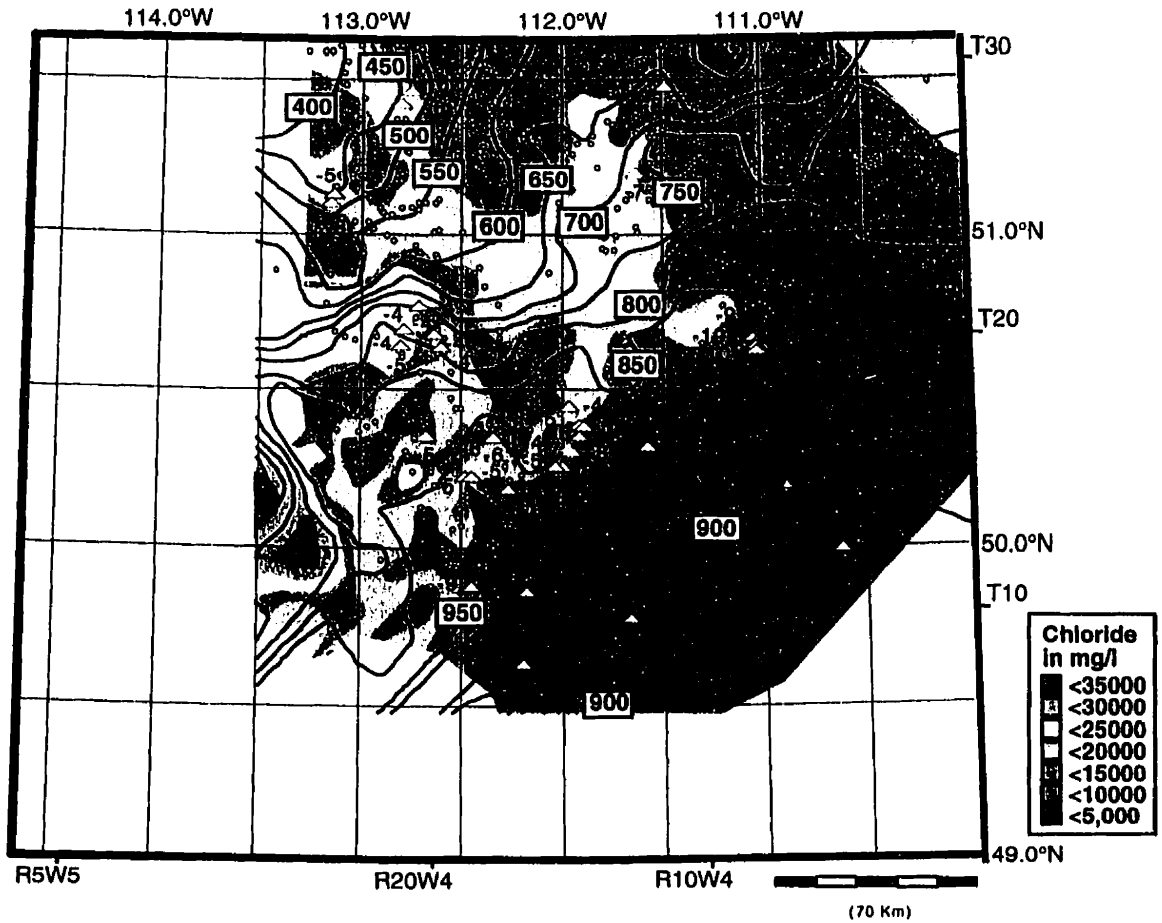

Figure 3.8. Upper Mannville aquifer potentiometric surface (labelled solid contour lines) overlain on the chloride (coloured contours 5,000 mg/l) and $\delta^{18}O$ distribution (shown as numbers). Arrows show the interpreted flow paths. Oxygen isotope data includes that of Cody and Hutcheon (1994).

west of 113°. The potentiometric surface coincides with those of the Lower Mannville and Mississippian with a broad, low head gradient in the south and east alternating to a steeper gradient towards the northwest. The change in head gradient roughly coincides with the increasing chloride concentration gradient. The values of $\delta^{18}O$ increase from south to north and east to west. The potential flow direction is from the south towards the north and northeast and towards the regional low. Fluid flow paths, in terms of head distribution and water chemistry, extend from the southwest to the north and northeast. Flow is redirected towards the low in the northwest, north of 50.7°. Lack of reservoir continuity south of 49.5° strongly suggests recharge from the underlying aquifers.

Viking/Bow Island aquifer fluid flow paths

Figure 3.9 illustrates the potentiometric surface of the Viking/Bow Island aquifer. A regional high occurs in the south with values in excess of 850 m. Lows occur along the western margin of the map area. Freshwater equivalent hydraulic head contours are widely spaced in the east indicating hydraulic connectivity. West of 112.5° the head gradient increases, particularly in the south. The potentiometric surface indicates a flow

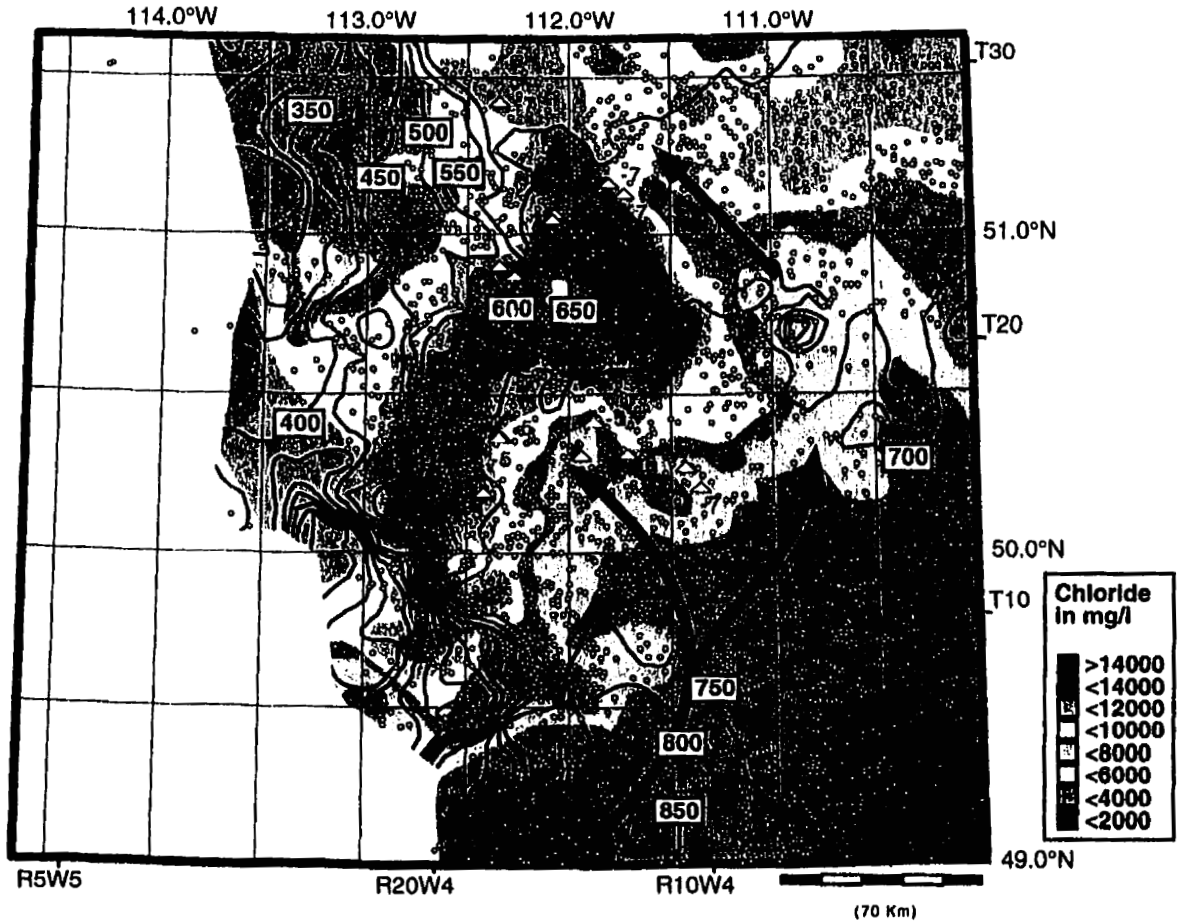

Figure 3.9. Viking/Bow Island aquifer potentiometric surface (labelled solid contour lines) overlain on the chloride (coloured contours 2,000 mg/l) and $\delta^{18}O$ distribution (shown as numbers). Arrows show the interpreted flow paths. Oxygen isotope data includes that of Hitchon and Friedman (1969).

potential from the south to the northeast and northwest. The salinity and head gradients south of 51° roughly coincide, indicating transport and flow potential may be related. The distribution of oxygen isotope composition correlates with chloride content in the southern half of the study area but shows no relation in the north. $\delta^{18}O$ ratios are lower at higher Cl in the north than in the south. Variations in chloride content, used in conjunction with head contours, suggest south to northeast flow with a small component of northwest directed flow, west of 111.5°.

Pressure – Depth plots

Pressure – depth plots were generated for each of the aquifers (**Figures 3.10, 3.11, 3.12, 3.13, 3.14, and 3.15**). Overlain on each plot are pressure gradients based on fresh water (hydrostatic 1,000 kg/m^3), rock (lithostatic 2,600 kg/m^3), oil (oil 870 kg/m^3), and gas (gas 120 kg/m^3).

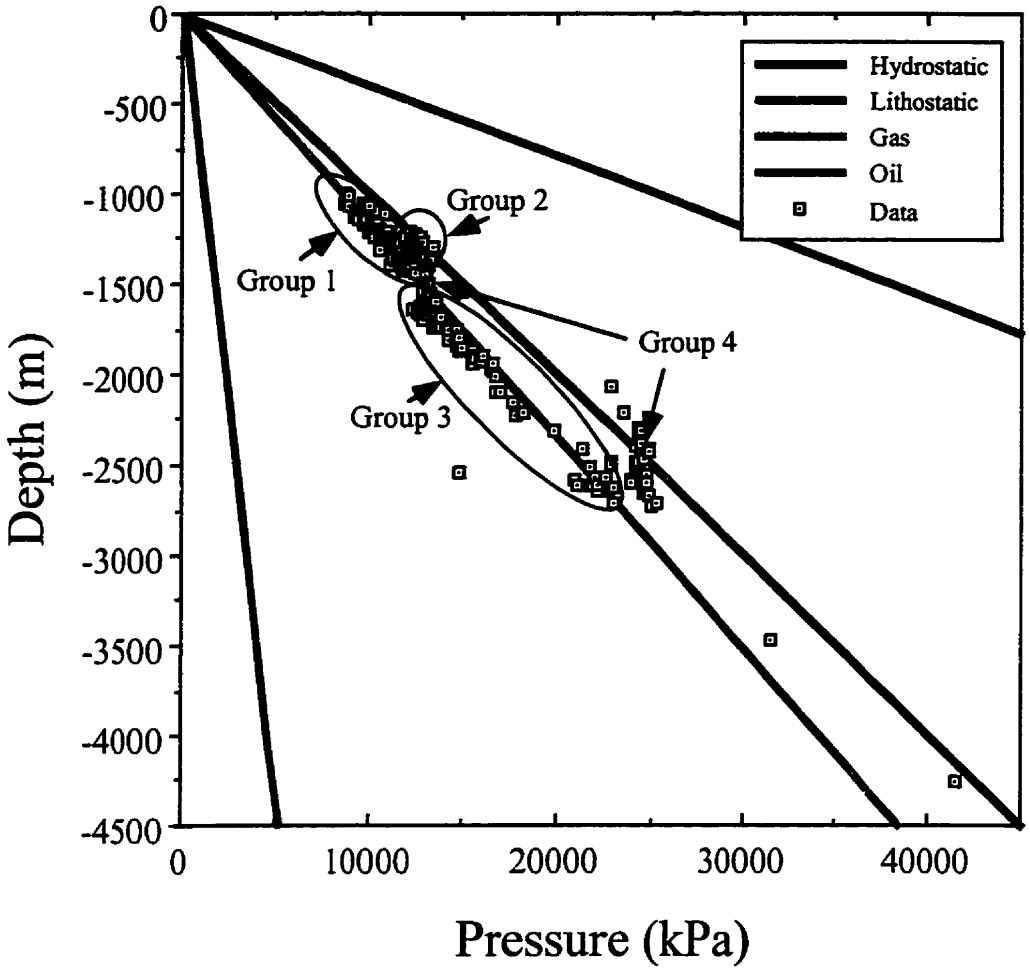

Figure 3.10. Nisku/Arcs aquifer pressure-depth plot. The P-D gradients reflect compartments that are recognised regionally on the potentiometric surface and chloride distribution maps. Group 1 occurs in the north, east of the potentiometric low in the north. Group 2 occurs in the south, east of 112.8°W. Group 3 occurs west of 112.8°W. Group 4 corresponds to the potentiometric low in the north. Note the gas pressure gradient connection Group 1 and 2 with Group 3.

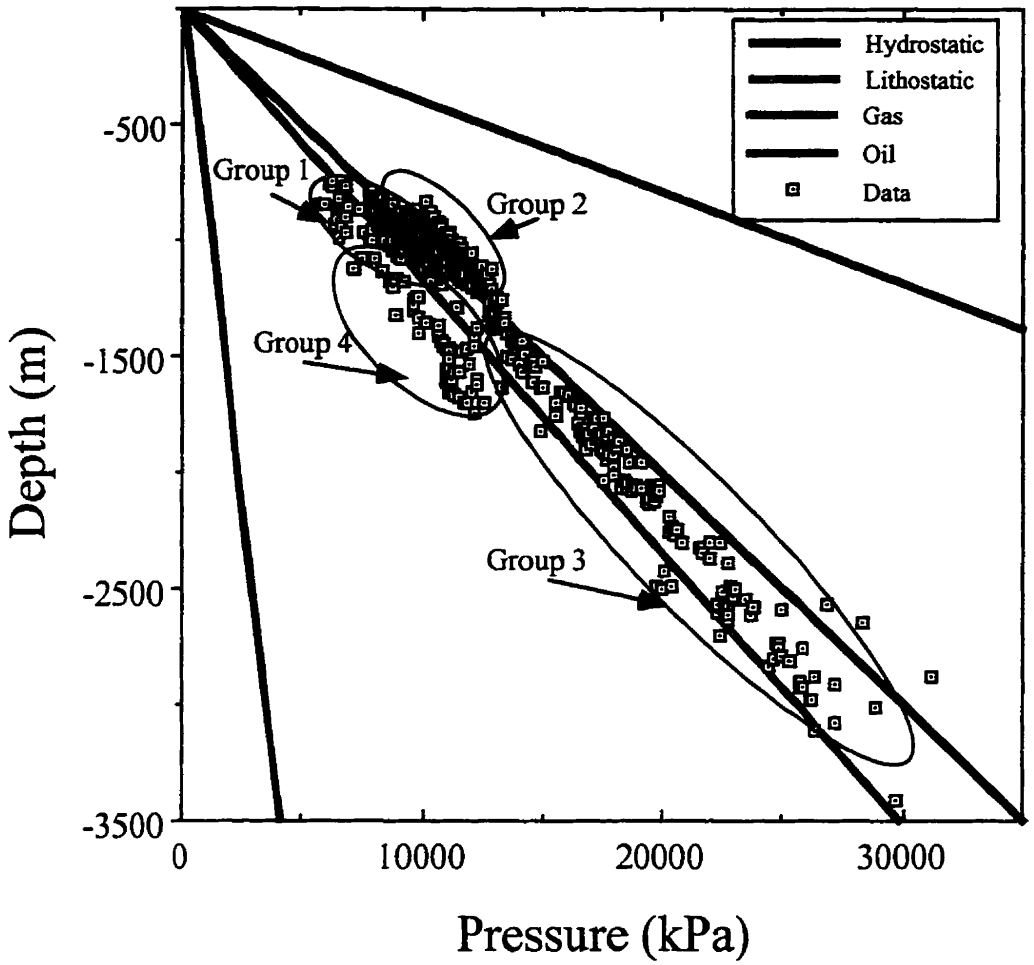

Figure 3.11. Mississippian aquifer pressure-depth plot. The P-D gradients reflect compartments that are recognised regionally on the potentiometric surface and chloride distribution maps. Group 1 occurs in the north, east of the potentiometric low in the north. Group 2 occurs in the south, east of 112.8°W and corresponds to the low chloride (<10,000 mg/l) region. Group 3 occurs west of 112.8°W. Group 4 corresponds to the regional potentiometric low in the north. Note the gas pressure gradient connection Group 2 with Group 3.

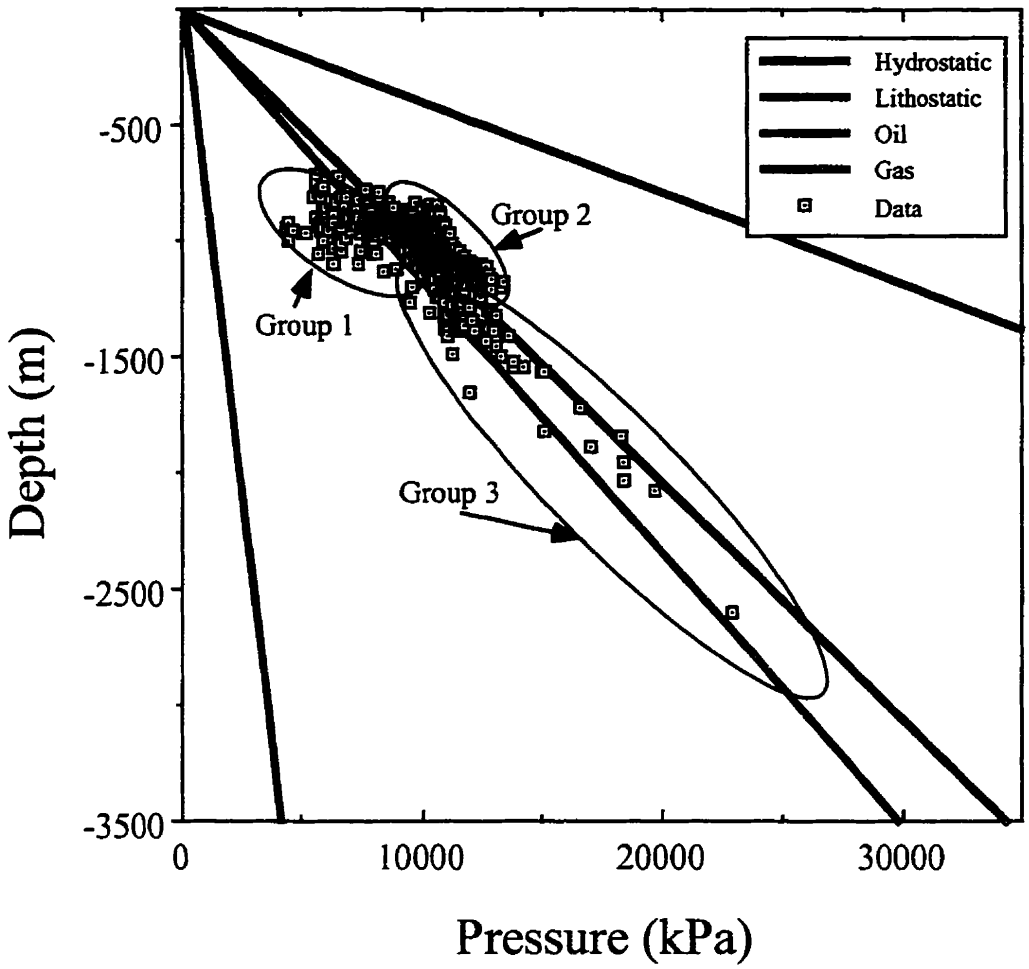

Figure 3.12. Sawtooth aquifer pressure-depth plot. The P-D gradients reflect compartments that are recognised regionally on the potentiometric surface and chloride distribution maps. Group 1 occurs in the southeast. Group 2 occurs east of 112.8°W and west of 111°W. Group 3 occurs west of 112.8°W. Note the gas pressure gradient connection Group 2 with Group 3.

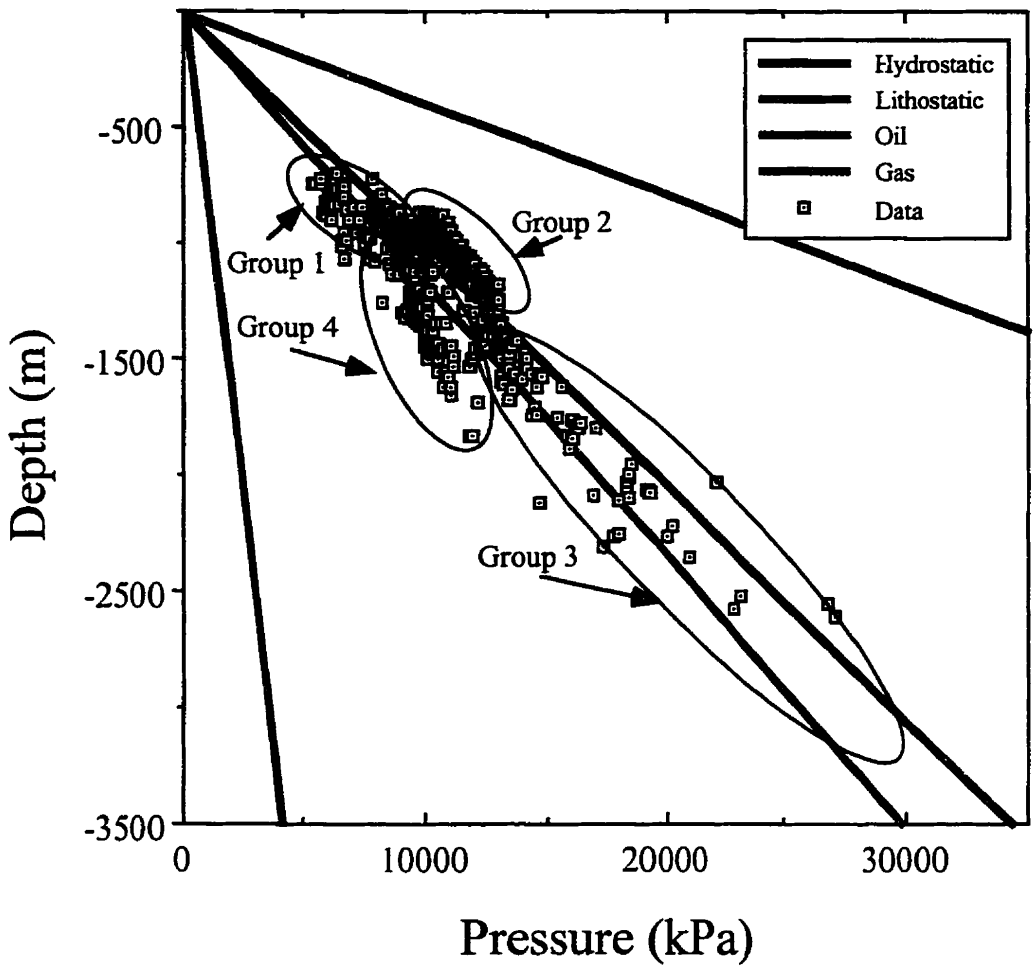

Figure 3.13. Lower Mannville aquifer pressure-depth plot. The P-D gradients reflect compartments that are recognised regionally on the potentiometric surface and chloride distribution maps. Group 1 occurs east of 111°W in the northeast and southeast. Group 2 occurs east of 112.8°W and west of 111°W south of the change in head gradient observed on the potentiometric surface map. Group 3 occurs west of 112.8°W. Group 4 corresponds to the region of potentiometric lows in the north. Note the gas pressure gradient connection Group 2 with Group 3.

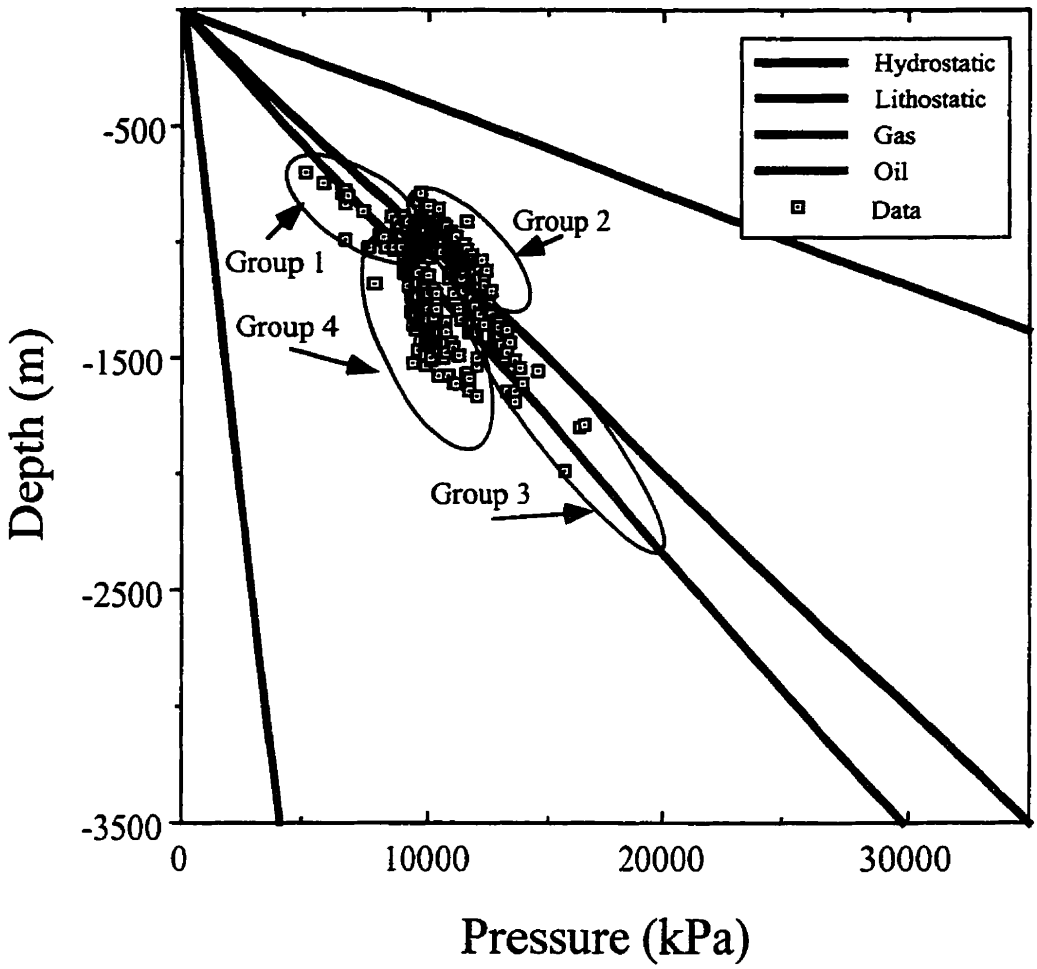

Figure 3.14. Upper Mannville aquifer pressure-depth plot. The P-D gradients reflect compartments that are recognised regionally on the potentiometric surface and chloride distribution maps. Group 1 occurs east of 111 in the northeast. Group 2 occurs east of 112.8°W and west of 111°W south of the change in head gradient observed on the potentiometric surface map. Group 3 occurs west of 112.8°W. Group 4 corresponds to the region of potentiometric lows in the north. Note the gas pressure gradient connection Group 2 with Group 3.

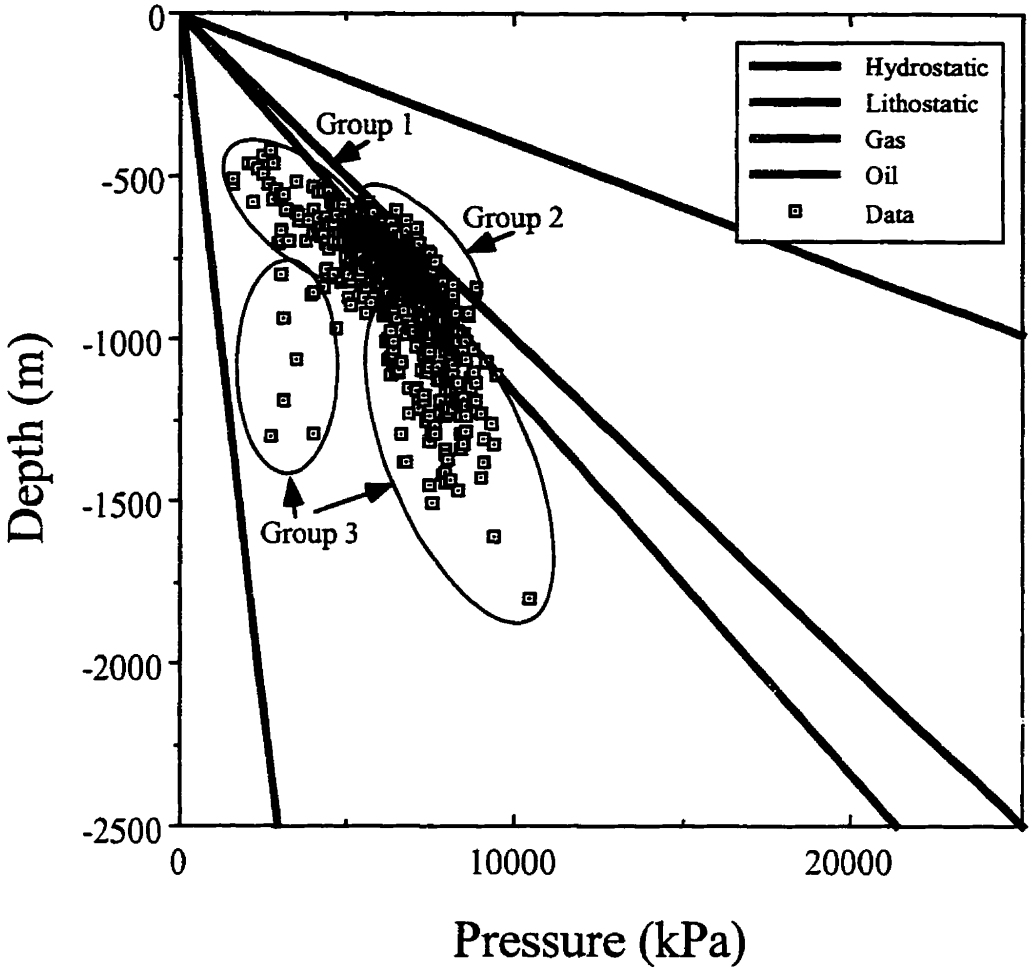

Figure 3.15. Viking/Bow Island aquifer pressure-depth plot. The P-D gradients reflect compartments that are recognised regionally on the potentiometric surface and chloride distribution maps. Group 1 occurs east of 111 in the northeast and southeast. Group 2 occurs east of 112.8°W and west of 111°W. Group 3 occurs west of 112.5°W.

The P-D plots illustrate several key features:

1. Pressure – depth plots display gradients similar to those of fresh water and gas controlled systems (**Figure 3.10 to 3.15**).
2. Up to four different compartments can be recognized and these compartments correspond to regions defined in the potentiometric surface maps and chloride distributions.
3. Mississippian, Sawtooth, Lower Mannville and Upper Mannville pressure gradients are similar indicating a single hydrostratigraphic system (**Figures 3.11, 3.12, 3.13 and 3.12**).
4. A gas induced pressure gradient separates the regional potentiometric low in the north from surrounding areas (**Figures 3.10, 3.11, 3.12, 3.13, 3.14, and 3.15**).
5. West of approximately 112.8°W aquifers display an hydrostatic pressure gradient but they are separated from the eastern region by a gas induced pressure gradient except for the Viking/Bow Island aquifer in which the western region is under gas density dependent gradients (**Figures 3.10, 3.11, 3.12, 3.13, 3.14, and 3.15**).

Oxygen isotopic composition and water-rock interaction

Water-rock interactions have been suggested to explain the enrichment of waters in the heavier isotopes of oxygen and hydrogen (Clayton *et al.*, 1966; Hitchon and Friedman,

1969; and Longstaffe, 1986). In particular, oxygen isotopic equilibration between water and carbonate rocks is important because carbonate minerals are a large reservoir of easily exchangeable oxygen atoms (Kharaka and Carothers, 1986). The possibility of control over the ^{18}O content of the water by isotope exchange between water and carbonates is investigated by plotting the $\delta^{18}O$ against temperature (**Figures 3.16, 3.17, 3.18, 3.19, 3.20, and 3.21**). The diagrams show the temperature equilibrium values of $\delta^{18}O(H_2O)$ for the range of $\delta^{18}O$ compositions of calcites or dolomites from the Mississippian and Nisku/Arcs carbonates and calcite cements of the clastic rocks using the calcite-water and dolomite-water fractionation factors of Friedman and O'Neil (1977), and two dolomite-water fractionation factors from Land (1983). Superimposed on these diagrams are the analyzed $\delta^{18}O$ ratios of the waters at reservoir temperature. The oxygen isotopic composition of Nisku/Arcs dolomite is +26‰ (Hitchon and Friedman, 1969; Whitaker and Mountjoy, 1996) and calcite in Mississippian limestones is approximately +19‰ to +21‰ (Hitchon and Friedman, 1969; Connolly *et al.*, 1990), and those of calcite cement in Mannville clastic rocks are +15‰ to +18‰ (Hitchon and Friedman, 1969; Connolly *et al.*, 1990) and +19‰ to +23‰ for the Viking Formation (Hitchon and Friedman, 1969; Longstaffe and Ayalon, 1987; McLellan, 1995).

The majority of the waters sampled from Nisku/Arcs reservoirs are not in temperature equilibrium with the host rock below 70°C (**Figure 3.16**). The higher temperature

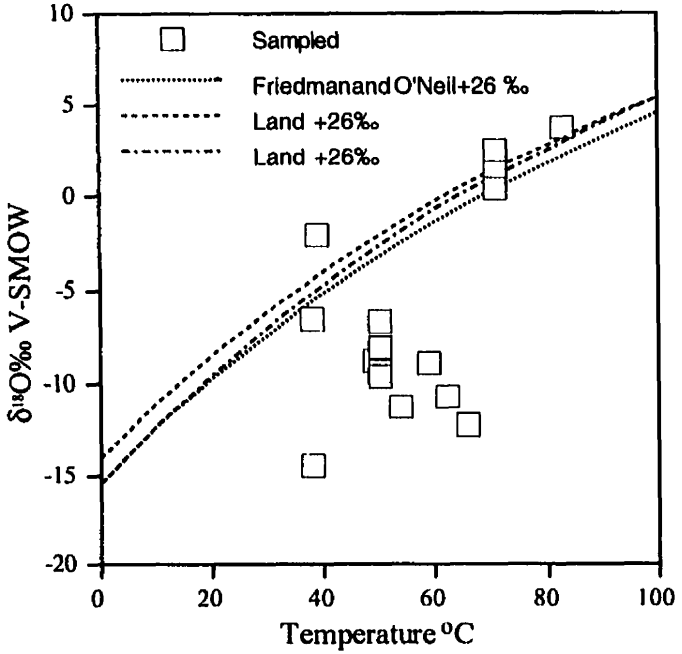

Figure 3.16. Plot of the relation between Nisku/Arcs aquifer water and carbonates in the $\delta^{18}O$ vs temperature format. The lines represent the oxygen isotopic composition of water in equilibrium with dolomite that has $\delta^{18}O$=+26‰ using the isotope fractionation factors of Friedman and O'Neil (1977) and Land (1983).

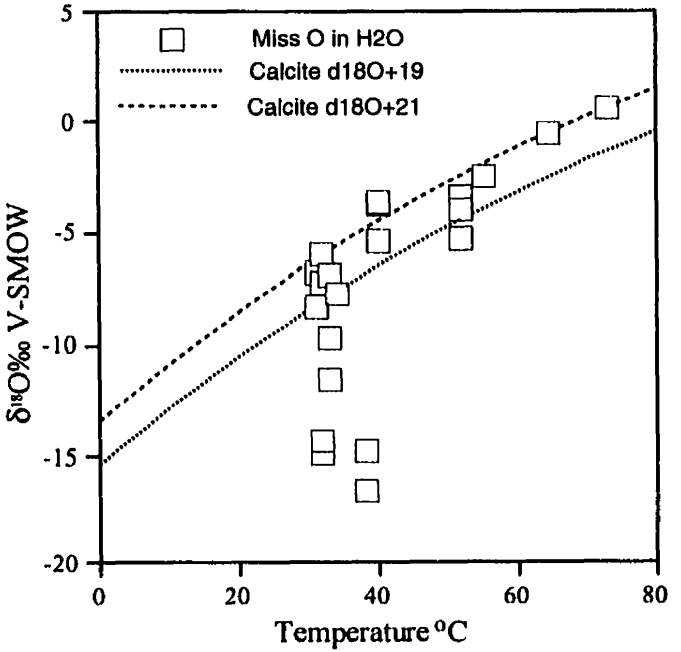

Figure 3.17. Plot of the relation between Mississippian aquifer water and carbonates in the $\delta^{18}O$ vs temperature format. The lines Calcite $\delta^{18}O$=+19‰, and $\delta^{18}O$=+21‰ represent the oxygen isotopic composition of water in equilibrium with calcite that has $\delta^{18}O$=+19‰ to +21‰ using the isotope fractionation factor of Friedman and O'Neil (1977).

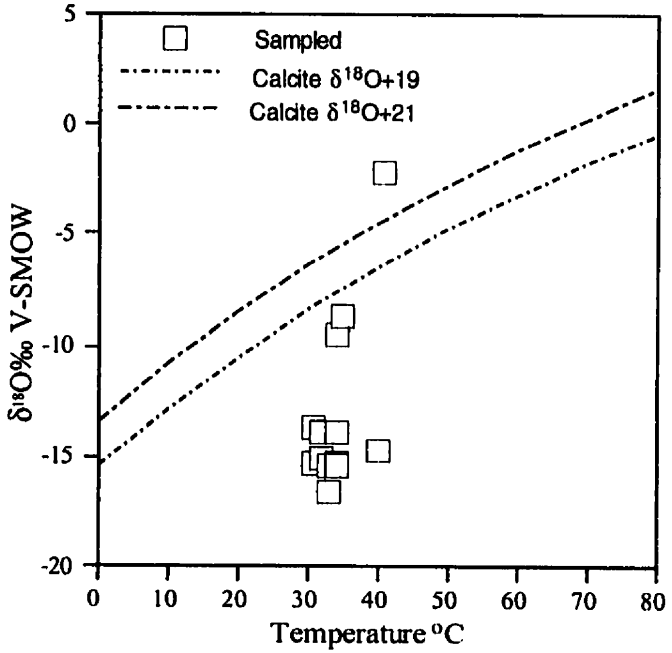

Figure 3.18. Plot of the relation between Sawtooth aquifer water and carbonates in the $\delta^{18}O$ vs temperature format. The lines Calcite $\delta^{18}O$=+19‰, and $\delta^{18}O$=+21‰ represent the oxygen isotopic composition of water in equilibrium with Mississippian calcite that has $\delta^{18}O$=+19‰ to +21‰ using the isotope fractionation factor of Friedman and O'Neil (1977).

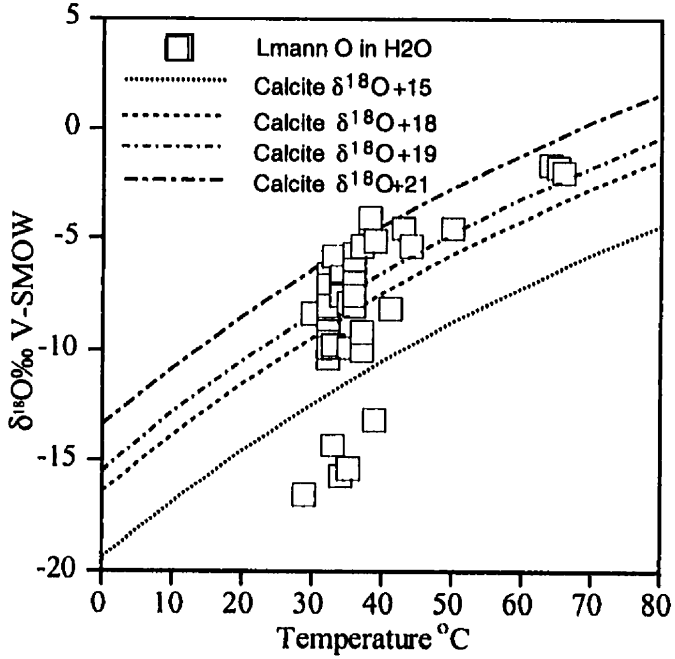

Figure 3.19. Plot of the relation between Lower Mannville aquifer water and carbonates in the $\delta^{18}O$ vs temperature format. The lines Calcite $\delta^{18}O$=+19‰, and $\delta^{18}O$=+21‰ represent the oxygen isotopic composition of water in equilibrium with Mississippian calcite that has $\delta^{18}O$=+19‰ to +21‰ and $\delta^{18}O$=+15‰, and $\delta^{18}O$=+18‰ represent calcite cement that has $\delta^{18}O$=+15‰ to +18‰ using the isotope fractionation factor of Friedman and O'Neil (1977).

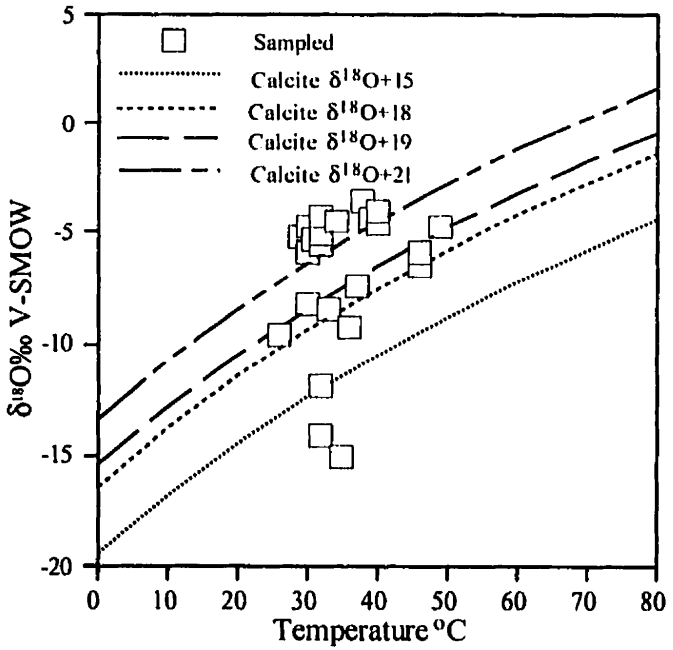

Figure 3.20. Plot of the relation between Upper Mannville aquifer water and carbonates in the $\delta^{18}O$ vs temperature format. The lines Calcite $\delta^{18}O$=+19‰, and $\delta^{18}O$=+21‰ represent the oxygen isotopic composition of water in equilibrium with Mississippian calcite that has $\delta^{18}O$=+19‰ to +21‰ and $\delta^{18}O$=+15‰, and $\delta^{18}O$=+18‰ represent calcite cement that has $\delta^{18}O$=+15‰ to +18‰ using the isotope fractionation factor of Friedman and O'Neil (1977).

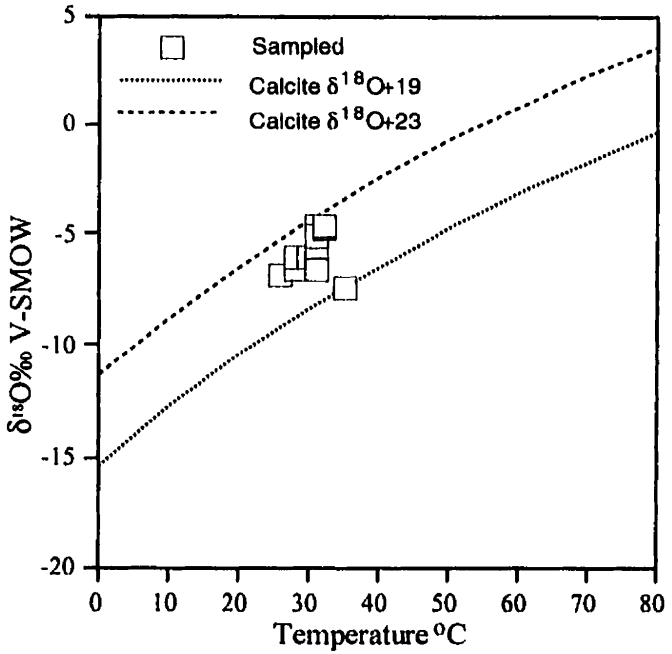

Figure 3.21. Plot of the relation between Viking/Bow Island aquifer water and carbonates in the $\delta^{18}O$ vs temperature format. The lines Calcite $\delta^{18}O$=+19‰, and $\delta^{18}O$=+23‰ represent the oxygen isotopic composition of water in equilibrium with calcite cement that has $\delta^{18}O$=+19‰ to +23‰ using the isotope fractionation factor of Friedman and O'Neil (1977).

samples (70 °C and higher) appear to be in isotope equilibrium with dolomite. $\delta^{18}O$ values that are not in isotopic equilibrium with the host rock are interpreted to reflect a component of the isotopic signature of meteoric water.

The Mississippian to Upper Mannville hydrostratigraphic group diagrams include the Mississippian calcite-water fractionation curves because of the close hydrologic relationship between the different aquifers. **Figures 3.17, 3.18, 3.19, and 3.20** illustrate that many of the low temperature samples are not in isotopic equilibrium with the Mississippian limestones. The majority of these samples have <5,000 mg/l chloride and the $\delta^{18}O$ values reflect input of meteoric water. A number of samples fall within the range defined by Lower Mannville and Upper Mannville calcite cements. Of these, two Lower Mannville (16-20-1-8W4, 4-7-5-4W4) and two Upper Mannville waters (02/11-6-29-20W4 and 02/11-6-29-20W4) were collected proximal to the measured calcite data. The close relationship suggests that the calcite was probably precipitated from the current fluid and reflects isotopic equilibrium. The remainder of the data plot within or above the range defined by equilibrium with Mississippian calcite. These data are from waters collected from within the narrow mixing zone (defined in the chloride maps), and from the higher chloride waters to the north and west of the mixing zone (**Figures 3.5, 3.7, and 3.8**).

The Viking/Bow Island aquifer data cluster in a region defined by the upper and lower limits of equilibration with coexisting calcite cements (**Figure 3.21**). Isotopic equilibrium with a calcite cement in a clastic rock is more likely evidence of precipitation of the cement from the existing formation water as the mass of water is considerably greater than the mass of cement. A simple mass balance calculation (moles of O in calcite = moles of O in water) requires nearly 2 kg of calcite (or approximately 9% volume at 10% porosity) per kg of water for the calcite to control the oxygen isotopic composition of the water. Cements typically make up less than a few percent of the rock (for porous and permeable rocks) and cannot account for the mass needed. Longstaffe (1989) lists a number of researchers who have used paragenetic sequences and oxygen isotopic compositions of authigenic phases to estimate the isotopic composition of formation waters based on evidence that the authigenic phases were not equilibrated with current water composition. Their results indicate that diagenetic mineral phases may not significantly alter the isotopic composition of the water.

Isotopic compositions that fall above the Devonian dolomite and Mississippian calcite isotope composition-temperature curves may reflect higher temperatures of equilibration. The current reservoir temperatures are lower than those experienced prior to Late Oligocene to Miocene erosion in the Alberta basin. The Upper Mannville samples in particular have a considerable number of analyses that lie above the calcite curve.

Temperatures calculated to reflect equilibrium with calcite are 5° to 15°C higher than current reservoir temperatures. There is however, no way of determining accurate temperatures with this method, as some mixing with meteoric water has occurred.

Connolly *et al.* (1990) found that the waters in central Alberta are not isotopically equilibrated with the carbonates in the associated rocks. In this study it appears that many of the waters are in temperature equilibrium with the carbonates and cements. The waters in the Upper and Lower Mannville appear to show, with considerable scatter, $\delta^{18}O$ values similar to values for waters in temperature equilibrium with Mississippian limestone. This may be explained if the waters flowed into the clastic units from the underlying Mississippian carbonates and have retained the oxygen isotopic composition of equilibration with the Mississippian calcite.

$\delta^{18}O$-Cl

Variations in the isotopic composition of formation waters may be the result of mixing or of water-rock interaction (Kyser, 1987; Longstaffe, 1987). Although the $\delta^{18}O$ content of waters can be affected by water-rock interaction, if ^{18}O behaves largely conservatively (extent of water-rock interaction is small), plotting $\delta^{18}O$ values against chloride content can reveal variations in chemistry due to mixing.

The Nisku/Arcs formation water samples (**Figure 3.22**) generally, have increasing $\delta^{18}O$ ratios with increasing chloride. At Cl <30,000 mg/l the oxygen isotopic composition displays considerable scatter. The lowest chloride content waters have $\delta^{18}O$ ratios of –9 to –10‰ and four of the samples (at <30,000 mg/l Cl) have lower $\delta^{18}O$ ratios at higher chloride content. The four samples (02/9-13-20-20W4, 3-18-22-16W4, 02/6-13-28-21W4, and 6-29-29-19W4) come from wells sampled in the northern part of the study area (**Table 3.1**). In the previous chapter it was determined that chloride displays conservative behavior and mixing of a marine evaporative brine with dilute meteoric water controls the chloride content. A single mixing event should result in a linear increase in $\delta^{18}O$ ratios with increasing chloride. The non-linear relationship indicates that meteoric water has mixed with water of varying chloride content. The variations in chloride content suggest dilution from an earlier event. The oxygen isotopic data variations at <30,000 mg/l Cl imply that at least two meteoric incursions have occurred. The most recent event is represented by the low chloride water in the southeast (**Figure 3.4**). Samples collected south of 50.5° are located along the western edge of the low chloride recharge water suggesting that the composition of these waters has been influenced by the most recent meteoric event.

The $\delta^{18}O$ content plotted versus chloride concentration of the Mississippian to Upper Mannville hydrostratigraphic group show similar patterns for most of the aquifers

(Figures 3.23, 3.24, 3.25, and 3.26). From these diagrams and **Table 3.1** several trends can be distinguished:

1. For chloride concentrations below ~5,000 mg/l, $\delta^{18}O$ ratios increase markedly from –16‰ to –7.5‰ as Cl concentrations increase.
2. Between 5,000 and ~10,000 mg/l Cl there is a distinct change in slope with $\delta^{18}O$ values increasing from –7.5‰ to ~–5‰.
3. Above ~10,000 mg/l, chloride content and $\delta^{18}O$ ratios appear to be largely independent except for the Mississippian where a linear increase is observed.
4. The Lower Mannville and Upper Mannville samples from the northeast and Lower Mannville waters from south of the Jurassic subcrop edge have more negative $\delta^{18}O$ ratios at higher chloride contents (**Table 3.1, Figures 3.25 and 3.26**).

At low chloride content the $\delta^{18}O$ values are similar to present-day precipitation. The data for the <5,000 mg/l chloride suggest that the oxygen isotopic composition of these waters is largely controlled by mixing with meteoric water. Between 5,000 and 10,000 mg/l Cl the change in $\delta^{18}O$ ratios reflects a narrow mixing zone of waters with a minor meteoric contribution and waters that are at, or near, isotopic equilibrium with Mississippian calcite. Above approximately 10,000 mg/l chloride, the data reflect isotopic equilibrium with Mississippian calcite and do not correlate with chloride content.

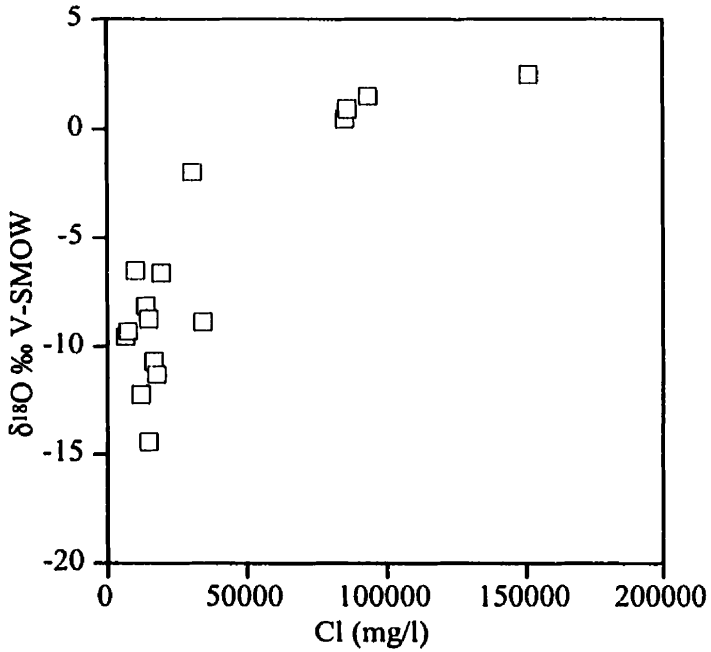

Figure 3.22. Nisku/Arcs aquifer water $\delta^{18}O$ ‰ vs Cl. Low chloride waters tend to have $\delta^{18}O$ values displaying meteoric influence and a non-linear relationship to Cl. At high Cl, $\delta^{18}O$ values are typical of an evolved brine.

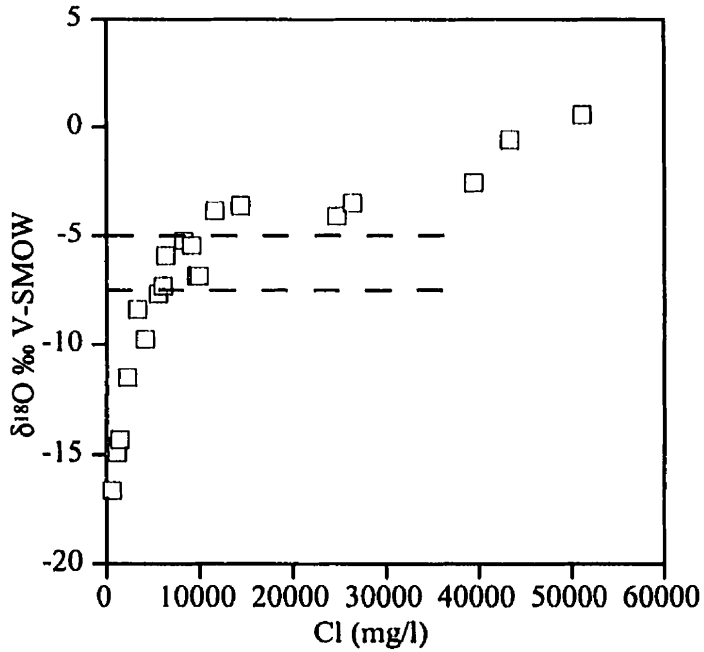

Figure 3.23. Mississippian aquifer water $\delta^{18}O$ ‰ vs Cl. Low chloride waters show a linear increase in $\delta^{18}O$ values that reflect mixing with meteoric water. A change in slope at -7.5‰ and at -5‰ mark the boundaries of the isotope trends.

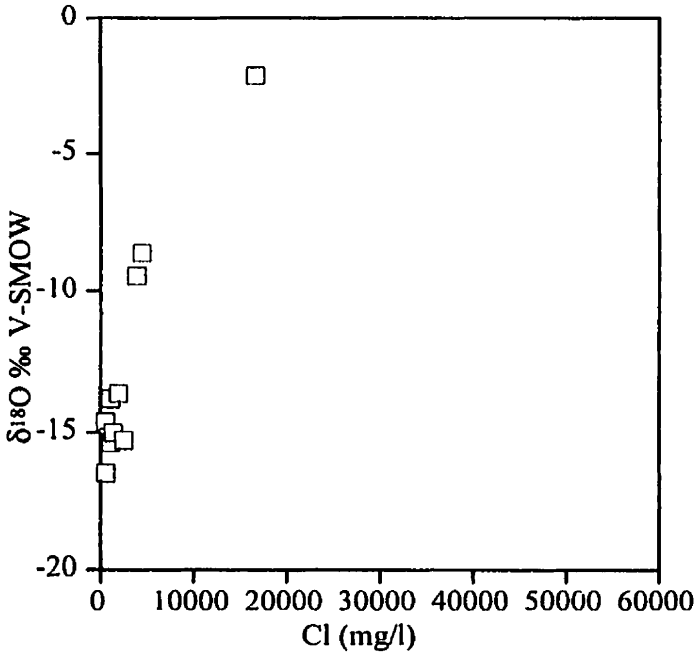

Figure 3.24. Sawtooth aquifer water $\delta^{18}O$ ‰ vs Cl. Low chloride waters show a linear increase in $\delta^{18}O$ values that reflect mixing with meteoric water.

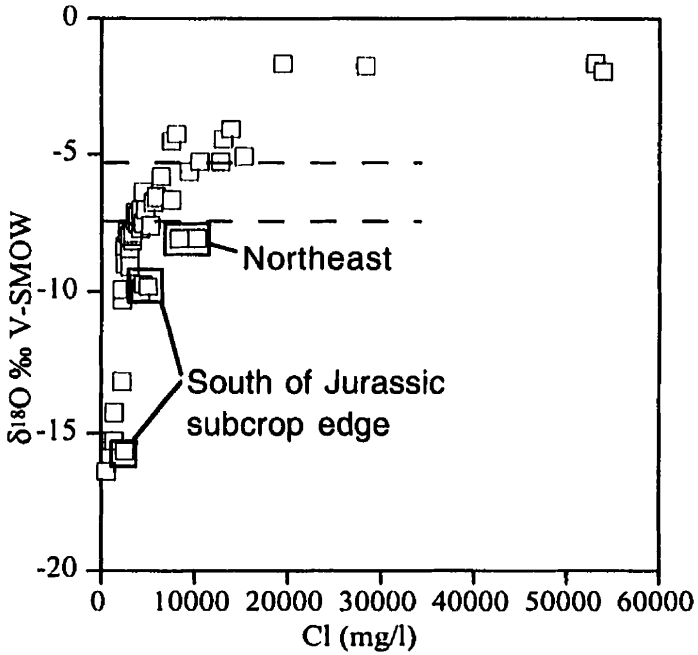

Figure 3.25. Lower Mannville aquifer water $\delta^{18}O$ ‰ vs Cl. Low chloride waters show a linear increase in $\delta^{18}O$ values that reflect mixing with meteoric water. A change in slope at approximately -7.5‰ and at -5‰ mark the boundaries of the isotope trends. Data that do not fit the general trend are from geographically limited areas in the southeast and northeast.

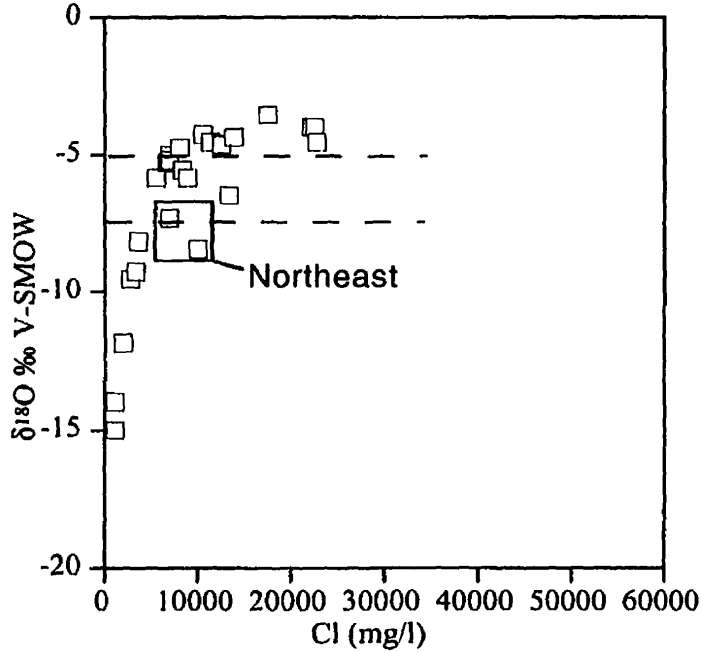

Figure 3.26. Upper Mannville aquifer water $\delta^{18}O$ ‰ vs Cl. Low chloride waters show a linear increase in $\delta^{18}O$ values that reflect mixing with meteoric water. A change in slope at approximately -7.5‰ and at -5‰ mark the boundaries of the isotope trends. Data from the northeast have higher Cl content than expected for the ^{18}O content.

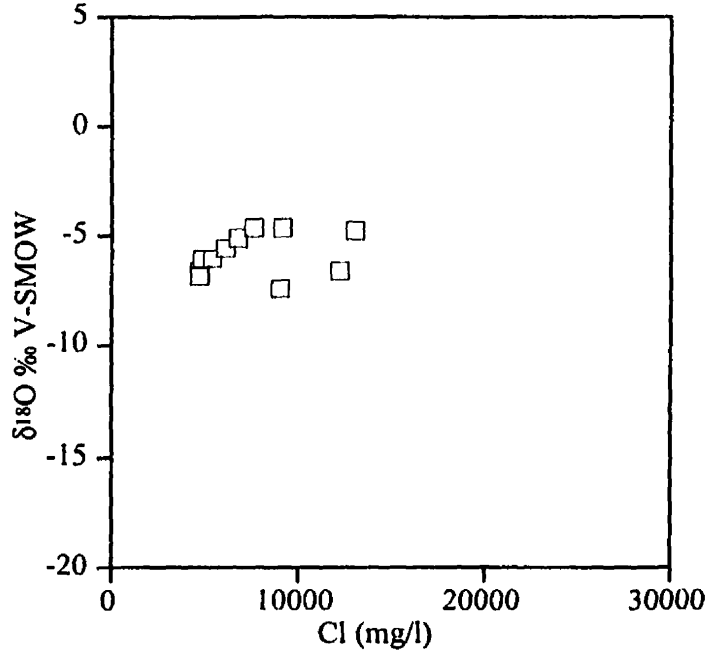

Figure 3.27. Viking/Bow Island aquifer water $\delta^{18}O$ ‰ vs Cl. At <9,000 mg/l Cl, waters show a linear increase in $\delta^{18}O$ values that reflect mixing with meteoric water. Above 9,000 mg/l, data are scattered.

In the previous chapter, it was determined that, like the Nisku/Arcs formation water, the Mississippian to Upper Mannville formation waters originated as residual evaporite brines that have been diluted to varying extent by meteoric water. The oxygen isotopic data suggest that at least two mixing and dilution events must have occurred. The earlier event had to have taken place prior to the introduction of the waters into the Lower and Upper Mannville aquifers as the waters appear to have equilibrated with Mississippian calcite. The current flow regime has resulted in $\delta^{18}O$ values that reflect mixing with present-day meteoric water.

The plot of the Viking/Bow Island $\delta^{18}O$ to Cl is consistent with mixing at low Cl (<9,000 mg/l), but shows considerable scatter at higher Cl (**Figure 3.27**). Low chloride waters are from the south and higher Cl content is in the north (**Table 3.1**). The waters from the south appear to reflect mixing with meteoric water, however the intercept with the $\delta^{18}O$ axis is approximately −10‰, which is 6‰ higher than present-day precipitation.

δD-Cl

Deuterium is considered to behave more conservatively than oxygen in aquifer waters because the amount of available hydrogen in minerals tends to small relative to the amount in the water (Longstaffe, 1987). Plotting values of δD against chloride can be a useful technique in determining changes in composition of waters due to mixing.

Figures 3.28, 3.29, 3.30, 3.31, 3.32, and 3.33 illustrate plots of δD vs Cl content. Like the $\delta^{18}O$ vs Cl plots, there is a general increase in δD with increasing chloride. All of the aquifers display trends similar to those observed in the $\delta^{18}O$ vs Cl. At greater than 10,000 mg/l Cl the Lower Mannville and Mississippian are considerably different. Lower Mannville waters display an enrichment in deuterium with higher chloride whereas the Mississippian shows little change from those of lower Cl.

The origin of this difference is not known, but may reflect a greater availability of hydrogen in the clastic rocks relative to the carbonates. However, Longstaffe (1989) points out that most hydrous phases are depleted in deuterium relative to water. Exchange of hydrogen with mineral phases in the clastic rocks should result in a shift towards more negative values of δD at the temperatures experienced by these rocks, not the more positive values as observed (**Figure 3.31**).

Discussion

The Devonian Nisku/Arcs Formation forms an individual hydrostratigraphic unit. Freshwater hydraulic head values are lower than the overlying Mississippian to Upper Mannville except for a low in the north, and the distribution of chloride shows only a general correlation. The $\delta^{18}O$ ratios of the waters are more negative at higher chloride content than the overlying units and the regional variation in the oxygen isotopic

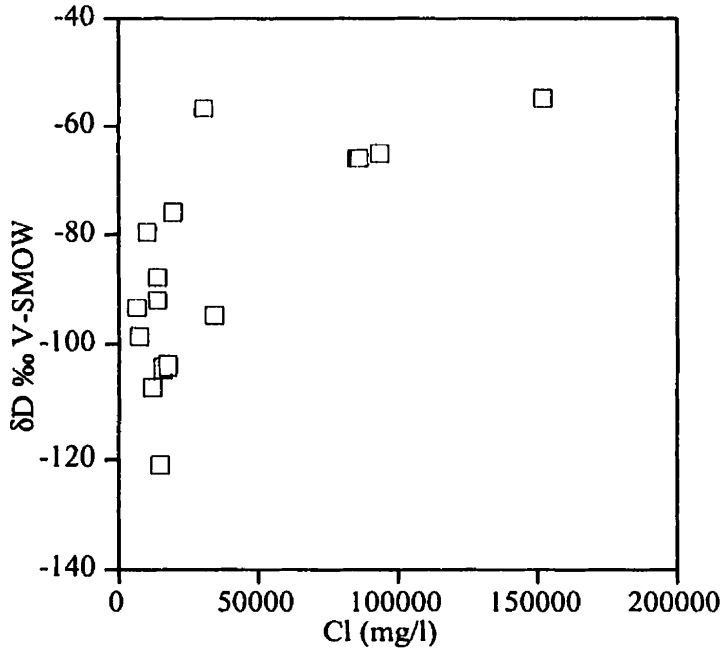

Figure 3.28. Nisku/Arcs aquifer water δD‰ vs Cl. Low chloride waters tend to have δD values suggesting the data reflect at least two meteoric mixing events.

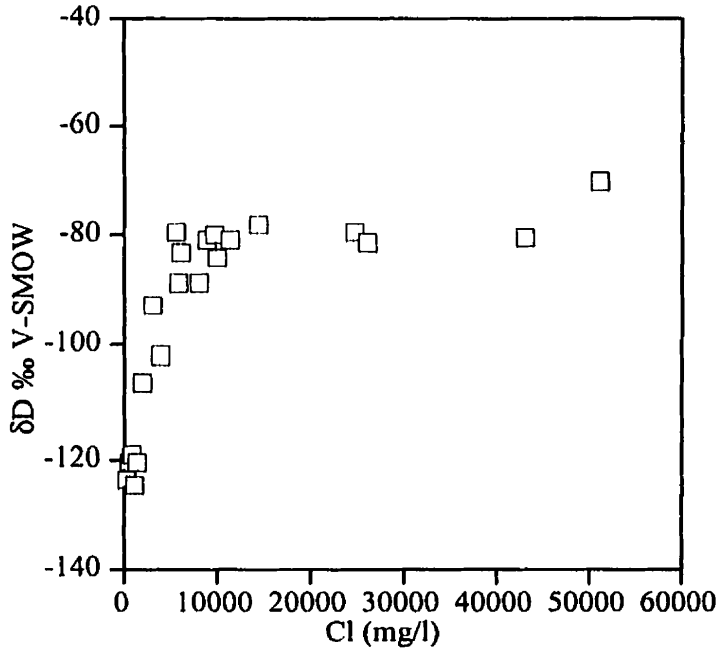

Figure 3.29. Mississippian aquifer water δD‰ vs Cl. Low chloride waters display a linear increase in δD up to 5,000 mg/l Cl. At higher Cl, δD values show little change with increasing Cl.

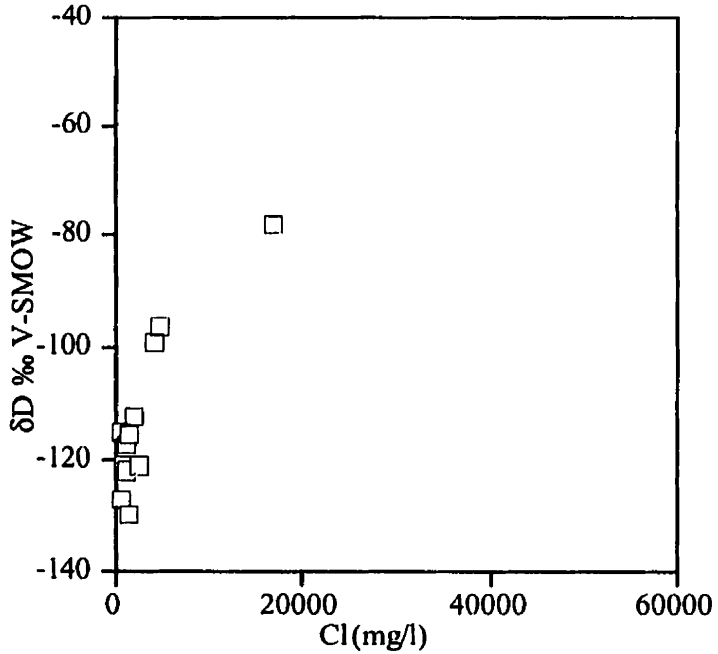

Figure 3.30. Jurassic Sawtooth aquifer water δD‰ vs Cl. Low chloride waters display a linear increase in δD values up to 5,000 mg/l Cl.

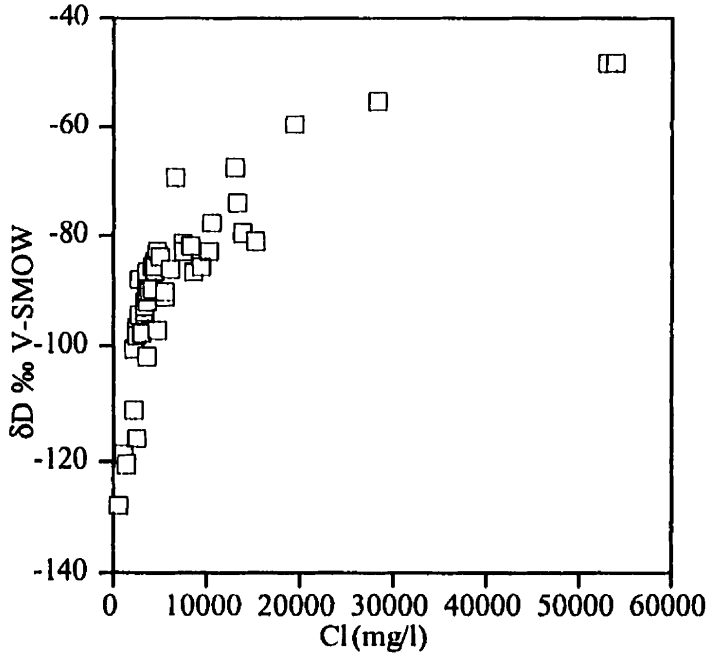

Figure 3.31. Lower Mannville aquifer water δD‰ vs Cl. Low chloride waters display a linear increase in δD values up to 5,000 mg/l Cl. At higher Cl, δD values show a more gradual increase with Cl and are significantly different from the Mississippian aquifer waters.

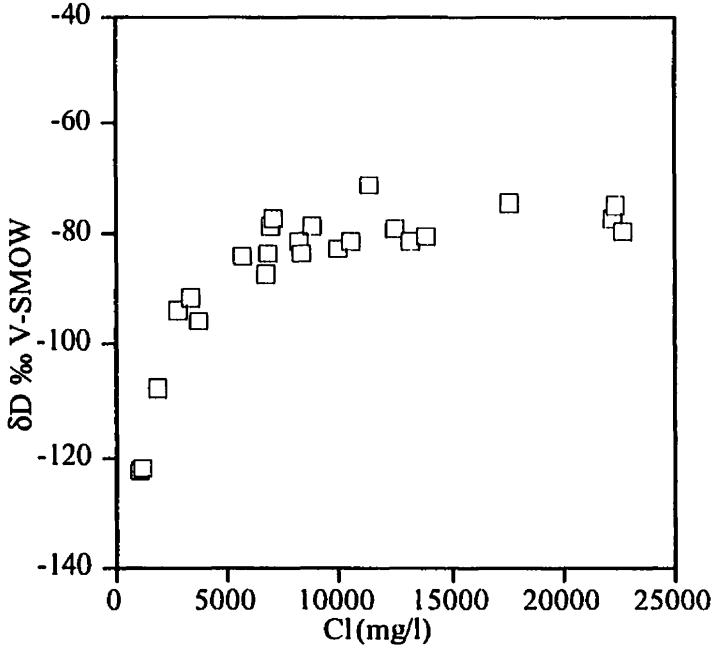

Figure 3.32. Upper Mannville aquifer water δD‰ vs Cl. Low chloride waters display a linear increase in δD values up to 5,000 mg/l Cl. At higher Cl, δD values lie between the Mississippian and Lower Mannville trends.

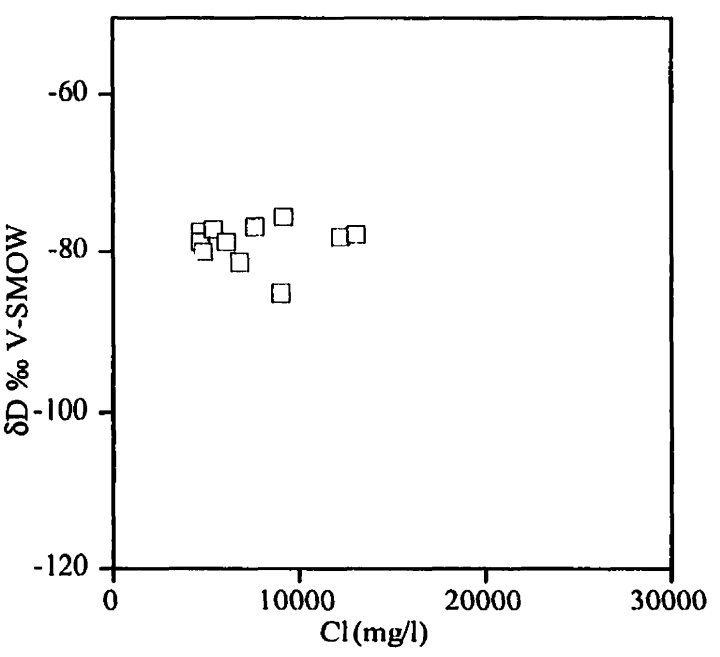

Figure 3.33. Viking/Bow Island aquifer water δD‰ vs Cl. The data all lie at δD =-80‰ +/-5‰ regardless of Cl content.

composition is considerably different. These observations indicate that the Nisku/Arcs aquifer is not in hydraulic communication with the overlying aquifers.

Hitchon (1969a,b) identified the Rocky Mountain foothills, the Sweetgrass arch and the Cypress Hills as major topographic controls on fluid flow in the southern portion of the WCSB. Flow, initiated by recharge at the topographic highs, was interpreted to be directed northward by the highly permeable beds of the Upper Devonian and Carboniferous (Hitchon, 1969b). Downey (1986) determined that Devonian-aged strata outcropping in Montana and Wyoming provide a conduit for meteoric water and recharge waters are directed towards the north into the Williston Basin through these conduits. The southeastern portion of the study area comprises the western extent of the Williston Basin, suggesting that recharge of the Nisku/Arcs aquifer is related to the topographic highs in Montana and Wyoming. The correlation between chloride content and potentiometric surface in the southeast indicates that meteoric recharge waters are related to the Williston Basin. Freshwater hydraulic head contours and cross sections (**Figures 3.5, 3.11-3.15**) indicate fluid flow in the Nisku/Arcs Formation appears to be directed from the south towards the north, similar to the conclusions of Hitchon (1969b). Topography driven flow relating to recharge in the foothills, however, may be impeded by a strong downslope component of density driven flow. In the west, large increases in chloride content and hydraulic head coincide with increases in the depth of burial. Along

the axis of the hinge zone (**Figure 3.1**), deep-seated normal faults extending to the Precambrian basement with throws of up to 300m were observed in a seismic and gravimetric study by Paukert (1982). Movement on these faults was interpreted to occur during Carboniferous and Lower Cretaceous times. The faults have resulted in considerable offset of the strata (Paukert, 1982) leading to the potential loss of lateral continuity of reservoir units. The steep salinity and head gradients and the gas induced pressure gradients separating the more deeply buried western region from the east are consistent with a lack of reservoir continuity.

The isotopic composition of Nisku/Arcs formation waters does not show a consistent relationship with chloride content. Hitchon and Friedman (1969) and Connolly *et al.* (1990b) interpreted variations in the $\delta^{18}O$ and δD ratios of Devonian formation waters to be remnants of the effect of the influx of meteoric water subsequent to the Laramide Orogeny. Positive deviations in the oxygen isotopic composition were interpreted to reflect exchange with carbonates (Hitchon and Friedman, 1969; Spencer, 1987) and/or evaporative concentration of the heavier isotope and mixing with fresh water (Connolly *et al.*, 1990b). Samples from east of 113° display $\delta^{18}O$ values that reflect mixing with meteoric water. In the west, the water appears to be in isotopic equilibrium with the host rock dolomite. The temperature-equilibrium plot indicates that oxygen isotope equilibration with dolomite at low temperature has not occurred. However, the regional

distribution of $\delta^{18}O$ values cannot be reconciled by simple mixing with meteoric water. Oxygen isotopic compositions of the Nisku/Arcs Formation water in the north tend to be more negative at higher chloride content than in the south. The difference is interpreted to be the result of at least two meteoric mixing events. The earlier event (or events) probably resulted in the extensive dilution of saline brine. The brine was quite likely displaced to the west and north. The high chloride content in the west reflects the composition of the displaced water. The later meteoric event appears to originate from the south and most likely is represented by the <10,000 mg/l Cl water observed in **Figure 3.4.**

Hitchon and Friedman (1969) proposed the distribution of deuterium in formation waters is the result of mixing of meteoric water and diagenetically modified seawater. Exchange with hydrogen sulfide was considered to be insignificant but the effect of membrane filtration by shales was qualitatively considered possible (Hitchon and Friedman, 1969). Connolly *et al.* (1990b) suggest that the shift in deuterium content of formation waters in the Alberta basin is due to concentration of deuterium during evaporation of seawater. Membrane filtration was determined to be of minor significance as the pressure differentials, meant to generate flow through shales, were not high enough to produce sufficient flow potential (Connolly *et al.*, 1990b). The results of this study are in

agreement with those of Connolly *et al.* (1990b). The enrichment in deuterium, without any further evidence as to its origin, may be the result of evaporative concentration.

The Mississippian to Upper Mannville aquifers behave as a single hydrostratigraphic group except in the south where the Jurassic aquitard prevents communication between the different units and the Upper Mannville consists of discontinuous thin sands. The chloride and oxygen isotopic composition of the waters for all four aquifers are similar. Potentiometric surfaces and pressure-depth plots all provide evidence for continuity between the different aquifers.

The waters in the south are typical of meteoric recharge with low chloride, and oxygen and deuterium isotopic composition similar to meteoric water. The flow of the low salinity waters appears to be controlled by the continuity of the aquifer units, both laterally and vertically. Toth and Corbet (1987) interpreted hydraulic head distributions in the Taber region of southern Alberta to reflect a strong upward component for flow from Mississippian into Mannville aquifers. Cody (1993) and Cody and Hutcheon (1999) also suggest cross-formational flow from the Mississippian into the Lower Cretaceous in southern Alberta. Recharge of meteoric waters is interpreted to be through the Mississippian and Jurassic Sawtooth Formation and up into the Upper and Lower Mannville north of the Jurassic subcrop edge, similar to flow paths suggested by Toth and Corbet (1987). The variations in chloride distribution and hydraulic head for the

Mississippian and Jurassic are consistent with recharge by meteoric waters from the south and east. Variations in chloride concentration and oxygen isotope distribution suggest that south of the Jurassic subcrop edge, flow in the Lower Mannville is sluggish or stagnant. Chloride and ^{18}O contents increase from south to north between 49° and 49.6°, at approximately 49.6°, lower values are observed, which can only be explained by the introduction of Mississippian- and Jurassic-hosted waters that have chemical and isotopic signatures similar to the low chloride and negative $\delta^{18}O$ waters north of 49.6°.

Cody (1993) and Cody and Hutcheon (1994) interpreted variations in water chemistry in the Mannville Group to be the result of gravity driven, south to north flow of meteoric recharge waters. In their study, changes in the oxygen isotopic composition of waters were interpreted to reflect mixing of meteoric water and water enriched in the heavier isotope (Cody and Hutcheon, 1994). Schwartz *et al.* (1981) used hydraulic conductivity, freshwater hydraulic head and water chemistry to interpret flow in Mississippian to Upper Cretaceous aquifers in southern Alberta. They recognized a pattern of south to north flow, with permeable units recharged by meteoric water in the south. Flushing of connate waters, recognized through variations in chemistry, was observed to correlate with zones of high hydraulic conductivity (Schwartz *et al.*, 1981). The highest hydraulic conductivities, found in the deepest aquifers (Mississippian and Jurassic), display more extensive flushing (Schwartz *et al.*, 1981). This is consistent with the results in this study,

which indicate the Lower Mannville formation waters south of the Jurassic subcrop are not in good hydraulic communication with those to the north and that flow is focused through the Mississippian-Jurassic aquifer system.

Flow is directed northward and eastward in the Mississippian and enters in to the northwest-southeast trending channel sands of the Lower and Upper Mannville where they cut down into Mississippian strata. The lack of east-west continuity of the channels supports the interpretation of lateral flow being dominated by flow in the Mississippian. Flow direction changes north and northeast of 50.3° and 112.5°. The abrupt change in chloride content, hydraulic head gradient, pressure gradient, and $\delta^{18}O$ along a northeast trending line suggests that north-directed flow is impeded, perhaps through permeability changes, and is redirected towards the northeast. The higher chloride water in the north and west is probably not a mixture of saline water with the meteoric water that is to the south, otherwise a mixing relationship on the $\delta^{18}O$ vs Cl diagrams of the higher chloride waters with low chloride waters would be apparent. The only mixing observed is between the meteoric water and waters with less than 10,000 mg/l Cl. The moderately saline waters that extend out into the central portion of the study area, even down to Cl concentrations of 10,000 mg/l, appear to reflect an older mixing event and are somewhat isolated from the current flow system of recharge from the south. The oxygen isotopic compositions are at, or near, temperature equilibration with Mississippian limestone.

This can only be possible if the waters were equilibrated prior to flow into the Lower and Upper Mannville. The dilute waters, which may have originated from the east, then equilibrated with the Mississippian limestone and subsequently flowed into the clastic reservoirs.

The waters to the north and northeast of the 10,000 to 15,000 mg/l chloride waters are also quite distinctive, but fit into the general trend of decreasing chloride content of the saline waters. The waters have moderate to low salinity, but unlike the low salinity waters to the south, they have low bicarbonate, and $\delta^{18}O$ contents that suggest equilibrium with either the Mannville cements or the Mississippian limestone. These waters may represent a continuation of the older, more evolved meteoric-saline mixed water, perhaps by recharge from the east during erosion of overlying strata initiated in the Oligocene (Abercrombie and Fullmer, 1992).

Similar arguments as those made for the Nisku/Arcs west-east fluid flow can be used to interpret flow potential in the Mississippian to Upper Mannville hydrostratigraphic group. Steep chloride and head gradients in the west and a change in pressure gradient between the systems suggest a lack of reservoir continuity. Bachu (1995) suggested topography-driven flow related to recharge in the foothills was insignificant in southern Alberta and the dominant flow direction was south to north with recharge in the Sweetgrass Hills in Montana.

The south to north flow of the Mississippian to Upper Mannville aquifers appears to be controlled by structural highs located south of the Canada U.S. border. Hydraulic head contours and the distribution of chloride suggest that flow follows the Sweetgrass/Bow Island arch particularly along the northern side (**Figure 3.1**). Flow appears to be focused towards the northeast from the central region. The result is an arcuate band of higher salinity water that closely coincides with the location of the Vulcan Low (**Figure 3.1**). It is difficult at this point to speculate as to the cause of the change in flow, the obvious influence of the Sweetgrass/Bow Island Arch on flow and the homogeneity of the rock units suggests a tectonic rather than sedimentary origin. It is possible that faults associated with movement of the Vulcan Low (Brandley *et al.* 1993) and the Sweetgrass/Bow Island Arch (Lorenz, 1982) act as barriers to fluid flow. Movement on these faults was interpreted to occur during Carboniferous and Late Cretaceous times. Changes in permeability described above may reflect a lack of continuity of the aquifers.

The Viking/Bow Island aquifer comprises a separate hydrostratigraphic unit. The distribution of chloride displays lows in the south and northwest with a broad high extending southwest to northeast. Chloride concentrations are lower than the underlying aquifers and oxygen isotope values have a narrow range. Schwartz *et al.* (1981) constructed regional maps of freshwater equivalent hydraulic head, distribution of

chloride and oxygen isotopic composition. They interpreted a more limited flow potential in the Viking/Bow Island based on variations in Cl, δD, and $\delta^{18}O$. A similar interpretation is evident in this study. The Viking/Bow Island waters are relatively dilute and show a narrow range in composition. The $\delta^{18}O$ value increases with increasing Cl at low Cl concentrations, but comparison with the data of Schwartz *et al.* (1981) indicates very little change in the isotopic composition except in the extreme southern area where a rapid increase is observed.

Hitchon and Friedman (1969) suggest that the enrichment of ^{18}O in the Viking/Bow Island formation waters results from exchange with carbonate cements. The Viking/Bow Island formation waters appear to be in temperature equilibrium with authigenic calcite. The isotopic composition of calcite cement suggests that it was precipitated from the current formation water and the mass of cement is not great enough to alter the composition of the formation water. Longstaffe and Ayalon (1987) determined that the formation of calcite in the Viking to the northwest of the study area was relatively early, with calcite precipitation occurring during early burial and deepest burial. If calcite precipitation took place at similar times in the south, then the waters are relatively unchanged since the early to mid Tertiary. The majority of calcite cements in the Viking/Bow Island Formation in southern Alberta have been interpreted as a late stage authigenic cement (McLellan, 1995). The results of McLellan (1995), however, only

express the relative timing while those of Longstaffe and Ayalon (1987) are interpreted in relation to orogenic activity and burial history. The difference between the two paragenetic sequences may merely be a result of subsequent diagenesis of rocks in the study area of Longstaffe and Ayalon (1987) and not from the temporal occurrence of the events. Head values of the Viking/Bow Island are subhydrostatic and a steep gradient is observed in the south where recharge occurs. Based on the isotopic composition of the waters in this study and those of Schwartz *et al.* (1981), flow is interpreted to be sluggish and variations in the oxygen isotopic composition and chloride content may reflect an earlier meteoric recharge event.

Conclusions

1. The present day fluid flow of the Devonian Nisku/Arcs, Mississippian, Jurassic Sawtooth, Lower Cretaceous Lower Mannville, Upper Mannville and Viking/Bow Island aquifers is dominated by a south to north component and is topography driven.
2. West to east flow resulting from recharge in the Rocky Mountain foothills is minimized by density-driven flow and decreased hydraulic communication.
3. Water chemistry in the Mississippian to Upper Mannville aquifers is controlled by flow in the Mississippian, the lateral continuity of the clastic aquifers, and, potentially

by structural features like the Sweetgrass/Bow Island arch system and the Vulcan Low.

4. Extensive mixing and dilution of the formation waters has occurred.
5. At least two mixing and dilution events are recognized for all of the aquifers. The earlier event appears to have occurred prior to uplift and erosion of the Late Oligocene.
6. The formation waters of the Nisku/Arcs, Mississippian, Lower and Upper Mannville have $\delta^{18}O$ values that reflect a carbonate rock equilibrated system at temperatures of >30°C for the Mississippian and younger aquifers and >70°C for the Nisku/Arcs.
7. Some waters may have $\delta^{18}O$ values that reflect isotopic equilibration with carbonates at higher temperatures and have retained that signature during uplift and erosion.
8. The influx of fresh water has resulted in lower chloride content and $\delta^{18}O$ values consistent with mixing of meteoric water and isotopically modified formation waters.
9. A narrow mixing zone between waters reflecting meteoric recharge and isotopically modified formation waters is recognized in the Mississippian to Upper Mannville aquifers.

Future Work

Our understanding of the origin and evolution of WCSB formation waters is constantly evolving. Meteoric water has had an obvious and considerable influence on the regional distribution and chemical composition of the waters. Unfortunately the effect of dilution has often resulted in changes in composition that obscure the origin of the brine-end member. Spencer (1987) and Connolly et al. (1990a,b) used bromide content to interpret the origin of the saline brine end-member. Based on sodium and potassium to bromide ratios, the evolution of the brine end-member was required to involve some reaction with rocks containing feldspars or clays. It would be worthwhile to obtain accurate bromide data to test whether the Nisku/Arcs formation waters in southern Alberta also retain some evidence of interaction with silicates. As it stands the data indicate no such reaction is necessary but the additional constraint on composition that bromide could provide would at the least allow comparison with the waters in the central and northern reaches of the basin.

Mineralogical control on the composition of water is often quite subtle. Small changes in pH and dissolved silica activity as solution chemistry changes through physical processes like mixing, appear to keep the system at or close to equilibrium with respect to the aluminosilicate phases. At low temperatures do phases other than the silica polymorphs influence the dissolved silica content? The answer appears to be affirmative and it would

be of value to look at dissolved silica content from a wider range samples from the WCSB to see if trends observed by Abercrombie et al. (1994) for data from other basins, can be recognized.

What is the source of the high pCO_2 and bicarbonate content in southern Alberta. Certainly BSR contributes to high values, but why is the carbon isotopic composition of bicarbonate generally close to that of the carbonate rocks? Taking a mass balance approach to answer this problem may be the most appropriate. How much carbon from the different sources results in the observed isotopic composition? To what degree does methanogenesis affect the composition? All of these questions need to be, and can be, addressed.

Perhaps of interest to hydrogeologists would be to try to accurately determine flux and flow rates. By how much does the permeability change to result in redirection of flow? Establishing flow paths using water chemistry and potentiometric surfaces is just the first step in a long series. Where does all of this water go? For that matter, is it really that much water? Detailed studies of smaller areas are needed. Perhaps focussing on where the water is going to would better delineate the flow paths.

General Conclusions

The extent of fluid flow in the southern portion of the Alberta is considerable. It is questionable as to whether topography-driven recharge in the current flow regime has extensively modified the formation waters though. Older events appear to dominate the regional variations in composition.

Mineralogical control on solution composition is subtle at these low temperatures. Unless of course if salts are being dissolved. Changes in composition are small, the rocks seem to be content with controlling pH and by doing so the system is controlled.

How much mass can be transported in a system that is close to equilibrium? That depends on the solubility and the solubility of silicate minerals is low.

References Cited

Aagard P. and Helgeson H. C. (1983) Activity/composition relations among silicates and aqueous solutions: II. Chemical and thermodynamic consequences of ideal mixing of atoms on homological sites in montmorillonites, illites, and mixed-layer clays. *Clays and Clay Minerals* **31**(3), 207-217.

Abercrombie H. J. and Fullmer E. G. (1992) Regional hydrogeology and fluid geochemistry of the Mannville Group, western Canada sedimentary basin: Synthesis and reinterpretation. In *Water-Rock Interaction*, Vol. Volume 2: Moderate and High Temperature Environments (ed. Y. K. Kharaka and A. S. Maest), A.A. Balkema, pp. 1101-1104.

Abercrombie H. J., Hutcheon I. E., Bloch J. D. a., and de Caritat P. (1994) Silica activity and the smectite-illite reaction. *Geology* **22**, 539-542.

Appelo C. A. J. and Postma D. (1996) *Geochemistry, Groundwater and Pollution*. A.A. Balkema.

Bachu S. (1995) Synthesis and model of formation-water flow, Alberta basin, Canada. *A.A.P.G. Bulletin* **79**(8), 1159-1178.

Bachu S., Sauveplane C. M., Lytviak A. T., and Hitchon B. (1987) Analysis of fluid and heat regimes in sedimentary basins: techniques for use with large data bases. *A.A.P.G. Bulletin* **71**(7), 822-843.

Bachu S. and Underschultz J. R. (1993) Hydrogeology of formation waters, northeastern Alberta basin. *A.A.P.G. Bulletin* **77**(10), 1745-1768.

Bachu S. and Underschultz J. R. (1995) Large-scale underpressuring in the Missippippian-Cretaceous succession, southwestern Alberta basin. *A.A.P.G. Bulletin* **79**(7), 989-1004.

Bailey N. J. L., Krouse H. R., Evans C. R., and Rogers M. A. (1973) Alteration of crude oil by waters and bacteria - Evidence from geochemical and isotope studies. *A.A.P.G. Bulletin* **57**(7), 1276-1291.

Berman R. G. (1988) Internally-consistent thermodynamic data for minerals in the system Na_2O-K_2O-CaO-MgO-FeO-Fe_2O_3-Al_2O_3-SiO_2-TiO_2-H_2O-CO_2. *Journal of Petrology* **29**(2), 445-522.

Berman R. G. and Brown T. H. (1985) Heat capacity of minerals in the system Na_2O-K_2O-CaO-MgO-FeO-Fe_2O_3-Al_2O_3-SiO_2-TiO_2-H_2O-CO_2: representation, estimation, and high temperature extrapolation. *Contributions to Mineralogy and Petrology* **89**, 168-183.

Berner J. A. (1985) Sulfate reduction, organic matter decomposition and pyrite formation. *Philo. Trans. of the Royal Society of London* **A315**, 25-38.

Bethke C. M. (1985) A numerical model of compaction-driven groundwater flow and heat transfer and its application to the paleohydrology of intracratonic sedimentary basins. *Journal of Geophysical Research* **90**(B8), 6817-6828.

Billings G. K., Hitchon B., and Shaw D. R. (1969) Geochemistry and origin of formation waters in the western Canada sedimentary basin. 2. Alkali metals. *Chemical Geology* **4**, 211-223.

Brandley R.T., Thurston, J., and Krause, F.F., 1993. Basement tectonic control on carbonate ramp deposition: Lower Carboniferous Mount Head Formation, Southwest Alberta and Southeast British Columbia. Alberta Transects Workshop (March 1-2), Lithoprobe Report #31, G.M. Ross (ed.), p. 98-118.

Bruggenwert M. G. M. and Kamphorst A. (1982) Survey of experimental information on cation exchange in soil systems. In *Soil Chemistry*, Vol. 5 (ed. G. H. Bolt), pp. 141-203.

Caldwell M. E., Garrett R. M., Prince R. C., and Suflita J. M. (1998) Anaerobic biodegradation of long-chain n-alkanes under sulfate reducing conditions. *Environmental Science and Technology* **32**(14), 2191-2195.

Carothers W. W. and Kharaka Y. K. (1980) Stasble carbon isotopes of HCO_3^- in oil-field waters-implications for the origin of CO_2. *Geochimica et Cosmochimica Acta* **44**, 323-332.

Carpenter A. B. (1978) Origin and chemical evolution of brines in sedimentary basins. *Oklahoma Geological Survey Circular* **79**, 60-77.

Cathles L. M. and Smith A. T. (1983) Thermal constraints on the formation of Mississippi Valley-type lead-zinc deposits and their implications for episodic basin dewatering and deposit genesis. *Economic Geology* **78**, 983-1002.

Chermak J. A. and Rimstidt J. D. (1989) Estimating the thermodynamic properties of silicate minerals at 298K from the sum of polyhedral contributions. *American Mineralogist* **74**, 1023-1031.

Clayton R. N., Friedman I., Graf D. L., Mayeda T. K., Meents W. F., and Shimp N. F. (1966) The origin of saline formation waters 1. Isotopic composition. *Journal of Geophysical Research* **71**(16), 3869-3882.

Cody J. D. (1993) Geochemistry of Formation Fluids in the Mannville Group (Lwr. Cret.), Southern Alberta. M.Sc., University of Calgary.

Cody J. D. and Hutcheon I. E. (1994) Regional water and gas geochemistry of the Mannville Group and associated horizons, southern Alberta. *Bulletin of Canadian Petroleum Geology* **42**(4), 449-464.

Cody J. D., Hutcheon I. E., and Krouse H. R. (1999) Fluid flow, mixing and the origin of CO2 and H2S by bacterial sulfate reduction in the Mannville Group, southern Alberta, Canada. *Marine and Petroleum Geology* **16**, 495-510.

Coleman M. L., Sheppard T. J., Durham J. J., Rouse J. D., and Moore G. R. (1982) Reduction of water with zinc for hydrogen isotope analysis. *Analytical Chemistry* **54**, 199-260.

Connan J. (1984) Biodegradation of crude oils in reservoirs. In *Advances in Petroleum Geochemistry* (ed. J. Brooks and D. H. Welte), Academic Press, pp. 299-335.

Connolly C. A., Walter L. M., Baadsgaard H., and Longstaffe F. J. (1990a) Origin and evolution of formation waters, Alberta basin, western Canada sedimentary basin. I. Chemistry. *Applied Geochemistry* **5**, 375-395.

Connolly C. A., Walter L. M., Baadsgaard H., and Longstaffe F. J. (1990b) Origin and evolution of formation waters, Alberta basin, western Canada sedimentary basin. II. Isotope systematics and water mixing. *Applied Geochemistry* **5**, 397-413.

Craig H. (1961) Isotopic variations in meteoric waters. *Science* **133**, 1702-1703.

Dahlberg E. C. (1982) *Applied Hydrodynamics in Petroleum Exploration*. Spring-Verlag, 161 p.

Davies P. B. (1987) Modeling areal, variable-densitry, ground-water flow using equivalent freshwater head -- Analysis of potentially significant errors. *Proceedings of the NWWA Conference on Solving Ground Water Problems with Models*, Denver, Colorado, pp. 888-903.

Deming D. and Nunn J. A. (1991) Numerical simulations of brine migration by topographically driven recharge. *Journal of Geophysical Research* **96**(B2), 2485-2499.

Deming D., Nunn J. A., and Evans D. G. (1990) Thermal effects of compaction-driven groundwater flow from overthrust belts. *Journal of Geophysical Research* **95**(B5), 6669-6683.

Downey J. S. (1986) *Geohydrology of bedrock aquifers in the Northern Great Plains in parts of Montana, North Dakota, South Dakota, and Wyoming*. USGS. Professional Paper 1402-E

Epstein S. and Mayeda T. (1953) Variation of O^{18} content of waters from natural sources. *Geochimica et Cosmochimica Acta* **4**, 213-224.

Farshori M. Z. and Hopkins J. C. (1989) Sedimentology and petroleum geology of fluvial and shoreline deposits of the Lower Cretaceous Sunburst Sandstone Member, Mannville Group, southern Alberta. *Bulletin of Canadian Petroleum Geology* **37**(4), 371-388.

Foscolos A. E., Reinson G. E., and Powell T. G. (1982) Controls on clay-mineral authigenesis in the Viking Sandstone, central Alberta, 1. Shallow depths. *Canadian Mineralogist* **20**, 141-150.

Friedman I. and O'Neil J. R. (1977) Compilation of stable isotope fractionation factors of geochemical interest. In *Data of Geochemistry*, Vol. Prof. Paper 440-KK (ed. M. Fleisher). USGS.

Garrels R. M. (1984) Montmorillonite/illite stability diagrams. *Clays and Clay Minerals* **32**(3), 161-166.

Garven G. (1985) The role of regional fluid flow in the genesis of the Pine Point deposit, western Canada sedimentary basin. *Economic Geology* **80**, 307-324.

Gat J. R. (1981) Groundwater. In *Stable Isotope Hydrology: Deuterium and Oxygen-18 in the Water Cycle*, Vol. Technical Report Series No. 210, IAEA, pp. 223-240.

Ge S. and Garven G. (1994) A theoretical model for thrust-induced deep groundwater expulsion with application to the Canadian Rocky Mountains. *Journal of Geophysical Research* **99**(B7), 13851-13868.

Ghent E. D. and Miller B. E. (1974) Zeolite and clay-carbonate assemblages in the Blairmore Group (Cretaceous), southern Alberta Foothills, Canada. *Contributions to Mineralogy and Petrology* **44**, 313-329.

Guven N. (1988) Smectites. In *Hydrous Phyllosilicates (exclusive of micas)*, Vol. 19 (ed. P. H. Ribbe), MSA Reviews in Mineralogy, pp. 497-560.

Harvie C. E., Moller N., and Weare J. H. (1984) The prediction fo mineral solubilities in natural waters: The Na-K-Mg-Ca-H-Cl-So4-OH-HCO3-CO3-CO2-H20 system to high ionic strengths at 25 C. *Geochimica et Cosmochimica Acta* **48**, 723-751.

Hayes B. J. R. (1986) Stratigraphy of the basal Cretaceous Lower Mannville formation, southern Alberta and north-central Montana. *Bulletin of Canadian Petroleum Geology* **34**(1), 30-48.

Helgeson H. C. (1969) Thermodynamics of hydrothermal systems at elevated temperatures and pressures. *American Journal of Science* **267**, 729-804.

Helgeson H. C., Delany J. M., Nesbitt H. W., and Bird D. K. (1978) Summary and critique of the thermodynamic properties of rock-forming minerals. *American Journal of Science* **278A**, 1-229.

Helgeson H. C., Kirkham D. H., and Flowers G. C. (1981) Theoretical prediction of the thermodynamic properties of aqueous electrolytes at high temperatures and pressures. IV. Calculation of activity coefficients, osmotic coefficients, and apparent molal and standard and relative partial molal properties to 600°C and 5kb. *American Journal of Science* **281**, 1249-1516.

Hitchon B. (1969a) Fluid flow in the western Canada sedimentary basin. 1. Effect of topography. *Water Resources Research* **5**(1), 186-195.

Hitchon B. (1969b) Fluid flow in the western Canada sedimentary basin. 2. Effect of geology. *Water Resources Research* **5**(2), 460-469.

Hitchon B., Bachu S., Lytviak A. T., and Sauveplane C. M. (1986) Integrated hydrological data bases: Their use and misuse. *NWWA Can-Am Hydroconference on Hydrology of Sedimentary Basins: Application to Exploration and Exploitation*, 115-117.

Hitchon B., Bachu S., and Underschultz J. R. (1990) Regional subsurface hydrogeology, Peace River Arch area, Alberta and British Columbia. *Bulletin of Canadian Petroleum Geology* **38A**, 196-217.

Hitchon B., Billings G. K., and Klovan J. E. (1971) Geochemistry and origin of formation waters in the western Canada sedimentary basin--III. Factors controlling chemical composition. *Geochimica et Cosmochimica Acta* **35**, 567-598.

Hopkins J. C., Hermanson S. W., and Lawton D. C. (1982) Morphologies of channels and channel-sand bodies in the Glauconitic sandstone member (Upper Mannville), Little Bow area, Alberta. *Bulletin of Canadian Petroleum Geology* **30**(4), 274-285.

Hubbert M. K. (1956) Darcy's law and the field equations of the flow of underground fluids. *Darcy Centennial Hydrology Symposium*, 222-239.

Hutcheon I. and Abercrombie H. (1990) Carbon dixide in clastic rocks and silicate hydrolysis. *Geology* **18**, 541-544.

Hutcheon I., Shevalier M., and Abercrombie H. J. (1993) pH buffering by metastable mineral-fluid equilibria and evolution of carbon dixide fugacity during burial diagenesis. *Geochimica et Cosmochimica Acta* **57**, 1017-1027.

James D. P. (1985) Stratigraphy, Sedimentology, and Diagenesis of Upper Jurassic and Lower Cretaceous Strata, Southwestern Alberta. Ph.D., University of Oxford.

Johnson J. W., Oelkers E. H., and Helgeson H. C. (1992) SUPCRT92: A software package for calculating the standard molal thermodynamic properties of minerals, gases, aqueous species, and reactions from 1 to 5000 bars and 0 to 1000°C. *Computers and Geosciences*.

Karavas F. A., Riediger C. L., Fowler M. G., and Snowdon L. R. (1998) Oil families in Mannville Group reservoirs of southwestern Alberta, western Canada sedimentary basin. *Organic Geochemistry* **29**(1-3), 769-784.

Karvonen R. L. and Pemberton S. G. (1997) The Upper Mannville Group of southeast Alberta, Canada: An example of multiple incised valley fill deposits. In *Petroleum Geology of the Cretaceous Mannville Group, Western Canada*, Vol. Memoir 18 (ed. S. G. Pemberton and D. P. James), CSPG, pp. 124-139.

Kharaka Y. K. (1986) Origin and evolution of water and solutes in sedimentary basins. *Third Canadian/American Conference on Hydrogeology*, 173-195.

Kharaka Y. K. and Carothers W. W. (1986) Oxygen and hydrogen isotope geochemistry of deep basin brines. In *Handbook of Environmental Isotope Geochemistry*, Vol. 2 (ed. P. Fritz and J. Fontes), pp. 305-360.

Kharaka Y. K., Gunter W. D., Aggarwal P. K., Hull R. W., and Perkins E. H. (1987) *SOLMINEQ.87: Acomputer program code for geochemical modeling of water-rock interactions*. USGS. Water Resources Investigations Report 87-5082

Kissling D. L. and Slingsby A. (1992) Depositional , digenetic and reservoir parameters of the Upper Devonian Nisku Shelf, Alberta and Montana. In *CSPG Core Workshop*, pp. 46.

Kittrick J. A. (1971) Stability of montmorillonites: I. Belle Fourche and Clay Spur montmorillonites. *Soil Sci. Soc. Amer. Proc.* **35**, 140-145.

Krouse H. R., Viau C. A., Eliuk L. S., Ueda A., and Halas S. (1988) Chemical and isotopic evidence of thermochemical sulphate reduction by light hydrocarbon gases in deep carbonate reservoirs. *Nature* **333**(2 June), 415-419.

Kyser T. K. (1987) Equilibrium fractionation factors for stable isotopes. In *Stable isotope chemistry of low temperature processes*, Vol. 13 (ed. T. K. Kyser), MAC pp. 1-83.

Land L. S. (1983) The application of stable isotopes to studies of the origin of dolomite and to problemsof diagenesis of clastic sediments. In *Stable Isotopes in Sedimentary Geology*, Vol. Short Course 10, SEPM, pp. 4.1-4.22.

Langmuir D. (1997) *Aqueous Environmental Geochemistry*. Prentice Hall. 600 p.

Lico M. S., Kharaka Y. K., Carothers W. W., and Wright V. A. (1982) *Methods of collection and analysis of geopressured geothermal and oil field waters*. United States Geological Survey. USGS Water Supply Paper 2194

Longstaffe F. and Ayalon A. (1987) Oxygen-isotope studies of clastic diagenesis in the Lower Cretaceous Viking Formation, Alberta: implications for the role of meteoric water. In *Diagenesis of Sedimentary Sequences*, Vol. Special Publication No. 36 (ed. J. D. Marshall), Geological Society, pp. 277-296.

Longstaffe F. J. (1986) Mineralogical and oxygen-isotope studies of clastic diagenesis: Implications for fluid flow in sedimentary basins. *Third Canadian/American Conference on Hydrogeology: Hydrogeology of Sedimentary Basins: Application to Exploration and Exploitation*, 204-220.

Longstaffe F. J. (1987) Stable isotope studies in diagenetic processes. In *Stable isotope chemistry of low temperature processes*, Vol. 13 (ed. T.K. Kyser), MAC, pp. 187-257.

Longstaffe F. J. (1989) Stable isotopes as tracers in clastic diagenesis. In *Burial Diagenesis*, Vol. 15 (ed. I. E. Hutcheon), MAC, pp. 201-257.

Lorenz J. C. (1982) Lithospheric flexure and the history of the Sweetgrass arch, northwestern Montana. *Rocky Mountain Association of Geologists* **1982 Symposium**, 77-89.

Machel H. G., Krouse H. R., and Sassen R. (1995) Products and distinguishing criteria of bacterial and thermochemical sulfate reduction. *Applied Geochemistry* **10**, 373-389.

Mackenzie F. T. and Garrels R. M. (1965) Silicates; reactivity with seawater. *Science* **150**(3692), 57-58.

Manzano B. K., Riediger C., and Fowler M. (2000) Mesozoic oil families, southern Alberta: Application of aromatic compounds. CSPG Annual Convention *GeoCanada 2000.* Calgary, Alberta, Posters with Abstracts.

May H. M., Kinniburgh D. G., Helmke P. A., and Jackson M. L. (1986) Aqueous dissolution, solubilities and thermodynamic stabilities of common aluminosilicate clay minerals: Kaolinite and smectites. *Geochimica et Cosmochimica Acta* **50**, 1667-1677.

McCafferey M. A., Lazar B., and Holland H. D. (1987) The evaporation path of seawater and the coprecipitation of Br^- and K^- with halite. *Journal of Sedimentary Petrology* **57**, 928-937.

McLellan S. R. (1995) Fluid flow, gas isotope geochemistry and diagenesis in the Bow Island Formation (Lower Cretaceous) of southern Alberta. M.Sc., University of Calgary.

Nesbitt B. E. and Muehlenbachs K. (1994) Paleohydrogeology of the Canadian Rockies and origins of brines, Pb-Zn deposits and dolomitization in the western Canada sedimentary basin. *Geology* **22**(March), 243-246.

Neuzil C. E. and Pollock D. W. (1982) Erosional unloading and fluid pressures in hydraulically "tight" rocks. *Journal of Geology* **91**, 179-193.

Nordstrom, D.K. and Munoz, J.L. (1996) Geochemical Thermodynamics (2nd Edition). Boston. Blackwell Scientific Publications.

Nriagu J. O. (1975) Thermochemical approximation for clay minerals. *American Mineralogist* **60**, 834-839.

Olson G. J., Dockins W. S., McFeters G. A., and Iverson W. P. (1981) Sulfate reducing and methanogenic bacteria from deep aquifers in Montana. *Geomicrobiology Journal* **2**, 327-339.

Orr W. L. (1977) Geological and geochemical controls on the distribution of hydrogen sulfide in natural gas. In *Advances in Organic Geochemistry* (ed. R. Campos and J. Goni), pp. 571-597.

Paukert, G.W., 1982. Geophysical Study of Precambrian Basement Fault Structure and Related Cretaceous Sratigraphic Variation in Southern Alberta. Unpublished M.Sc. Thesis, University of Calgary, 114 p.

Potocki D. and Hutcheon I. E. (1992) Lithology and diagenesis of sandstones in the western Canada foreland basin. In *Foreland Basins and Fold Belts*, Memoir 55 (ed. R. W. L. Macqueen, D.A.Leckie), A.A.P.G., pp. 229-257.

Poulton, T.P., Christopher, J.E., Hayes, B.J.R., Losert, J., Tittemore, J. and Gilchrist, R.D., 1994, Jurassic and Lowermost Cretaceous Strata of the Western Canada Sedimentary Basin. In G. D. Mossop and I Shetson (eds.), The Geological Atlas

of the Western Canada Sedimentary Basin. Calgary. Canadian Society of Petroleum Geologists and Alberta Research Council, p. 297-316.

Ransom B. and Helgeson H. C. (1993) Compositional end members and thermodynamic components of illite and dioctahedral aluminous smectite solid solutions. *Clays and Clay Minerals* **41**(5), 537-550.

Ransom B. and Helgeson H. C. (1994) Estimation of the standard molal heat capacities, entropies, and volumes of 2:1 clay minerals. *Geochimica et Cosmochimica Acta* **58**(21), 4537-4547.

Ransom B. and Helgeson H. C. (1995) A chemical and thermodynamic model of dioctahedral 2:1 layer clay minerals in diagenetic processes: Dehydration of dioctahedral aluminous smectite as a function of temperature and depth in sedimentary basins. *American Journal of Science* **295**, 245-281.

Richards, B.C., Barclay, J.E., Bryan, D., Harting, A., Henderson, C.M. and Hinds, R.C., 1994, Carboniferous Strata of the Western Canada Sedimentary Basin. In G. D. Mossop and I Shetson (eds.), The Geological Atlas of the Western Canada Sedimentary Basin. Calgary. Canadian Society of Petroleum Geologists and Alberta Research Council, p. 221-250.

Robie R. A., Hemingway B. S., and Fisher J. R. (1978) *Thermodynamic properties of minerals and related substances at 298.15K and 1 bar pressure and at higher temperature.* USGS. Bulletin 1452.

Robinson G. R. and Haas Jr. J. L. (1983) Heat capacity, relative enthalpy, and calorimetric entropy of silicate minerals: an empirical method of prediction. *American Mineralogist* **68**, 541-553.

Ross G. M., Parrish R. P., Villeneuve M. E., and Bowring S. A. (1991) Geophysics and geochronology of the crystalline basement of the Alberta basin, western Canada. *Canadian Journal of Earth Sciences* **28**, 512-522.

Routson R. C. and Kittrick J. A. (1971) Illite solubility. *Soil Sci. Soc. Amer. Proc.* **35**, 714-718.

Rueter P., Rabus R., Wilkes H., Aeckersberg F., Rainey F. A., Jannasch H. W., and Widdel F. (1994) Anaerobic oxidation fo hydrocarbons in crude oil by new types of sulfate-reducing bacteria. *Nature* **372**(1 December), 455-458.

Runnels D. D. (1969) Diagenesis, chemical sediments and the mixing of natural waters. *Journal of Sedimentary Petrology* **39**, 1188-1202.

Schwartz F. W., Muehlenbachs K., and Chorley D. W. (1981) Flow-system controls of the chemical evolution of groundwater. *Journal of Hydrology* **54**, 225-243.

Simpson G. P. (1999) Sulfate reduction and fluid chemistry of the Devonian Leduc and Nisku Formations in south-central Alberta. Ph.D., University of Calgary.

Smith, D.G., 1994, Paleogeographic Evolution of the Western Canada Foreland Basin. In G. D. Mossop and I Shetson (eds.), The Geological Atlas of the Western Canada Sedimentary Basin. Calgary. Canadian Society of Petroleum Geologists and Alberta Research Council, p. 277-296.

Smith J. T. and Ehrenberg S. N. (1989) Correlation of carbon dioxide abundance with temperature in clastic hyrdocarbon reservoirs: relationship to inorganic chemical equilibrium. *Marine and Petroleum Geology* **6**, 129-135.

Spencer R. J. (1987) Origin of Ca-Cl brines in Devonian formations, western Canada sedimentary basin. *Applied Geochemistry* **2**, 373-384.

Tardy Y. and Duplay J. (1992) A method of estimation the Gibbs free energies of formation of hydrated and dehydraed clay minerals. *Geochimica et Cosmochimica Acta* **56**(8), 3007-3029.

Tardy Y., Duplay J., and Fritz B. (1987) Stability fields of smectites and illites as a function of temperature and chemical composition. *Intl. Mtg. on Geochemistry of the Earth Surface and Processes of Mineral Formation*, 461-494.

Tardy Y. and Fritz B. (1981) An ideal solid solution model for calculating solubility of clay minerals. *Clay Minerals* **16**, 361-373.

Tardy Y. and Garrels R. M. (1974) A method of estimation the Gibbs energies of formation of layer silicates. *Geochimica et Cosmochimica Acta* **38**, 1101-1116.

Tardy Y. and Garrels R. M. (1976) Prediction of Gibbs energies of formation-I. Relationships among Gibbs energies of formation of hydroxides, oxides, and aqueous solutions. *Geochimica et Cosmochimica Acta* **40**, 1051-1056.

Tardy Y. and Garrels R. M. (1977) Prediction of Gibbs energies of formation of compounds from the elements-II. Monovalent and divalent metal silicates. *Geochimica et Cosmochimica Acta* **41**, 87-92.

Thode H. G., Wanless R. K., and Wallouch R. (1954) The origin of native sulfur deposits from isotope fractionation studies. *Geochimica et Cosmochimica Acta* **5**, 286-298.

Toth J. (1989) Large-scale characteristics of pore-fluid potential fields in the Alberta basin, Canada. *Eos* **October 24**, 1096.

Toth J. and Corbet T. (1987) Post-Paleocene evolution of regional groundwater flow systems and their relation to petroleum accumulations, Taber area, southern Alberta, Canada. In *Fluid Flow in Sedimentary Basins and Aquifers*, Vol. Geological Society Special Publication No. 34 (ed. J. C. Goff and B. P. J. Williams), Blackwell Scientific Publications, pp. 45-77.

Weaver R. M., Jackson M. L., and Syers J. K. (1971) Magnesium and silicon activities in matrix solutions of montmorillonite-containing sols in relation to clay mineral stability. *Soil Sci. Soc. Amer. Proc.* **35**, 823-830.

Whelan J. A. (1987) Stable isotope hydrology. In *Stable isotope chemistry of low temperature processes*, Vol. 13 (ed. T. K. Kyser), MAC, pp. 159-160.

Whiticar M. J., Faber E., and Schoell M. (1986) Biogenic methane formation in marine and freshwater environments: CO_2 reduction vs. acetate fermentation-Isotope evidence. *Geochimica et Cosmochimica Acta* **50**, 693-709.

Whittaker S. G. and Mountjoy E. W. (1996) Diagenesis of an Upper Devonian carbonate-evaporite sequence: Birdbear Formation, southern interior plains, Canada. *Jounal of Sedimentary Research* **66**(5), 965-975.

Wood J. M. (1990) Sequence stratigraphy, sedimentology and petroleum geology of the Glauconitic and adjacent strata, Lower Cretaceous Mannville Group, southern Alberta. Ph.D., University of Calgary.

Wood J. M. and Hopkins J. C. (1992) Traps associated with paleovalleys and interfluves in an unconformity bounded sequence: Lower Cretaceous Glauconitic member, southern Alberta, Canada. *A.A.P.G. Bulletin* **76**(6), 904-926.

Wright, C.N., McMechan, M.E. and Potter, D.E.G., (1994). Structure and Architecture of the Western Canada Sedimentary Basin. In G. D. Mossop and I Shetson (eds.), The Geological Atlas of the Western Canada Sedimentary Basin. Calgary. Canadian Society of Petroleum Geologists and Alberta Research Council, p. 25-40.

Zaitlin B. A. (1997) The stratigraphic organization of incised-valley systems: Implications for exploration and exploitation in the western Canada sedimentary basin. *CSPG Reservoir and Noon Hour Talk* **24**(6), 3-6.